Dissertation

Adenine nucleotide – modulated $CD8^+$ T cell differentiation and effector functions

by Niels Christian Lory
Matriculation no.: 6744676
AG Prof. Dr. Hans-Willi Mittrücker
Universitätsklinik Hamburg-Eppendorf

supervised by

Prof. Dr. Hans-Willi Mittrücker
Prof. Dr. Dr. Andreas H. Guse

Zur Erlangung der Doktorwürde an der Universität Hamburg, Fachbereich Biologie der Fakultät für Mathematik, Informatik und Naturwissenschaften.

Gutachter

Gutachter dieser Arbeit sind Prof. Dr. Hans-Willi Mittrücker und Prof. Dr. Dr. Andreas H. Guse

Disputation: 06.07.2022

Acknowledgements

I would like to thank everyone in the working group. In particular, Joanna Schmid, Karsten Yang and Daniel Reimers who have been very supportive especially in the beginning of my work. Further I would like to thank all contributors to the publications included in this work and Karsten Yang and Christian Casar for their efforts in the single cell CITE sequencing experiment. I would like to thank Prof. Dr. Dr. Andreas H. Guse, Prof. Dr. Samuel Huber and Prof. Dr. Hans-Willi Mittrücker for their supervision.

Contents

List of Figures

List of Tables

Abbreviations

2dADPR	2-deoxy-ADPR
ACA	59 N- p-amylcinnamoyl anthranilic acid
ADPR	adenosine diphosphate ribose
ADPRP	2-phospho adenosine diphosphoribose
ADT	antibody derived tag
AHNAK	neuroblast differentiation-associated protein
AHRGI	rho guanine nucleotide exchange factor 18
AKT	RAC-alpha serine/threonine-protein kinase, also called protein kinase B
AP-1	activator protein 1
AP-1	activator protein 1
APC	antigen presenting cells
ART2	ADP-ribosyltransferase 2
ATP	adenosine triphosphate
BCL2	apoptosis regulator Bcl-2
BIM	Bcl2-interacting mediator of cell death, also called Bcl2-L-11
BLT	N-α-benzyloxycarbonyl-L-lysine thiobenzyl ester
BMDM	bone marrow derived macrophages
cADPR	cyclic ADP-ribose
CaM	calmodulin
CCL2	C-C motif chemokine 2
***Cd38*$^{-/-}$**	CD38 deficient
CD38	cyclic ADP ribose hydrolase
CD49d	integrin alpha-4
CITE	cellular indexing of transcriptomes and epitopes
CSF-2	colony stimulating factor 2
CX3CR1	CX3C chemokine receptor 1
CXCL2	C-X-C motif chemokine 2
DAG	diacylglycerol
DUOX	nicotinamide adenine dinucleotide phosphate oxidase

EAE	experimental autoimmune encephalomyelitis
E. coli	*Escherichia coli*
ER	endoplasmic reticulum
ERK	extracellular signal-regulated kinases
ETS1	protein C-ets-1
FACS	fluorescence-activated cell sorting
fMLP	N-Formylmethionyl-leucyl-phenylalanine
FOS	c-Fos
FOXO1	forkhead box protein O1
FOXO3	forkhead box protein O3
FoxP3	forkhead box protein P3
FPR	fMet-Leu-Phe receptor
GILZ	glucocorticoid-induced leucine zipper
Glut1	glucose transporter 1
GRB2	growth factor receptor-bound protein 2
GZMA	granzyme A
HN1L/JPT2	hematological and neurological expressed 1-like protein/ jupiter microtubule associated homolog 2
IFNγ	interferon γ
IFNGR1	interferon γ receptor 1
IKK	inhibitor of nuclear factor κ-B kinase
IL	interleukin
IL18R	interleukin-18 receptor 1
IL18rap	interleukin-18 receptor accessory protein
IP3	inositol 1,4,5-trisphosphate
IP3R	IP3 receptor
ISG	interferon-stimulated genes
ITAM	immunoreceptor tyrosine-based activation motif
ITGA4	integrin α-4
ITK	tyrosine-protein kinase ITK also known as interleukin-2-inducible T-cell kinase
JNK	c-Jun N-terminal kinase
JUN	c-Jun
KLF3	CACCC-box-binding protein
KLRG1	killer cell lectin-like receptor subfamily G member 1
K. pneumoniae	*Klebsiella pneumoniae*
LAT	linker for activation of T cells

LCK	lymphocyte-specific protein tyrosine kinase
L. monocytogenes	*Listeria monocytogenes*
MAP3K7	Mitogen-activated protein kinase kinase kinase 7
MAPK	mitogen-activated protein kinase
MCU	mitochondrial Ca^{2+} uniporter
MHC	major histocompatibility complex
mTOR	mammalian target of rapamycin / mechanistic target of rapamycin
NAADP	nicotinic acid adenine dinucleotide
NAD	nicotinamide adenine dinucleotide
NADP	nicotinamide adenine dinucleotide phosphate
NET	neutrophil extracellular traps
NFAT	nuclear factor of activated T-cells
NFAT	nuclear factor of an activated T cell
NF-κB	nuclear factor κB
NK	natural killer
NUDT9H	nudix hydrolase 9 homologous domain
NUR77	nuclear receptor 4A1 also called NUR77
ORAI1	calcium release-activated calcium channel protein 1
OVA	ovalbumin
OVA	ovalbumin
$OVA_{257-264}$	SIINFEKL
P2X	purinergic ionotropic receptor
***P2x4*$^{-/-}$**	P2X4 deficient
***P2x7*$^{-/-}$**	P2X7 deficient
P2X7-nb	P2X7 inhibiting nanobody
P. aerugenosa	*Pseudomonas aerugenosa*
PAMP	pathogen-associated molecular patterns
PANX1	pannexin 1
PARP	poly (ADP-ribose) polymerase
PCA	principal components analysis
PI3K	phosphatidylinositol 3-kinase
PI3K	phosphoinositide 3-kinases
PIK3IP1	phosphoinositide-3-kinase-interacting protein 1
PIP2	phosphatidylinositol 4,5-bisphosphate
PIP2	phosphatidylinositol 4,5-bisphosphate
PKCθ	protein kinase C θ

PLCγ1	phospholipase Cγ1
PMCA	plasma membrane Ca^{2+} ATPase
PMCA1	plasma membrane Ca^{2+} ATPase 1
PTGS2	prostaglandin G/H synthase 2
***Rag1*$^{-/-}$**	RAG1-deficient
RAP1b	Ras-related protein Rap-1b
RORγt	retinoic acid receptor-related orphan receptor-γt
ROS	reactive oxygen species
RYR	ryanodine receptors
RYR1	type 1 ryanodine receptor
SERCA	sarcoplasmic/ER Ca^{2+} ATPases
SIRT	sirtuin
SOCE	store operated Ca^{2+} entry
SPN	sialophorin
STIM1	stromal interaction molecule 1
STIM2	stromal interaction molecule 2
T-bet	T-box transcription factor TBX21
TCF1	T cell factor 1
TCR	T cell receptor
T_{FH}	T follicular helper
TLR	toll-like receptor
TNFα	tumor necrosis factor α
TPC	two pore segment channel
T_{reg}	T regulatory
TRPM	transient receptor potential cation channel subfamily M
***Trpm2*$^{-/-}$**	TRPM2-deficient
TXNIP	thioredoxin-interacting protein
UMAP	uniform manifold approximation and projection
VAV1	proto-oncogene vav 1
WT	wild type
ZAP70	zeta-chain-associated protein kinase 70
ZEB	zinc finger E-box-binding homeobox
ZEB2	zinc finger E-box-binding homeobox 2

Abstract

Stimulation of the T cell receptor with specific antigen leads to Ca^{2+} signaling in T cells which is essential for their function. Cyclic ADP ribose hydrolase (CD38), transient receptor potential cation channel subfamily M (TRPM) 2, purinergic ionotropic receptor (P2X) 4 and P2X7 are modulators of Ca^{2+} signaling which we hypothesized to be involved in activation and differentiation of T cells. We used CD38-deficient mice to investigate the role of CD38 in $CD8^+$ T cells *in vivo* in *Listeria monocytogenes* infection models. In competitive T cell transfer experiments, *Cd38*$^{-/-}$ $CD8^+$ T cells showed a disadvantage compared to wild type $CD8^+$ T cells. The $CD8^+$ T cell response to *Listeria monocytogenes* infection however, was not altered in *Cd38*$^{-/-}$ mice and we could not detect an altered phenotype of *Cd38*$^{-/-}$ $CD8^+$ T cells. We could detect differentially expressed genes associated with an effector rather than memory state of *Cd38*$^{-/-}$ $CD8^+$ T cells compared to wild type $CD8^+$ T cells. In the publication "TRPM2 is not required for T cell function and differentiation" [Lory et al., 2022] we investigated the function of TRPM2 in T cells . We utilized *in vitro* T cell receptor stimulation, *Listeria monocytogenes* infection of TRPM2-deficient (*Trpm2*$^{-/-}$) mice and competitive T cell transfers which revealed TRPM2 does not affect $CD8^+$ T cell function. We investigated the function of the purinergic ionotropic receptors P2X4 and P2X7 in $CD4^+$ T cells *in vitro*. P2X4 deficient $CD4^+$ T cells did not show an altered response to T cell receptor stimulation after 16 hours and in a proliferation assay. P2X7 deficient $CD4^+$ T cells however showed reduced proliferation and reduced expression of the immediate early activation marker NUR77 after stimulation. The results are part of the publication "P2X4 and P2X7 are essential players in basal T cell activity and Ca^{2+} signaling milliseconds after T cell activation" by Brock et al. [Brock et al., 2022] which focuses on the role of P2X4 and P2X7 in the formation of early localized Ca^{2+} microdomains. In conclusion, our results show that CD38 may be involved in the proliferation or survival of $CD8^+$ T cells and development of memory T cells, P2X7 is important for activation and proliferation of $CD4^+$ T cells and that TRPM2 is not required for $CD8^+$ T cell function.

German abstract

Stimulation des T-Zell-Rezeptors durch ein spezifisches Antigen führt zu einer Ca^{2+}-Signalkaskade in T-Zellen, die für die Funktion von T-Zellen wesentlich ist. CD38, TRPM2, P2X4 und P2X7 sind Modulatoren der Ca^{2+}-Signale, von denen wir annehmen, dass sie an der Aktivierung und Differenzierung von T-Zellen beteiligt sind. Wir haben die Rolle von CD38 in $CD8^+$ T-Zellen *in vivo* in *Listeria monocytogenes* (*L. monocytogenes*) -Infektionsmodellen in CD38-defizienten Mäusen untersucht. Kompetitive T-Zell Transferexperimente zeigten, dass CD38-defiziente $CD8^+$ T-Zellen im Vergleich zu Wildtyp $CD8^+$ T-Zellen im Nachteil sind. Die Immunantwort der $CD8^+$ T-Zellen auf eine Infektion mit *L. monocytogenes* war bei CD38-defizienten Mäusen jedoch nicht verändert, und wir konnten keinen veränderten Phänotyp von CD38-defizienten $CD8^+$ T-Zellen feststellen. Wir konnten differentiell exprimierte Gene nachweisen, die eher mit einem Effektoren- als mit einem Gedächtniszell- Zustand von CD38-defizienten $CD8^+$ T-Zellen im Vergleich zu Wildtyp $CD8^+$ T-Zellen assoziiert werden. In der Veröffentlichung "TRPM2 is not required for T cell function and differentiation" [Lory et al., 2022] untersuchten wir die Funktion von TRPM2 in T-Zellen. Wir nutzten *in vitro* T-Zell-Rezeptor-Stimulation, *L. monocytogenes*-Infektion von TRPM2-defizienten Mäusen und kompetitive T-Zell-Transfers, die zeigten, dass TRPM2 für die Funktion von $CD8^+$ T-Zellen nicht notwendig ist. Wir untersuchten die Funktion von P2X4 und P2X7 in $CD4^+$ T-Zellen *in vitro*: P2X4-defiziente $CD4^+$ T-Zellen zeigten nach 16 Stunden Stimulation und in einem Proliferationsassay keine veränderte Reaktion auf die Stimulation des T-Zell-Rezeptors. P2X7-defiziente $CD4^+$ T-Zellen zeigten dagegen eine verminderte Proliferation und verringerte Expression des frühen Aktivierungsmarkers NUR77 nach der Stimulation. Die Ergebnisse sind Teil der Publikation "P2X4 and P2X7 are essential players in basal T cell activity and Ca^{2+} signaling milliseconds after T cell activation" von Brock et al. [Brock et al., 2022], die sich mit der Rolle von P2X4 und P2X7 bei der Bildung von frühen lokalisierten Ca^{2+}-Mikrodomänen befasst. Zusammenfassend zeigen unsere Ergebnisse, dass CD38 an der Proliferation oder dem Überleben von $CD8^+$ T-Zellen und möglicherweise der Entwicklung von Gedächtnis-T-Zellen beteiligt ist, dass P2X7 für die Aktivierung und Proliferation von $CD4^+$ T-Zellen wichtig ist und, dass TRPM2 nicht für die Funktion von $CD8^+$ T-Zellen erforderlich ist.

1 | Introduction

1.1 The innate and adaptive immune system

Pathogens that enter the body encounter several defense mechanisms. As a first level of defense, the epithelial layers, skin and mucosal tissues, hinder the entrance of pathogens into the body by forming physical barriers. Secondly, invading pathogens are targeted by cells of the innate immune system which recognize conserved molecular motives called pathogen-associated molecular patterns (PAMP). The cells of the innate immune system derive from the myeloid lineage and include neutrophils, eosinophils basophils, monocytes, mast cells, natural killer (NK) cells and macrophages as well as their progenitors.

These cells perform several functions that are crucial to limit the spread of pathogens: Phagocytes engulf and dispose of pathogenic cells and debris. Antigen presenting cells, in particular dendritic cells, process foreign antigens, transport them to lymphoid organs and present them to cells of the adaptive immune system, thereby initiating the activation of antigen-specific cells. Furthermore, the production of cytokines at the site of infection leads to recruitment of adaptive immune cells and enhances the immune response. Another aspect of innate immunity is the complement system which consists of a number of small proteins that circulate in the blood. Upon activation, these proteins form cylindrical membrane attack complexes that undermine the membrane integrity of pathogenic cells.

The innate immune system provides a rapid response to pathogens entering the body but it is less effective in removing pathogens than the specific response mounted by adaptive immune cells. While the innate response starts within the first minutes to hours of an infection, the adaptive response only becomes effecitve after four to five days. [Murphy and Weaver, 2016]

The adaptive immune system primarily consists of B cells and T cells which carry antigen-specific receptors. These receptors are generated in a process of V(D)J recombination, creating an

extensive repertoire of receptors that can recognize a large number of epitopes which potentially can be derived from pathogens. T cells originate from common lymphoid progenitor cells in the bone marrow. After migrating to the thymus, they rearrange their T cell receptor (TCR) genes. T cells with a functional T cell receptor (TCR) subsequently undergo a process of positive selection to determine their ability to bind major histocompatibility complex (MHC) molecules. This process is followed by a negative selection, to ensure that the TCR does not recognize self-antigen. In the thymus, the conventional T cell subpopulations $CD4^+$ T cells and $CD8^+$ T cells are formed and migrate to secondary lymphoid organs. [Murphy and Weaver, 2016]

T cells residing in secondary lymphoid tissues are activated by dendritic cells, which migrate from sites of infection to lymphoid tissues. There, naïve T cells recognize the presented antigen and start to proliferate and differentiate to aquire specific effector functions, depending on their lineage. The clonal expansion of T cells which carry a specific TCR for antigens derived from the invading pathogen marks the start of the adaptive immune response. $CD4^+$ T cells can then further differentiate into T helper cell subsets, such as T_H1, T_H2, T follicular helper (T_{FH}), T_H17 and T regulatory (T_{reg}) cells with distinct functions. [Chatzileontiadou et al., 2021]

Following activation, $CD8^+$ T cells mature to cytotoxic T cells which are characterized by their ability to kill infected cells and to produce tumor necrosis factor α (TNFα) and interferon γ (IFNγ).

The high numbers of effector T cells that are generated during an immune response are not sustained after infection, most effector T cells go into apoptosis after the infection is cleared. A small percentage of the expanded T cell clones, however, differentiates into memory T cells which can be re-activated upon re-encounter of their specific antigen. [Murphy and Weaver, 2016]

1.2 T cell activation and TCR dependent Ca^{2+} signaling

Stimulation of the TCR activates several signaling cascades that are important in activating a resting T cell. Here, I will focus on the Ca^{2+} signaling in T cell activation and only touch on co-receptor signaling through the glycoprotein CD28 and cytokine interactions.

The TCR of conventional T cells is formed by a heterodimer of an α- and β subunit which are connected by a disulfide bridge. The α- and β subunit are membrane anchored glycoproteins with an extracellular receptor domain. Stimulation of the extracellular domain of the TCR evokes intracellular signaling through CD3 proteins, a protein complex associated with the TCR. The CD3 complex consists of six subunits, the CD3γ chain, CD3δ chain and two CD3ϵ chains connected

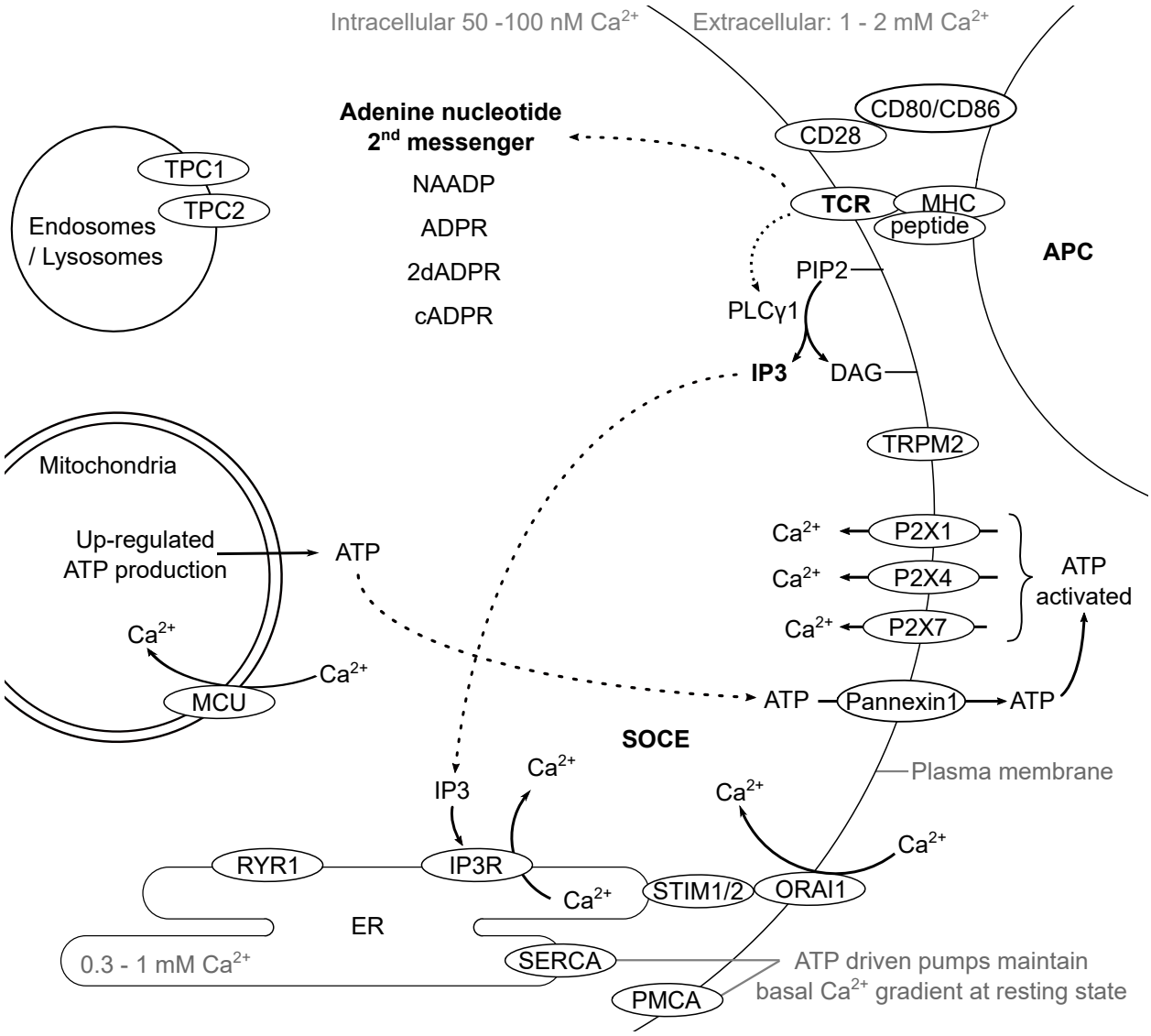

Figure I.1: **TCR stimulation and Ca^{2+} signaling in T cells** The very first events after TCR stimulation are Ca^{2+} microdomains which are evoked by the generation of adenine nucleotide 2nd messengers. Following these Ca^{2+} microdomains, generation of IP3 by PLCγ1 leads to accelerated Ca^{2+} efflux from the ER through IP3R. Ca^{2+} efflux from the ER activates STIM1 and STIM2 which then engage ORAI1 in the plasma membrane and induce further Ca^{2+} entry into the cell (SOCE). The increased Ca^{2+} concentration causes uptake of Ca^{2+} through the MCU into the mitochondria, resulting in increased ATP production. ATP is released from the cell through pannexin 1 and activates P2RX channels. Increased cytosolic Ca^{2+} concentration results in the activation of NFAT and other factors important for T cell activation (For reasons of space not included in this schematic).

with two CD3 chains called CD3ζ. TCR signaling is initiated by the recognition of antigen that is presented by MHC I or MHC II molecules on presenting cells. In addition to the T cell receptor, the co-receptor proteins CD4 or CD8 (comprised of CD8α and CD8β) interact with the MHC proteins at the immune synapse. CD4 and CD8 bind to different MHC classes and define different roles of the $CD4^+$ and $CD8^+$ T cell populations: Whereas CD4 recognizes MHC II, found mostly on professional antigen presenting cells (APC)'s, such as B cells, activated macrophages and activated dendritic cells, CD8 binds MHC I, found on all nucleated somatic cells. Antigen processing in APC results in the presentation of intracellular pathogen fragments through MHC I and presentation of extracellular pathogen-derived antigen after endocytosis of the exogenous antigen / pathogen on MHC II. [Murphy and Weaver, 2016, Gaud et al., 2018]

When the TCR complex binds to MHC molecules carrying its specific antigen, a phosphorylation cascade ensues, starting with the recruitment of lymphocyte-specific protein tyrosine kinase (LCK) associated with a CD4 or CD8 co-receptor. Subsequently, intracellular motifs of CD3, immunoreceptor tyrosine-based activation motifs (ITAMs), are phosphorylated by LCK, allowing zeta-chain-associated protein kinase 70 (ZAP70) to bind to CD3ζ and also ZAP70 itself to be phosphorylated by LCK. ZAP70 phosphorylates growth factor receptor-bound protein 2 (GRB2), which recruits proto-oncogene vav 1 (VAV1) to the linker for activation of T cells (LAT). LAT is a membrane anchored platform for several proteins important in T cell activation. While ZAP70 recruits VAV1, LCK phosphorylates VAV1 to activate it. VAV1 activates c-Jun N-terminal kinase (JNK) mitogen-activated protein kinase (MAPK) and p38 MAPK pathways which lead to the activation of the transcription factors c-Jun (JUN) and c-Fos (FOS) and to actin polymerization needed for cell motility. [Gaud et al., 2018] An additional target of LCK is the kinase tyrosine-protein kinase ITK also known as interleukin-2-inducible T-cell kinase (ITK) which phosphorylates and activates phospholipase Cγ1 (PLCγ1) bound to LAT. This allows PLCγ1 to cleave phosphatidylinositol 4,5-bisphosphate (PIP2) at the membrane, leading to the release of two second messenger molecules: Soluble inositol 1,4,5-trisphosphate (IP3) and membrane anchored diacylglycerol (DAG). DAG activates the protein kinase C θ (PKCθ) which in turn activates the transcription factors nuclear factor κB (NF-κB) and activator protein 1 (AP-1) [Gaud et al., 2018].

The production of IP3 leads to an extensive Ca^{2+} signaling cascade: At the resting state, an extracellular Ca^{2+} concentration of 1-2 mM opposed to 50-100 nM in the cell is maintained by plasma membrane Ca^{2+} ATPases (PMCAs). The resting Ca^{2+} concentration in the endoplasmic reticulum (ER) ranges from 300 μM to 1 mM. [Trebak and Kinet, 2019] IP3 opens the ligand-

gated IP3 receptor (IP3R) channels in the ER membrane, inducing an efflux of Ca^{2+} from the ER lumen into the cytosol. The membrane potential in the "resting" state of T cells is maintained by sarcoplasmic/ER Ca^{2+} ATPases (SERCA), in particular SERCA2B and SERCA3, which actively pump Ca^{2+} into the ER using adenosine triphosphate (ATP) [Trebak and Kinet, 2019]. An efflux of Ca^{2+} from the ER triggers stromal interaction molecule 1 (STIM1) and stromal interaction molecule 2 (STIM2) in the ER membrane which sense the decreased Ca^{2+} concentration and activate calcium release-activated calcium channel protein 1 (ORAI1) channels in the plasma membrane. The activation of ORAI1 Ca^{2+} channels leads to a substantial Ca^{2+} influx to the cell. This mechanism is called store operated Ca^{2+} entry (SOCE). The interaction of STIM1 and STIM2 with ORAI1 channels occurs likely at ER-plasma membrane junctions. [Wolf et al., 2015, Diercks et al., 2018]

The increased Ca^{2+} concentration after IP3R opening and SOCE leads to the binding of Ca^{2+} to calmodulin (CaM) and its activation. [Trebak and Kinet, 2019] Ca^{2+}-calmodulin activates isoforms of the nuclear factor of an activated T cell (NFAT) transcription factors which triggers activation and differentiation of T cells through transcriptional regulation. [Trebak and Kinet, 2019] In addition, the increase of Ca^{2+} in the cytosol through IP3R and plasma membrane channels is extended to mitochondria. Ca^{2+} enters mitochondria through mitochondrial Ca^{2+} uniporter (MCU). An increase in Ca^{2+} concentration in the mitochondria leads to an increased ATP production which causes further signaling through pannexin 1 and P2X channels and prepares T cells for proliferation and cytokine production. [Trebak and Kinet, 2019] Calcium influx into the cytosol through SOCE is counteracted by TRPM4, which depolarizes the plasma membrane upon sensing of Ca^{2+} by allowing an influx of Na^{+} [Vig and Kinet, 2009, Launay et al., 2002, Launay et al., 2004].

Besides the production of DAG and IP3, additional 2^{nd} messenger molecules are generated upon TCR stimulation. Early events after TCR-stimulation include the formation of cyclic ADP-ribose (cADPR) and nicotinic acid adenine dinucleotide (NAADP) which may act on TRPM2 and type 1 ryanodine receptor (RYR1) or two pore segment channels (TPCs). These second messenger mediated events will be discussed in the next section. [Guse et al., 1999, Guse and Wolf, 2016, Roggenkamp et al., 2021, Gunaratne et al., 2021]

1.3 Adenine nucleotide 2^{nd} messengers and Ca^{2+} signaling

Within milliseconds of TCR stimulation, temporally and spatially restricted Ca^{2+} microdomains are formed [Wolf et al., 2015, Diercks et al., 2018]. This occurs before IP3-IP3R signaling and

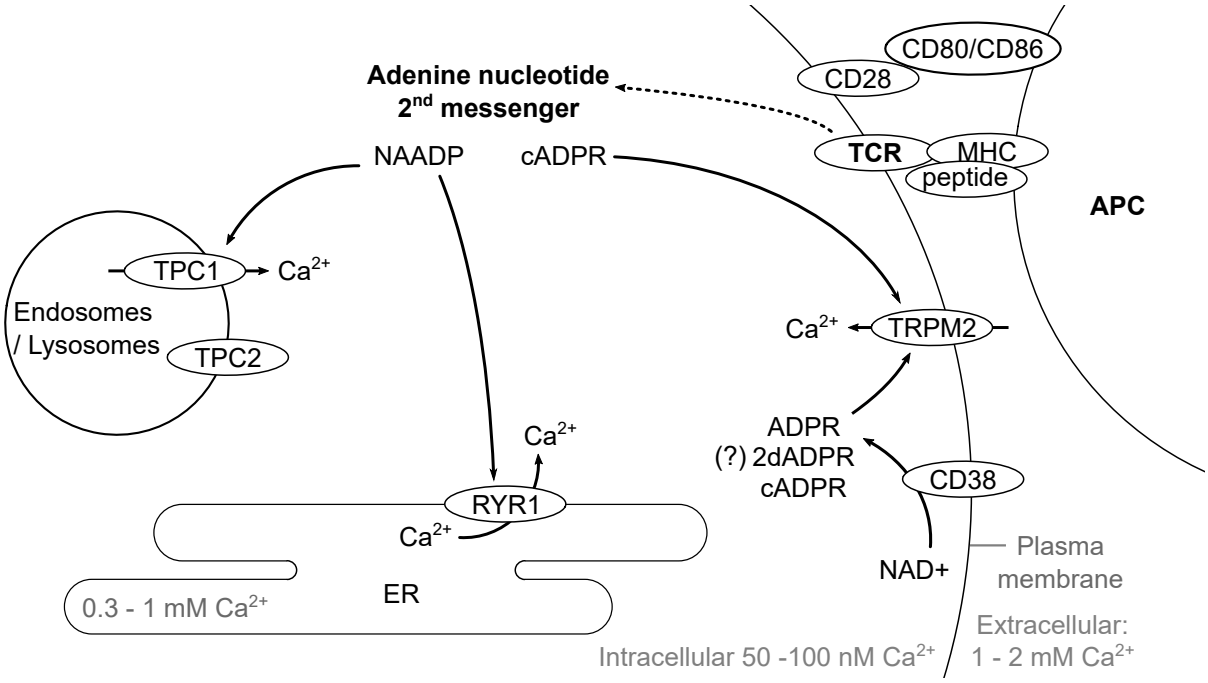

Figure I.2: **Adenine nucleotide 2nd messengers and Ca^{2+} signaling** NAADP, ADPR and cADPR 2dADPR are formed rapidly after TCR stimulation. NAADP was shown to interact with a binding protein HN1L/JPT2. The complex colocalizes with RYR1 channels at the ER and co-immunoprecipitate with the TPC1 channel which localize to endosomes / lysosomes. NAADP, ADPR, 2dADPR and cADPR open TRPM2 in the plasma membrane, with potential influence on the Ca^{2+} signaling in T cells.

SOCE build up an increase of global Ca^{2+} concentration. These Ca^{2+} microdomains are evoked by NAADP, which is formed rapidly after TCR stimulation, NAADP binds to hematological and neurological expressed 1-like protein/ jupiter microtubule associated homolog 2 (HN1L/JPT2) and this complex interacts with and activates RYR1 [Gerasimenko et al., 2003, Yamasaki et al., 2005, Gasser et al., 2006, Roggenkamp et al., 2021, Dammermann et al., 2009]. Besides ryanodine receptors (RYR)1 the NAADP-HN1L/JPT2 complex was shown to activate TPC1 [Davis et al., 2012, Gunaratne et al., 2021]. Silencing the HN1L/JPT2 gene in Jurkat T cells not only decreased Ca^{2+} microdomain frequency but lead to decreased global calcium signaling [Roggenkamp et al., 2021]. Further, NAADP was shown to activate TRPM2 in the plasma membrane. However, TRPM2 was found not to be crucial for the formation of Ca^{2+} microdomains [Beck et al., 2006].

A further 2^{nd} messenger which is formed after TCR stimulation is cADPR. Upon TCR ligation and cADPR-levels are increased over a sustained period of time [Guse et al., 1999]. The adenine 2^{nd} messenger cADPR opens RYR3 in the ER and was shown to activate TRPM2 channels in the plasma membrane. However, this result it is controversial. [Beck et al., 2006, Fliegert et al., 2020]

Two other adenine nucleotide 2^{nd} messengers, adenosine diphosphate ribose (ADPR) and 2-deoxy-ADPR (2dADPR), which may be produced by the multi-functional enzyme CD38 act on TRPM2 and could play a role in the activation and differentiation of T cells [Fliegert et al., 2020, Fliegert et al., 2017].

Table 1.1: Adenine nucleotides and Ca^{2+} channels

Name	permeability	location	ligands
TRPM2	Ca^{2+} Na^{+}, K^{+}	Plasma membrane, lysosome	ADPR, 2dADPR, H_2O_2, (cADPR, NAADP)
P2X4	Ca^{2+} Na^{+}	Lysosomes, cell membrane	ATP
P2X7	Ca^{2+} Na^{+}	Cell membrane	ATP
RYR1	Ca^{2+}	ER	NAADP
TPC1*	Ca^{2+}	Endosomes, lysosomes	NAADP
	Na^{+}		PI(3,5)P2**
TPC2*	Ca^{2+}	Endosomes, lysosomes	NAADP
	Na^{+}		PI(3,5)P2

*Ion selective permeability is dependent on the activating ligand; **Voltage dependent

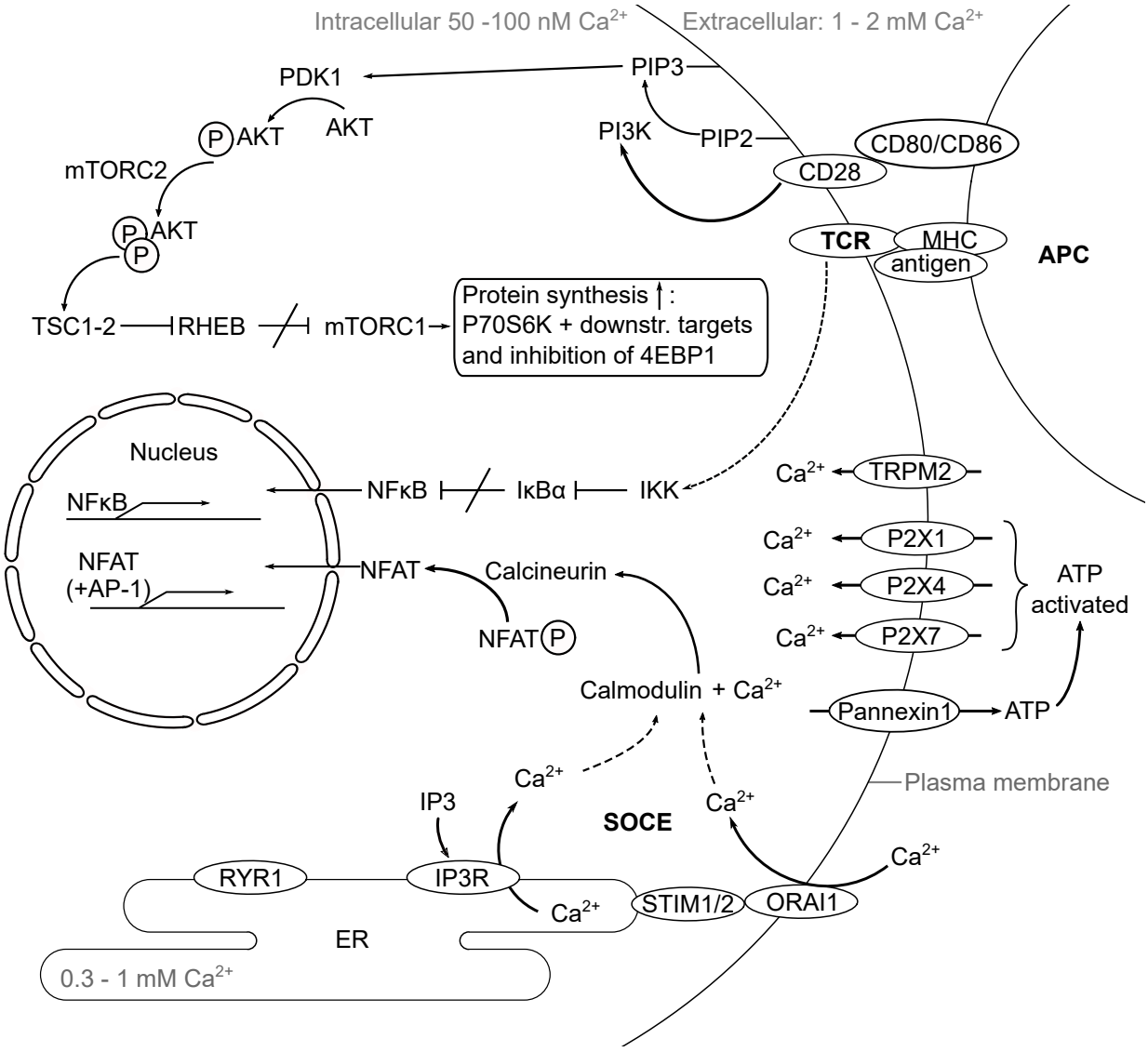

Figure I.3: **TCR stimulation: NFAT and mTOR signaling** TCR activation and subsequent calcium influx lead to the translocation of NFAT through the activation of calcineurin by Ca^{2+}-calmodulin. The co-receptor CD28, engaged by CD80 or CD86, activates PI3K, which phosphorylates PIP2 into PIP3. PIP3 activates PDK1 which phosphorylates AKT, phosphorylated AKT is recognized by the mTORC2 and further phosphorylated. The activated AKT now in turn activates TSC1-2 which inhibits RHEB, the inhibitor of mTORC1. mTORC1 activity leads to the activation of translation initiating factors and increased protein synthesis in the cell. IKK is activated in the p62-Bcl10-Malt1-IKK clusters or signalosomes formed upon TCR stimulation and phosphorylation of the IκBα inhibitor of NFκB leads to NFκB translocation to the nucleus where it functions as a potent transcription factor.

1.4 Metabolic reprogramming: NFAT and PI3K/AKT/mTOR signaling

T cells undergo a substantial change in metabolic activity and pass checkpoints to enter the cell cycle to expand when their specific antigen is presented to them. Increased cytosolic Ca^{2+} concentration after TCR stimulation leads to translocation and consequently activation of NFAT transcription factor isoforms. Cytosolic Ca^{2+} binds to calmodulin, forming a calmodulin-Ca^{2+} complex which activates the serine/threonine phosphatase calcineurin. Calcineurin in turn dephosphorylates NFAT, which is translocated to the nucleus and drives transcription through formation of a complex with AP-1. This is the case in all T cell subsets except in T_{reg} cells where forkhead box protein P3 (FoxP3) inhibits AP-1 transcription activity. [Lee et al., 2008, Sumpter et al., 2008, Hogan, 2017] The NFAT-AP-1 complex causes transcription of lineage-determining transcription factors of T cell subsets such as T-box transcription factor TBX21 (T-bet) in T_H1 cells, retinoic acid receptor-related orphan receptor-γt (RORγt) in T_H17 cells and the production of cytokines such as interleukin (IL)-2 and IFNγ in $CD8^+$ T cells. The interaction of NFAT with lineage specific transcription factors shapes the cytokine composition and surface receptor expression of activated T cells. [Klein-Hessling et al., 2017, Lee et al., 2018] NFAT is not only for important for differentiation of T cells but also for effector functions: The NFAT isotype NFATc1 is necessary for cytotoxicity of $CD62L^{low}$ $CD44^{high}$ $CD8^+$ effector T cells and NFATc1 deficiency causes altered expression of a large number of genes in activated $CD8^+$ effector T cells including most genes involved in glycolysis [Klein-Hessling et al., 2017].

Besides NFAT regulation, signaling through phosphoinositide 3-kinases (PI3K), RAC-alpha serine/threonine-protein kinase, also called protein kinase B (AKT) and mammalian target of rapamycin / mechanistic target of rapamycin (mTOR) is another vital pathway in T cell activation that regulates cell growth and energy metabolism [Shyer et al., 2020]. Proliferation is dependent on this pathway as mTOR was shown to be necessary for entry into the cell cycle [Shyer et al., 2020, Shi et al., 2011, Finlay et al., 2012, Doedens et al., 2013, Zeng et al., 2016]. It was shown, that SOCE activates mTOR signaling in quiescent T cells after TCR stimulation [Vaeth et al., 2017] but it is activated predominantly through the co-receptor CD28 which is the main driver of glucose transporter 1 (Glut1) up-regulation [Frauwirth et al., 2002, Shyer et al., 2020]. Downstream of CD28, PI3K phosphorylates AKT which in turn activates mTOR. Signaling through mTOR drives glucose uptake and glycolysis and in tandem with TCR signaling activates the proto-oncogene pro-

tein MYC, a transcription factor with crucial role in the metabolic switch [Shyer et al., 2020]. A potent transcription factor, NF-κB, is translocated into the nucleus through activation of inhibitor of nuclear factor κ-B kinase (IKK) by the p62-Bcl10-Malt1-IKK signalosome [Paul et al., 2014].

By activating the NFAT, NF-κB and mTOR pathways through TCR stimulation and engagement of the CD28 co-receptor, T cells undergo a substantial change in energy metabolism and cell cycle regulation as well as transcriptional regulation [Shyer et al., 2020, Vaeth et al., 2017]. Naïve T cells, which did not encounter antigenic stimulation after development, show a low/basal glycolytic rate and nutrient uptake, while they rely on oxidative phosphorylation or fatty acid oxidation for their energy needs [Pearce et al., 2013]. Trough TCR stimulation and SOCE signaling, T cells up-regulate glucose and amino acid transporters and nutrient uptake. T cells then switch to aerobic glycolysis, which allows them to proliferate and mount an appropriate immune response. [Frauwirth et al., 2002, Carr et al., 2010, Sinclair et al., 2013, Pearce et al., 2013]

1.5 CD38

The multi-functional ecto-enzyme CD38 is expressed in cells of the innate and adaptive immune system, including B cells, neutrophils, monocytes, NK cells and several T cell subsets as well as a wide variety of tissues which are not part of the immune system [Malavasi et al., 1992,Malavasi et al., 2008]. CD38 catalyzes the reaction from nicotinamide adenine dinucleotide (NAD) to ADPR and cADPR and was originally thought to catalyze the conversion of nicotinamide adenine dinucleotide phosphate (NADP) to NAADP as well. This was however, demonstrated under acidic conditions in the presence of 30 mM nicotinic acid and 1 mM NAD at pH 5.5 [Aarhus et al., 1995]. It is not known whether these conditions are met in a living cell. A more likely course is the degradation of NAADP to 2-phospho adenosine diphosphoribose (ADPRP) by CD38 as described by Schmid et al. in 2011 in the Jurkat cell line and murine CD38 deficient ($Cd38^{-/-}$) cells [Schmid et al., 2011]. Recently, nicotinamide adenine dinucleotide phosphate oxidase (DUOX)1 and DUOX2 were identified as NAADP generating enzymes [Gu et al., 2021]. The major fraction of the cell membrane protein CD38 faces the extracellular space with its active site. A second, flipped orientation which results in the CD38's active site facing to the cytosol, was discovered in 2012 for a smaller portion of CD38 protein in the cell [Zhao et al., 2012]. The inward facing orientation could allow CD38 to be involved in the calcium signaling after TCR stimulation [Da Silva et al., 1998].

CD38 could modulate calcium signaling during TCR stimulation and subsequent T cell activation

by generation of NAADP in lysosomes, which then could activate RYR1 or TPC channels. A second way of modulation of calcium signaling by CD38 could be CD38 mediated generation of ADPR and/or 2dADPR which activates TRPM2 in the plasma membrane [Fliegert et al., 2017].

CD38 is essential for the innate immune response to *Listeria monocytogenes* infection in mice. It has been shown to be expressed on neutrophils, inflammatory monocytes and dendritic cells at the site of *Listeria monocytogenes* infection. Lischke et al. found that the bacterial burden of *L. monocytogenes* 60 hours after infection was significantly increased in *Cd38*$^{-/-}$ mice compared to wild type mice. The increased bacterial titers and increased mortality were accompanied by decreased frequencies of neutrophils and inflammatory monocytes in spleen and liver of infected *Cd38*$^{-/-}$ mice. The frequency of dendritic cells in spleen and liver however was not affected by CD38 deficiency as well as the response of $CD8^+$ T cells to primary infection. In secondary infection *Cd38*$^{-/-}$ mice did not show a defective response to *Listeria monocytogenes* infection, as demonstrated by bacterial titers, indicating that CD38 deficiency does not affect the effectiveness of the memory T cell response in this assay. [Lischke et al., 2013] Infection with *Mycobacterium avium* showed a different course of bacterial burden. At day one after infection Viegas et al. found decreased titers in *Cd38*$^{-/-}$ mice compared to wild type mice. At day 30 the bacterial titers were found to be the same as in wild type mice while they finally were found to be increased in *Cd38*$^{-/-}$ mice at day 45 after infection compared to wild type mice. Through *in vitro* stimulation of spleen cells with sonicated *Mycobacterium avium* bacteria, a decrease in IFNγ production was measured for *Cd38*$^{-/-}$ spleen cells. [Viegas et al., 2007] A third infection model, utilizing *Streptococcus pneumoniae*, was applied to *Cd38*$^{-/-}$ mice by Partida-Sánchez et al.. *Cd38*$^{-/-}$ mice showed an increased mortality compared to wild type mice in this model. As seen in *Listeria monocytogenes* infection, neutrophil infiltration at the site of infection was severely disturbed. The reason for the decreased neutrophil migration may be explained by the inability of *Cd38*$^{-/-}$ neutrophils to move directional towards N-Formylmethionyl-leucyl-phenylalanine (fMLP), a formylated peptide derived from bacteria which is sensed by the fMet-Leu-Phe receptor (FPR) on neutrophils. [Partida-Sanchez et al., 2001, Partida-Sánchez et al., 2004b] In addition to bacterial infections, the response of *Cd38*$^{-/-}$ mice to *Entamoeba histolytica* infection was studied by Estrada-Figueroa et al. in 2011. Similar to bacterial infection models, neutrophil infiltration at the site of infection - the liver - was decreased compared to wild type mice. mRNA analysis of tissue from liver abscesses showed delayed expression of cytokines and "inflammation mediators" TNFα, IL-1β, IL-6, prostaglandin G/H synthase 2 (PTGS2), IL-10 and colony stimulating factor 2 (CSF-2). [Estrada-Figueroa et al., 2011] Further, CD38 is induced

in macrophages and contributes to the secretion of pro-inflammatory cytokines IL-6 and IL-12p40 [Amici et al., 2018]. Partida-Sanchez et al. performed more extensive experiments on the migration of *Cd38*$^{-/-}$ dendritic cells. They reported a defective migration of *Cd38*$^{-/-}$ dendritic cells to lymph nodes and *Cd38*$^{-/-}$ precursor dendritic cells to sites of infection. Additionally they showed activation of T cells by *Cd38*$^{-/-}$ dendritic cells was less effective in transfer assays with wild type T cells and *Cd38*$^{-/-}$ dendritic cells. [Partida-Sánchez et al., 2004a] NK cells showed enhanced cytotoxicity and increased production of TNFα, IFNγ and N-α-benzyloxycarbonyl-L-lysine thiobenzyl ester (BLT) thioesterase when stimulated with anti-CD38 cross-linking antibodies [Sconocchia et al., 1999].

CD38 was further reported to function as an adhesion molecule on lymphocytes, interacting with CD31 in endothelial cells [López-Cortés et al., 2021, Deaglio et al., 1998].

In T cells, CD38 was first identified as an activation marker, initially termed "T10" [Bhan et al., 1980]. A CD4$^+$ T cell sub-population of CD45RB$^{\text{low}}$ CD38$^+$ CD4$^+$ T cells was demonstrated to have an inhibiting effect on proliferation and activation of T cells [Read et al., 1998, Martins and Aguas, 1999]. Bahri et al. demonstrated the suppressing capacity of CD8$^+$ CD38$^{\text{high}}$ T cells which were cultivated with the addition of IL-15. In *in vitro* assays they showed a suppressive effect on proliferation of CD4$^+$ T cells which requires IFNγ and cell to cell contact. [Bahri et al., 2012]

The catalytic activity of CD38 reduces NAD levels outside of the cell. Reduced NAD levels subsequently decrease ADP-ribosyltransferase 2 (ART2) mediated apoptosis. Chen et al. showed increased T cell death of *Cd38*$^{-/-}$ cells in NAD killing assays and an increased sensitivity of *Cd38*$^{-/-}$ CD4$^+$ CD25$^+$ T$_{\text{reg}}$ cells *in vitro*. They further showed increased ART2-dependent susceptibility of *Cd38*$^{-/-}$ NOD mice in an autoimmune diabetes model. [Chen et al., 2006] Further, the conversion of NAD to ADPR by CD38 was shown to be important for the suppressive function of CD4$^+$ and CD8$^+$ regulatory T cells in *in vitro* experiments. Fedele et al. describe that the produced ADPR is converted by CD203a into AMP, which is then converted into adenosine by CD73. They demonstrated that suppression conferred by T$_{\text{reg}}$ cells in a mixed lymphocyte reaction assay correlated with adenosine generation. [Fedele et al., 2015]

The suppressive capability of CD38$^+$ CD4$^+$ T$_{\text{reg}}$ cells was confirmed by Patton et al. in *in vitro* CD4$^+$ T cell proliferation assays [Patton et al., 2011]. In patient studies of the anti-CD38 antibody Daratumumab, which is used to deplete CD38$^+$ cells in multiple myeloma patients, the number of CD4$^+$ T helper cells and CD8$^+$ T cells were found to be increased, which may be caused by the depletion of CD38$^+$ T$_{\text{reg}}$ cells [Morandi et al., 2019, McMahon and Luger, 2019, Syed, 2019, Krejcik et al., 2016]. Muñoz et al. reported that CD38 clusters at the contact zone of T cells and antigen

presenting cells in an LCK-dependent manner. [Muñoz et al., 2008] Katsuyama et al. showed that over-expression of CD38 in $CD8^+$ T cells reduced degranulation. They further claimed that CD38 reduces NAD levels in the cell which causes decreased EOMES, RUNX3, and T-bet expression through a signaling cascade involving sirtuin (SIRT) 1. [Katsuyama et al., 2020]

We investigated the $CD8^+$ T cell response to *Listeria monocytogenes* infection in *Cd38*$^{-/-}$ mice to shed light on a possible function of the multi-functional protein in T cells.

[Chakraborty and Mehrotra, 2020]

1.6 TRPM2

The central protein we investigated in the publication "TRPM2 Is Not Required for T-Cell Activation and Differentiation", TRPM2 has been shown to be involved in $CD4^+$ T cell activation. [Melzer et al., 2012]

The nonselective voltage independent cation channel TRPM2 facilitates Na^+ and Ca^{2+} influx into the cell. TRPM2 is part of the transient receptor potential cation channels subfamily M which consists of eight members [Huang et al., 2020]. Except TRPM4 and TRPM5 the TRPM members are calcium permeable channels mediating Ca^{2+} influx into the cell, while TRPM4 and TRPM5 are activated by Ca^{2+} [Launay et al., 2002, Hofmann et al., 2003]. The TRPM2 channel is found in monocytes [Yamamoto et al., 2008,Shimizu et al., 2015], macrophages [Kashio et al., 2012,Zou et al., 2013, Yao et al., 2016], neutrophils [Wehage et al., 2002, Partida-Sanchez et al., 2007, Lange et al., 2008], dendritic cells [Sumoza-Toledo et al., 2011] and effector T cells [Melzer et al., 2012]. [Fliegert et al., 2020] In myeloid cells, it is involved in oxidative stress response, phagosome maturation and migration [Partida-Sanchez et al., 2007,Sumoza-Toledo et al., 2011,Knowles et al., 2013,Wang et al., 2016, Beceiro et al., 2017, Di et al., 2017, Morad et al., 2021].

NAADP, ADPR, 2dADPR and cADPR have been reported as activating ligands of TRPM2 [Beck et al., 2006, Knowles et al., 2013, Fliegert et al., 2020, Kolisek et al., 2005] Additionally, H_2O_2 is described as an activator of TRPM2, conferring susceptibility to cell death through sustained opening of the channel [Hara et al., 2002]. The role of NAADP as a TRPM2 agonist was only demonstrated using micromolar range concentrations of the molecule. TRPM2 activation by NAADP was enhanced when using it in tandem with cADPR. [Beck et al., 2006,Lange et al., 2008] However, TRPM2-activation by cADPR is controversial, due to potential contamination of commercially available cADPR preparations with ADPR [Beck et al., 2006,Fliegert et al., 2020, Heiner

et al., 2006]. In essence, TRPM2 was only reliably shown to be activated by the NAD derivatives ADPR and 2dADPR and by H_2OH_2. For adenine nucleotide 2nd messenger signaling, the essential part of the TRPM2 channel is the nudix hydrolase 9 homologous domain (NUDT9H) which is -like NUDT9- activated by ADPR and was also demonstrated to accept 2dADPR in the case of TRPM2 [Gattkowski et al., 2021].

A function of TRPM2 has been described for a variety of innate immune cells. *Trpm2*$^{-/-}$ mice infected with *Pseudomonas aerugenosa* (*P. aerugenosa*) showed increased mortality and bacteria persisting in the lung. Through confocal microscopy of human lung sections and patch clamp experiments with bone marrow derived macrophages (BMDM), TRPM2 was shown to locate to phagosomes of human alveolar macrophages and to be activated by ADPR and H_2O_2. Phagosome acidification in macrophages was demonstrated to be impaired in *Trpm2*$^{-/-}$ mice and resulted in defective killing of *P. aerugenosa*. [Di et al., 2017] In another study applying bacterial infection models, *Trpm2*$^{-/-}$ mice were investigated during *L. monocytogenes* infection. The effects of *L. monocytogenes* infection were found to be similar to *P. aerugenosa*. Knowles et al. reported an increased mortality from sublethal infection doses and increased bacterial burden in liver and spleen which were comparable in magnitude to the bacterial titer in IFNγR deficient mice. Further, they observed decreased IFNγ serum levels and IFNγ^+ NK cell- and CD8$^+$ T cell counts 24 hours post infection in *Trpm2*$^{-/-}$ mice. IFNγ levels however did not differ between wild type and *Trpm2*$^{-/-}$ NK cells and CD8$^+$ T cells in the respective IFNγ^+ subsets. [Knowles et al., 2011] Robledo-Avila et al. described increased TNFα, IL-6, IL-10, and C-C motif chemokine 2 (CCL2) serum levels at early time points of *L. monocytogenes* infection in *Trpm2*$^{-/-}$ mice. In contrast to Kowles et al. they did not observe a difference in IFNγ and IL-12 serum levels. Depletion of neutrophils via anti-Ly6G antibodies before infection caused necrotic areas in spleen and abscesses in the liver which were decreased in number in *Trpm2*$^{-/-}$ mice. When tested for their ability to kill bacteria, neutrophils deficient in TRPM2 were found more efficient than wild type neutrophils. Additionally, *Trpm2*$^{-/-}$ neutrophils showed increased degranulation and production of reactive oxygen species (ROS). [Robledo-Avila et al., 2020] While the ability to kill bacteria was found to be increased for neutrophils in *L. monocytogenes* infection, a similar study from Qian et al. using *Escherichia coli* (*E. coli*) infection showed decreased fMLP induced p38 MAPK phosphorylation and elastase release from neutrophils required to kill gram negative bacteria. The bacteria burden in *E. coli* infected *Trpm2*$^{-/-}$ mice was higher than in wild type mice similar to the results of *L. monocytogenes* infection studies. [Qian et al., 2018] Similar results were found by Tripathi et al.

who found *Trpm2*$^{-/-}$ neutrophils were defective in neutrophil extracellular traps (NET)-mediated killing of bacteria. Further they showed neutrophils NET-formation is disturbed in *Trpm2*$^{-/-}$ mice during *Klebsiella pneumoniae* (*K. pneumoniae*) infection. *K. pneumoniae* infection in parallel to *L. monocytogenes* and *E. coli* infection was found to cause increased mortality in *Trpm2*$^{-/-}$ mice which also showed increased bacterial burden. [Tripathi et al., 2018]

In contrast to bacterial infections, TRPM2-deficiency has been shown to be attenuating disease in autoimmune models and an ischemic stroke model: An ischemic stroke has a phase of initial hypoxia which causes cell death and is followed by sterile inflammation during which neutrophils and macrophages migrate to the site of the infarct. Infiltration of macrophages and neutrophils at infarct sites was significantly reduced in *Trpm2*$^{-/-}$ mice. *Trpm2*$^{-/-}$ mice showed decreased volume of infarcts in the brain as well as ameliorated neurological scores. The pharmacological inhibition of TRPM2 by administering 59 N- p-amylcinnamoyl anthranilic acid (ACA) was also demonstrated to be attenuating ischemic stroke. However, infiltration of NK cells $CD4^+$, $CD8^+$, and $\gamma\delta$ T cells in infarcts was not changed in *Trpm2*$^{-/-}$ mice. [Gelderblom et al., 2014] Infiltration of NK cells, $CD4^+$, $CD8^+$, and $\gamma\delta$ T cells in infarcts was not changed in *Trpm2*$^{-/-}$ mice. In a study on experimental lupus, Garcia-Rodriguez et al. demonstrated that *Trpm2*$^{-/-}$ monocytes, macrophages and neutrophils were less prone to pristane-induced apoptosis [Wolf et al., 2015]. Yamamoto et al. showed that TRPM2 is cruical for C-X-C motif chemokine 2 (CXCL2) and TNFα production, NF-κB translocation and extracellular signal-regulated kinases (ERK) signaling in monocytes. They further found *Trpm2*$^{-/-}$ mice to be protected in an ulcerative colitis model through decreased CXCL2, IFNγ and IL-12 levels and reduced numbers of neutrophils present at the site of inflammation. In this model, neutrophil migration was reduced but not macrophage infiltration. [Yamamoto et al., 2008] Melzer et al. could show that the TRPM2 channel is upregulated in $CD4^+$ T cells after anti-CD3/anti-CD28 stimulation. *Trpm2*$^{-/-}$ $CD4^+$ T cells showed decreased proliferation and production of IL-2, IFNγ and IL-17 in vitro. In the experimental autoimmune encephalomyelitis (EAE) model, *Trpm2*$^{-/-}$ mice were partially protected. *Trpm2*$^{-/-}$ mice showed less severe clinical scores compared to wild type mice. Further, they report reduced inflammation and demyelination of the spinal chord in *Trpm2*$^{-/-}$ mice and reduced inflammatory infiltrates in the EAE model. [Melzer et al., 2012] However, initial Ca^{2+} signals in *Trpm2*$^{-/-}$ $CD4^+$ T cells were not found to be different from wild type cells [Wolf et al., 2015].

1.7 Purinergic receptors P2X4 and P2X7

In the study on P2X receptors, "P2X4 and P2X7 are essential players in basal T cell activity and Ca^{2+} signaling milliseconds after T cell activation" we investigated the role of P2X4 and P2X7 in T cell activation.

The ATP-gated P2X channels P2X4 and P2X7 are part of a seven-member family of ATP-activated Na^{+} and Ca^{2+} conductive channels [Di Virgilio et al., 2018, Schenk et al., 2009, Burnstock and Boeynaems, 2014, Ruiz-Rodríguez et al., 2019]. P2X4 is located in lysosomal membranes, but translocated to the plasma membrane at the immune synapse upon TCR stimulation [Woehrle et al., 2010, Murrell-Lagnado and Frick, 2019, Kanellopoulos et al., 2021] while the P2X7 channel is located in the plasma membrane. Both P2X4 and P2X7 have been demonstrated to function in T cells, and modulating global Ca^{2+} signaling during T-cell activation [Grassi, 2020, Woehrle et al., 2010, Yip et al., 2009, Ledderose et al., 2014].

The activation of the two P2X channels is initiated by the IP3R mediated SOCE Ca^{2+} influx leading to Ca^{2+} uptake of mitochondria through MCU. Mitochondria then produce ATP which is exported to the extracellular space by pannexin 1 channels at the immune synapse [Woehrle et al., 2010]. This mechanism is thought to enhance weak TCR signaling to generate an unimpaired T-cell response by linking enhanced mitochondrial bioenergetics with Ca^{2+} signaling [Trebak and Kinet, 2019, Ledderose et al., 2014].

When overexpressing P2X7 in K562 and LG14 cell lines, Baricordi et al. showed increased proliferation when stimulating with ATP already in 1999 [Baricordi et al., 1999]. Woehrle et al. showed P2X4 and P2X7 are expressed in primary human $CD4^{+}$ T cells. P2X4 was shown to be contributing to NFAT activation and IL-2 expression together with P2X1. In addition to P2X1 and P2X4, pannexin 1 (PANX1) was found to be translocated to the immune synapse. [Woehrle et al., 2010] Yip et al. showed ATP release after TCR stimulation and found both P2X4 and P2X7 to be necessary for subsequent Ca^{2+} mobilization and IL-2 synthesis in the Jurkat human cell line. Through an NFAT-luciferase reporter assay, they showed increased activation of NFAT when overexpressing P2X7, while in the absence of P2X7, IL-2 production was reduced when stimulating mouse $CD4^{+}$ T cells with ATP. [Yip et al., 2009] Danquah et al. showed that the inhibition of the P2X7 channel with specific nanobodies ameliorated contact dermatitis and experimental glomerulonephritis and could block IL-1β release from human monocytes. [Danquah et al., 2016]

Schenk et al. reported that mice treated with oxidized ATP, which inhibits P2X channels, were

protected against colitis in adoptive T-cell transfer models. They found reduced IL-17 producing cell numbers and increased T_{reg} cell numbers in the colitis model. They concluded that the most likely cause for the protection in the colitis model was P2X7 inhibiting T_{reg} cell conversion to T_H17 cells. Further, T_{reg} cell function of P2X7 deficient mice was shown to be enhanced in suppression assays. [Schenk et al., 2011]. Finally, T cell migration and the activity and subcellular localization of mitochondria at the pseudopods facing movement direction were demonstrated to be dependent on the P2X4 receptor in Jurkat and primary human $CD4^+$ T cells [Ledderose et al., 2018].

We investigated the role of P2X4 and P2X7 in the activation and proliferation of $CD4^+$ T cells *in vitro*.

2 | Results

2.1 CD38 does not impact $CD8^+$ T cell function and phenotype in the acute response to *Listeria monocytogenes* infection but *Cd38*$^{-/-}$ $CD8^+$ T cells show a competitive disadvantage

We investigated the role of CD38 in the activation and differentiation of $CD8^+$ T cells in the acute immune response at day 5 and day 8 after initial infection. Compared to wild-type mice, *Cd38*$^{-/-}$ mice are highly susceptible to *L. monocytogenes* infection and were shown to have increased bacterial titers and increased mortality [Lischke et al., 2013]. This effect is caused by non-functioning innate immune cell populations. To minimize the effect of CD38 deficient innate immune cells on survival of the mice and to characterize $CD8^+$ T cells *in vivo*, we treated the mice with Ampicillin via the drinking water starting at day two post infection to clear the mice from bacteria [Lischke et al., 2013, Mercado et al., 2000].

Cd38$^{-/-}$ and wild type (WT) mice were infected with a recombinant *L. monocytogenes* strain secreting ovalbumin (OVA), a white egg protein from chicken (*Gallus domesticus*). OVA contains the SIINFEKL ($OVA_{257\text{-}264}$) peptide which is immunodominant in C57BL/6 mice and induces strong MHC class I (H-$2K^b$) restricted $CD8^+$ T cell responses. $OVA_{257\text{-}264}$-specific T cells can be identified with $OVA_{257\text{-}264}$-dextramers, consisting of $OVA_{257\text{-}264}$-peptide loaded recombinant MHC class I proteins bound to a fluorochrome-conjugated dextran backbone. The frequency of $OVA_{257\text{-}264}$-specific $CD8^+$ T cells however, was not altered in *Cd38*$^{-/-}$ mice when compared to WT mice. This was the case in spleen and liver, the two organs which show the highest bacterial titers in *L. monocytogenes* infection (Figure 1 a). We investigated cell surface markers which are indicative for the T cell response to infection. Killer cell lectin-like receptor subfamily G member 1 (KLRG1) is a surface protein up-regulated in differentiated $CD8^+$ effector T cells and NK cells. The frequency

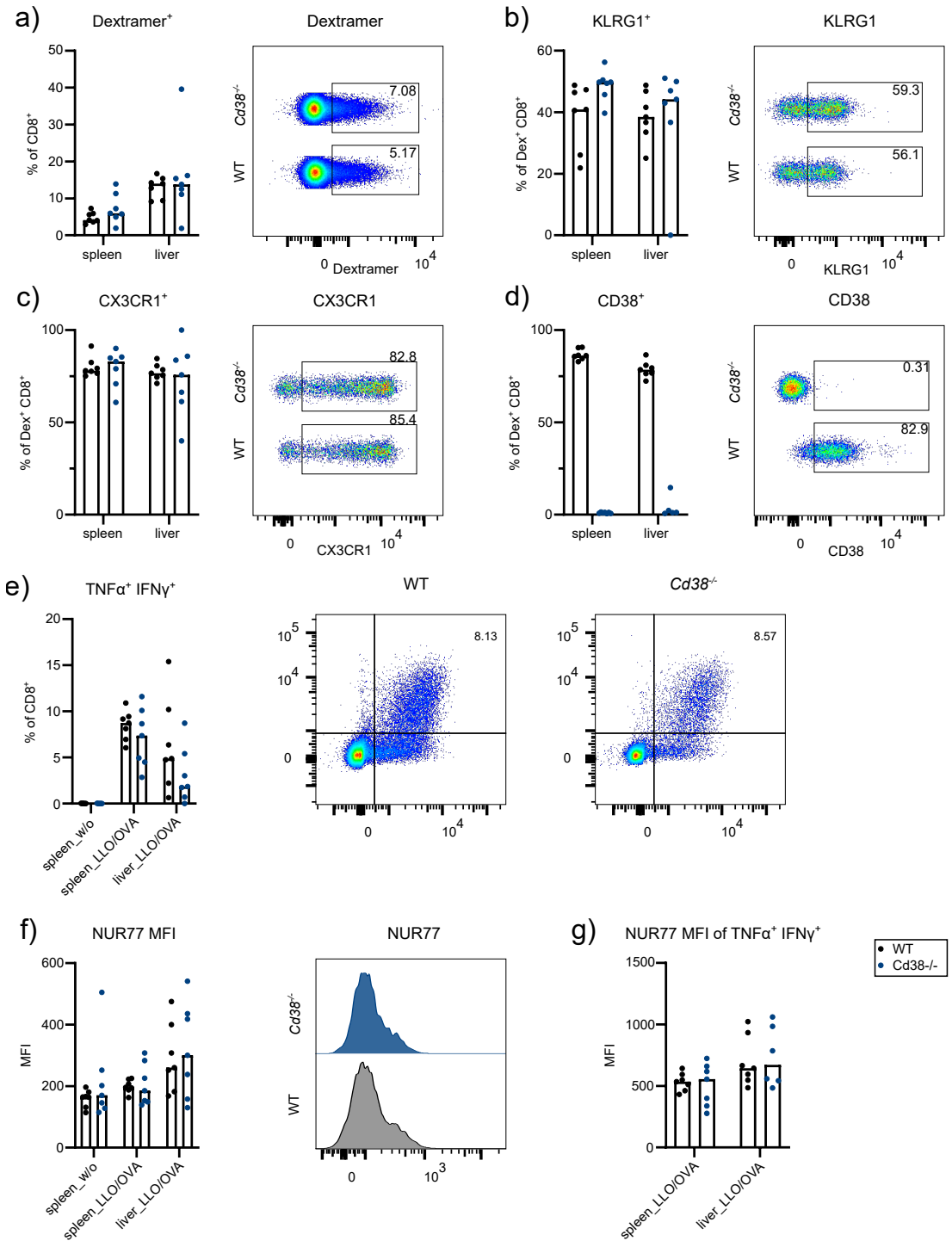

Figure 1: ***Listeria monocytogenes* infection of *Cd38*$^{-/-}$ mice for 8 days.** Wild type and *Cd38*$^{-/-}$ mice were infected with *Listeria monocytogenes* secreting ovalbumin. Mice were treated with ampicillin 2 days post-infection. Mice were sacrificed and organs were taken after 8 days. a) Ovalbumin-specific CD8$^+$ T cells were detected with dextramers carrying MHC I loaded with SIINFEKL and attached to an APC fluorochrome. b) Cell surface marker KLRG1 on dextramer positive CD8$^+$ T cells. c) Cell surface marker CX3CR1 on dextramer positive CD8$^+$ T cells. d) Frequency of CD38$^+$ in dextramer positive CD8$^+$ T cells. e) Frequency of TNFα and IFNγ double positive CD8$^+$ T cells after 4h stimulation with SIINFEKL peptide. f) NUR77 expression level of all CD8$^+$ T cells after stimulation. g) NUR77 expression level in TNFα^+ IFNγ^+ CD8$^+$ T cells

of KLRG1$^+$ cells in OVA$_{257\text{-}264}$-specific CD8$^+$ T cells in *Cd38*$^{-/-}$ mice was not altered compared to cells from WT mice (Figure 1 b). CX3C chemokine receptor 1 (CX3CR1), which is highly expressed on CD8$^+$ effector T cells did not show different surface levels between OVA$_{257\text{-}264}$-specific CD8$^+$ T cells from WT and *Cd38*$^{-/-}$ mice (Figure 1 c). As expected, CD38 could not be detected on CD8$^+$ T in *Cd38*$^{-/-}$ mice, while OVA$_{257\text{-}264}$-specific CD8$^+$ T cells of WT mice were to a large part CD38$^+$ (Figure 1 d). Stimulation of CD8$^+$ T cells with the OVA$_{257\text{-}264}$-peptide revealed no difference between WT and *Cd38*$^{-/-}$ mice: CD8$^+$ T cells which have encountered an antigen produce the cytokines TNFα and IFNγ. TNFα can activate endothelial cells to produce adhesion molecules and chemokines that recruit more T cells to the site of infection. IFNγ can activate macrophages which kill intracellular bacteria and other cells to promote antiviral / bacterial resistance. IFNγ can also induce the up-regulation of expression of interferon-stimulated genes (ISG) which include MHC proteins. [Murphy and Weaver, 2016] The percentage of CD8$^+$ T cells responding with TNFα and IFNγ production did not differ between WT and *Cd38*$^{-/-}$ mice (Figure 1 e). The immediate early activation marker nuclear receptor 4A1 also called NUR77 (NUR77), which is directly induced by TCR stimulation [Ashouri and Weiss, 2017], did not show different expression levels in WT and *Cd38*$^{-/-}$ CD8$^+$ T cells (Figure 1 f). Further, the expression level of NUR77 was not different between activated WT and *Cd38*$^{-/-}$ CD8$^+$ T cells which were TNFα^+ and IFNγ^+ (Figure 1 g).

To further reduce the influence of cells of the innate immune system on the investigated CD8$^+$ T cells, WT and *Cd38*$^{-/-}$ OT-1 CD8$^+$ T cells were transferred to WT recipient mice. This model allows the observation of WT and *Cd38*$^{-/-}$ CD8$^+$ T cells in the exact same infection-environment. Antigen specific OT1 CD8$^+$ T cells were transferred to WT recipient mice which were infected with a *L. monocytogenes* strain that secretes OVA. The ratio of *Cd38*$^{-/-}$ to WT CD8$^+$ T cells compared to the ratio at day 0 was reduced significantly in the spleen and liver (Figure 2 a). However we did not find a difference in the phenotype of *Cd38*$^{-/-}$ CD8$^+$ T cells at day 5. CD44 and CD62L are cell surface markers used to identify naïve CD8$^+$ T cells (CD44$^{\text{low}}$CD62L$^{\text{high}}$), activated effector CD8$^+$ T cells which have encountered their specific antigen (CD44$^{\text{high}}$CD62L$^{\text{low}}$) and central memory CD8$^+$ T cells (CD44$^{\text{high}}$CD62L$^{\text{high}}$). WT and *Cd38*$^{-/-}$ CD8$^+$ T cells did not differ in the frequency of CD44$^{\text{hi}}$ CD62L$^{\text{lo}}$ CD8$^+$ T cells (Figure 2 b). KLRG1 expressing CD8$^+$ T cell frequencies did not differ between WT and *Cd38*$^{-/-}$ CD8$^+$ T cells (Figure 2 c).

Spleen cells were stimulated for 4 hours with the OVA$_{257\text{-}264}$-peptide to investigate the activation of CD8$^+$ T cells *ex vivo*. The frequency of TNFα and IFNγ producing cells was not altered in *Cd38*$^{-/-}$ CD8$^+$ T cells compared to WT CD8$^+$ T cells (Figure 2 d). The immediate early activation marker

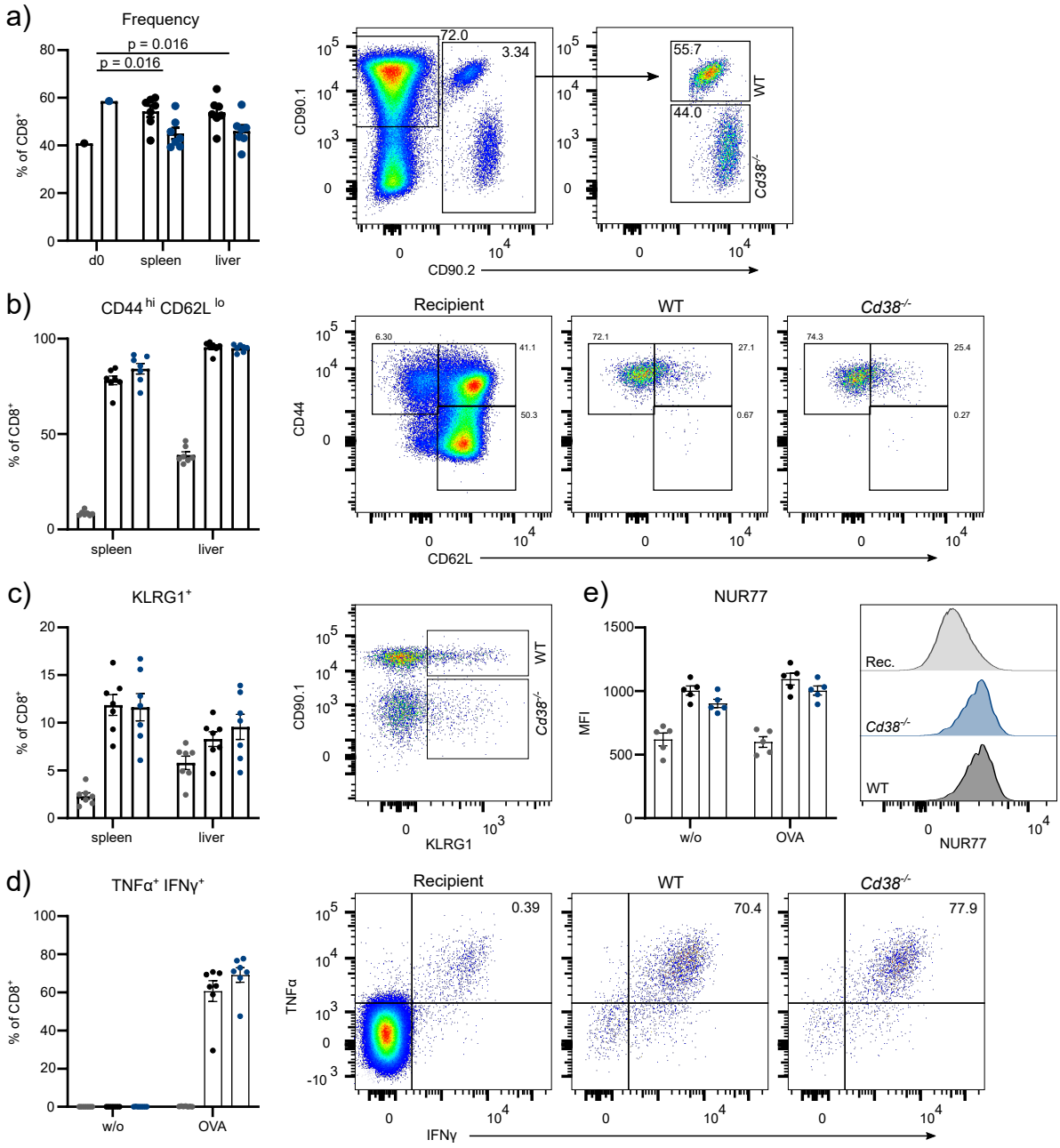

Figure 2: **Competitive *Cd38*$^{-/-}$ OT-1 CD8$^+$ T cell transfer for 5 days.** CD90.1$^+$ CD90.2$^+$ and CD90.1$^-$ CD90.2$^+$ spleen cells from wild type OT-1 mice and *Cd38*$^{-/-}$ OT-1 mice, respectively, were transferred to CD901.1 recipient mice. The recipient mice were infected with *Listeria monocytogenes* secreting ovalbumin. Mice were sacrificed 5 days after infection and transfer. a) Frequency of CD8$^+$ T cells at day 0, before transfer, and frequency at day 5 in spleen and liver of recipient mice. Statistical analysis was done using the one-sample Wilcoxon signed rank test, comparing the ratio of % *Cd38*$^{-/-}$ divided by % WT CD8$^+$ T cells at day 5 with day 0 are shown. b) Frequency of CD44^{hi} CD62L^{lo} CD8$^+$ effector T cells. c) Frequency of KLRG1$^+$ CD8$^+$ T cells. d) Frequency of TNFα^+ IFNγ^+ CD8$^+$ T cells after 4 h stimulation with the SIINFEKL peptide e) Expression level of NUR77 on CD8$^+$ T cells. Subfigures b-e) show population frequencies and expression levels in relation to the respective CD90.1$^+$ CD90.2$^+$ (WT), CD90.1$^-$ CD90.2$^+$ (*Cd38*$^{-/-}$) and CD90.1$^+$ CD90.2$^-$ (recipient) CD8$^+$ T cell subsets.

NUR77 did not differ in expression levels between WT and *Cd38*$^{-/-}$ CD8$^+$ T cells (Figure 2 e).

Cd38$^{-/-}$ CD8$^+$ T cells did not show an altered phenotype compared to WT CD8$^+$ T cells in the acute response to *L. monocytogenes* infection. We did observe a reduced frequency of *Cd38*$^{-/-}$ CD8$^+$ T cells in the spleen and the liver compared to WT CD8$^+$ T cells after 5 days in the T cell transfer assay. This indicates a lower proliferation or reduced survival of *Cd38*$^{-/-}$ CD8$^+$ T cells during the acute response to *L. monocytogenes* infection.

2.2 CD38 deficiency did not alter the phenotype but the stability of CD8$^+$ T cells in T cell memory experiments

CD38 did not appear to have a significant impact on the function and phenotype of CD8$^+$ T cells in acute infection other than a reduced frequency of *Cd38*$^{-/-}$ CD8$^+$ T cells in competitive T cell transfers. We nvestigated CD38 in T cell memory experiments and its function in memory T cell populations. In parallel to the earlier described infection of *Cd38*$^{-/-}$ for 8 days, we infected mice with *L. monocytogenes* and sacrificed the mice after 8 weeks to investigate CD8$^+$ T cell populations at this later time point in their development. The mice were treated with ampicillin via the drinking water from day 2 post-infection.

We investigated CD8$^+$ memory T cells generated by *L. monocytogenes* infection and used CD69 as a marker for tissue-residency [Kumar et al., 2017, Mackay et al., 2013, Siracusa et al., 2019]. We did not observe an altered frequency of OVA$_{257\text{-}264}$-specific CD69$^+$ CD8$^+$ T cells in spleen, liver, lung and kidney of *Cd38*$^{-/-}$ mice compared to WT mice (Figure 3 a). Further, the phenotype of OVA$_{257\text{-}264}$-specific *Cd38*$^{-/-}$ CD8$^+$ T cells did not differ from wild type OVA$_{257\text{-}264}$-specific CD8$^+$ T cells for the investigated surface markers: In spleen, liver, lung and kidney the frequencies of OVA$_{257\text{-}264}$-specific CD44^{hi} CD62L^{lo} CD8$^+$ effector memory T cells as well as OVA$_{257\text{-}264}$-specific KLRG1$^+$ CD8$^+$ T cells did not differ between wild type and *Cd38*$^{-/-}$ mice (Figure 3 b&c). The frequency of OVA$_{257\text{-}264}$-specific CD38$^+$ CD8$^+$ was reduced in *Cd38*$^{-/-}$ mice as expected, while OVA$_{257\text{-}264}$-specific CD38$^+$ CD8$^+$ T cells were present in all investigated organs in WT mice (Figure 3 d).

The cytokine production capabilities of CD8$^+$ memory T cells were not altered in *Cd38*$^{-/-}$ mice: The frequency of CD8$^+$ T cells which produce TNFα and IFNγ upon stimulation with OVA$_{257\text{-}264}$-peptide did not differ between WT and *Cd38*$^{-/-}$ mice (Figure 3 e). Further, the expression level of NUR77 did not differ between OVA$_{257\text{-}264}$-peptide stimulated wild type and *Cd38*$^{-/-}$ CD8$^+$ T cells

(Figure 3 f).

Taken together, CD8$^+$ memory T cells were not affected in *Cd38*$^{-/-}$ mice compared to WT mice in the 8 weeks *L. monocytogenes* infection assay.

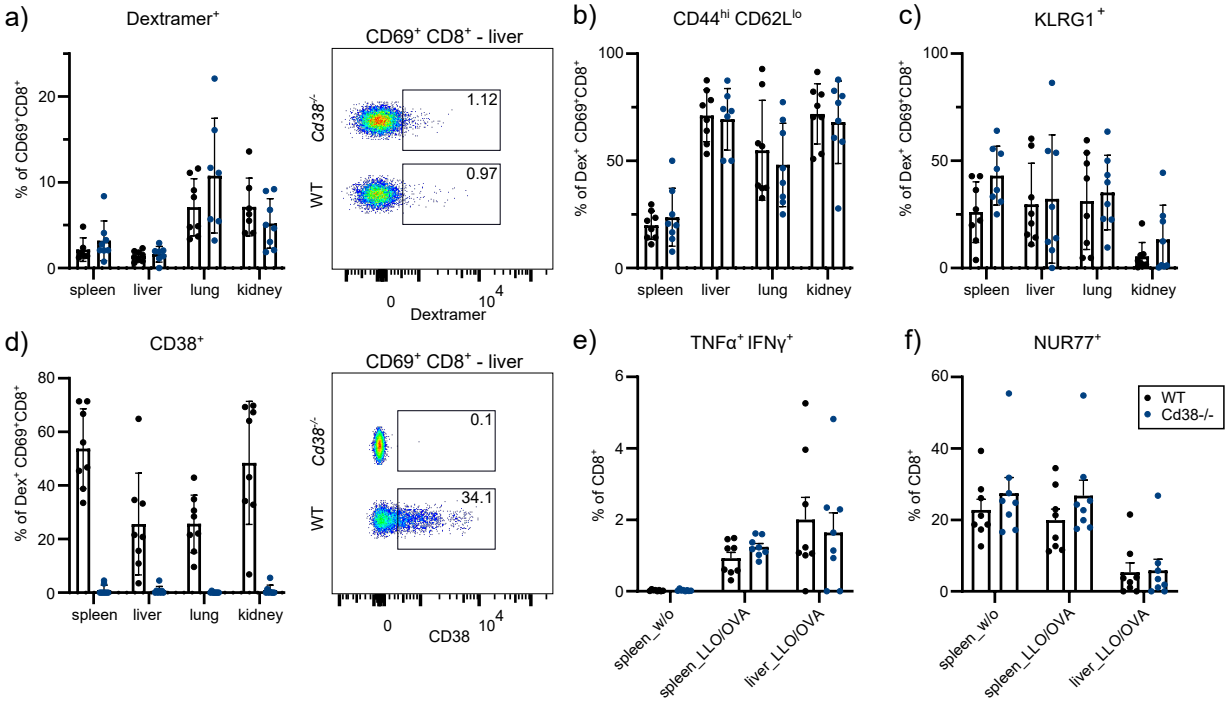

Figure 3: ***Listeria monocytogenes* infection of *Cd38*$^{-/-}$ mice for 8 weeks.** *Cd38*$^{-/-}$ and wild type mice were infected with *Listeria monocytogenes* secreting ovalbumin and treated with ampicillin 2 days after infection. a) Ovalbumin specific CD69$^+$ CD8$^+$ T cells were detected with dextramers carrying MHC I loaded with SIINFEKL and attached to an APC fluorochrome. b) Percentage of CD44^{hi} CD62L^{lo} CD8$^+$ T cells in the dextramer$^+$ CD69$^+$ CD8$^+$ T cell subset. c) Percentage of KLRG1$^+$ CD8$^+$ T cells in the dextramer$^+$ CD69$^+$ CD8$^+$ T cell subset. d) Percentage of CD38$^+$ CD8$^+$ T cells in the dextramer$^+$ CD69$^+$ CD8$^+$ T cell subset. e) Frequency of TNFα and IFNγ double positive CD8$^+$ T cells in total CD8$^+$ T cells after 4h stimulation with OVA$_{257\text{-}264}$-peptide. f) NUR77 expression in CD8$^+$ T cells after OVA$_{257\text{-}264}$-peptide stimulation.

We further used competitive T cell transfer experiments with a duration of 8 weeks to investigate CD8$^+$ memory T cells in *Cd38*$^{-/-}$ mice. As described in section 2.1, we reduced effects of the innate immune system on the T cell response using this experimental design. In contrast to 5 day transfer experiments, OT-1 CD8$^+$ T cells were transferred to RAG1-deficient (*Rag1*$^{-/-}$) mice, which do not produce B- and T lymphocytes, in order to avoid graft versus host rejection of the transferred T cells [Mombaerts et al., 1992].

As a control experiment, two donor mice, which both carried wild type *Cd38* alleles, were used and ovalbumin specific wild type OT-1 CD8$^+$ T cells with different congenic markers were transferred

(CD90.1$^+$ CD90.2$^+$ vs. CD90.1$^-$ CD90.2$^+$). The control showed no difference in frequency between the transferred cells whereas the *Cd38*$^{-/-}$ OT-1 CD8$^+$ T cells showed a lower frequency compared to the co-transferred OT-1 CD8$^+$ T cells (Figure 4 a). This result is also found in the liver and the lung, showing a more pronounced effect than in the spleen (Figure 4 b). CX3CR1 is involved in adhesion and migration of T cells and up-regulated in CD8$^+$ effector and memory T cells (immgen.org) [Heng et al., 2008]. The frequency of CX3CR1$^+$ CD8$^+$ T cells was not changed in *Cd38*$^{-/-}$ CD8$^+$ T cells (Figure 4 c). Apoptosis regulator Bcl-2 (BCL2) is expressed in KLRG1^{low} CD127^{high} pre-memory CD8$^+$ T cells where it counteracts the apoptotic function of Bcl2-interacting mediator of cell death, also called Bcl2-L-11 (BIM) [Hardwick and Soane, 2013, Li et al., 2020, Kurtulus et al., 2011, Joshi et al., 2007, Kaech and Cui, 2012]. BCL2 expression was not affected by CD38 deficiency in CD8$^+$ T cells in the 8 week transfer assay (Figure 4 d). Finally, T cell activation and cytokine production were not affected after the 8 week transfer experiments: CD8$^+$ T cells were stimulated with the OVA$_{257\text{-}264}$-peptide and two derivatives with amino acid substitutions at position 4 of the peptide (OVA$_{257\text{-}264}$N260Q and OVA$_{257\text{-}264}$N260V). The amino acid substitutions lower the affinity of the MHC I -peptide complex to the transgenic TCR of CD8$^+$ OT-1 T cells allowing for a gradual increase in stimulation strength. *Cd38*$^{-/-}$ CD8$^+$ T cells did not show different frequencies of TNFα^+ IFNγ^+ cells compared to WT CD8$^+$ T cells when stimulated with the different OVA$_{257\text{-}264}$-derived peptides (Figure 4 f). The expression of the immediate early activation marker NUR77 was not altered in *Cd38*$^{-/-}$ CD8$^+$ T cells in response to the different stimuli compared to WT CD8$^+$ T cells (Figure 4 g).

Summarized, the phenotype and activation of CD8$^+$ memory T cells was not affected by CD38-deficiency but the frequency of *Cd38*$^{-/-}$ CD8$^+$ T cells was reduced compared to WT CD8$^+$ memory T cells in the competitive transfer assay. This could be due to a reduced stability of *Cd38*$^{-/-}$ CD8$^+$ memory T cells, or reduced proliferation in the acute response to *L. monocytogenes* infection (See figure 2).

2.3 Single cell CITE sequencing of *Cd38*$^{-/-}$ CD8$^+$ T cells revealed a delayed progression towards CD8$^+$ memory T cells

We performed a single cell RNA cellular indexing of transcriptomes and epitopes (CITE) sequencing experiment to gain insight into transcriptional changes in *Cd38*$^{-/-}$ OT-1 CD8$^+$ T cells. Single cell RNA CITE sequencing incorporates the use of antibodies which are are labeled with oligo-

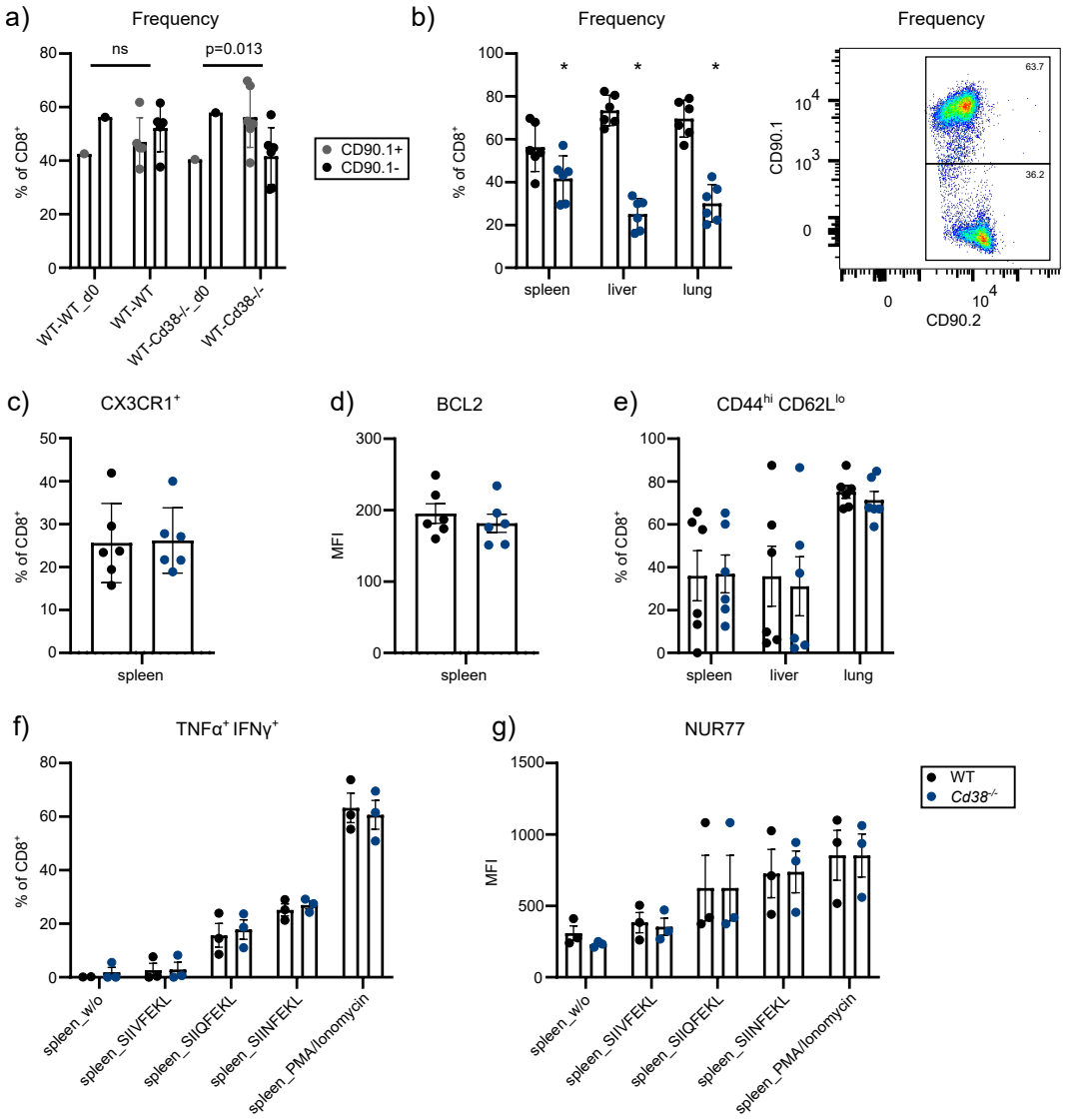

Figure 4: **Competitive *Cd38*$^{-/-}$ OT-1 CD8$^+$ T cell transfer for 8 weeks** Spleen cells of *Cd38*$^{-/-}$ OT-1 and OT-1 mice were transferred to recipient mice, which were infected with *Listeria monocytogenes* secreting ovalbumin. 5000 CD8$^+$ T cells each were transferred. After 8 weeks, the mice were sacrificed. a) Ratio of transferred T cells after 8 weeks in the spleen, compared to the ratio of transferred cells at day 0. OT-1 / OT-1 control transfer with parallel OT1 / *Cd38*$^{-/-}$ OT-1 CD8$^+$ T cell transfer. b) Ratio of OT-1 and *Cd38*$^{-/-}$ OT1 CD8$^+$ T cells in spleen, liver and lung. c) Frequency of CX3CR1$^+$ CD8$^+$ T cells. d) Intracellular staining of the BCL2 transcription factor. e) Frequency of CD44^{hi} CD62L^{lo} CD8$^+$ T cells f) Frequency of TNFα^+ IFNγ^+ CD8$^+$ T cells after stimulation for 4 hours. g) NUR77 MFI of CD8$^+$ T cells after 4 hour stimulation. Statistical analysis (a&b) was done using the one-sample Wilcoxon signed rank test, comparing the ratio of % *Cd38*$^{-/-}$ divided by % WT CD8$^+$ T cells after 8 weeks with day 0 are shown.

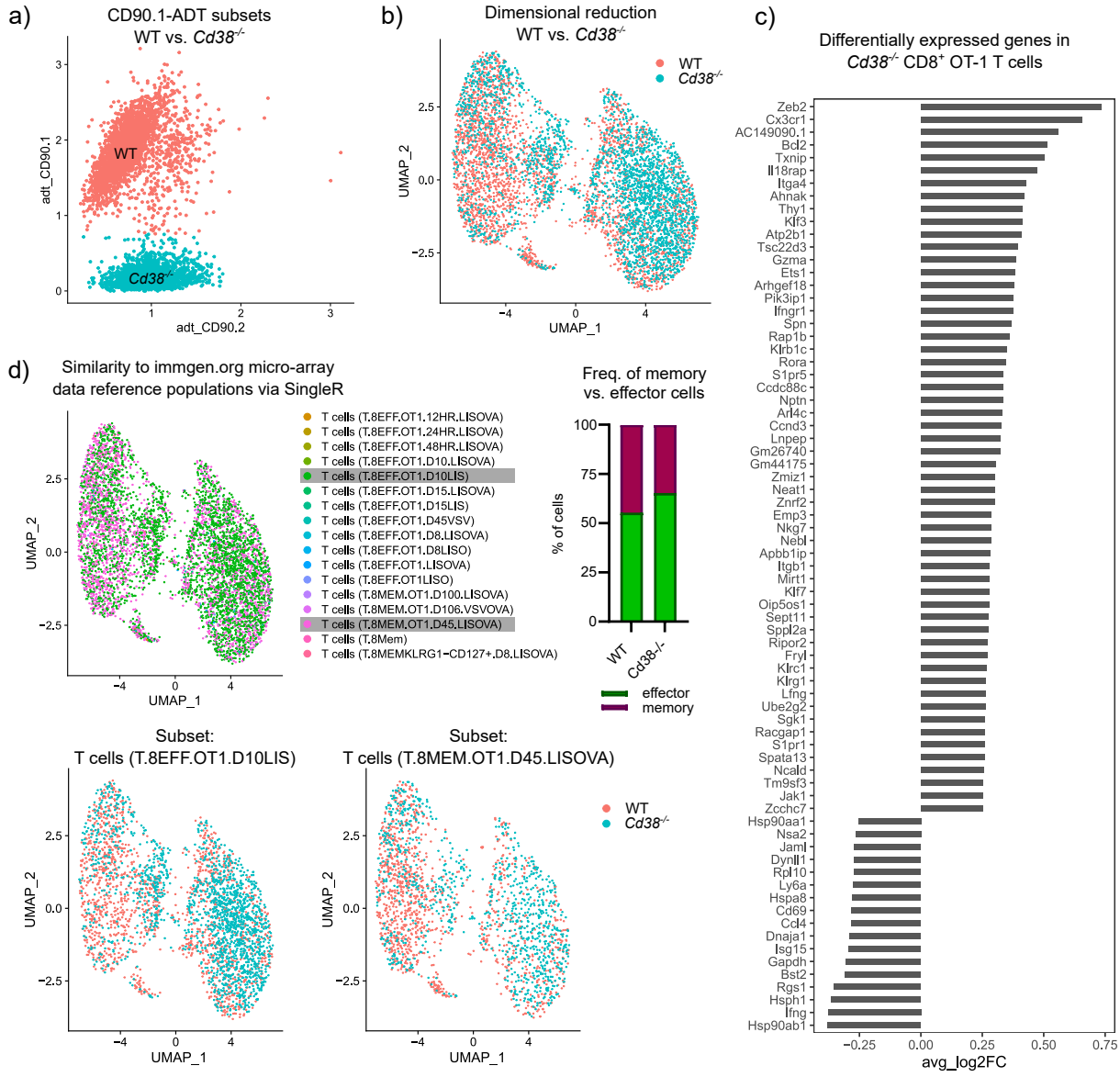

Figure 5: **Single Cell CITE-seq. of *Cd38*$^{-/-}$ CD8^{+} T cells.** OT-1 and *Cd38*$^{-/-}$ OT-1 CD8^{+} T cells were transferred to recipient mice which were infected with *Listeria monocytogenes* secreting ovalbumin. At day 11 post infection, CD8^{+} and CD69^{+} cells from the liver were sorted and labeled with CITE-seq. antibodies. Single cell CITE-seq. was performed with a sequencing depth of 50,000 reads per cell for 25,000 cells per genotype. a) Wild type (CD90.1^{+} CD90.2^{+}) and *Cd38*$^{-/-}$ (CD90.1^{-} CD90.2^{+}) cells were selected based on CD90.1 and CD90.2 normalized ADT counts. b) UMAP dimensionality reduction of normalized RNA expression data (ADT information was not included for this analysis) - of sequenced CD8^{+} cells, with indicated genotype. c) Log_2 fold differential expression of genes in *Cd38*$^{-/-}$ cells compared to wild type OT-1 cells. d) UMAP of CD8^{+} cells labeled based on immgen.org micro array sequencing data of sorted reference populations. Percentage of cells and UMAPs of OT-1 and *Cd38*$^{-/-}$ OT-1 cells are shown for predominant clusters "T cells (T.8EFF.OT1.D10LIS)" (effector) and "T cells (T.8MEM.OT1.D45.LISOVA)" (memory).

nucleotides which can be detected by sequencing. Similar to flow cytometry staining, CITE-seq antibodies can be used to distinguish immune cell populations by their cell surface protein composition. The CITE-seq antibody labeling is sequenced separately and the result is stored in an antibody derived tags (ADTs)-library that contains the read-count per cell which is then normalized and combined with the RNA-sequencing result based on unique sequence-tags identifying individual cells. OT-1 $CD8^+$ T cells and *Cd38*$^{-/-}$ OT-1 $CD8^+$ T cells were investigated at day 11 after infection of recipient mice in a competitive T cell transfer. Tissue resident and activated $CD8^+$ T cells from the liver were sorted for $CD69^+$ $CD8^+$ T cells. Additionally, $CD90.1^+$ $CD90.2^+$ wild type OT-1 cells and $CD90.1^-$ $CD90.2^+$ *Cd38*$^{-/-}$ OT-1 cells were sorted to ensure an equal number of cells were sequenced. 25,000 cells of each genotype were mixed again and labeled with CITE-seq. antibodies before sequencing. Single cell RNA sequencing was done with a read depth of 50,000 reads per cell.

$CD8^+$ T cells were selected for the presence of CD8α-RNA, CD8α-ADT and CD90.2-ADTs. WT and *Cd38*$^{-/-}$ $CD8^+$ OT-1 T cells were then distinguished by their CD90.1-ADT normalized read count (Figure 5 a). A uniform manifold approximation and projection (UMAP) dimensionality reduction of the RNA sequencing results was performed without the inclusion of ADT-information (except for the mentioned selection of the CD8α^+ subset). The UMAP analysis, which is based on a principal components analysis (PCA), showed little clustering of WT versus *Cd38*$^{-/-}$ OT-1 $CD8^+$ T cells. Two large clusters emerged with a tendency of *Cd38*$^{-/-}$ ($CD90.1^-$) cells to locate in the right cluster and vice versa (Figure 5 b). Differentially expressed genes of *Cd38*$^{-/-}$ $CD8^+$ OT-1 T cells compared to WT $CD8^+$ OT-1 T cells showed a maximum $\log_2$-fold change of 0.73 for *Zeb2*, 0.66 for *Cx3cr1*, 0.56 for *Ac149090.1* and 0.51 for *Bcl2*. 73 genes(Cutoff at a $\log_2$-fold change of $\pm$ 0.25), showed a $\log_2$-fold change of $\pm$ 0.5 or less (Figure 5 c).

A gene ontology inquiry based on the differentially expressed genes revealed up-regulated genes in *Cd38*$^{-/-}$ OT-1 $CD8^+$ cells include gene sets associated to "leukocyte tethering or rolling" (85.51 fold enriched, $p = 0.00000026$) and "positive regulation of natural killer cell mediated cytotoxicity" (38.48 fold enriched, $p = 0.00008$) (Figure 5 c; Table S.1) Interestingly, the gene ontology inquiry results for biological processes included a set of genes attributed to "immune effector process[es]" that was significantly enriched (6.37 fold enriched; $p = 0.0103$). The shared genes between the differentially expressed genes up-regulated in *Cd38*$^{-/-}$ $CD8^+$ OT-1 T cells and the "immune effector process" gene set are Spn, Apbb1ip, Lfng, Klrc1, Rora, Cx3cr1, Il18rap and Nkg7. The results for a gene ontology inquiry for biological processes to analyze the gene set found down-regulated in *Cd38*$^{-/-}$ $CD8^+$ OT-1 T cells, included a significantly enriched gene set associated with "negative regulation

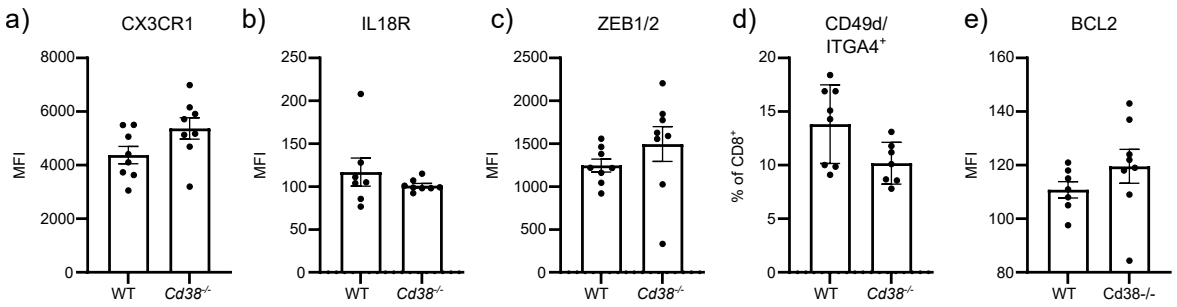

Figure 6: **Flow cytometry analysis of differentially expressed genes in *Listeria monocytogenes* infection of *Cd38*$^{-/-}$ mice** *Cd38*$^{-/-}$ and wild type mice were infected with *Listeria monocytogenes* and sacrificed after 8 weeks. Differentially expressed genes found in the single cell CITE-seq experiment were investigated via flow cytometry in CD8$^+$ T cells. a) CX3CR1 staining of CD8$^+$ T cells from the spleen. b) IL-18R staining of CD8$^+$ T cells from the spleen. c) Staining of CD8$^+$ T cells with ZEB-specific antibody covering ZEB1 and ZEB2. d) Frequency of ITGA4/CD49d$^+$ CD8$^+$ T cells. e) BCL2 staining of CD8$^+$ T cells. MFI: mean fluorescence intensity

of establishment of protein localization to mitochondrion" ($>$ 100 fold enriched; p = 0.000031) and "regulation of establishment of protein localization to mitochondrion" ($>$ 100 enriched; p = 0.0002) and "regulation of tau-protein kinase activity" ($>$ 100 fold enriched; p = 0.00005). A complete list of gene ontology inquiry results is shown in table S.1 and S.2. [Ashburner et al., 2000, Ontology, 2021, Mi et al., 2019]

When compared via the SingleR R-package [Aran et al., 2019] to micro-array sequencing data of sorted immune cell populations from the immunological genome project (immgen.org) [Heng et al., 2008], 95% of cells were found similar to either a CD8$^+$ OT-1 memory T cell population "T cells (T.8MEM.OT1.D45.LISOVA)" or a CD8$^+$ OT-1 effector T cell population "T cells (T.8EFF.OT1.D10LIS)" (See figure S.1). The sequencing data of both reference populations was obtained from CD8$^+$ OT-1 T cells which were transferred to recipient mice which were infected with *L. monocytogenes* secreting OVA. Cells of the reference population "T cells (T.8EFF.OT1.D10LIS)" were analyzed 10 days post infection. Cells of the reference population "T cells (T.8MEM.OT1.D45.LISOVA)" were analyzed 45 days post infection [Heng et al., 2008].

The portion of cells associated with the memory (T cells (T.8MEM.OT1.D45.LISOVA)) versus effector (T cells (T.8EFF.OT1.D10LIS)) like transcriptomic profile differed between *Cd38*$^{-/-}$ OT-1 and OT-1 CD8$^+$ T cells. *Cd38*$^{-/-}$ OT-1 CD8$^+$ T cells contained smaller percentage of cells with a memory like transcriptome than WT OT-1 CD8$^+$ T cells. (Figure 5 d)

Because the single cell CITE RNA sequencing is a single experiment and the transcript level of

genes does not necessarily correlate with protein levels in the cell, we investigated protein levels of genes which were identified as differentially expressed between WT and *Cd38*$^{-/-}$ CD8$^+$ OT-1 T cells (Figure 5 c). We investigated CX3CR1, interleukin-18 receptor 1 (IL18R), zinc finger E-box-binding homeobox (ZEB)1 and ZEB2, integrin alpha-4 (CD49d)/integrin α-4 (ITGA4) and BCL2 8 weeks after infection.

The chemokine receptor CX3CR1 is expressed in terminally differentiated CD8$^+$ effector T cells. CX3CR1 is involved in adhesion and migration of T lymphocytes. [Gerlach et al., 2016] CX3CR1 was found to be higher expressed in *Cd38*$^{-/-}$ than in WT OT-1 CD8+ T cells and we observed a trend of increased protein levels in *Cd38*$^{-/-}$ CD8+ T cells after 8 weeks of infection, however this result was not significant (Figure 6 a). The interleukin-18 receptor accessory protein (IL18rap) interacts with the IL-18 receptor and is part of the signal transduction of the response to IL-18. IL18rap is up-regulated in CD8$^+$ OT-1 T cells about 48 hours post infection with *L. monocytogenes* in immgen.org reference populations [Debets et al., 2000, Cheung et al., 2005, Born et al., 1998, Heng et al., 2008] Flow cytometry analysis of IL18R levels in *Cd38*$^{-/-}$ and WT CD8+ T cells did not show a difference (Figure 6 b). The multi zinc finger transcription factor zinc finger E-box-binding homeobox 2 (ZEB2) is up-regulated in KLRG1$^+$ CD8$^+$ effector T cells [Omilusik et al., 2015, Kim et al., 2020, Barata et al., 2019]. We found that ZEB1/ZEB2 levels were not significantly increased in *Cd38*$^{-/-}$ CD8+ T cells but showed a tendency, as seen in the differential expression analysis. The ZEB antibody was not specific for ZEB2 which may have masked a difference in ZEB protein level (Figure 6 c). CD49d or ITGA4 is an integrin which recognizes fibronectin on endothelial cells and has been found to interact with fractalkine and was hypothesized to play a role in the interaction of T cells with target cells [Fujita et al., 2012]. The frequency of ITGA4$^+$ CD8$^+$ T cells was slightly decreased in *Cd38*$^{-/-}$ mice compared to wild type CD8$^+$ T cells. In contrast, *Cd38*$^{-/-}$ CD8+ OT-1 T cells exhibited increased *Itga4* mRNA levels compared to WT CD8$^+$ OT-1 T cells in the differential expression analysis (Figure 6 d). BCL2 levels of *Cd38*$^{-/-}$ CD8$^+$ T cells were slightly increased compared to wild type CD8$^+$ T cells, however not significantly (Figure 6 e).

Summarized, we could not detect significantly altered levels of the proteins selected based on in the differential expression analysis in *Cd38*$^{-/-}$ compared to WT CD8$^+$ T cells. However, we did observe trends of increased protein levels for 3 of the 5 investigated proteins which support the findings of the single cell RNA CITE sequencing.

Publications

In the following I will include two publications I was part of, "TRPM2 Is Not Required for T-Cell Activation and Differentiation" [Lory et al., 2022] and "P2X4 and P2X7 are essential players in basal T cell activity and Ca^{2+} signaling milliseconds after T cell activation" by Brock et al. [Brock et al., 2022]. Preceding you will find a statement listing my contributions to these publications.

17.01.2022

Sehr geehrte Damen und Herren,

ich habe die zwei Veröffentlichungen die ich für die kumulative Dissertation nutzen möchte angehängt und zusammengefasst, welche Beiträge ich dazu geleistet habe. Ich würde ich mich sehr über Ihre Zustimmung zu meinem Antrag freuen.

Mit freundlichen Grüßen

Niels Christian Lory

TRPM2 Is Not Required for T-Cell Activation and Differentiation
(published January 2022 in Frontiers in Immunology)

- Experimente und Analyse/Visualisierung der Daten für Figure 1, 2a+b, 3, 4, 5
- Experimente und Analyse/Visualisierung für supplementary Figure 1 und 2
- Verfassen der ersten Version des Manuskripts
- Experimente für die Revision
- Planung des Projektes zusammen mit Prof. Dr. Mittrücker und Prof. Dr. Huber

P2X4 and P2X7 are essential players in basal T cell activity and Ca^{2+} signaling milliseconds after T cell activation (Provisionally accepted in Science Advances)

- Experimente und Analyse/Visualisierung für supplementary Figure 3
- Verfassen des Methodenteils für supplementary Figure 3

Hiermit bestätige ich die Richtigkeit der Angaben zur Beteiligung von Niels Christian Lory zu den oben genannten Publikationen.

HH 12.1.2022
Ort, Datum

Prof. Dr. Hans-Willi Mittrücker

frontiers in Immunology

ORIGINAL RESEARCH
published: 14 January 2022
doi: 10.3389/fimmu.2021.778916

TRPM2 Is Not Required for T-Cell Activation and Differentiation

Niels C. Lory[1,2†], Mikolaj Nawrocki[2,3†], Martina Corazza[2,3], Joanna Schmid[1], Valéa Schumacher[1], Tanja Bedke[2,3], Stephan Menzel[1,4], Friedrich Koch-Nolte[1], Andreas H. Guse[5], Samuel Huber[2,3‡] and Hans-Willi Mittrücker[1,2‡]*

[1] Department for Immunology, University Medical Center Hamburg-Eppendorf, Hamburg, Germany, [2] Hamburg Center for Translational Immunology (HCTI), University Medical Center Hamburg-Eppendorf, Hamburg, Germany, [3] Section of Molecular Immunology and Gastroenterology, I. Department of Medicine, University Medical Center Hamburg-Eppendorf, Hamburg, Germany, [4] The Calcium Signalling Group, Department of Biochemistry and Molecular Cell Biology, University Medical Center Hamburg-Eppendorf, Hamburg, Germany, [5] Mildred Scheel Cancer Career Center HaTriCS4, University Medical Center Hamburg-Eppendorf, Hamburg, Germany

Antigen recognition by the T-cell receptor induces a cytosolic Ca^{2+} signal that is crucial for T-cell function. The Ca^{2+} channel TRPM2 (transient receptor potential cation channel subfamily M member 2) has been shown to facilitate influx of extracellular Ca^{2+} through the plasma membrane of T cells. Therefore, it was suggested that TRPM2 is involved in T-cell activation and differentiation. However, these results are largely derived from *in vitro* studies using T-cell lines and non-physiologic means of TRPM2 activation. Thus, the relevance of TRPM2-mediated Ca^{2+} signaling in T cells remains unclear. Here, we use TRPM2-deficient mice to investigate the function of TRPM2 in T-cell activation and differentiation. In response to TCR stimulation *in vitro*, *Trpm2*$^{-/-}$ and WT $CD4^+$ and $CD8^+$ T cells similarly upregulated the early activation markers NUR77, IRF4, and CD69. We also observed regular proliferation of *Trpm2*$^{-/-}$ $CD8^+$ T cells and unimpaired differentiation of $CD4^+$ T cells into Th1, Th17, and Treg cells under specific polarizing conditions. *In vivo*, *Trpm2*$^{-/-}$ and WT $CD8^+$ T cells showed equal specific responses to *Listeria monocytogenes* after infection of WT and *Trpm2*$^{-/-}$ mice and after transfer of WT and *Trpm2*$^{-/-}$ $CD8^+$ T cells into infected recipients. $CD4^+$ T-cell responses were investigated in the model of anti-CD3 mAb-induced intestinal inflammation, which allows analysis of Th1, Th17, Treg, and Tr1-cell differentiation. Here again, we detected similar responses of WT and *Trpm2*$^{-/-}$ $CD4^+$ T cells. In conclusion, our results argue against a major function of TRPM2 in T-cell activation and differentiation.

Keywords: TRPM2, T cells, T-cell activation, TCR signaling, ADPR, calcium signaling

Abbreviations: ADPR, adenosine 5′-diphosphate-ribose; cADPR, cyclic adenosine 5′-diphosphate-ribose; 2dADPR, 2′-deoxyadenosine 5′-diphosphoribose; IP_3, D-*myo*-inositol 1,4,5-trisphosphate; Lm, *Listeria monocytogenes*; LmOVA, ovalbumin recombinant *Listeria monocytogenes*; NAADP, nicotinic acid adenine dinucleotide phosphate; OVA, ovalbumin; PMA, phorbol 12-myristate 13-acetate; RYR, ryanodine receptor; TPC, two-pore channel; TRPM2, transient receptor potential cation channel subfamily M member 2.

OPEN ACCESS

Edited by:
Andrew D. Wells, Children's Hospital of Philadelphia, United States

Reviewed by:
Prabhakaran Kumar, University of Illinois at Chicago, United States
Weishan Huang, Louisiana State University, United States
Jorge Mora, Moderna Inc., United States

***Correspondence:**
Hans-Willi Mittrücker
h.mittruecker@uke.de

†These authors have contributed equally to this work and share first authorship

‡These authors have contributed equally to this work and share last authorship

Specialty section:
This article was submitted to T Cell Biology, a section of the journal Frontiers in Immunology

Received: *17 September 2021*
Accepted: *20 December 2021*
Published: *14 January 2022*

Citation:
Lory NC, Nawrocki M, Corazza M, Schmid J, Schumacher V, Bedke T, Menzel S, Koch-Nolte F, Guse AH, Huber S and Mittrücker H-W (2022) TRPM2 Is Not Required for T-Cell Activation and Differentiation. Front. Immunol. 12:778916. doi: 10.3389/fimmu.2021.778916

INTRODUCTION

T-cell receptor (TCR) stimulation causes a rapid increase of the free cytoplasmic Ca^{2+} concentration. The intensity of this Ca^{2+} signal correlates with the strength of the TCR signal and has strong impact on the activation and differentiation processes of T cells (1–4). Triggering of the TCR induces the rapid formation of the 2nd messengers nicotinic acid adenine dinucleotide phosphate (NAADP), cyclic adenosine 5′-diphosphate-ribose (cADPR), and D-*myo*-inositol 1,4,5-trisphosphate (IP_3). NAADP targets ryanodine receptor 1 (RYR1) in the ER membrane and possibly two pore channels in the lysosomal membranes resulting in the formation of Ca^{2+} microdomains within milliseconds. Subsequent activation of IP_3 receptors and RYR in the ER membrane by IP_3 and cADPR further enhances Ca^{2+} release from the ER. Ca^{2+} depletion of the ER is sensed by stromal interaction module-1 (STIM1) which activates entry of extracellular Ca^{2+} *via* ORAI/CRAC channels in the plasma membrane and thereby causes the extended and global cytoplasmic Ca^{2+} signal required for effective T-cell activation (5–8).

Transient receptor potential cation channel subfamily M member 2 (TRPM2) was also identified as Ca^{2+} channel in T cells, but its function in T cells and particularly in TCR signaling is still unclear. TRPM2 is a Ca^{2+}-permeable non-selective cation channel in the plasma membrane. The channel is expressed in cells of the central nervous system but is also found in leukocytes, particularly in cells of the myeloid lineage, e.g., neutrophils, macrophages, and dendritic cells (DCs). In these cells, TRPM2 has been linked to diverse functions, such as oxidative stress response, phagosome maturation, and migratory processes (9–15). *Trpm2* mRNA and TRPM2 protein have been detected in T cells (16–19); however, compared to cells of the myeloid lineage, mRNA expression is relatively low in all analyzed T-cell subsets [**Supplementary Figure 1** and www.immgen.org (20)].

TRPM2 is activated by adenosine 5′-diphosphate-ribose (ADPR), and recently, high-resolution structures of TRPM2 with bound ADPR were reported (18, 21–23). Using ADPR microinjection and uncaging of ADPR derivatives, activation of TRPM2 by ADPR was demonstrated in T cells (16–18, 24). Endogenous ADPR is also detected in T cells, and strong stimulation of T cells causes an increase in the ADPR concentration (17). NAADP and cADPR have been described as further agonists for TRPM2, either alone or in synergy with ADPR; however, the activity of these nucleotides on TRPM2 is controversial (5, 16, 25). TRPM2 can also sense reactive oxygen species, although the relevance of this function for T cells is unclear (19, 26). Recently, 2′-deoxyadenosine 5′-diphosphoribose (2dADPR) was identified as a further TRPM2 agonist in T cells. 2dADPR can be isolated from T cells and was more potent than ADPR in stimulation of TRPM2 currents (27).

Currently, hydrolysis of NAD by the NAD-glycohydrolase CD38 is considered to be the main source of ADPR in T cells and CD38 might also be required for 2dADPR formation (11, 25). CD38 is a type II transmembrane protein with its enzymatic activity in the extracellular part. However, a fraction of CD38 is found with an inverted orientation and thus is able to catalyze ADPR formation in the cytoplasm (28). In addition, ADPR may be cleaved from poly- or mono-ADP-ribosylated proteins. In conclusion, these data demonstrate an ADPR/2dADPR–TRPM2 pathway in T cells that can facilitate a Ca^{2+} influx into the cytoplasm (11, 25). However, these results are largely derived from cell lines, e.g., Jurkat cells, and rely on rather artificial activation protocols. Therefore and in light of the relatively low expression of *Trpm2* in primary T cells, it is unclear to which extent they represent a relevant function of TRPM2 in primary T cells.

TRPM2-deficient (*Trpm2*$^{-/-}$) mice are viable and fertile (29, 30). Interestingly, TRPM2 deficiency profoundly affects the immune system of these mice. *Trpm2*$^{-/-}$ mice are highly susceptible in several bacterial infection models (14, 30–33). On the other hand, mice show milder disease in inflammation and autoimmune models (19, 29, 34, 35). In most of these studies, altered susceptibility to disease can be linked to an impaired function of granulocytes, macrophages, or dendritic cells. So far, only two studies specifically analyzed T cells from *Trpm2*$^{-/-}$ mice. Wolf and colleagues found similar early Ca^{2+} responses following TCR stimulation of $CD4^+$ T cells from WT and *Trpm2*$^{-/-}$ mice (7). In contrast, Melzer et al. observed reduced proliferation and cytokine production of total spleen cells and of purified $CD4^+$ T cells from *Trpm2*$^{-/-}$ mice (19). To our knowledge, the function of TRPM2 in T cells has not been specifically addressed in mouse models *in vivo*.

Here, we analyze the response of $CD4^+$ and $CD8^+$ T cells from *Trpm2*$^{-/-}$ mice *in vitro* and in infection and inflammation models *in vivo*. We show that *Trpm2*$^{-/-}$ T cells are not impaired in the expression of early activation markers and in proliferation and differentiation to effector T-cell subsets *in vitro*. *In vivo*, *Trpm2*$^{-/-}$ $CD8^+$ T cells show regular responses in the *Listeria monocytogenes* infection model both after infection of *Trpm2*$^{-/-}$ mice and after transfer of deficient T cells into infected recipients. Following anti-CD3 mAb-induced intestinal inflammation, *Trpm2*$^{-/-}$ and WT mice develop a similar disease and equally accumulate defined Th-cell subsets in the intestinal mucosa. A largely regular response of *Trpm2*$^{-/-}$ $CD4^+$ T cells to anti-CD3 mAb treatment is also observed after T cell transfer into WT recipients. In conclusion, our results so far suggest that TRPM2 is not required for $CD4^+$ and $CD8^+$ T-cell activation and differentiation.

METHODS

Mice

Trpm2$^{-/-}$ mice (*Trpm2*^{tm1Yamo}) (29), *Rag1*$^{-/-}$ mice (B6.129S7 –*Rag1*^{tm1Mom}/J) (36), OT-1 mice [Tg(TcraTcrb)1100Mjb] (37), and CD90.1 congenic mice (B6.PL-*Thy1*^{a}/CyJ) were on the C57BL/6 background. All other mice used in this study were derived from intercrosses of these mouse strains. Mice were housed under specific pathogen-free conditions at the University Medical Center Hamburg-Eppendorf. The housing was done under standard conditions with food and water ad libitum in individually ventilated cages. Mice were monitored on a daily

basis. Animal experiments were approved by the local committee for animal experiments of the City of Hamburg (registration numbers: N033/2018, N067/2020). Age- and sex-matched mice were used.

Listeria monocytogenes Infection

Mice were i.p. infected with 10^4 CFU of a *Listeria monocytogenes* strain recombinant for ovalbumin (LmOVA) (38). Inocula were controlled by plating on TSB agar plates. From day 2 on, mice were treated with 2 mg/ml ampicillin in the drinking water. Endogenous T-cell responses were analyzed on day 8 postinfection. For T-cell co-transfer studies, CD90.1 congenic mice or *Rag1*$^{-/-}$ mice were infected with LmOVA. On the same day, infected mice received a mix of WT and *Trpm2*$^{-/-}$ OT-1 CD8$^+$ T cells. Spleen cells from WT CD90.1$^+$CD90.2$^+$ OT-1 cells and *Trpm2*$^{-/-}$ CD90.1$^-$CD90.2$^+$ OT-1 cells were purified and mixed to reach a 1:1 ratio of CD8$^+$ T cells. Recipient mice intravenously received a total of approx. 10,000 CD8$^+$ T cells. Responses in CD90.1 congenic and *Rag1*$^{-/-}$ recipients were analyzed after 5 days and after 8 weeks, respectively. For analysis of endogenous T-cell response and for 8-week transfer experiments, 2 µg per mouse anti-CD45 mAb (30-F11, AF700) mAb was injected i.v., 3 min before sacrificing to label intravascular cells.

Isolation and Stimulation of Cells

Cells from spleen were isolated by pressing the organ successive through 70- and 40-µm cell strainers. Cells from the kidney, lung, and liver were digested for 40 min at 37°C with 10 U/ml DNase I (Sigma-Aldrich, St. Louis, MO) and 400 µg/ml Collagenase D (Roche, Mannheim, Germany). Leukocytes were enriched by density gradient centrifugation (37.5% Easycoll, Merck Millipore, Darmstadt, Germany) and then filtered through a 30-µm strainer. Erythrocytes were depleted with lysis buffer (155 mM NH_4Cl, 10 mM $KHCO_3$, 10 µM EDTA, pH 7.2). After removal of Peyer's patches, the small intestine was opened longitudinally and washed in PBS 1% FCS. Then, the small intestine was cut into small pieces of approx. 0.5-cm length and incubated in the presence of 5 mM EDTA in complete medium at 37°C for 30 min while shaking. Intraepithelial lymphocytes (IEL) in the supernatant were collected and enriched by centrifugation. For isolation of lamina propria lymphocytes (LPL), the remaining tissue was digested with collagenase IV (100 U/ml, Roche Diagnostics GmbH, Mannheim) and DNase I (10 U/ml Sigma-Aldrich) in complete medium at 37°C for 45 min while shaking. The digested intestinal tissue was further homogenized by passing through a metal strainer, and pooled IEL and LPL fractions were enriched by a 40%/67% Percoll gradient centrifugation. Lymphocytes were collected from the interphase.

For induction of cytokines, cells were incubated for 4 h in IMDM medium supplemented with fetal calf serum, glutamine, gentamicin, and 2-mercaptoethanol. Cells were simulated for 4 h, with phorbol 12-myristate 13-acetate (PMA, 50 ng/ml, Sigma-Aldrich) and ionomycin (1 µM, Sigma Aldrich) or with the ovalbumin$_{257-264}$ peptide (10^{-6} M, SIINFEKL) (JPT, Berlin, Germany). Brefeldin A (10 µg/ml, Sigma Aldrich) was added to the cultures to prevent cytokine secretion. In controls, medium only contained brefeldin A.

For induction of CD69, IRF4, and NUR77, spleen cells were cultured for 4, 24, or 48 h in 96W plates coated with anti-CD3ϵ mAb (2 µg/ml, clone: 145-2C11). Anti-CD28 mAb (1 µg/ml, clone: 37.51) was added to the culture. In some of the assays, cells were CFSE labeled prior to stimulation. A division index was calculated with the FlowJo software (Tree Star, Ashland, OR, USA). For long-term culture, cells were stimulated with anti-CD3 mAb, antiCD28, mAb and IL-2 (100 U/ml IL-2, Proleukin S, Novartis, Nürnberg, Germany). After 3 days, cells were washed and further cultured with IL-7 (10 ng/ml mIL-7, PeproTech, Hamburg, Germany).

In Vitro Differentiation of CD4$^+$ T Cells

Lymphocytes were isolated from spleen and lymph nodes of WT and *Trpm2*$^{-/-}$ mice. Naive CD4$^+$ CD25$^-$ CD44$^-$ T cells were enriched by depletion of CD25$^+$ and CD44$^+$ cells followed by enrichment of CD4$^+$ T cells using MACS according to the manufacturer's instruction (Miltenyi Biotec, Bergisch-Gladbach, Germany). The purity of CD4$^+$ T cells obtained was about 80% as determined by flow cytometry. For each differentiation condition, the cells were cultured in a 96-well plate at 2×10^5 cells per well in 200 µl of full Click's medium (Irvine Scientific, Santa Ana, USA) supplemented with cytokines and antibodies. For differentiation of Th1 cells, naive CD4$^+$ T cells were cultured in the presence of 100 U/ml mIL-2, 10 ng/ml mIL-12, 10 µg/ml anti-IL-4 mAb (clone: 11B11), and 2 µg/ml anti-CD28 mAb (clone: 37.51) in plates coated with 10 µg/ml anti-CD3ϵ mAb (clone: 145 2C1). For the differentiation of Th17 cells, naive CD4$^+$ T cells were cultured in the presence of 10 ng/ml mIL-6 and 0.25 ng/ml hTGF-β1, 10 µg/ml anti-IL-4 mAb, 10 µg/ml anti-IFN−γ mAb (clone: XMG1.2), and 2 µg/ml anti-CD28 mAb in plates coated with 10 µg/ml anti-CD3ϵ mAb. For differentiation of Treg cells, naive CD4$^+$ T cells were cultured in the presence of 50 U/ml mIL-2 and 2 ng/ml hTGF-β1 and 2 µg/ml anti-CD28 mAb in plates coated with 2 µg/ml anti-CD3ϵ mAb. For differentiation of Tr1 cells, naive CD4$^+$ T cells were cultured in the presence of 30 ng/ml mIL-27 and 0.25 ng/ml hTGF-β1 and 2 µg/ml anti-CD28 mAb in plates coated with 10 µg/ml anti-CD3 mAb. Cytokines and antibodies were purchased from BioLegend (San Diego, CA) and Miltenyi Biotec. After 3 days, T cells were restimulated with PMA (50 ng/ml, Sigma-Aldrich) and ionomycin (1 µM, Sigma-Aldrich) for 4 h in the presence of monensin (2 µM, BioLegend) and expression of cytokines and Foxp3 was determined by intracellular antibody staining.

Antibody Staining and Flow Cytometry

After isolation from tissue or after cell culture, cells were incubated in PBS with 1% rat serum and 10 µg/ml anti-Fc-receptor mAb (clone 2.4G2, Bio X Cell, West Lebanon, NH). For extracellular staining, fluorochrome-conjugated antibodies and a fixable dead cell stain (AF750 life/dead staining or Pacific Orange succinimidyl ester, Life Technologies, Carlsbad, CA) were added. Cells were incubated for 15 min on ice. Intracellular antibody staining was conducted with the Foxp3/Transcription Factor

Staining Buffer Set (eBioscience, Carlsbad, CA) according to the manufacturer's protocol. Cells were washed with PBS 1% FCS and incubated with antibodies for intracellular staining in PBS 1% FCS for 20 min at RT.

Fluorochrome-conjugated antibodies against murine CD3 (clone 17A2, BV421), CD4 (clone RM4-5, FITC/AF700/BV605/BV785), CD8α (clone 53-6.7, PerCP/BV650), CD38 (clone 90, PE-Cy7), CD40L (clone MR1, PerCP-Cy5.5), CD44 (clone IM7, APC/BV785), CD45 (clone 30-F11, APC-Cy7/AF700/BV510/BV785), CD62L (clone MEL-14, APC/PerCP), CD69 (clone H1.2F3, PE-Cy7/V450/BV785), CD90.1 (clone HIS51, FITC/eFlour 450), CD90.2 (clone 53-2.1, PerCP), CD127 (clone A7R34, BV421), CX3CR1 (clone SA011F11, PE), Ly6C (clone AL-21, FITC), Ly6G (clone 1A8, PerCP-Cy5.5), CTLA4 (clone UC10-4F10-11, PE), PD1 (clone 29F.1A12, BV421), LAG3 (clone C9B7W, APC), IFN-γ (clone XMG1.2, APC-Cy7/BV785), IL-10 (clone JES5-16E3/APC/PE), PE), IL-17A (clone TC11-18H10.1, BV785/AF488/APC), TNF-α (clone MP6-XT22; V450), Foxp3 (clones NRRF-30, PE and FJK-16s, APC), IRF4 (clone 3E4, PE-Cy7), KI-67 (clone SolA15, PE), KLRG1 (clone 2F1, BV605), and NUR77 (clone 12.14, PE) were obtained from BioLegend, eBioscience, Thermo Fisher (Darmstadt, Germany) or BD Bioscience (Heidelberg, Germany). The anti-mouse TRPM2 mAb (clone A128) was developed by DNA immunization of rats with a plasmid expressing the full-length cDNA of mouse TRPM2. For analysis of TRPM2 expression, spleen cells were stained intracellularly with unconjugated anti-TRPM2 mAb and then stained with anti-rat-IgG antibodies (R-PE, polyclonal, Dianova, Hamburg, Germany). APC-conjugated H-2K^b/SIINFEKL dextramers were obtained from Immudex (Copenhagen, Denmark).

Cells were analyzed using Canto II, Celesta or Fortessa flow cytometers (BD Biosciences, Franklin Lakes, NJ, USA) and FlowJo software (Tree Star, Ashland, OR, USA).

Anti-CD3 mAb Induced Intestinal Inflammation

Mice were i.p. injected with 15 μg anti-CD3 mAb (clone: 145 2C11) on days 0, 2, and 4. Mice were analyzed 4 h after the last injection. For the T-cell transfer approach, cells were isolated from spleen and peripheral lymph nodes of WT and *Trpm2*$^{-/-}$ mice. Total CD4$^+$ cells were enriched with MACS according to the manufacturer's instructions. Recipient *Rag1*$^{-/-}$ mice received 2×10^6 CD4$^+$ cells i.v. After 4 weeks, recipients were treated i.p. with 2 μg anti-CD3 mAb on days 0, 2, and 4 and were analyzed 4 h after the last injection.

Quantitative RT-PCR

CD4$^+$ and CD8$^+$ T cells were isolated from spleens of WT and *Trpm2*$^{-/-}$ mice and purified by MACS (Miltenyi Biotec, Bergisch Gladbach, Germany). Total RNA from pooled CD4$^+$ and CD8$^+$ T cells was isolated using TRIzol® reagent (Invitrogen) according to the manufacturer's protocol. RNA was reverse transcribed with the high-capacity cDNA synthesis Kit (Thermo Fisher, Darmstadt, Germany). cDNA concentrations for *Ryr1*, *Tpcn1*, *Tpcn2*, *Orai1*, and the control *Hprt* were determined with TaqMan PCR using primer and probes from Thermo Fisher: *Hprt* Mm03024075_m1, *Ryr1* Mm01175211_m1, *Tpcn1* Mm00455326_m1, *Tpcn2* Mm00628260_m1, and *Orai1* Mm00774349_m1.

Statistics

Statistical analyses were performed with Prism software (GraphPad Software Inc., La Jolla, CA). Results were analyzed with the tests indicated in the figure legends. A p-value of <0.05 was considered significant ($p < 0.05$) and is indicated with *.

RESULTS

TRPM2 Deficiency Does Not Impair CD8$^+$ T-Cell Activation *In Vitro*

Ca^{2+} signaling is central for T-cell activation and differentiation, and Ca^{2+} influx facilitated by TRPM2 could enhance or modulate these processes. In a first set of experiments, the expression of TRPM2 was determined in CD8$^+$ T cells (**Figure 1A** and **Supplementary Figure 2A**). Compared to Ly6C$^+$ and Ly6G$^+$ myeloid cells (inflammatory monocytes and neutrophils), we detected only a low level of TRPM2 expression in CD8$^+$ T cells from WT mice which was markedly reduced in CD8$^+$ T cells from *Trpm2*$^{-/-}$ mice. Spleen cells from WT and *Trpm2*$^{-/-}$ mice were stimulated with anti-CD3ϵ and anti-CD28 mAb, and the expression of CD69 and of the transcription factors IRF4 and NUR77 (NR4A1) was determined by flow cytometry. Expression of these proteins is induced within a few hours of TCR stimulation and can be used to determine the quality of the TCR signal. After 4 h, we observed strong upregulation of all three proteins and expression of IRF4 was further increased after 24 and 48 h of culture (**Figures 1B, C**). CD8$^+$ T cells from WT and *Trpm2*$^{-/-}$ mice showed similar upregulation of the proteins. Then, spleen cells were labeled with CFSE and proliferation was determined by loss of the CFSE label. Cells were stimulated with anti-CD3ϵ and anti-CD28 mAb, and after 1, 2, 3, and 4 days, CFSE staining was determined (**Figures 1D, E** and **Supplementary Figure 2B**). T-cell activation resulted in cumulative loss of CFSE staining in CD8$^+$ T cells; however, there was no difference in proliferation between WT and *Trpm2*$^{-/-}$ cells. TRPM2 could also modulate the T-cell response at later time points. Therefore, CD8$^+$ T cells from WT and *Trpm2*$^{-/-}$ mice were mixed and activated with anti-CD3ϵ and anti-CD28 mAb. After 3 days, activated cells were cultured in medium containing IL-7 (**Figure 1F**). After 21 days, CD8$^+$ T cells expressed only low levels of CD69 and of the proliferation marker Ki-67 but had upregulated CD38. Importantly, the ratio of WT to *Trpm2*$^{-/-}$ CD8$^+$ T cells was similar to the ratio at the start of the culture, indicating that the lack of TRPM2 did not alter the T-cell response.

TRPM2 Deficiency Does Not Impair CD4$^+$ T-Cell Activation and Differentiation *In Vitro*

Similar to WT CD8$^+$ T cells, WT CD4$^+$ T cells expressed only low levels of TRPM2 and staining was reduced in *Trpm2*$^{-/-}$ CD4$^+$ T cells (**Figure 2A**). The early response following TCR

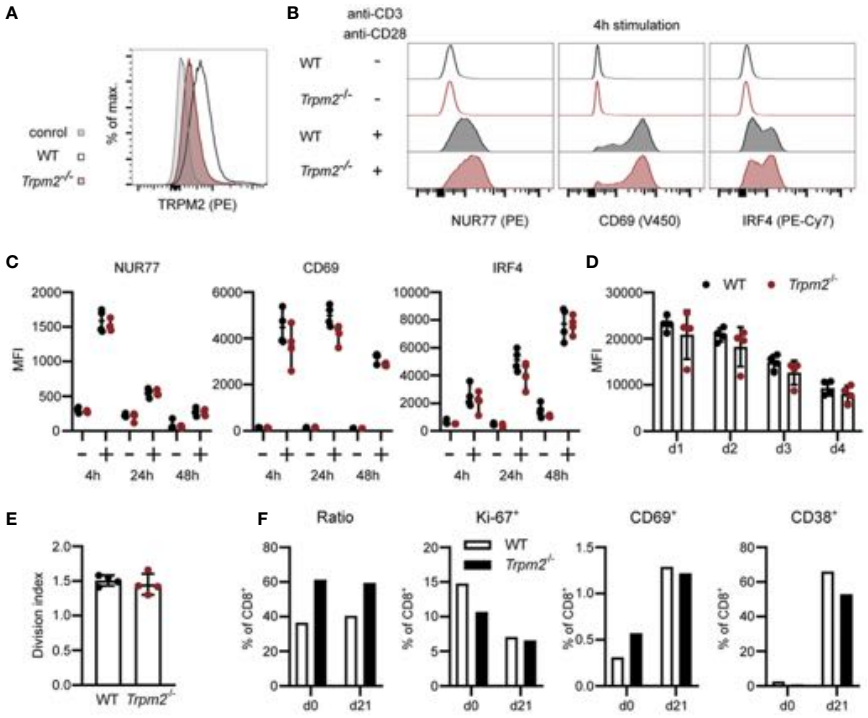

FIGURE 1 | TRPM2 deficiency does not impair CD8$^+$ T-cell activation *in vitro*. **(A)** CD8$^+$ T cells were intracellularly stained with anti-TRPM2 mAb and PE-conjugated anti-rat IgG antibody (control: WT cells stained only with the secondary antibody). **(B, C)** Spleen cells from WT and *Trpm2*$^{-/-}$ mice were stimulated for 4, 24, or 48 h with plate-coated anti-CD3ε mAb and soluble anti-CD28 mAb. Expressions of CD69, NUR77, and IRF4 were determined by extra- and intracellular antibody staining. Representative staining **(B)** and results **(C)** for CD8$^+$ T cells are shown. **(D, E)** Spleen cells were CFSE-labeled and stimulated with anti-CD3ε mAb and anti-CD28 mAb. Representative results for the mean fluorescence intensity (MFI) of CFSE of CD8$^+$ T cells on days 1–4 **(D)** and the division index for day 4 **(E)** are given. **(F)** WT (CD90.1$^+$) and *Trpm2*$^{-/-}$ (CD90.2$^+$) spleen cells were mixed and stimulated with anti-CD3ε and anti-CD28 for 3 days. Then, cells were washed and incubated with IL-7. On day 21, cells were analyzed by extra- and intracellular antibody staining. Representative results for the ratio of CD90.1$^+$ and CD90.2$^+$ CD8$^+$ T cells and for the expression of the proliferation markers Ki-67 and of CD69 and CD38 are shown. Bars and scatters in **(C–E)** give the mean ± SEM and were analyzed with the unpaired t-test. All experiments were conducted at least twice.

stimulation was also determined in CD4$^+$ T cells (**Figures 2B, C**). CD4$^+$ T cells showed rapid upregulation of CD69, NUR77, and IRF4, but there was no difference between WT and *Trpm2*$^{-/-}$ CD4$^+$ T cells. We also determined the induction of the inhibitory receptors CTLA4, PD1, and LAG3 (**Supplementary Figure 3**). We observed an equal expression of these receptors on WT and *Trpm2*$^{-/-}$ CD4$^+$ T cells. Differentiation of CD4$^+$ Th cells is regulated by cytokine signals from the environment but also by the strength of the TCR stimulus and the quality of the TCR-induced Ca^{2+} signal. Thus, modulation of the Ca^{2+} signal by TRPM2 could influence the fate of Th-cell differentiation. Purified CD4$^+$ T cells from WT and *Trpm2*$^{-/-}$ mice were stimulated under defined conditions to induce IFN-γ$^+$ Th1 cells, IL-17A$^+$ Th17 cells, Foxp3$^+$ regulatory T cells (Treg cells), and Foxp3$^-$ IL-10$^+$ regulatory 1 T cells (Tr1 cells). After 3 days, T cells were activated with PMA and ionomycin, and expression of Foxp3 and cytokines was determined by intracellular staining and flow cytometry (**Figure 2D**). Consistent with the conditions of differentiation, we detected upregulation of IFN-γ, IL-17A, IL-10, and Foxp3; however, WT and *Trpm2*$^{-/-}$ CD4$^+$ T cells did not significantly differ in the generation of IFN-γ$^+$ Th1 cells, IL-17A$^+$ Th17 cells, and Foxp3$^+$ Treg cells. In the experiment shown, there was a small reduction of *Trpm2*$^{-/-}$ Tr1 cells; however, this reduction was not consistent in other experiments.

Absence of TRPM2 could be compensated by higher expression of other Ca^{2+} channels. Therefore, mRNA was isolated from WT and *Trpm2*$^{-/-}$ T cells and the expression of *Ryr1*, *Tpcn1*, *Tpcn2*, and *Orai1* coding for Ca^{2+} channels that might compensate for the absence in T cells was measured by RT-PCR (**Supplementary Figure 4**). We detected similar mRNA levels for all analyzed Ca^{2+} channels in WT and *Trpm2*$^{-/-}$ T cells.

In conclusion, our data so far provide no evidence for a substantial role of TRPM2 in the activation and differentiation of CD4$^+$ and CD8$^+$ T cells.

TRPM2 Deficiency Does Not Impair CD8$^+$ T-Cell Activation *In Vivo*

In order to analyze the role TRPM2 in CD8$^+$ T cells *in vivo*, we used the *Listeria monocytogenes* infection model. WT and *Trpm2*$^{-/-}$ mice were infected with an ovalbumin-recombinant

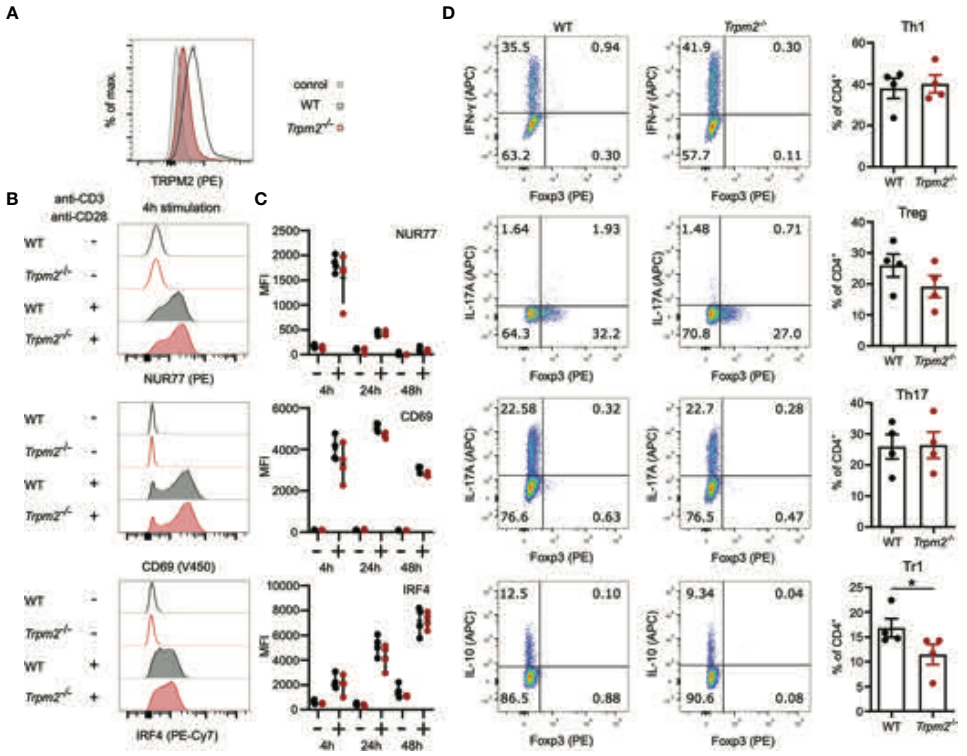

FIGURE 2 | TRPM2 deficiency does not impair CD4$^+$ T-cell activation and differentiation *in vitro*. **(A)** CD4$^+$ T cells were intracellularly stained with anti-TRPM2 mAb and PE-conjugated anti-rat IgG antibody (control: WT cells stained only with the secondary antibody). **(B, C)** Spleen cells from WT and *Trpm2*$^{-/-}$ mice were stimulated for 4, 24, or 48 h with plate-coated anti-CD3ε mAb and soluble anti-CD28 mAb. Expressions of CD69, NUR77, and IRF4 were determined by extra- and intracellular antibody staining. Representative staining **(B)** and results **(C)** for CD4$^+$ T cells are shown. **(C)** Purified naïve CD4$^+$ T cells were stimulated with plate-bound anti-CD3ε mAb and soluble anti-CD28 mAb and cultured under Th1-, Th17-, Treg-, and Tr1-polarizing conditions. After 4 days, T cells were stimulated with PMA/ionomycin in the presence of monensin, and cytokine and Foxp3 expression was measured by flow cytometry. Shown are representative dot plots and corresponding bar graphs. Th1 cells were defined as IFN-γ$^+$ CD4$^+$ T cells, Th17 cells as IL-17A$^+$ CD4$^+$ T cells, Treg cells as Foxp3$^+$ CD4$^+$ T cells, and Tr1 cells as Foxp3$^-$ IL-10$^+$ CD4$^+$ T cells. Bars and scatters in **(C, D)** give the mean ± SEM and were analyzed with the unpaired t-test. *p < 0.05. All experiments were conducted at least twice.

strain of *L. monocytogenes* (LmOVA) which induce a strong CD8$^+$ T cell response against the OVA$_{257\text{-}264}$ peptide (38). Since *Trpm2*$^{-/-}$ mice are more susceptible to *L. monocytogenes* (30, 31), mice were treated after 2 days with ampicillin in the drinking water which results in the rapid elimination of Listeria but does only marginally effect the T-cell response (39). Eight days postinfection, frequencies and total numbers of ovalbumin-specific CD8$^+$ T cells were determined using OVA$_{257\text{-}264}$H-2K^b dextramers (**Figures 3A–C**). WT and *Trpm2*$^{-/-}$ mice showed similar numbers of dextramers$^+$ CD8$^+$ T cells in spleen and liver, the main sites of listeria replication. Dextramer$^+$ CD8$^+$ T cells in both mouse strains were CD44^{hi}CD62L^{lo} and similar frequencies expressed CX3CR1 and KLRG1, indicative for highly activated effector T cells (**Figures 3D–F**). Dextramer$^+$ CD8$^+$ T cells did also not differ with regard to the upregulation of CD38 (**Figure 3G**). Spleen and liver cells were also incubated with OVA$_{257\text{-}264}$ peptide, and the induction of TNF-α and IFN-γ was determined by intracellular cytokine staining (**Figure 3H**). Again, we observed similar frequencies of TNF-α$^+$IFN-γ$^+$ CD8$^+$ T cells. There was also no difference in the production of IFN-γ and TNF-α by CD4$^+$ T cells in response to polyclonal restimulation (**Figure 3I**).

More excessive initial inflammation and altered function of TRPM2-deficient innate immune cells could mask a defect of CD8$^+$ T cells in *Trpm2*$^{-/-}$ mice. Therefore, we used a competitive T-cell transfer assay to characterize the function of TRPM2 in CD8$^+$ T cells. *Trpm2*$^{-/-}$ mice were crossed with OT-1 mice which are transgenic for an MHC class I-restricted OVA$_{257\text{-}264}$-specific TCR (37). CD8$^+$ T cells from WT and *Trpm2*$^{-/-}$ mice were mixed roughly at a 1:1 ratio, and 1 × 10^4 CD8$^+$ T cells were transferred into recipient mice infected with LmOVA. Donor and recipient cells differed in the expression of CD90.1 and CD90.2, which allowed identification of the different cell populations. Five days post transfer and infection, CD8$^+$ T cells derived from both donors could be detected in spleen and liver (**Figures 4A, B**). However, the ratio of WT to *Trpm2*$^{-/-}$ cells in both tissues was similar to that of the transferred CD8$^+$ T-cells and both populations were similar in their expression profiles of CD44, CD62L, and KLRG1 (**Figures 4C–E**). In addition, after stimulation with the OVA$_{257\text{-}264}$ peptide, WT and *Trpm2*$^{-/-}$

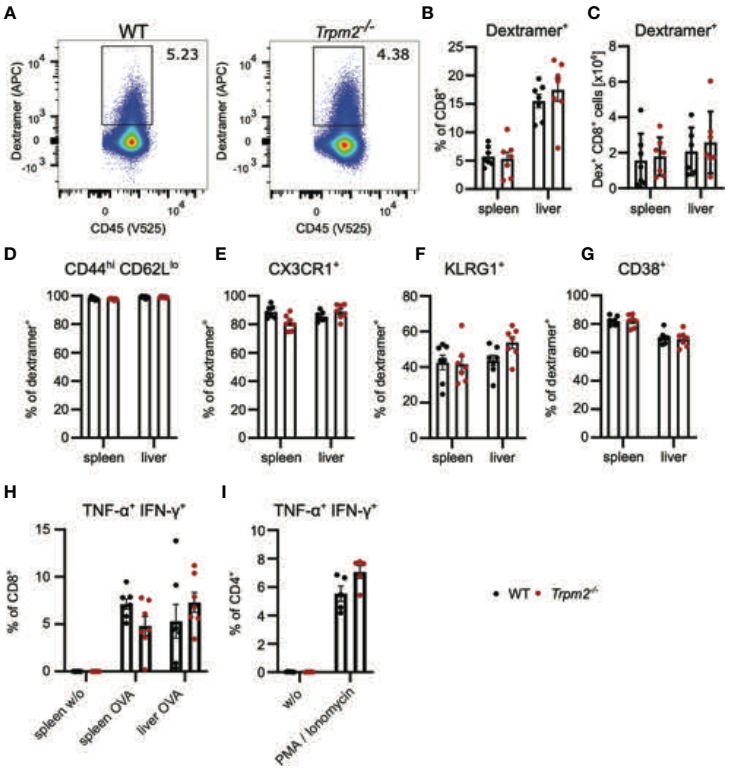

FIGURE 3 | TRPM2 deficiency does not impair the CD8$^+$ T-cell response to *L. monocytogenes*. *Trpm2*$^{-/-}$ and WT mice were infected with LmOVA. Mice were treated with ampicillin in the drinking water from day 2 on until analysis at day 8. Ovalbumin-specific CD8$^+$ T cells were detected with H–2K^b OVA$_{257-264}$-dextramers. **(A)** Representative dextramers staining of CD8-gated T cells. **(B)** Frequencies and **(C)** numbers of dextramers$^+$ CD8$^+$ T cells in spleen and liver of infected mice. **(D–G)** Percentage of CD44^{hi}CD62L^{lo} **(D)**, CX3CR1$^+$ **(E)**, KLRG1$^+$ **(F)**, and CD38$^+$ **(G)** cells among dextramer$^+$ CD8$^+$ T cells. **(H)** Spleen and liver cells were stimulated for 4 h with OVA$_{257-264}$ peptide and the expression of IFN-γ and TNF-α in CD8$^+$ T cells was determined by intracellular cytokine staining. **(I)** Spleen cells were stimulated for 4 h with PMA/ionomycin, and the expression of IFN-γ and TNF-α in CD4$^+$ T cells was determined by intracellular cytokine staining. Bars in **(C–I)** give the mean ± SEM and were analyzed with the unpaired t-test. Data from one of three experiments are shown.

OT-1 T-cells showed similar induction of IFN-γ and TNF-α and of NURF77 (**Figures 4F, G**). Thus, TRPM2 deficiency restricted to CD8$^+$ T cells did not significantly impair their response during acute infection.

The competitive transfer assay was also used to determine the role of TRPM2 in CD8$^+$ memory T-cell formation. To exclude rejection of donor cells, *Rag1*$^{-/-}$ mice were used as recipients. Eight weeks post transfer and LmOVA infection, donor cells in the spleen, liver, lung, kidney, and bone marrow were analyzed. In the spleen, liver, and bone marrow, we observed ratios of WT to *Trpm2*$^{-/-}$ cells similar to the ratio of the transferred cell population (**Figure 5A**). Interestingly, WT cells were slightly more prominent in lung and kidney, indicating a disadvantage of *Trpm2*$^{-/-}$ CD8$^+$ T cells in migration into or survival within these tissues. Phenotypical characterization revealed similar expression profiles for CD44 and CD62L cells with high frequencies of CD44^{hi}CD62L^{lo} effector/effector memory T cells in the liver, lung, and kidney, and somewhat lower frequencies of these cells in the spleen and bone marrow (**Figure 5B**). Upon peptide restimulation of CD8$^+$ T cells from the spleen of recipients, we observed similar frequencies of TNF-α$^+$IFN-γ$^+$ and NUR77$^+$ T cells in both CD8$^+$ T-cell populations (**Figures 5C, D**).

TRPM2 Deficiency Does Not Impair CD4$^+$ T-Cell Differentiation *In Vivo*

In order to test the response of *Trpm2*$^{-/-}$ CD4$^+$ T cells *in vivo*, we used the model of anti-CD3 mAb-induced intestinal inflammation. In this model, repeated injection of anti-CD3 mAb causes systemic T-cell activation. A main hallmark of the model is the activation and accumulation of Th1 and Th17 cells in the small intestine resulting in inflammation of the intestinal mucosa, and diarrhea and weight loss as disease manifestations. As a consequence of the inflammation, Th17 cells differentiate to IL-10-secreting Tr1 cells and enhanced frequencies of both Tr1 cells and conventional Foxp3$^+$ Treg cells are found in the small intestinal mucosa. Thus, the anti-CD3 application model allows the analyses of Th1, Th17, and Treg cell responses as well as the formation of Tr1 cells (40–43). Four days after anti-CD3 mAb treatment, mice had lost about 15% of their weight; however,

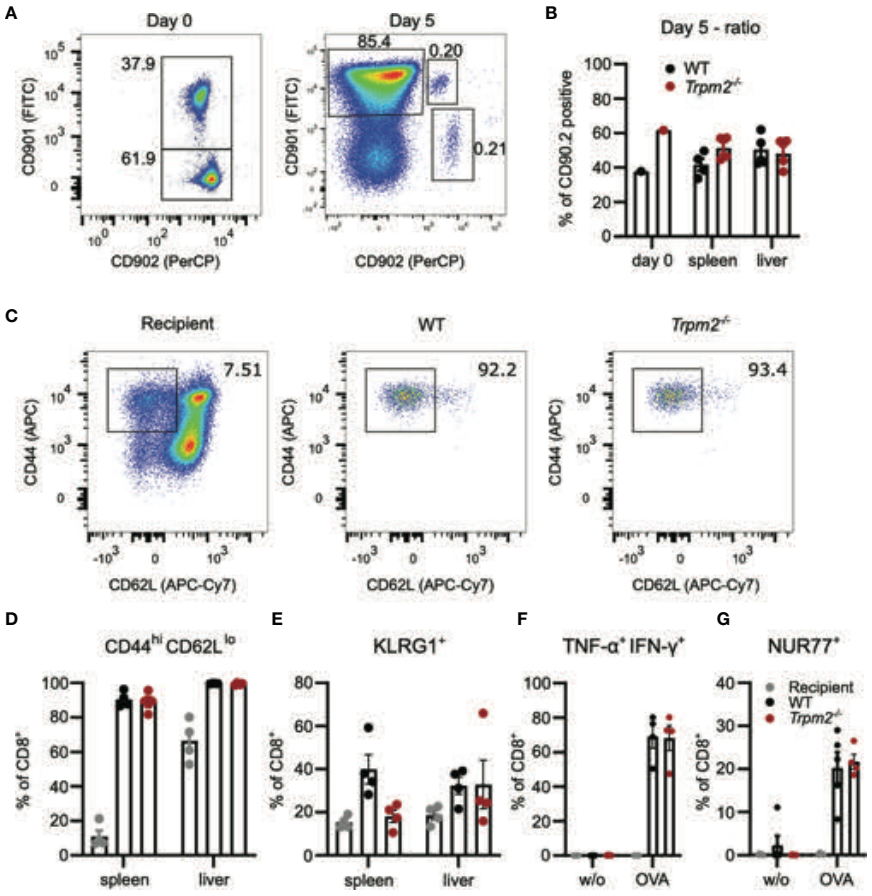

FIGURE 4 | TRPM2 deficiency does not impair the acute CD8$^+$ T-cell response to *L. monocytogenes* in a T-cell transfer model. *Trpm2*$^{-/-}$ CD8$^+$ OT-1 T cells (CD90.1$^-$ CD90.2$^+$) and WT CD8$^+$ OT-1 T cells (CD90.1$^+$CD90.2$^+$) were mixed roughly at a ratio 1:1 and 10^4 CD8$^+$ T cells were i.v. transferred to CD90.1$^+$CD90.2$^-$ WT mice. Recipients were infected on the same day with LmOVA and analyzed 5 days later. **(A)** Representative dot plots for CD90.1 and CD90.2 staining of the transferred CD8$^+$ T-cell population (Day 0) and of the CD8$^+$ T cells from the spleen at day 7. (In the experiment shown, we transferred cells with a 2:3 ratio of WT to *Trpm2*$^{-/-}$ CD8$^+$ T cells.) **(B)** Frequencies of WT and *Trpm2*$^{-/-}$ cells among CD8$^+$ donor T cells at day 0 (mix before transfer) and day 5 postinfection. **(C)** Representative dot plots for CD44 and CD62L expression of donor and recipient CD8$^+$ T cells. **(D)** Frequencies of CD44^{hi}CD62L^{lo} donor and recipient CD8$^+$ T cells in spleen and liver. **(E)** Frequencies of KLRG1$^+$ donor and recipient CD8$^+$ T cells in spleen and liver. **(F)** Spleen cells were stimulated for 4 h with OVA$_{257-264}$ peptide and the frequencies of IFN-γ$^+$ TNF-α$^+$ donor and recipient CD8$^+$ T cells was determined by intracellular cytokine staining. **(G)** Frequencies of NUR77$^+$ donor and recipient CD8$^+$ T cells after OVA$_{257-264}$ peptide stimulation of spleen cells. Bars give the mean ± SEM. Results in **(D–G)** and were analyzed with ANOVA with Dunnett's multiple-comparison test. Experiments were conducted twice.

weight loss was similarly extensive in WT and *Trpm2*$^{-/-}$ mice (**Figure 6A**). Characterization of T cells from the small intestinal mucosa revealed similar frequencies and numbers of CD4$^+$ Th1, Th17, Treg, and Tr1 cells in WT and *Trpm2*$^{-/-}$ mice (**Figure 6B**). Thus, deficiency of TRPM2 did not affect the CD4$^+$ T-cell response in this model.

As discussed in the context of the infection model, TRPM2 deficiency in cells other than T cells could mask an altered CD4$^+$ T-cells response. Therefore, *Rag1*$^{-/-}$ mice were reconstituted with CD4$^+$ T cells from either WT or *Trpm2*$^{-/-}$ mice and then treated with anti-CD3 mAb. Under these conditions, weight loss was less pronounced but similar in mice reconstituted with WT and *Trpm2*$^{-/-}$ cells (**Figure 7A**). Recipients did not differ in the frequencies and numbers of intestinal IFN-γ$^+$ Th1 cells, IL-17A$^+$ Th17 cells, and IFN-γ$^+$IL-17A$^+$ CD4$^+$ T cells as well as in frequencies and numbers of Foxp3$^+$ cells (**Figure 7B**).

In conclusion, we could not demonstrate a substantial role of TRPM2 in the *in vivo* response of CD4$^+$ T cells.

DISCUSSION

Upon TCR stimulation, we observed a similar induction of IRF4, NUR77, and CD69 after 4, 24, and 48 h in both CD4$^+$ and CD8$^+$ T cells from WT and *Trpm2*$^{-/-}$ mice. This result is consistent with the regular early Ca^{2+} signal after TCR stimulation of *Trpm2*$^{-/-}$ T cells reported by Wolf and colleagues (7) and indicates that TRPM2 is not required for early T-cell activation. In line with

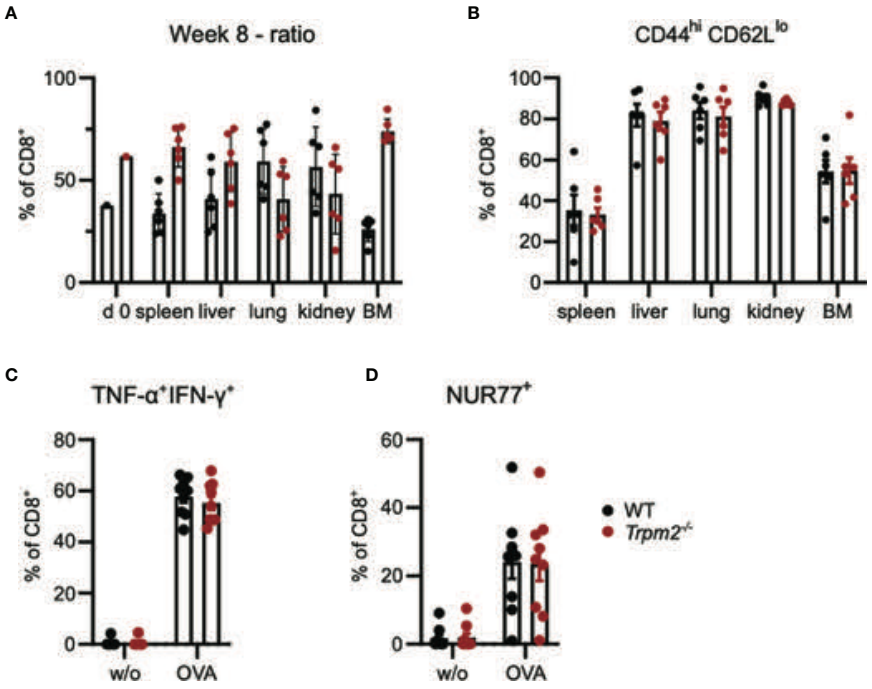

FIGURE 5 | TRPM2 deficiency does not impair the long-term CD8$^+$ T-cell response to *L. monocytogenes* in a T-cell transfer model. 5,000 *Trpm2*$^{-/-}$ CD8$^+$ OT-1 T cells (CD90.1$^-$CD90.2$^+$) and 5,000 WT CD8$^+$ OT-1 T cells (CD90.1$^+$CD90.2$^+$) were mixed and i.v. transferred to *Rag1*$^{-/-}$ mice. Recipients were infected on the same day with LmOVA and analyzed 8 weeks later. **(A)** Frequencies of WT and *Trpm2*$^{-/-}$ cells among CD8$^+$ donor T cells at day 0 (mix before transfer) and 8 weeks postinfection in spleen, liver, lung, kidney, and bone marrow (BM). **(B)** Frequencies of CD44^{hi}CD62L^{lo} donor CD8$^+$ T cells in different tissues. **(C)** Spleen cells were stimulated for 4 h with $OVA_{257-264}$ peptide, and the frequencies of IFN-γ$^+$ TNF-α$^+$ donor and recipient CD8$^+$ T cells were determined by intracellular cytokine staining. **(D)** Frequencies of NUR77$^+$ donor and recipient CD8$^+$ T cells after $OVA_{257-264}$ peptide stimulation of spleen cells. Bars in give the mean ± SEM. Results in **(B–D)** and were analyzed with the unpaired t-test. One representative experiment of three is shown.

this concept, *Trpm2*$^{-/-}$ CD8$^+$ T cells were not impaired in their proliferation after polyclonal stimulation *in vitro* and in their response to *L. monocytogenes* infection *in vivo*. The absence of effect is further consistent with the relatively low expression levels of mRNA for *Trpm2*, *Cd38*, and *Bst1/Cd157* (coding for a NAD-glycohydrolase closely related to CD38 (44) (**Supplementary Figure 1**, Immgen.org (20)) and of TRPM2 protein (**Figures 1A**, **2A** and **Supplementary Figure 2A**)

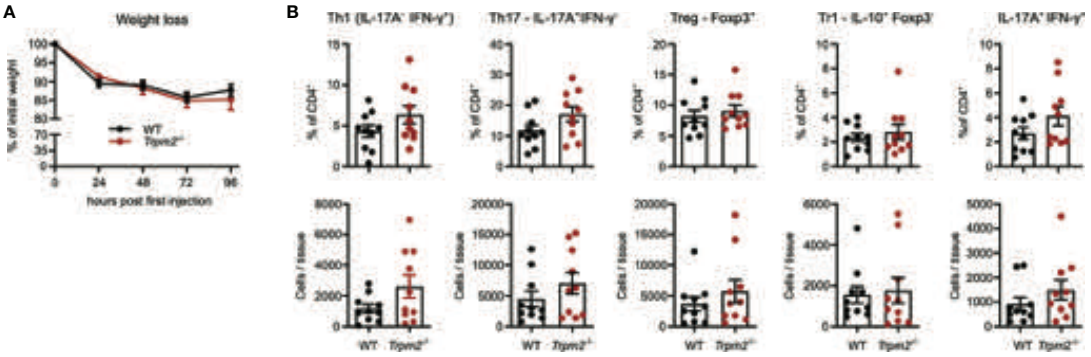

FIGURE 6 | TRPM2 deficiency does not impair the CD4$^+$ T-cell response in response to anti-CD3 mAb induced intestinal inflammation. Mice were i.p. injected with anti-CD3 mAb on days 0, 2, and 4 and analyzed 4 h after the last injection. **(A)** Percentage of initial body weight. **(B)** Frequencies and numbers of different CD4$^+$ T-cell populations in the small intestinal mucosa. Bars depict mean ± SEM. Results were analyzed with the Mann–Whitney test. Data were pooled from two independent experiments.

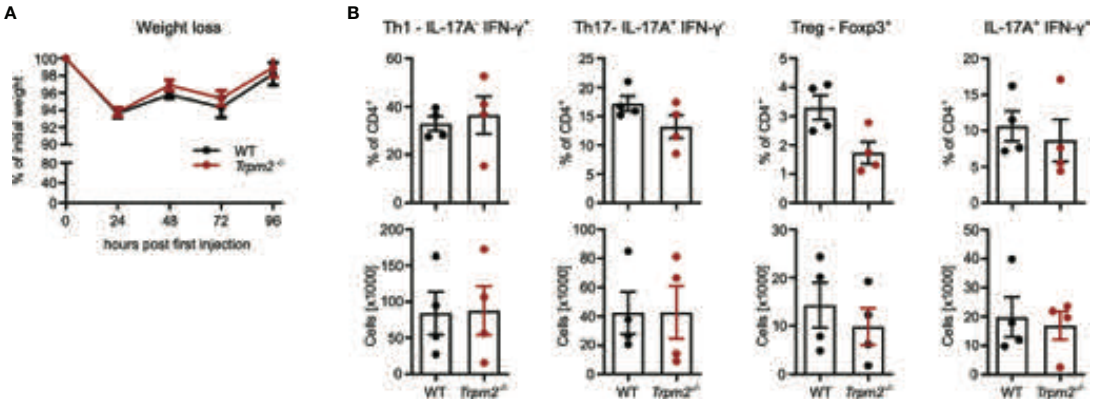

FIGURE 7 | TRPM2 deficiency does not impair response of transferred CD4$^+$ T cells in the model of anti-CD3 mAb induced intestinal inflammation. Total CD4$^+$ T cells from WT and *Trpm2*$^{-/-}$ mice were transferred into *Rag1*$^{-/-}$ mice. After 4 weeks, recipients were treated with anti-CD3 mAb on days 0, 2, and 4 and were analyzed 4 h after the last injection. **(A)** Percentage of initial body weight. **(B)** Frequencies and numbers of different CD4$^+$ T-cell populations in the small intestinal mucosa. Bars depict mean ± SEM. Results were analyzed with the Mann–Whitney test.

in naive mouse CD4$^+$ and CD8$^+$ T cells. Our results are in contrast to results from Melzer et al., who reported reduced *in vitro* proliferation and cytokine production of *Trpm2*$^{-/-}$ T cells (19). Currently, we have no valid explanation for these inconsistent results.

Differentiation of CD4$^+$ Th cells is regulated by signals from the environment, in particular inflammatory cytokines, but also by the quality of the TCR-signal (2–4). Thus, TRPM2-facilitated Ca^{2+} signaling could affect Th-cell differentiation. However, under defined *in vitro* conditions, we observed similar Th1, Th17, Tr1, an Treg-cell differentiation of purified WT and *Trpm2*$^{-/-}$ CD4$^+$ T cells. Consistent with the results from the *in vitro* assays, Th-cell differentiation was also only marginally affected in anti-CD3 mAb-induced inflammation, which is associated with intestinal accumulation of Th1, Th17, Tr1, and Treg cells (40–43). Thus, TRPM2 has, at least in our experimental models, no major function in CD4$^+$ Th-cell differentiation. Interestingly, *Trpm2*$^{-/-}$ mice and WT mice developed comparable symptoms to anti-CD3 mAb treatment. This differs to the attenuated disease of *Trpm2*$^{-/-}$ mice in the dextran sulfate sodium (DSS) model (29). In contrast to the anti-CD3 mAb model in which disease is caused by the response of T cells, the DSS colitis model is primarily driven by innate immune mechanisms after damage and bacterial infiltration of the colon mucosa. Consistent with this notion, the milder course of DSS colitis of *Trpm2*$^{-/-}$ mice is associated with reduced neutrophil but similar T cell accumulation (29).

TRPM2 could be relevant at later stages of the T-cell response for instance due to increased expression levels of TRPM2 or of ADPR generating enzymes. mRNA expression analysis did not reveal major changes in *Trpm2* levels in different T-cell subsets sorted from naïve and infected mice. In contrast, the expression of CD38 was upregulated on effector and memory T-cell subsets (**Figure 1F** and **Supplementary Figure 1**). However, our results from long-term *in vitro* coculture and the analysis of CD8$^+$ T cells 8 weeks post co-transfer and infection argue against such a late function, since we detect no major changes in the ratio of WT and *Trpm2*$^{-/-}$ donor cells in cell culture and in the spleen and liver, the main organs of *L. monocytogenes* infection in the mouse. Interestingly, there was a slightly reduced accumulation of *Trpm2*$^{-/-}$ CD8$^+$ T cells in the lung and kidney. Thus, TRPM2 might be required for the migration of T cells to these tissues or the survival of T cells within these tissues. The CD38–ADPR–TRPM2 axis has been linked to chemokine signaling in myeloid cells (9), and it is possible that this pathway is also active in chemokine signaling in T cells and thereby required for migration of activated T cells to peripheral tissues such as lung and kidney. However, this function would be restricted to only certain tissues and chemokine receptors since we did not observe impaired migration of CD8$^+$ T cells to liver and bone marrow or of CD4$^+$ T cells to the intestinal mucosa.

In summary, our results do not support a major function of TRPM2 in T-cell activation and differentiation. However, we cannot exclude a role of TRPM2 in T-cell subsets or differentiation stages not analyzed in our assays. Our analyses were entirely conducted with mouse T cells and in mouse models. Thus, we can also not exclude that TRPM2 has a more substantial role in human T cells.

DATA AVAILABILITY STATEMENT

The original contributions presented in the study are included in the article/**Supplementary Material**. Further inquiries can be directed to the corresponding author.

ETHICS STATEMENT

The animal study was reviewed and approved by Behörde für Justiz und Verbraucherschutz der Freien und Hansestadt Hamburg.

AUTHOR CONTRIBUTIONS

Conceptualization: NL, MN, AHG, SH, H-WM. Data curation: NL, MN, MC, JS, VS. Methodology: NL, MN, TB, SM, FK-N, SH, H-WM. Formal analysis: NL, MN. Project administration: SH, H-WM. Writing, review, editing: all authors. All authors contributed to the article and approved the submitted version.

FUNDING

This work was supported in part by the Deutsche Forschungsgemeinschaft (project number 335447717, SFB1328: to SH, H-WM, FK-N, and AHG). SH has an endowed Heisenberg-Professorship awarded by the Deutsche Forschungsgemeinschaft. MN has a scholarship from the Else Kröner Stiftung (iPRIME).

ACKNOWLEDGMENTS

We thank Dr. Dietmar Zehn for LmOVA and Dr. Yasuo Mori for *Trpm2*$^{-/-}$ mice.

SUPPLEMENTARY MATERIAL

The Supplementary Material for this article can be found online at: https://www.frontiersin.org/articles/10.3389/fimmu.2021.778916/full#supplementary-material

REFERENCES

1. Le Borgne M, Raju S, Zinselmeyer BH, Le VT, Li J, Wang Y, et al. Real-Time Analysis of Calcium Signals During the Early Phase of T Cell Activation Using a Genetically Encoded Calcium Biosensor. *J Immunol* (2016) 196(4):1471–9. doi: 10.4049/jimmunol.1502414
2. Corse E, Gottschalk RA, Allison JP. Strength of TCR-Peptide/MHC Interactions and *In Vivo* T Cell Responses. *J Immunol* (2011) 186(9):5039–45. doi: 10.4049/jimmunol.1003650
3. Guichard V, Bonilla N, Durand A, Audemard-Verger A, Guilbert T, Martin B, et al. Calcium-Mediated Shaping of Naive CD4 T-Cell Phenotype and Function. *Elife* (2017) 6:e27215. doi: 10.7554/eLife.27215
4. Rogers PR, Croft M. Peptide Dose, Affinity, and Time of Differentiation can Contribute to the Th1/Th2 Cytokine Balance. *J Immunol* (1999) 163(3):1205–13.
5. Ernst IM, Fliegert R, Guse AH. Adenine Dinucleotide Second Messengers and T-Lymphocyte Calcium Signaling. *Front Immunol* (2013) 4:259. doi: 10.3389/fimmu.2013.00259
6. Trebak M, Kinet J-P. Calcium Signalling in T Cells. *Nat Rev Immunol* (2019) 19(3):154–69. doi: 10.1038/s41577-018-0110-7
7. Wolf IM, Diercks B-P, Gattkowski E, Czarniak F, Kempski J, Werner R, et al. Frontrunners of T Cell Activation: Initial, Localized Ca2+ Signals Mediated by NAADP and the Type 1 Ryanodine Receptor. *Sci Signal* (2015) 8(398):ra102–ra. doi: 10.1126/scisignal.aab0863
8. Diercks BP, Werner R, Weidemuller P, Czarniak F, Hernandez L, Lehmann C, et al. ORAI1, STIM1/2, and RYR1 Shape Subsecond Ca(2+) Microdomains Upon T Cell Activation. *Sci Signal* (2018) 11(561):eaat0358. doi: 10.1126/scisignal.aat0358
9. Partida-Sanchez S, Gasser A, Fliegert R, Siebrands CC, Dammermann W, Shi G, et al. Chemotaxis of Mouse Bone Marrow Neutrophils and Dendritic Cells is Controlled by Adp-Ribose, the Major Product Generated by the CD38 Enzyme Reaction. *J Immunol* (2007) 179(11):7827–39. doi: 10.4049/jimmunol.179.11.7827
10. Sumoza-Toledo A, Lange I, Cortado H, Bhagat H, Mori Y, Fleig A, et al. Dendritic Cell Maturation and Chemotaxis is Regulated by TRPM2-Mediated Lysosomal Ca2+ Release. *FASEB J* (2011) 25(10):3529–42. doi: 10.1096/fj.10-178483
11. Knowles H, Li Y, Perraud A-L. The TRPM2 Ion Channel, an Oxidative Stress and Metabolic Sensor Regulating Innate Immunity and Inflammation. *Immunol Res* (2013) 55(1):241–8. doi: 10.1007/s12026-012-8373-8
12. Wang G, Cao L, Liu X, Sieracki NA, Di A, Wen X, et al. Oxidant Sensing by TRPM2 Inhibits Neutrophil Migration and Mitigates Inflammation. *Dev Cell* (2016) 38(5):453–62. doi: 10.1016/j.devcel.2016.07.014
13. Beceiro S, Radin JN, Chatuvedi R, Piazuelo MB, Horvarth DJ, Cortado H, et al. TRPM2 Ion Channels Regulate Macrophage Polarization and Gastric Inflammation During Helicobacter Pylori Infection. *Mucosal Immunol* (2017) 10(2):493–507. doi: 10.1038/mi.2016.60
14. Di A, Kiya T, Gong H, Gao X, Malik AB. Role of the Phagosomal Redox-Sensitive TRP Channel TRPM2 in Regulating Bactericidal Activity of Macrophages. *J Cell Sci* (2017) 130(4):735–44. doi: 10.1242/jcs.196014
15. Morad H, Luqman S, Tan C-H, Swann V, McNaughton PA. TRPM2 Ion Channels Steer Neutrophils Towards a Source of Hydrogen Peroxide. *Sci Rep* (2021) 11(1):9339. doi: 10.1038/s41598-021-88224-5
16. Beck A, Kolisek M, Bagley LA, Fleig A, Penner R. Nicotinic Acid Adenine Dinucleotide Phosphate and Cyclic ADP-Ribose Regulate TRPM2 Channels in T Lymphocytes. *FASEB J* (2006) 20(7):962–4. doi: 10.1096/fj.05-5538fje
17. Gasser A, Glassmeier Gn, Fliegert R, Langhorst MF, Meinke S, Hein Dr, et al. Activation of T Cell Calcium Influx by the Second Messenger ADP-Ribose. *J Biol Chem* (2006) 281(5):2489–96. doi: 10.1074/jbc.M506525200
18. Sano Y, Inamura K, Miyake A, Mochizuki S, Yokoi H, Matsushime H, et al. Immunocyte Ca2+ Influx System Mediated by LTRPC2. *Science* (2001) 293(5533):1327–30. doi: 10.1126/science.1062473
19. Melzer N, Hicking G, Göbel K, Wiendl H. TRPM2 Cation Channels Modulate T Cell Effector Functions and Contribute to Autoimmune CNS Inflammation. *PloS One* (2012) 7(10):e47617. doi: 10.1371/journal.pone.0047617
20. Heng TS, Painter MW. The Immunological Genome Project: Networks of Gene Expression in Immune Cells. *Nat Immunol* (2008) 9(10):1091–4. doi: 10.1038/ni1008-1091
21. Perraud A-L, Fleig A, Dunn CA, Bagley LA, Launay P, Schmitz C, et al. ADP-Ribose Gating of the Calcium-Permeable LTRPC2 Channel Revealed by Nudix Motif Homology. *Nature* (2001) 411(6837):595–9. doi: 10.1038/35079100
22. Wang L, Fu T-M, Zhou Y, Xia S, Greka A, Wu H. Structures and Gating Mechanism of Human TRPM2. *Science* (2018) 362(6421):eaav4809. doi: 10.1126/science.aav4809
23. Huang Y, Winkler PA, Sun W, Lü W, Du J. Architecture of the TRPM2 Channel and its Activation Mechanism by ADP-Ribose and Calcium. *Nature* (2018) 562(7725):145–9. doi: 10.1038/s41586-018-0558-4
24. Yu P, Wang Q, Zhang L-H, Lee H-C, Zhang L, Yue J. A Cell Permeable NPE Caged ADP-Ribose for Studying TRPM2. *PloS One* (2012) 7(12):e51028. doi: 10.1371/journal.pone.0051028
25. Fliegert R, Riekehr WM, Guse AH. Does Cyclic ADP-Ribose (cADPR) Activate the Non-Selective Cation Channel Trpm2? *Front Immunol* (2020) 11:2018. doi: 10.3389/fimmu.2020.02018
26. Hara Y, Wakamori M, Ishii M, Maeno E, Nishida M, Yoshida T, et al. LTRPC2 Ca2+-Permeable Channel Activated by Changes in Redox Status Confers Susceptibility to Cell Death. *Mol Cell* (2002) 9(1):163–73. doi: 10.1016/S1097-2765(01)00438-5
27. Fliegert R, Bauche A, Wolf Perez AM, Watt JM, Rozewitz MD, Winzer R, et al. 2'-Deoxyadenosine 5'-Diphosphoribose is an Endogenous TRPM2 Superagonist. *Nat Chem Biol* (2017) 13(9):1036–44. doi: 10.1038/nchembio.2415
28. Zhao YJ, Lam CM, Lee HC. The Membrane-Bound Enzyme CD38 Exists in Two Opposing Orientations. *Sci Signal* (2012) 5(241):ra67. doi: 10.1126/scisignal.2002700

29. Yamamoto S, Shimizu S, Kiyonaka S, Takahashi N, Wajima T, Hara Y, et al. TRPM2-Mediated Ca 2+ Influx Induces Chemokine Production in Monocytes That Aggravates Inflammatory Neutrophil Infiltration. *Nat Med* (2008) 14(7):738–47. doi: 10.1038/nm1758
30. Knowles H, Heizer JW, Li Y, Chapman K, Ogden CA, Andreasen K, et al. Transient Receptor Potential Melastatin 2 (TRPM2) Ion Channel is Required for Innate Immunity Against Listeria Monocytogenes. *Proc Natl Acad Sci USA* (2011) 108(28):11578–83. doi: 10.1073/pnas.1010678108
31. Robledo-Avila FH, Ruiz-Rosado J, Brockman KL, Partida-Sánchez S. The TRPM2 Ion Channel Regulates Inflammatory Functions of Neutrophils During Listeria Monocytogenes Infection. *Front Immunol* (2020) 11:97. doi: 10.3389/fimmu.2020.00097
32. Qian X, Zhao H, Chen X, Li J. Disruption of Transient Receptor Potential Melastatin 2 Decreases Elastase Release and Bacterial Clearance in Neutrophils. *Innate Immun* (2018) 24(2):122–30. doi: 10.1177/1753425918759181
33. Tripathi JK, Sharma A, Sukumaran P, Sun Y, Mishra BB, Singh BB, et al. Oxidant Sensor Cation Channel TRPM2 Regulates Neutrophil Extracellular Trap Formation and Protects Against Pneumoseptic Bacterial Infection. *FASEB J* (2018) 32(12):fj201800605. doi: 10.1096/fj.201800605
34. Gelderblom M, Melzer N, Schattling B, Gob E, Hicking G, Arunachalam P, et al. Transient Receptor Potential Melastatin Subfamily Member 2 Cation Channel Regulates Detrimental Immune Cell Invasion in Ischemic Stroke. *Stroke* (2014) 45(11):3395–402. doi: 10.1161/STROKEAHA.114.005836
35. Garcia-Rodriguez S, Rosal-Vela A, Botta D, Cumba Garcia LM, Zumaquero E, Prados-Maniviesa V, et al. CD38 Promotes Pristane-Induced Chronic Inflammation and Increases Susceptibility to Experimental Lupus by an Apoptosis-Driven and TRPM2-Dependent Mechanism. *Sci Rep* (2018) 8 (1):3357. doi: 10.1038/s41598-018-21337-6
36. Mombaerts P, Iacomini J, Johnson RS, Herrup K, Tonegawa S, Papaioannou VE. RAG-1-Deficient Mice Have No Mature B and T Lymphocytes. *Cell* (1992) 68(5):869–77. doi: 10.1016/0092-8674(92)90030-G
37. Hogquist KA, Jameson SC, Heath WR, Howard JL, Bevan MJ, Carbone FR. T Cell Receptor Antagonist Peptides Induce Positive Selection. *Cell* (1994) 76 (1):17–27. doi: 10.1016/0092-8674(94)90169-4
38. Zehn D, Lee SY, Bevan MJ. Complete But Curtailed T-Cell Response to Very Low-Affinity Antigen. *Nature* (2009) 458(7235):211–4. doi: 10.1038/nature07657
39. Mercado R, Vijh S, Allen SE, Kerksiek K, Pilip IM, Pamer EG. Early Programming of T Cell Populations Responding to Bacterial Infection. *J Immunol* (2000) 165(12):6833–9. doi: 10.4049/jimmunol.165.12.6833
40. Esplugues E, Huber S, Gagliani N, Hauser AE, Town T, Wan YY, et al. Control of TH17 Cells Occurs in the Small Intestine. *Nature* (2011) 475(7357):514–8. doi: 10.1038/nature10228
41. Huber S, Gagliani N, Esplugues E, O'Connor J, Huber FJ, Chaudhry A, et al. Th17 Cells Express Interleukin-10 Receptor and are Controlled by Foxp3– and Foxp3+ Regulatory CD4+ T Cells in an Interleukin-10-Dependent Manner. *Immunity* (2011) 34(4):554–65. doi: 10.1016/j.immuni.2011.01.020
42. Gagliani N, Vesely MCA, Iseppon A, Brockmann L, Xu H, Palm NW, et al. Th17 Cells Transdifferentiate Into Regulatory T Cells During Resolution of Inflammation. *Nature* (2015) 523(7559):221–U5. doi: 10.1038/nature14452
43. Brockmann L, Soukou S, Steglich B, Czarnewski P, Zhao L, Wende S, et al. Molecular and Functional Heterogeneity of IL-10-Producing CD4(+) T Cells. *Nat Commun* (2018) 9(1):5457. doi: 10.1038/s41467-018-07581-4
44. Malavasi F, Deaglio S, Ferrero E, Funaro A, Sancho J, Ausiello CM, et al. CD38 and CD157 as Receptors of the Immune System: A Bridge Between Innate and Adaptive Immunity. *Mol Med* (2006) 12(11):334–41. doi: 10.2119/2006-00094.Malavasi

Conflict of Interest: The authors declare that the research was conducted in the absence of any commercial or financial relationships that could be construed as a potential conflict of interest.

Publisher's Note: All claims expressed in this article are solely those of the authors and do not necessarily represent those of their affiliated organizations, or those of the publisher, the editors and the reviewers. Any product that may be evaluated in this article, or claim that may be made by its manufacturer, is not guaranteed or endorsed by the publisher.

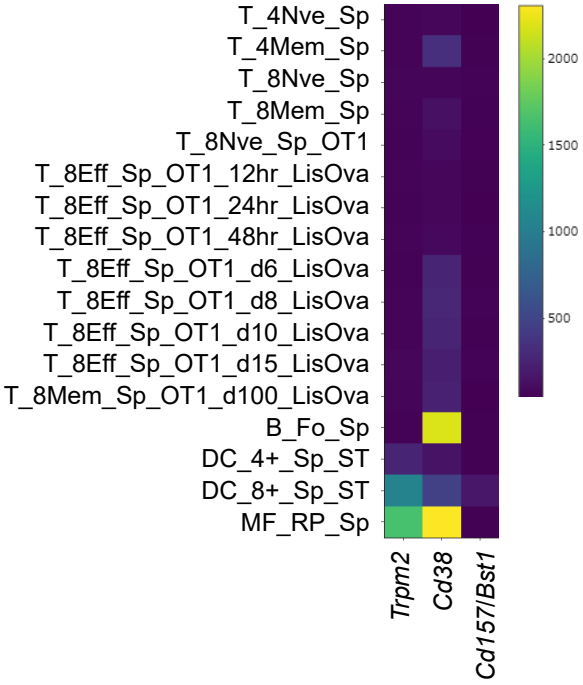

Supplementary Figure 1. mRNA expression of *Trpm2*, *Cd38*, *Bst/Cd157*. mRNA expression for selected mouse leucocyte populations was compiled from the microarray data set of the Immunological Genome Project Consortium (www.immgen.org). MF_RP_Sp: spleen red pulp macrophages; DC_8+_Sp_ST: spleen $CD8^+$ DC; DC_4+_Sp_ST: spleen $CD4^+$ DC; B_Fo_Sp: spleen follicular B cells; T_8Nve_Sp: spleen $CD8^+$ naive T cells; T_8Mem_Sp: spleen $CD8^+$ memory T cells; T_4Nve_Sp: spleen $CD4^+$ naive T cells; T_4Mem_Sp: spleen $CD4^+$ memory T cells; T_8Nve_Sp_OT1: spleen naïve OT-1 CD8 T cells; LisOVA values: OT-1 $CD8^+$ T cells transferred into mice infected with LmOVA and re-isolated at different time point post transfer. Scaling of expression: < 5 traces, 5-20 very low, 20-80 low, 80-800 medium, 800-8000 high.

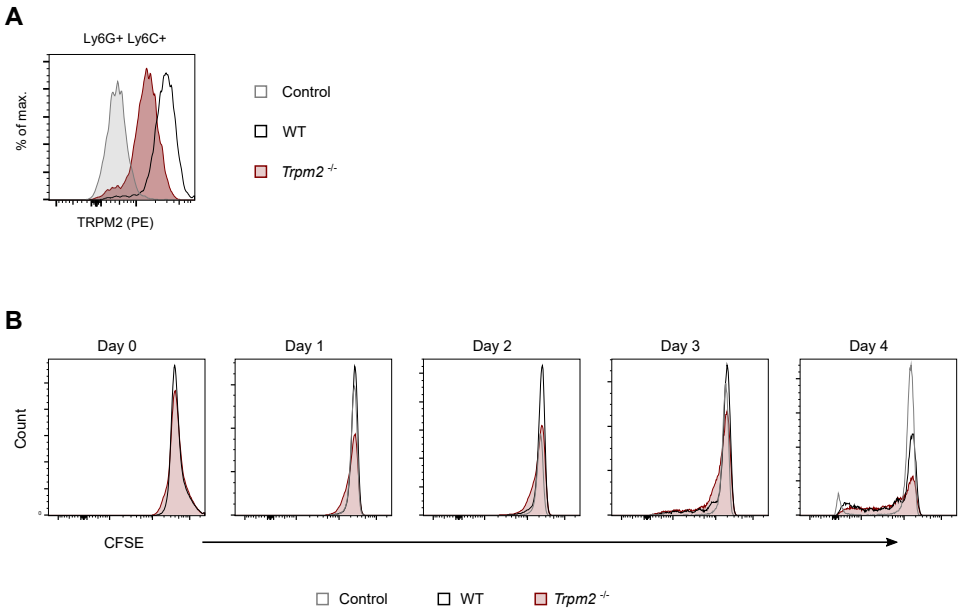

Supplementary Figure 2. TRPM2 expression on myeloid cells and proliferation of CD8$^+$ T cells. (**A**) Ly6C$^+$ and Ly6G$^+$ cells (inflammatory monocytes and neutrophil granulocyte) were intracellularly stained with anti-TRPM2 mAb and PE-conjugated anti-rat IgG antibody (control: WT cells stained only with the secondary antibody). (**B**) Spleen cells were CFSE-labelled and stimulated with anti-CD3ε mAb and anti-CD28 mAb or were cultured without stimulation. Representative results for CFSE intensity on days 0-4 of activated CD8$^+$ T cells from WT and *Trpm2*$^{-/-}$ mice of and non-activated CD8$^+$ T cells from WT mice (control) are shown.

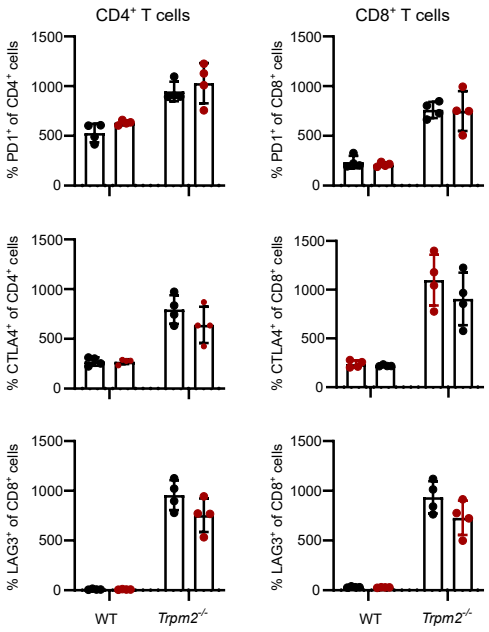

Supplementary Figure 3. Expression of inhibitory receptors on TRPM2-defiecient T cells. Spleen cells from WT and *Trpm2*$^{-/-}$ mice were stimulated for 24h with plate-coated anti-CD3ε mAb and soluble anti-CD28 mAb. Surface expression of PD1 and LAG3 and intracellular expression of CTLA4 was determined by extra and intracellular antibody staining. Bars depict mean ± SEM. Results were analyzed with unpaired t-test.

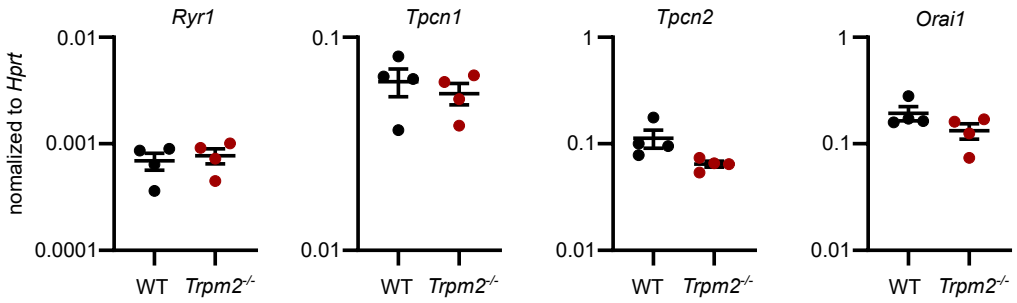

Supplementary Figure 4. Expression of Ca^{2+} channels in *Trpm2*$^{-/-}$ T cells. RNA was isolated from T cells from spleens of WT and *Trpm2*$^{-/-}$ mice. Expression of *Ryr1*, *Tpcn1*, *Tpcn2* and *Orai1* and *Hprt* was quantified in quadruplicates by TaqMan RT-PCR. Expression levels of Ca^{2+} channels were normalized to *Hprt* levels. Results were analyzed with Mann Whitney test.

SCIENCE ADVANCES | RESEARCH ARTICLE

CELL BIOLOGY

P2X4 and P2X7 are essential players in basal T cell activity and Ca^{2+} signaling milliseconds after T cell activation

Valerie J. Brock[1], Insa M. A. Wolf[1], Marco Er-Lukowiak[2], Niels Lory[3], Tobias Stähler[3], Lena-Marie Woelk[4], Hans-Willi Mittrücker[3], Christa E. Müller[5], Friedrich Koch-Nolte[3], Björn Rissiek[2], René Werner[4], Andreas H. Guse[1], Björn-Philipp Diercks[1]*

Initial T cell activation is triggered by the formation of highly dynamic, spatiotemporally restricted Ca^{2+} microdomains. Purinergic signaling is known to be involved in Ca^{2+} influx in T cells at later stages compared to the initial microdomain formation. Using a high-resolution Ca^{2+} live-cell imaging system, we show that the two purinergic cation channels P2X4 and P2X7 not only are involved in the global Ca^{2+} signals but also promote initial Ca^{2+} microdomains tens of milliseconds after T cell stimulation. These Ca^{2+} microdomains were significantly decreased in T cells from *P2rx4*$^{-/-}$ and *P2rx7*$^{-/-}$ mice or by pharmacological inhibition or blocking. Furthermore, we show a pannexin-1–dependent activation of P2X4 in the absence of T cell receptor/CD3 stimulation. Subsequently, upon T cell receptor/CD3 stimulation, ATP release is increased and autocrine activation of both P2X4 and P2X7 then amplifies initial Ca^{2+} microdomains already in the first second of T cell activation.

INTRODUCTION

Efficient immune response requires precisely coordinated signaling pathways, both for cell-to-cell communication and for intracellular signal transduction. Important examples for these molecules involved in T cell activation are Ca^{2+} ions that act intracellularly or adenosine triphosphate (ATP) as a proinflammatory purinergic mediator (*1*, *2*). The signaling pathways of these molecules are prominent targets for therapeutics (*3*–*6*). As T cell activation and signaling provide many potential spots for medical intervention, uncovering interactions between different signaling molecules will improve therapeutical approaches. T cell receptor (TCR)/CD3 complex–stimulated initial Ca^{2+} microdomains in T cells are evoked by the production of nicotinic acid adenine dinucleotide phosphate (NAADP), the most potent Ca^{2+}-mobilizing second messenger (*7*), targeting ryanodine receptor type 1 (RYR1). Furthermore, RYR1 and ORAI1 channels, the latter activated by clusters of "stromal interacting molecule" (STIM) 1 and 2, closely collaborate in this process, likely in endoplasmic reticulum (ER)–plasma membrane (PM) junctions (*8*, *9*). These initial Ca^{2+} microdomains are described as short-lived, highly dynamic Ca^{2+} signals with amplitudes of approximately 200 to 400 nM in primary mouse T cells arising in tens of milliseconds to seconds after stimulation of the TCR/CD3 complex (*8*, *9*). Furthermore, preformed clusters of STIM1 and ORAI1 were found in T cells, resulting in lower and less frequent Ca^{2+} microdomains already without direct stimulation of the TCR/CD3 complex, suggesting a low-grade preactivation of these cells (*9*). Recently, a long sought-after NAADP binding protein named "hematological and neurological expressed 1-like protein" (HN1L)/"Jupiter microtubule associated homolog 2" (JPT2) was found (*10*, *11*). Knockout (KO) of HN1L/JPT2 significantly reduced the number of Ca^{2+} microdomains in primary T cells (*10*), similar to inhibition of NAADP by NAADP antagonist BZ194 treatment or KO of RYR1 (*8*, *9*). Targeting NAADP signaling in a rat model of experimental autoimmune encephalomyelitis by BZ194 resulted in decreased proinflammatory cytokines and attenuated clinical symptoms (*6*).

P2X channels are ligand-gated ion channels activated by ATP (*12*–*14*). The two purinergic channels P2X4 and P2X7 have been shown to play an essential role in T cell function (*15*) and to amplify global Ca^{2+} signaling during T cell activation (*16*–*18*). Targeting P2X7 in a mouse model of contact hypersensitivity, a P2X7-inhibiting nanobody, namely, 13A7-HLE, decreased local inflammation by reducing inflammatory cytokine levels (*19*).

It is known that purinergic signaling is connected to Ca^{2+} signaling: An increasing Ca^{2+} concentration via store-operated Ca^{2+} entry (SOCE) through ORAI1 during T cell activation promotes the production of ATP inside the mitochondria immediately after TCR stimulation (*18*). ATP is transported to the cytosol and is subsequently released via pannexin-1 (PANX1) hemichannels, where it activates P2X4 and P2X7 channels in an autocrine manner, resulting in an influx of Ca^{2+}. These Ca^{2+} signals were visualized several minutes after TCR stimulation (*16*–*18*). Impaired purinergic signaling caused by inhibition of the P2X4 channel in human and mouse T cells prevents T cell proliferation and migration (*20*), demonstrating the important physiological role of purinergic signaling on general T cell function.

In the present study, by using *P2rx4*$^{-/-}$ and *P2rx7*$^{-/-}$ T cells or inhibiting compounds or nanobodies, we show that P2X4 and P2X7 are already involved in the initial step of T cell activation, the generation of initial Ca^{2+} microdomains tens of milliseconds after TCR stimulation. By inhibition of PANX1 or degradation of extracellular ATP, we demonstrate that PANX1 delivers ATP for the extracellular activation of the two P2X channels in this initial step of T cell activation. Moreover, we show that low-grade preactivation of unstimulated T cells not only is dependent on the interaction of STIM1 and ORAI1 (*9*) but also relies on basal ATP release via PANX1 and

[1]The Ca^{2+} Signalling Group, Department of Biochemistry and Molecular Cell Biology, University Medical Center Hamburg-Eppendorf, 20246 Hamburg, Germany. [2]Department of Neurology, University Medical Centre Hamburg Eppendorf, 20246 Hamburg, Germany. [3]Department of Immunology, University Medical Centre Hamburg Eppendorf, 20246 Hamburg, Germany. [4]Department of Computational Neuroscience, University Medical Centre Hamburg Eppendorf, 20246 Hamburg, Germany. [5]Department of Pharmacy, University of Bonn, 53121 Bonn, Germany.
*Corresponding author. Email: b.diercks@uke.de

autocrine activation of P2X4. Thus, our data indicate that purinergic signaling not only amplifies global Ca^{2+} events during T cell activation but also plays an essential role in fine-tuning the basal activity and the initial activation of T cells, opening up advanced possibilities for clinical interventions.

RESULTS

P2X4 and P2X7 are involved in the formation of initial Ca^{2+} microdomains in primary T cells

To analyze the impact of P2X4 and P2X7 on initial Ca^{2+} microdomains, we used a high-resolution Ca^{2+} live-cell imaging system with an acquisition rate of 40 frames/s (*8*, *9*) and freshly isolated primary $CD4^+$ T cells from wild-type (WT), *P2rx4*$^{-/-}$ and *P2rx7*$^{-/-}$ mice on a BALB/c background (*21*). Cells were stimulated with anti-CD3/anti-CD28–coated beads to mimic an immune synapse and stimulation via TCR/CD3 complex plus costimulation via CD28 (further termed TCR/CD3 stimulation). Initial Ca^{2+} microdomains were analyzed in a period from 0.5 s before and up to 15 s after bead contact (Fig. 1A). Directly (50 to 100 ms) after bead contact, WT T cells (Fig. 1A, top) showed increasing Ca^{2+} signals, starting with single local Ca^{2+} microdomains at the bead contact site and resulting in Ca^{2+} events spreading through the whole cell after 15 s. In contrast, T cells from *P2rx4*$^{-/-}$ and *P2rx7*$^{-/-}$ mice (Fig. 1A, middle and bottom) showed decreased Ca^{2+} microdomains directly in the initial period after bead contact. Ca^{2+} microdomains in the first 15 s occurred in 82% of the WT cells with an amplitude of 329 ± 14 nM and a frequency of approximately 0.29 signals per frame, which is equivalent to 12 signals per second. In *P2rx4*$^{-/-}$ and *P2rx7*$^{-/-}$ T cells, microdomains only occurred in 55 and 66% of the cells, with a significantly lower frequency of approximately 0.08 signals per frame (3 signals per second) and 0.1 signals per frame (5 signals per second; Fig. 1B). Moreover, the Ca^{2+} signals from *P2rx4*$^{-/-}$ T cells had a significantly lower amplitude of 266 ± 7 nM compared to the WT cells. By analyzing every 5 to 25 s after TCR stimulation (Fig. 1C), we observed a significantly decreased number of Ca^{2+} signals for cells from *P2rx4*$^{-/-}$ between 5 and 25 s after TCR stimulation, whereas cells from *P2rx7*$^{-/-}$ mice only show significantly decreased Ca^{2+} signals between 5 and 10 s compared to WT cells. The number of these highly dynamic Ca^{2+} microdomains directly at the artificial immune synapse was also decreased in the KOs 50 to 100 ms after stimulation compared to the WT (Fig. 1D), revealing an impact of P2X4 and P2X7 on Ca^{2+} microdomains tens of milliseconds after T cell stimulation.

Next, we compared the differences obtained by gene KOs (WT versus *P2rx4*$^{-/-}$ or *P2rx7*$^{-/-}$) to pharmacological inhibition using the chemical inhibitors for P2X4, 5-BDBD (*22*, *23*) (fig. S1) and PSB-15417 (*24*) (Fig. 2), and the inhibitory nanobody against P2X7, 13A7-dim-Alb (*19*) (Fig. 2). In control cells, Ca^{2+} microdomains occurred again directly (50 to 100 ms) after bead contact, whereas cells with inhibited P2X4 or P2X7 channels just show a few Ca^{2+} signals (Fig. 2A). In the first 15 s upon TCR stimulation, the Ca^{2+} microdomains were significantly decreased for both P2X4- and P2X7-inhibited cells, compared to the respective controls (Fig. 2B). The amplitude of the Ca^{2+} microdomains from cells upon P2X4 inhibition was again significantly reduced (Fig. 2B). The significantly decreased number of Ca^{2+} microdomains by inhibition of P2X4 and P2X7 as well as the decreased amplitude in cells upon P2X4 inhibition are in line with the results from P2X4 and P2X7 KO mice (Fig. 1).

Furthermore, between 2.5 s before and up to 25 s after TCR stimulation, a significant and consistent decrease of Ca^{2+} signals for the cells with inhibition of P2X4 (Fig. 2C, left) and P2X7 (Fig. 2C, right) was observed.

To analyze Ca^{2+} entry at the artificial immune synapse, we further compared Ca^{2+} microdomains in the outer sublayer of the cells at the contact site with the stimulating beads. The number of signals upon P2X4 and P2X7 inhibition was significantly reduced after TCR/CD3 stimulation compared to controls (Fig. 2D). Our results of P2X4 inhibition by PSB-15417 were confirmed with a second inhibitor for this channel, 5-BDBD (fig. S1). Here, we also observed significantly reduced Ca^{2+} signals in the first 15 s after TCR/CD3 stimulation (fig. S1B) as well as directly after stimulation at the artificial immune synapse (fig. S1D). These results substantiate that initial Ca^{2+} entry events were driven by P2X4 and P2X7 channels, leading to the question of interaction of the two channels during this initial phase. P2X4 and P2X7 show the highest sequence similarity compared to other P2X family members, and the *P2rx4* gene is located downstream of the *P2rx7* gene on the same chromosome (*25*, *26*). Moreover, homotrimers of P2X7 were already coimmunoprecipitated with P2X4 in macrophages, and Boumechache and colleagues (*27*) suggested an interaction of the channels inside the receptor complexes. To analyze colocalization during the formation of initial Ca^{2+} signals at the plasma membrane, superresolution imaging with optical reassignment (SoRa) was performed using directly conjugated nanobodies with the fluorophores CF568 and A647 against P2X4 and P2X7. Colocalization of the proteins was analyzed only at the plasma membrane of T cells to study the impact of interaction of P2X4 and P2X7 on Ca^{2+} influx (fig. S2A). During the basal state without stimulation, P2X4 and P2X7 proteins located at the plasma membrane show a slight colocalization of about 11%, and after a short (10-s) activation with soluble anti-CD3, colocalization increased to 15% (fig. S2B). In the first 10 s after stimulation of the cells, no significant increase in colocalization was observed, but after a longer activation time of 5 min, a significantly increased colocalization of P2X4 and P2X7 was observed (fig. S2B). These results indicate the interaction of P2X4 and P2X7 during global Ca^{2+} events, but for the generation of the initial Ca^{2+} microdomains, an extensive interaction of P2X4 and P2X7 seems not to be necessary.

Next, we analyze downstream signaling in *P2rx4*$^{-/-}$ or *P2rx7*$^{-/-}$ $CD4^+$ T cells, as it was reported that $CD4^+$ T cells from mice showed decreased migration upon inhibition of P2X4 and, to a lesser extent, P2X7 and P2X1 channels (*20*). Accordingly, we observed a significantly decreased and delayed global Ca^{2+} response after T cell stimulation with soluble anti-CD3 in *P2rx4*$^{-/-}$ and *P2rx7*$^{-/-}$ compared to $CD4^+$ WT cells (fig. S3, A to C). This further correlates with decreased expression of immediate early gene Nur77 after 18 hours for which the expression level closely reflects the strength of TCR stimulation (*28*) and decreased proliferation of $CD4^+$ T cells for *P2rx7*$^{-/-}$; however, expression of activation marker CD69 was not affected (fig. S3, D to H).

Immediate ATP release following TCR stimulation activates P2X4 and P2X7

P2X4 and P2X7 are activated by extracellular ATP binding to the channels, resulting in Ca^{2+} influx into T cell (*16*, *17*, *29*). Do we observe the same effects as above in Figs. 1 and 2 by removing the P2X4 and P2X7 channel activator, the extracellular ATP? To address this

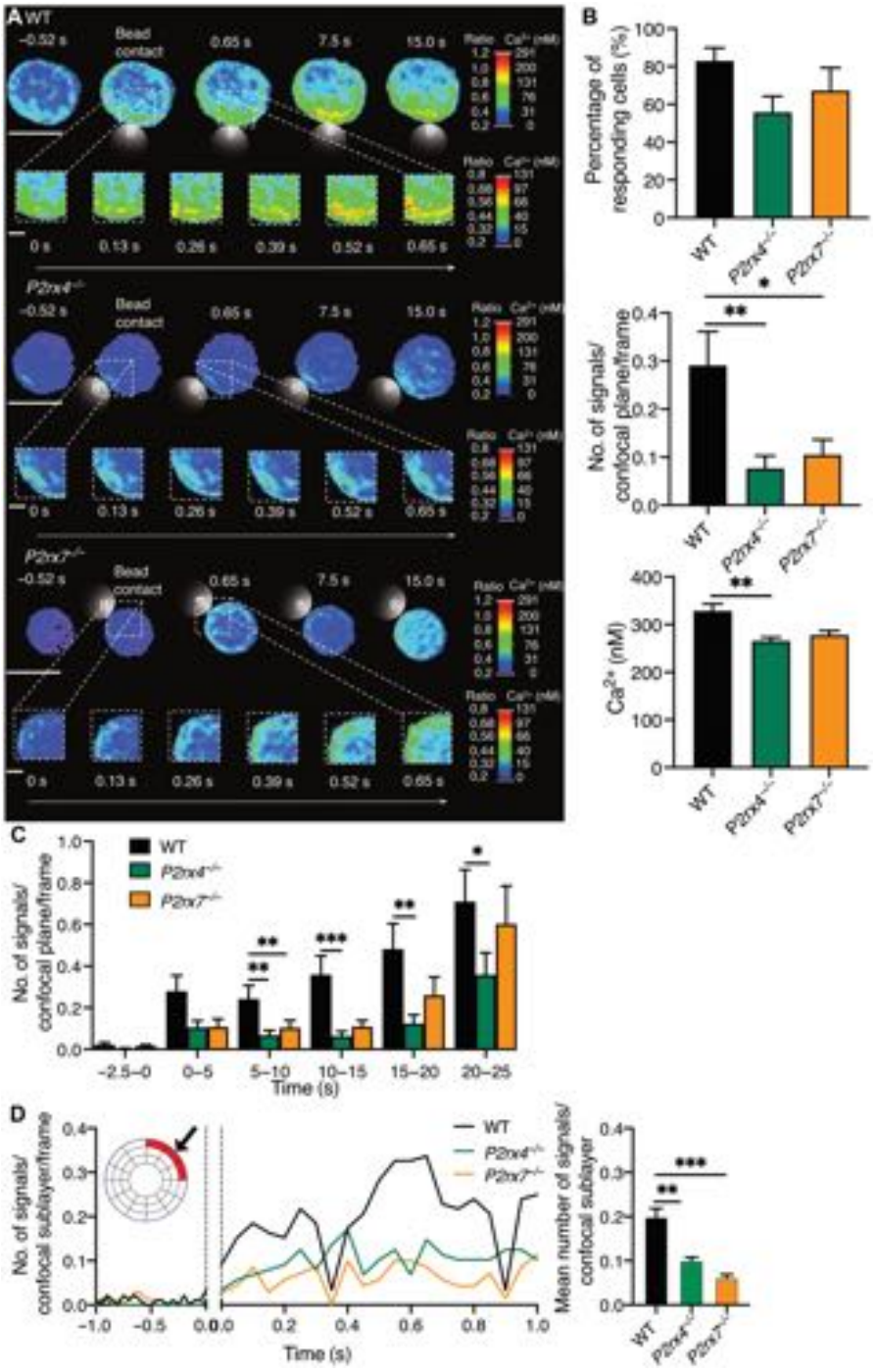

Fig. 1. Decreased Ca^{2+} microdomains in T cells from *P2rx4*$^{-/-}$ and *P2rx7*$^{-/-}$ KO mice. Ca^{2+} imaging of $CD4^+$ T cells of WT or *P2rx4*$^{-/-}$ and *P2rx7*$^{-/-}$ mice. Cells were stimulated with anti-CD3/anti-CD28–coated beads. A minimum of 10 different mice were used. (B to D) Data are means ± SEM; WT, $n = 46$ cells; *P2rx4*$^{-/-}$, $n = 47$ cells; *P2rx7*$^{-/-}$, $n = 39$ cells. Statistical analysis by Kruskal-Wallis test. (**A**) Representative cells of WT or *P2rx4*$^{-/-}$ and *P2rx7*$^{-/-}$ were shown for 0.52 s before and up to 15 s after stimulation with anti-CD3/anti-CD28–coated beads (scale bar, 5 μm) as well as for 0 to 0.65 s in 0.13-s steps zoomed into the region of bead contact (scale bar, 1 μm). (**B**) Quantification of the first 15 s after bead contact for $CD4^+$ T cells of WT or *P2rx4*$^{-/-}$ and *P2rx7*$^{-/-}$ mice. The percentage of responding cells, the number of Ca^{2+} microdomains per frame for whole cells (confocal plane), and the average Ca^{2+} concentration of these signals are shown. (**C**) Quantification of the number of Ca^{2+} microdomains per frame for the period 2.5 to 0 s before and every 5 s after bead contact up to 25 s after bead contact. (**D**) Analysis of the Ca^{2+} microdomains in the first second before and after TCR stimulation for the sublayers at the contact site (as indicated in red) (left). Quantification of the signals in the first second after bead contact (right). *$P < 0.05$, **$P < 0.005$, ***$P < 0.001$.

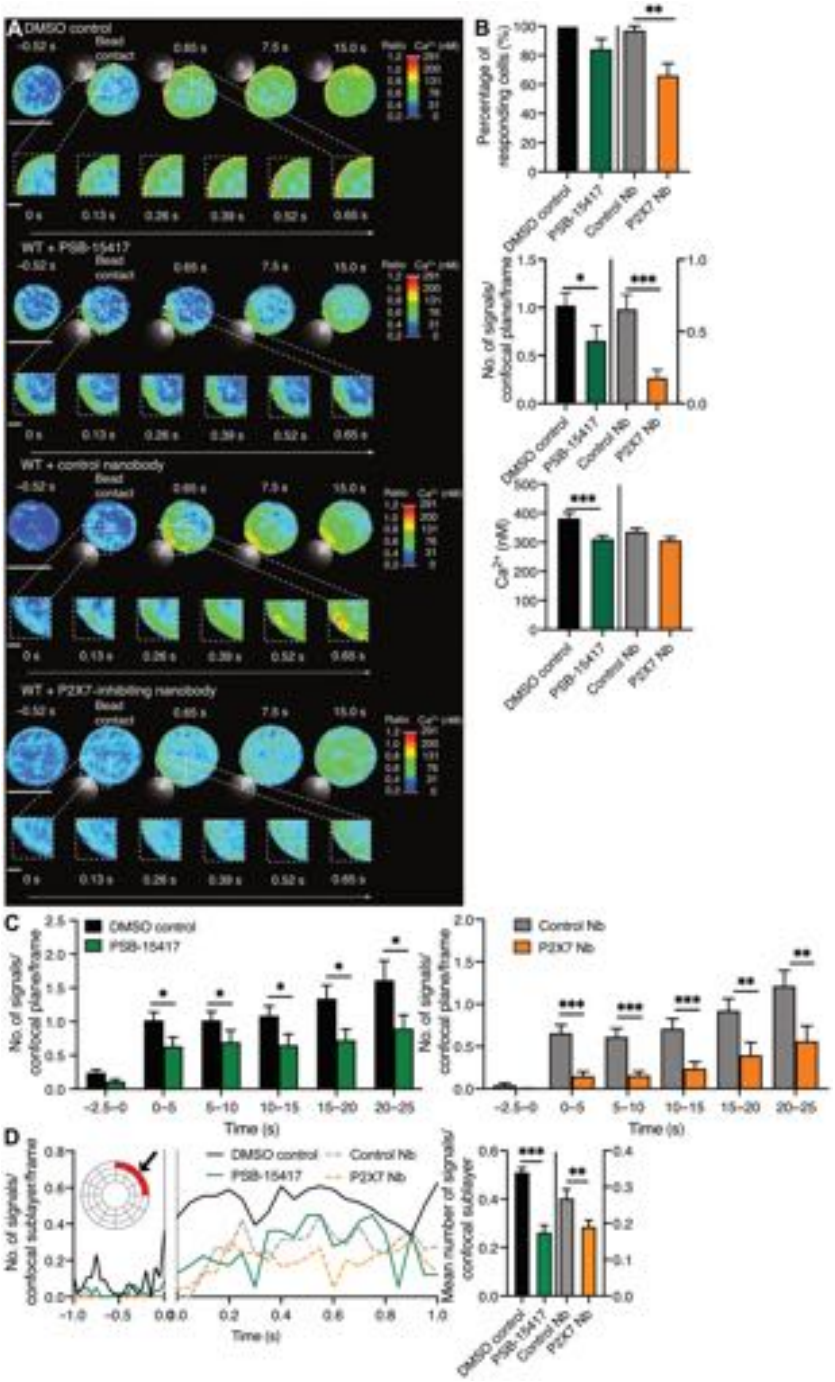

Fig. 2. Reduced Ca^{2+} microdomains in T cells with directly inhibited P2X4 and P2X7 channels. Ca^{2+} imaging of $CD4^+$ T cells of WT mice incubated with or without PSB-15417 (1 μM) for the inhibition of P2X4 or inhibiting nanobody (P2X7-Nb) 13A7-dim-Alb (1 μg/ml) for the inhibition of P2X7. A dimethyl sulfoxide (DMSO) control (0.01%) or an irrelevant nanobody (Control Nb; dummy-dim-Alb, 1 μg/ml) was used. Cells were stimulated with anti-CD3/anti-CD28–coated beads. A minimum of five different mice were used. (B to D) Data are means ± SEM; DMSO control, $n = 28$ cells; control nanobody, $n = 40$; cells treated with PSB-15417, $n = 29$ cells; cells treated with the P2X7-inhibiting nanobody, $n = 30$ cells. Statistical analysis by an unpaired two-tailed Mann-Whitney test. (**A**) , inhibited P2X4 and P2X7 channels were shown for 0.52 s before and up to 15 s after stimulation with anti-CD3/anti-CD28–coated beads (scale bar, 5 μm) as well as for 0 to 0.65 s in 0.13-s steps zoomed into the region of bead contact (scale bar, 1 μm). (**B**) Quantification of the first 15 s after bead contact for $CD4^+$ T cells of controls or inhibited P2X4 and P2X7. (**C**) Quantification of the number of Ca^{2+} microdomains per frame for the period 2.5 to 0 s before and every 5 s after bead contact up to 25 s after bead contact. DMSO control and cells treated with PSB-15417 were compared (left), as well as the control Nb with the P2X7-Nb (right). (**D**) Analysis of the Ca^{2+} microdomains in the first second before and after TCR stimulation for the sublayers at the contact site (as indicated in red) (left). Quantification of the signals in the first second after bead contact (right). $^*P < 0.05$, $^{**}P < 0.005$, $^{***}P < 0.001$.

question, we added apyrase, which hydrolyzes tri- and diphosphate groups of nucleotides (*30*, *31*). Three minutes before Ca^{2+} imaging, WT $CD4^+$ T cells were incubated with apyrase (10 U/ml). After 1 min of measurement, we stimulated the cells with anti-CD3/anti-CD28–coated beads. WT cells without apyrase incubation showed local Ca^{2+} microdomains increasing more and more after 15 s after bead contact through the cell (Fig. 3A, top). In comparison, cells treated with apyrase showed decreased local Ca^{2+} microdomains (Fig. 3A, bottom). In the first 15 s after activation in cells treated with apyrase, microdomains occurred with a significantly decreased frequency compared to the WT (WT, approximately 0.97 signals per frame; apyrase, approximately 0.25 signals per frame; Fig. 3B). In addition, investigating 5-s periods after TCR/CD3 stimulation also significantly reduced Ca^{2+} signals in cells treated with apyrase between 0 and 25 s compared to WT T cells not treated with apyrase that were observed (Fig. 3C). We conclude that the missing extracellular ATP because of degradation by apyrase (Fig. 3) resulted in decreased numbers of initial Ca^{2+} microdomains. As control, the same experiment was carried out using apyrase that was inactivated by boiling for 30 min (fig. S3). T cells incubated with boiled apyrase did not show any altered Ca^{2+} response (fig. S4). These results suggest a very fast release of ATP into the extracellular space. In addition, directly at the artificial immune synapse, we observed a reduced number of Ca^{2+} microdomains tens of milliseconds after stimulation in cells incubated with apyrase (Fig. 3D). Thus, ATP seems to be released immediately after stimulation of T cells, promoting the activation of the purinergic channels P2X4 and P2X7 to generate Ca^{2+} microdomains during the initial phase of Ca^{2+} signaling.

To further understand the mechanism of ATP release, we started to treat WT $CD4^+$ T cells with a mimetic inhibitor peptide for PANX1, termed ^{10}panx1. PANX1 is part of a family of glycoproteins, consisting of three family members PANX1 to PANX3 (*32*), expressed in $CD4^+$ T cells (*33*) acting as the main ATP-releasing channel (*34*, *35*). A typical T cell treated with the PANX1 inhibitor showed less Ca^{2+} signals after bead contact than the WT cell in the first 0.65 s and at the later time point of 15 s after T cell stimulation (Fig. 4A, top). Zoomed into the artificial immune synapse seconds after stimulation, only very few signals were detected for cells treated with ^{10}panx1 (Fig. 4A, bottom). Quantifying the first 15 s after bead contact, Ca^{2+} microdomains were significantly reduced in cells treated with ^{10}panx1 compared to WT T cells (Fig. 4B). To compare the temporal role of ATP release and the activation of the P2X channels in relation to the formation of Ca^{2+} microdomains, the number of Ca^{2+} microdomains was again analyzed 2.5 s before and in 5-s steps after T cell stimulation (Fig. 4C). T cells with reduced ATP release due to the inhibition of PANX1 showed significantly decreased Ca^{2+} signals between 0 and 5 s, 5 and 10 s, and 10 and 15 s. The initial Ca^{2+} microdomains at the artificial immune synapse significantly decreased in T cells treated with ^{10}panx1 compared to WT T cells already in the first second after bead contact (Fig. 4D). Together, T cells reveal a very fast apyrase- or ^{10}panx1-sensitive ATP release into the extracellular space via PANX1, which is responsible for the activation of P2X4 and P2X7, resulting in the amplification of initial Ca^{2+} microdomains.

Basal ATP release via PANX1 activates P2X4 in unstimulated T cells

To understand the fine-tuning of the Ca^{2+} signals after T cell stimulation, Diercks *et al.* (*9*) showed in 2018 that lower and less frequent Ca^{2+} microdomains in the absence of TCR/CD3 stimulation were already produced by preformed clusters of STIM1 and ORAI1. Therefore, we analyzed these Ca^{2+} microdomains using a high-resolution Ca^{2+} live-cell imaging system (*8*, *9*) in P2X4 and P2X7 KO T cells, in cells treated with the P2X4 inhibitor PSB-15417, or in cells treated with the PANX1 inhibitor ^{10}panx1 in the absence of TCR/CD3 stimulation (Fig. 5, A to C). Ca^{2+} microdomains occurred in nonstimulated WT or control T cells already with a lower frequency of approximately 0.07 to 0.2 signals per frame compared to Ca^{2+} microdomains upon TCR/CD3 stimulation with a frequency of approximately 0.3 to 1.0 signals per frame (Figs. 1 to 4B and 5, A to C, number of signals per confocal plane per frame). P2X4 KO cells showed, in the absence of TCR/CD3 stimulation, significantly reduced Ca^{2+} microdomain numbers during a 15-s period without stimulation, whereas *P2rx7*$^{-/-}$ cells showed no altered Ca^{2+} response compared to WT cells (Fig. 5A). The amplitude of the signals in *P2rx7*$^{-/-}$ T cells did not show differences to WT cells. Ca^{2+} signals were also significantly reduced in cells upon P2X4 inhibition by PSB-15417 (*24*), but the amplitude of the signals was not altered (Fig. 5B).

These results indicate a role of P2X4, but not of P2X7, in basal Ca^{2+} signaling in T cells in the absence of TCR/CD3 stimulation. Moreover, we demonstrate that the autocrine release of ATP is responsible for activating P2X4 in unstimulated cells by inhibiting the ATP release channel PANX1. In T cells treated with ^{10}panx1, the number and amplitude of Ca^{2+} signals were significantly decreased compared to the WT (Fig. 5C).

Together, the results reveal two different mechanisms, one for T cells in the absence of TCR/CD3 stimulation and one for the first seconds in activated T cells (Fig. 6, A and B). In the absence of TCR/CD3 stimulation, lower and less frequent Ca^{2+} microdomains (Figs. 5, A to C, and 6A) were promoted via STIM1 and ORAI1 (*9*), resulting in the activation of PANX1 (*36*, *37*). Subsequently, a low basal ATP release via PANX1 activates P2X4. After TCR/CD3 activation, increasing ATP release triggers not only P2X4 but now also the less sensitive P2X7 channel (*38*), leading to the formation of Ca^{2+} microdomains within tens of milliseconds (Figs. 1, 2, and 6B) comparable to our previous model of Ca^{2+} microdomain formation due to RYR1 or ORAI1 and STIM1/2 (*8*–*10*).

DISCUSSION

T cell Ca^{2+} microdomains are evoked upon TCR/CD3 stimulation by the production of NAADP that binds to HN1L/JPT2 and targets RYR1, as well as clusters of STIM1/2 with ORAI1 (*8*–*10*). Using specific inhibitors and cells from suitable KO mice, we identified two purinergic cation channels, namely, P2X4 and P2X7, which are involved in forming initial Ca^{2+} microdomains in tens of milliseconds after TCR/CD3 stimulation. In a similar setup to our experiments, a reduced number of Ca^{2+} microdomains within the first second after TCR/CD3 stimulation was demonstrated for *Orai1*$^{-/-}$, *Stim1*$^{-/-}$, *Stim2*$^{-/-}$, and *Stim1*$^{-/-}$/*2*$^{-/-}$ as well as *Ryr1*$^{-/-}$ T cells or by NAADP antagonism by BZ194 (*9*) and recently by knocking out the NAADP receptor HN1L/JPT2 (*10*). The interaction between STIM1/2 and ORAI1/2/3 and the alteration in Ca^{2+} signaling profiles (*9*) are predicted to have an important influence on downstream effects, like the activation of the nuclear factor of activated T cells (NFAT) (*39*). It was shown that the loss of either STIM1 or STIM2 impairs both the formation of Ca^{2+} microdomains (*9*) and translocation of NFAT1

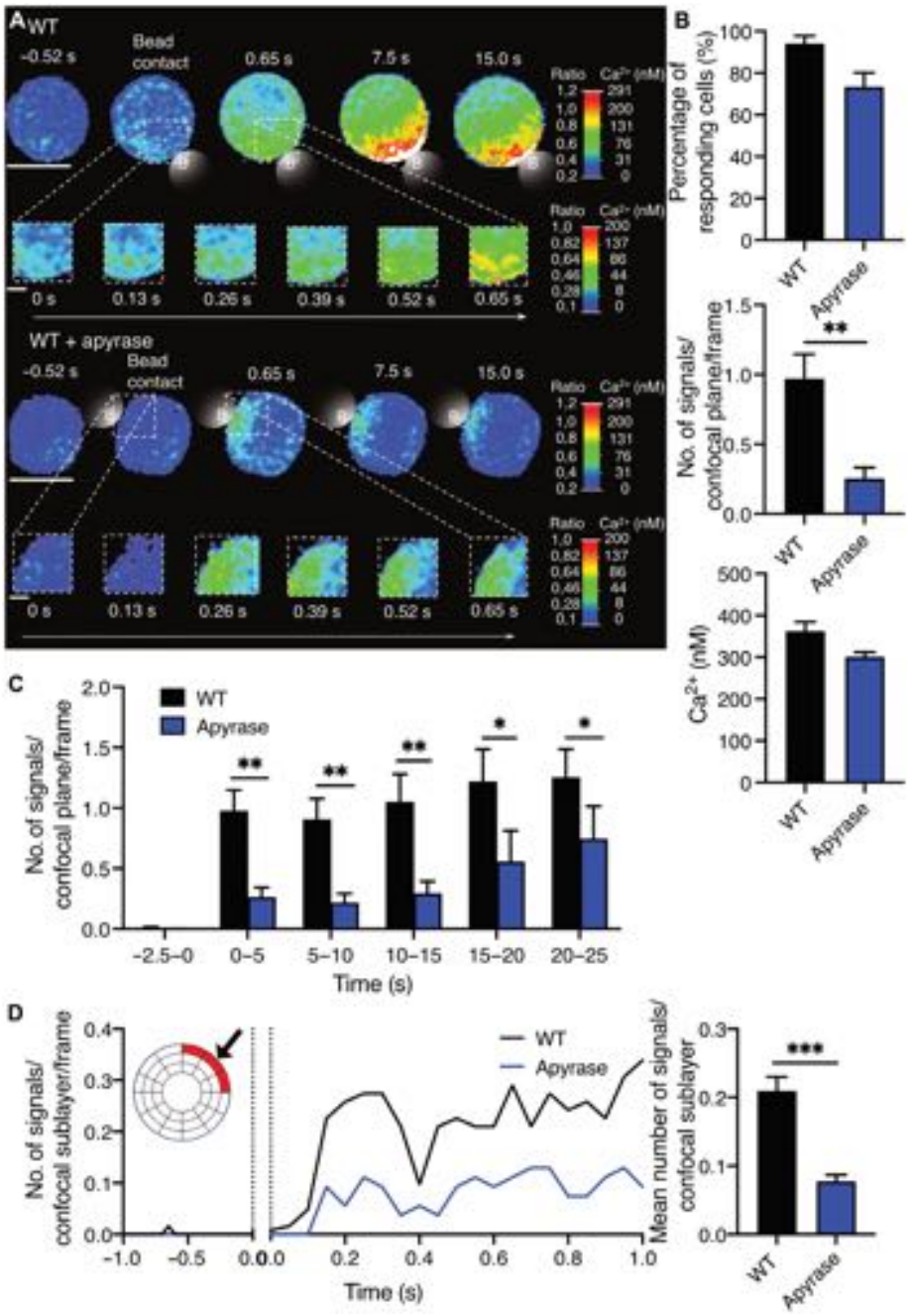

Fig. 3. Removal of extracellular ATP decreases Ca^{2+} microdomains. Ca^{2+} imaging of $CD4^+$ T cells of WT mice incubated with or without 10 U of apyrase. Cells were stimulated with anti-CD3/anti-CD28–coated beads. A minimum of five different mice were used. (B to D) Data are means ± SEM; WT, $n = 31$ cells; cells treated with apyrase, $n = 27$ cells. Statistical analysis was done using a nonparametric unpaired two-tailed Mann-Whitney test. (**A**) Representative cells of WT or cells treated with apyrase were shown for 0.52 s before and up to 15 s after stimulation with anti-CD3/anti-CD28–coated beads (scale bar, 5 μm) as well as for 0 to 0.65 s in 0.13-s steps zoomed into the region of bead contact (scale bar, 1 μm). (**B**) Quantification of the first 15 s after bead contact for $CD4^+$ T cells of WT or cells treated with apyrase. The percentage of responding cells, the number of Ca^{2+} microdomains per frame for whole cells (confocal plane), and the average Ca^{2+} concentration of these signals are shown. (**C**) Quantification of the number of Ca^{2+} microdomains per frame for the period 2.5 to 0 s before and every 5 s after bead contact up to 25 s after bead contact. (**D**) Analysis of the Ca^{2+} microdomains in the first second before and after TCR stimulation for the sublayers at the contact site (as indicated in red) (left). Quantification of the signals in the first second after bead contact (right). *$P < 0.05$, **$P < 0.005$, ***$P < 0.001$.

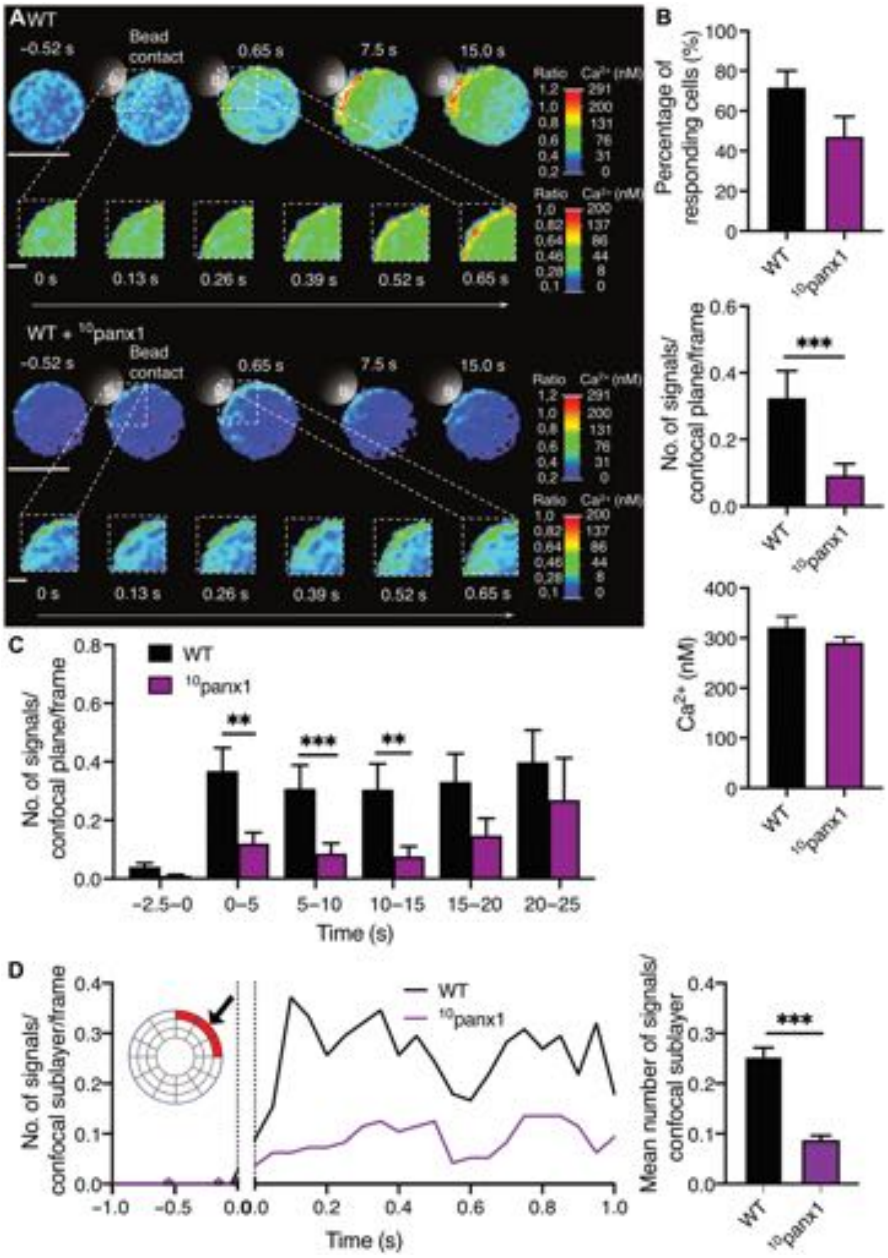

Fig. 4. Inhibition of PANX1 reduces the formation of Ca^{2+} microdomains. Ca^{2+} imaging of $CD4^+$ T cells of WT mice incubated with or without 200 μM PANX1 inhibitor ^{10}panx1 20 min before measurements. Cells were stimulated with anti-CD3/anti-CD28–coated beads. A minimum of 10 different mice were used. (B to D) Data are means ± SEM; WT, $n = 39$ cells; cells treated with ^{10}panx1, $n = 48$ cells. Statistical analysis by an unpaired two-tailed Mann-Whitney test. (**A**) Representative cells of WT or cells treated with ^{10}panx1 were shown for 0.52 s before and up to 15 s after stimulation with anti-CD3/anti-CD28–coated beads for whole cells (scale bar, 5 μm) as well as for 0 to 0.65 s in 0.13-s steps zoomed into the region of bead contact (scale bar, 1 μm). (**B**) Quantification of the first 15 s after bead contact for $CD4^+$ T cells of WT or cells treated with ^{10}panx1. The percentage of responding cells, the number of Ca^{2+} microdomains per frame for whole cells (confocal plane), and the average Ca^{2+} concentration of these signals are shown. (**C**) Quantification of the number of Ca^{2+} microdomains per frame for the period 2.5 to 0 s before and every 5 s after bead contact up to 25 s after bead contact. (**D**) Analysis of the Ca^{2+} microdomains in the first second before and after TCR stimulation for the sublayers at the contact site (as indicated in red) (left). Quantification of the signals in the first second after bead contact (right). $^{**}P < 0.005$, $^{***}P < 0.001$.

and NFAT4 (*40*). Furthermore, antagonizing NAADP by BZ194 results in decreased translocation of NFAT and attenuated clinical scores in rat experimental autoimmune encephalomyelitis (*6*, *41*). NFAT activation is also known to be triggered by purinergic signaling, and loss of P2X7 resulted in diminished NFAT activation (*17*, *42*, *43*). The similarities of downstream effects and alteration in initial Ca^{2+} signaling between the known channels involved in early T cell activation and the two purinergic cation channels P2X4 and P2X7

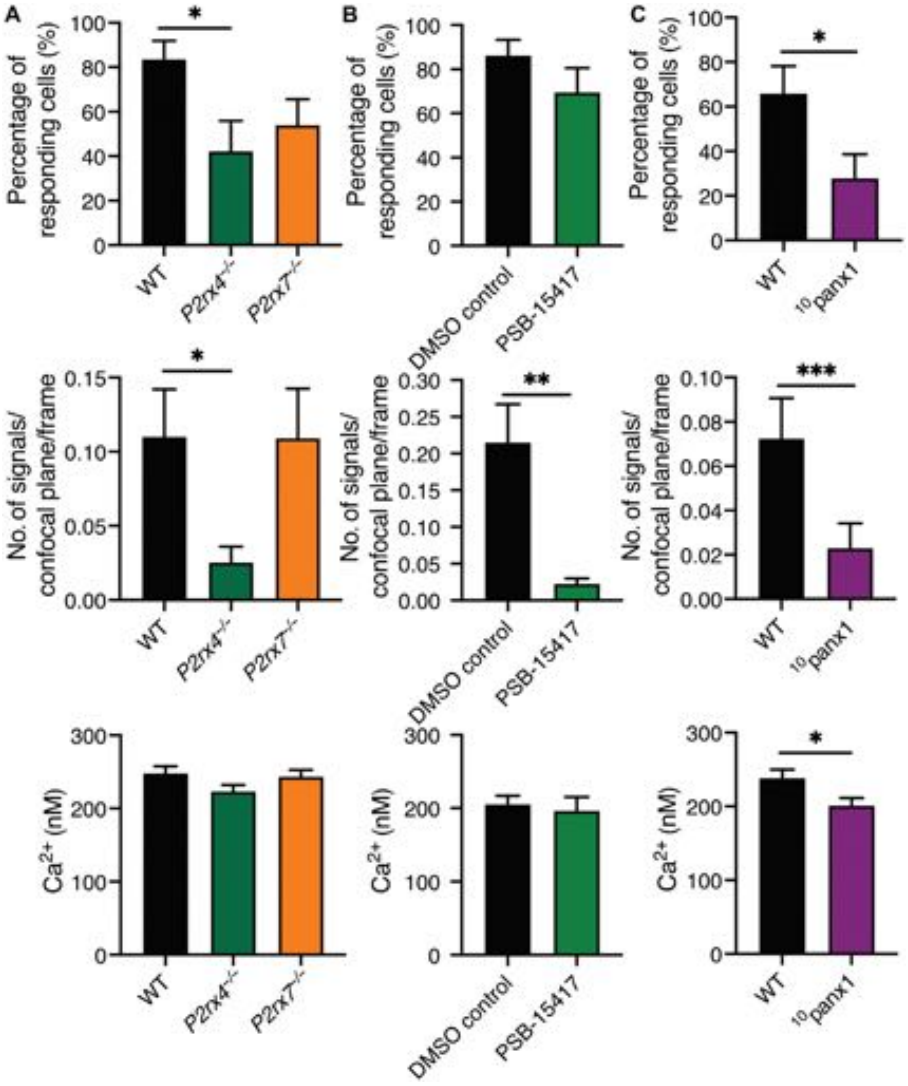

Fig. 5. Basal ATP release via PANX1 activates P2X4, promoting the formation of Ca^{2+} microdomains in the absence of TCR/CD3 stimulation. Ca^{2+} imaging of $CD4^+$ T cells of WT mice or *P2rx4*$^{-/-}$ and *P2rx7*$^{-/-}$ mice. WT cells were incubated with or without PSB-15417 (1 μM) for the inhibition of P2X4 or 200 μM PANX1 inhibitor ^{10}panx1 20 min before measurements. For the P2X4-inhibiting compound, a DMSO control (0.01%) was used. A minimum of four different mice were used. (A to C) Percentage of responding cells, number of Ca^{2+} microdomains per frame for whole cells (confocal plane), and average Ca^{2+} concentration of these signals. Data are means ± SEM; statistical analysis was done by a Kruskal-Wallis test or an unpaired two-tailed Mann-Whitney test. (**A**) Quantification of 15 s without stimulation for $CD4^+$ T cells of WT or *P2rx4*$^{-/-}$ and *P2rx7*$^{-/-}$ mice. WT, $n = 44$ cells; *P2rx4*$^{-/-}$, $n = 45$ cells; *P2rx7*$^{-/-}$, $n = 52$ cells. (**B**) Quantification of 15 s without stimulation for $CD4^+$ T cells of a DMSO control or cells treated with PSB-15417. DMSO control, $n = 35$ cells; cells treated with PSB-15417, $n = 26$ cells. (**C**) Quantification of 15 s without stimulation for $CD4^+$ T cells of WT or cells treated with ^{10}panx1. WT, $n = 40$ cells; cells treated with ^{10}panx1, $n = 47$ cells. $^*P < 0.05$, $^{**}P < 0.005$, $^{***}P < 0.001$.

analyzed in this study are notable. Thus, we need to expand our model of initial T cell activation, including the purinergic pathway on a level equivalent to SOCE and NAADP signaling (Fig. 6B). Upon TCR stimulation, not only the NAADP/HN1L-JPT2/RYR1 axis together with SOCE through STIM1/2 and ORAI1 but also P2X4 and P2X7 are involved in the formation of initial Ca^{2+} microdomains.

An interplay of SOCE with purinergic signaling was already found by Woehrle and colleagues (*16*) in Jurkat T cells, revealing colocalization of ORAI1 and STIM1 with P2X4 within 30 min of stimulation at the immune synapse. The low colocalization of P2X4 and P2X7 during the formation of initial Ca^{2+} microdomains before and after T cell stimulation in the current study indicates no interaction of these channels in the basal state of T cells and the first tens of milliseconds after TCR stimulation. In contrast, at later time points, an increased colocalization was observed, consistent with earlier studies (*27*, *44*). It was not confirmed that P2X4 and P2X7 form stable heteromers (*45*), and a mutual interaction for global Ca^{2+} signals could be assumed because of the impact of both channels on later stages of Ca^{2+} signaling (*12*–*14*, *16*–*18*, *46*) and the increased colocalization of P2X4 and P2X7 after 5 min of TCR stimulation (fig. S2). In addition, we showed the influence of both channels on the initial steps of T cell activation and Ca^{2+} microdomain formation,

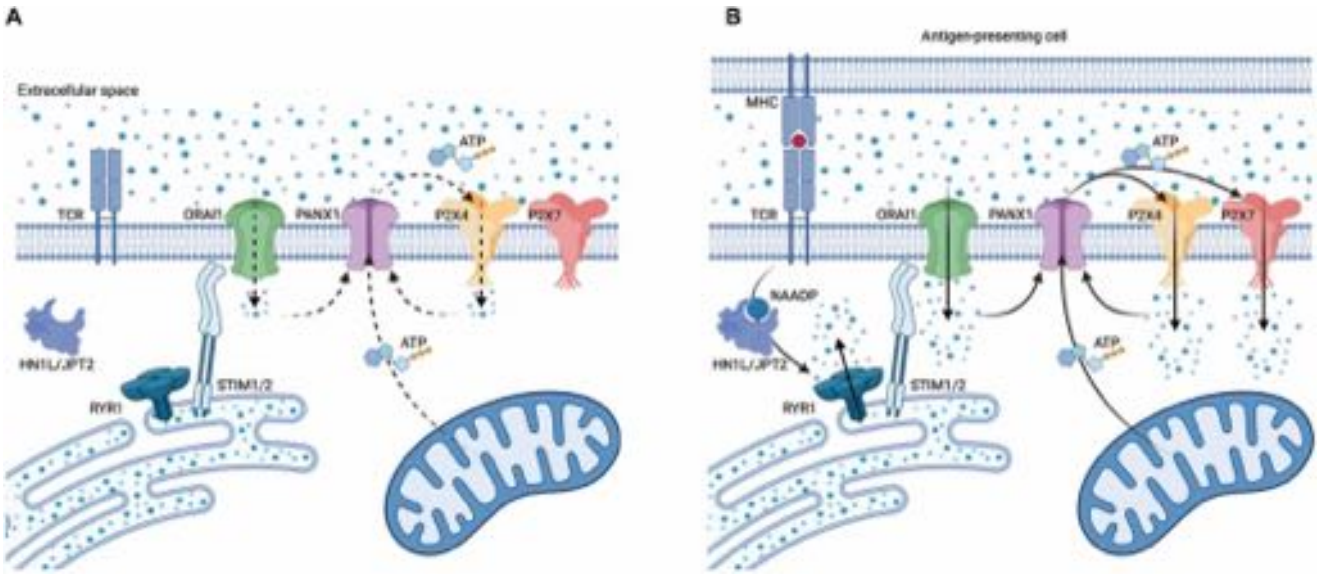

Fig. 6. Summary of Ca^{2+} microdomain formation in preactivated state and milliseconds after T cell activation. Ca^{2+} signaling before and milliseconds after stimulation of the TCR. Blue dots indicate Ca^{2+} signals, and dotted arrows indicate lower amounts of Ca^{2+} or ATP compared to solid arrows. Figures were created with BioRender. (**A**) A basal activity of T cells is due to preformed clusters of STIM1 and ORAI1 resulting in lower and less frequent Ca^{2+} microdomains. PANX1 is probably activated by these Ca^{2+} microdomains and releases low concentrations of ATP, which activates the sensitive purinergic channel P2X4, which also results in lower and less frequent Ca^{2+} microdomains. (**B**) Upon TCR stimulation, on the one hand, RYR1 is activated, probably by NAADP bound to HN1L/JPT2, resulting in local and transient Ca^{2+}release. NAADP-evoked Ca^{2+} release through RYR1 contributes directly to highly dynamic Ca^{2+} microdomains and promotes the activation of STIM1/2 and thus SOCE through ORAI1 channels, leading to an amplification of initial Ca^{2+} microdomains. On the other hand, increasing Ca^{2+} concentrations foster ATP release via PANX1 upon TCR stimulation, which activates P2X4 and the less sensitive P2X7 channel in an autocrine manner, and further promote again an amplification of initial Ca^{2+} microdomains.

but only P2X4 seems to be necessary for basal T cell activity without TCR/CD3 stimulation. Together, the results of colocalization and Ca^{2+} imaging indicate different time slots of P2X4 and P2X7 activity. Whereas P2X4 seems to be already active during antigen-presenting cell (APC) recognition and initial T cell activation, P2X7 is activated not until the initial TCR/CD3 stimulation. The different activation periods of P2X4 and P2X7 may influence downstream mechanisms, such as cytokine expression, T cell migration, or proliferation.

Several downstream effects in mice were previously described, for example, by Ulmann and co-workers (*47*) for P2X4 and Chessell and co-workers (*48*) for P2X7, who analyzed prostaglandin E_2 and different cytokine levels, like interleukin-6 (IL-6), in *P2rx4*$^{-/-}$ or *P2rx7*$^{-/-}$ mice after induced inflammatory pain, suggesting a prominent role of both purinergic channels during initial inflammatory signaling pathways. In human Jurkat T cells with silenced *P2rx4* or *P2rx7*, IL-2 transcription after stimulation with anti-CD3/anti-CD28–coated beads showed a significantly lower response (*16*, *17*). Moreover, inhibition of P2X4 and, to a lesser extent, P2X7 or P2X1 leads to decreased proliferation, and only inhibition of P2X4 reduced the migration of $CD4^+$ T cells from mice (*20*). When combining these published and our own data, the following model was generated: Initial Ca^{2+} microdomains of *P2rx4*$^{-/-}$ or *P2rx7*$^{-/-}$ T cells are decreased in the first tens of milliseconds after T cell stimulation, resulting in a delayed global Ca^{2+} response within minutes and decreased expression of the activation marker Nur77 after 18 hours, apparently translating into reduced proliferation in *P2rx7*$^{-/-}$ (fig. S3, G and H) and migration of T cells upon P2X4 inhibition (*20*).

ATP acts as an essential extracellular signaling molecule, with a crucial role in many cellular processes like cell-to-cell communication, inducing apoptosis, inflammatory reactions, or tumor growth (*49*–*53*). For example, human $CD4^+$ T cells incubated with 250 nM ATP showed increased secretion of cytokines like IL-2 (*52*). Our study suggests that ATP release through PANX1 activates P2X4 and P2X7 channels in an autocrine fashion (Figs. 3 and 4), consistent with earlier investigations (*16*, *46*, *54*, *55*). Hence, removal of extracellular ATP or inhibition of ATP release significantly decreased initial Ca^{2+} microdomains that were observed in tens of milliseconds after TCR/CD3 stimulation (Figs. 3D and 4D), revealing a very fast release of ATP and activation of the two P2X channels. Mitochondrial ATP production and release were also shown for this early time period after T cell stimulation (*18*), once more connecting Ca^{2+} signaling to purinergic signaling, whereby ATP production in the mitochondria depends on initial Ca^{2+} signaling in T cells (*56*, *57*).

More insights into the kinetics of this complex process were obtained by analyzing Ca^{2+} microdomains in T cells in the absence of TCR/CD3 stimulation. The fast release of ATP can be explained by the basal activity of PANX1 activating P2X4 to promote Ca^{2+} microdomains (Fig. 5C). After TCR/CD3 stimulation, the ATP release seems to be fostered to fully activate P2X4 and the less sensitive P2X7 channel (*38*) to promote Ca^{2+} microdomains. A basal T cell activity was also shown by preclustered STIM1 and ORAI1, promoting Ca^{2+} microdomains with lower amplitude and frequency already before T cell stimulation (*9*). We are now able to show the involvement of basal ATP release because of PANX1, resulting in P2X4 activation and the formation of less frequent Ca^{2+} microdomains in unstimulated T cells (Fig. 5, A to C). A basal mitochondrial ATP production in unstimulated cells claimed by Ledderose and colleagues (*58*) supports our findings of basal ATP release via PANX1

and preactivation of P2X4. Moreover, another purinergic channel, P2X1, was recently implicated in this basal phase of $CD4^+$ T cell function, being activated by lower ATP concentrations than P2X4 or P2X7 (*58*). In unstimulated Jurkat T cells, P2X1 and P2X7 act on the activity of mitochondria to produce ATP, revealing a positive feedback loop of purinergic signaling during basal T cell activity (*59*). The importance of the precisely regulated ATP homeostasis is elucidated in cancer cells. Here, the fine-tuning of extracellular ATP concentrations through the purinergic axis of P2X4, P2X7, and PANX1 can decide between a pathway of survival and tumor growth and a P2X7-mediated cell death (*59*–*61*). Different ATP concentrations induce different cellular responses. While ATP in the lower nanomolar range (1 to 50 nM) does not alter either proliferation or cell death of activated conventional $CD4^+$ T cells and regulatory T cells, intermediate concentrations of ATP (250 nM) result in the activation of conventional $CD4^+$ T cells. High concentrations (1 mM) of ATP decrease expression of CD54, CD49d, and CD25 during activation of conventional $CD4^+$ T cells but enhance proliferation, adhesion capacity, and migration of regulatory T cells (*52*). A low permanent ATP release in unstimulated T cells and the formation of Ca^{2+} microdomains might be necessary, or at least supportive, for a fast immune response and APC recognition. To this end, the interaction of purinergic and Ca^{2+} signaling in T cells not stimulated via the TCR/CD3 complex might be an early step of the immune response to be targeted for development of therapeutic interventions. One issue needs to be addressed at this point: There is a huge difference in the sensitivity to ATP concentrations in humans and mice. Cell death is induced in mice by ATP concentrations in the micromolar range, whereas in humans millimolar concentrations are needed (*62*). One possible explanation might be the missing P2Y11 channel in mice (*63*). P2Y11 inhibits the P2X7-dependent pore formation and, to this end, P2X7-mediated cell death, but not Ca^{2+} signaling (*64*). Interaction between P2X and P2Y receptors seems to be adjustable key in ATP balance; P2X1 activity, for example, was shown to be potentiated by coexpression with P2Y1 and P2Y2 (*65*). P2X and P2Y interactions during Ca^{2+} signaling and microdomain formation require further investigations, and the difference between human and mouse channel expression needs to be kept in mind.

In conclusion, we identify a previously unknown function of P2X4 that is required for the formation of Ca^{2+} microdomains in the absence of TCR/CD3 stimulation, probably via a low basal ATP release via PANX1 (Fig. 6A). Moreover, we show that both P2X4 and P2X7 have a central role in initial Ca^{2+} microdomain formation (Fig. 6B) already in tens of milliseconds after T cell stimulation, because these Ca^{2+} microdomains were blocked by hydrolyzing extracellular ATP or blocking PANX1. There are several mechanisms of PANX1 activation (*35*), but how PANX1 is activated during basal T cell activity is still unclear and needs to be addressed in further investigations. It was recently described that PANX1 is activated by increasing Ca^{2+} concentrations (*36*, *37*). To this end, the activation of PANX1 in the absence of TCR/CD3 stimulation might be due to preclustered STIM1 and ORAI1 promoting Ca^{2+} microdomains (*9*).

MATERIALS AND METHODS

Study design

The aim of the study was to analyze the influence of purinergic signaling on the formation of Ca^{2+} microdomains in T cells. Primary murine $CD4^+$ T cells were used, and Ca^{2+} imaging was done in cells with pharmacological or genetic inhibition of P2X4, P2X7, or PANX1 channels. Ca^{2+} microdomain acquisition and detection was performed as previously described (*66*). The Ca^{2+} microdomain detection threshold for microdomains after activation was set to 112 nM and for microdomains without TCR/CD3 stimulation to 90 nM Ca^{2+}. T cells with global and not spatiotemporally restricted Ca^{2+} amplitudes above the threshold of 90 nM were considered as preactivated and not included in this study. Colocalization of P2X4 and P2X7 before and after T cell activation was analyzed using SoRa. Downstream effects were analyzed in WT and genetically inhibited P2X4 and P2X7 $CD4^+$ T cells using flow cytometry. All Ca^{2+} imaging experiments were done three or more times to achieve cell numbers of a minimum of 20. All other experiments were done three times.

Reagents

The Ca^{2+} indicators Fluo4-AM and FuraRed-AM were obtained from Life Technologies. They were dissolved in dimethyl sulfoxide (DMSO), and aliquots were stored at −20°C until measurements. The monoclonal antibodies (mAbs) anti-mouse CD3 and anti-mouse CD28 were obtained from BD Biosciences. The inhibiting compound 5-BDBD was purchased from Tocris; PSB-15417 was provided by C. Müller (Department of Pharmacy, University of Bonn); and the P2X7-inhibiting nanobody 13A7-dim-Alb and the control nanobody dummy-dim-Alb (*19*) as well as directly conjugated nanobodies against P2X4 (dimer + CF568) and P2X7 (dimer + A647) were provided by F. Koch-Nolte (Department of Immunology, University Medical Centre Hamburg Eppendorf). All other reagents were ordered from Sigma-Aldrich.

Animal models

P2rx4$^{-/-}$ (*P2rx4*^{tm1Rass}; MGI (Mouse Genome Informatics):3665297) and *P2rx7*$^{-/-}$ mice (*P2rx7*^{tm1Gab}; MGI:2386080) were backcrossed for 13 generations onto the BALB/c background and were used for experiments along with WT BALB/c mice. All mice were bred at the animal facility of the University Medical Center (UKE). All experiments involving tissue derived from animals were performed with the approval of the responsible regulatory committee (Hamburger Behörde für Gesundheit und Verbraucherschutz, Veterinärwesen/Lebensmittelsicherheit, ORG 941).

Isolation of primary T cells

T cells were isolated from freshly dissected spleens and lymph nodes of WT or KO mice on a BALB/c background. The spleens and lymph nodes were ground through a cell strainer (Ø 40 μm) using the upturned plunger of a syringe in 30 ml of RPMI 1640 containing 25 mM Hepes and GlutaMAX-1 (Gibco, Life Technologies), adding penicillin and streptomycin (100 U/ml) and 7.5% (v/v) newborn calf serum (Biochrom, Merck Millipore). Cell suspension was centrifuged (1200 rpm, 5 min, 4°C), and the cell pellet was dissolved in 5 ml of ammonium-chloride-potassium buffer [4.3 g of ammonium chloride, 0.5 g of $KHCO_3$, and 0.0186 g of Na_2-EDTA in 400 ml of H_2O (pH 7.2 to 7.4)] for 3 to 5 min for lysis of the erythrocytes. After incubation, the lysis was stopped by adding 25 ml of RPMI medium and by centrifuging at 1200 rpm, 5 min, and 4°C. The supernatant was discarded, and cell pellet was dissolved in 2 ml of Dulbecco's phosphate-buffered saline (DPBS) without $CaCl_2$ and $MgCl_2$ (Gibco, Life Technologies). $CD4^+$ T cells were isolated using a negative selection kit according to the manufacturer's protocol (EasySep Mouse $CD4^+$ T Cell Enrichment Kit, STEMCELL

Technologies Inc.). The purity of cells was analyzed by fluorescence-activated cell sorting (FACS) and was up to 97 to 98%.

Local Ca^{2+} imaging in primary T cells and Ca^{2+} microdomain detection

Freshly isolated $CD4^+$ T cells from WT or *P2rx4*$^{-/-}$ or *P2rx7*$^{-/-}$ mice were loaded in RPMI (see above) with the two Ca^{2+} dyes Fluo4 (10 μM) and FuraRed (20 μM), and Ca^{2+} imaging with a frame rate of 40 frames/s was done as described in detail by Diercks *et al.* (*66*). Cells were resuspended in Ca^{2+} buffer [140 mM NaCl, 5 mM KCl, 1 mM $MgSO_4$, 1 mM $CaCl_2$, 20 mM Hepes (pH 7.4), 1 mM NaH_2PO_4, and 5 mM glucose] and imaged for 3 min on coverslips coated with 5 μl of bovine serum albumin (BSA) (5 mg/ml) and 5 μl of poly-L-lysine (0.1 mg/ml). After the first minute, they were either stimulated or not stimulated with anti-CD3/anti-CD28–coated beads adding 10 μl of the bead solution with a pipette, and Ca^{2+} changes were recorded for the last 2 min of measurements. During the postprocessing, all T cells were normalized on bead contact site and time.

For direct inhibition of P2X4 and P2X7, cells were incubated for 30 min before the Ca^{2+} measurements with a P2X4-inhibiting compound (5-BDBD, 10 μM) as well as PSB-15417 (1 μM) or a P2X7-inhibiting nanobody (13A7-dim-Alb, 1 μg/ml). The compounds were resolved in DMSO; to this end, a DMSO control (0.01 and 0.1%) for the measurements was used, as well as a nanobody control (dummy-dim-Alb; 1 μg/ml) for the measurements with the inhibiting nanobody. The addition of apyrase (10 U/ml) 3 min before measurements was used to remove the extracellular ATP. Moreover, a negative control was produced by heating the apyrase up for 30 min at 70°C. To inhibit the PANX1 hemichannel, cells were incubated with the PANX1 mimetic peptide ^{10}panx1 (*67*) at a concentration of 200 μM for 20 min.

Ca^{2+} microdomains, defined as small, compact connected sets of pixels with high $[Ca^{2+}]_i$ values, were detected with a threshold of 112 nM in cells activated with anti-CD3/anti-CD28–coated beads or without stimulation with a threshold of 90 nM in an automated MATLAB script (*66*). To analyze Ca^{2+} microdomains developing close to the bead contact (as shown in Figs. 1D to 4D), the cell shapes were approximated to be circular, all cells of the considered group/condition rotated such that the bead contact sites agreed for the cells, and the cell areas were subdivided in a dartboard-like manner detailed in (*66*). Ca^{2+} microdomain statistics (number of microdomains, associated Ca^{2+} concentration) were then computed for the different dartboard compartments and specified time windows. For Figs. 1D to 4D, the three outer compartments at the bead contact site that are highlighted in red in figures were analyzed.

Colocalization analysis with SoRa

Primary $CD4^+$ T cells from BALB/c mice were left unstimulated or stimulated with soluble anti-CD3 (0.5 mg/ml) for 10 s or 5 min and were seeded on slides coated with poly-L-lysine (0.1 mg/ml). The cells were fixed with 4% (w/v) paraformaldehyde (Alfa Aesar) for 15 min and permeabilized with 0.05% (v/v) saponin (Fluka) again for 15 min. They were incubated overnight at 4°C with 10% (v/v) of fetal bovine serum to block unspecific binding sites. Cells were stained with directly conjugated nanobodies against P2X4 (dimer + CF568; 1:50) and P2X7 (dimer +A647; 1:50) (provided by T. Stähler, Department of Immunology, University Medical Centre Hamburg Eppendorf) for 1 hour. Slides with fixed cells were mounted on coverslips upside down with Abberior Mount solid at 4°C overnight. Image acquisition was done using a superresolution spinning disk microscope (Visitron), a CSU-W1 SoRa optic (2.8×; Yokogawa), a ×100 magnification objective (Zeiss), and a scientific Complementary metal–oxide–semiconductor camera (Orca-Flash 4.0, C13440-20CU, Hamamatsu). The following lasers and filters were used: aP2X4-CF568: excitation, 561 nm laser; emission filter, 609/54 nm; aP2X7-A647: excitation, 640 nm laser; emission, 700/75 nm. Image deconvolution was based on the principle of Arigovindan *et al.* (*68*) [reimplemented and adapted by Woelk *et al.* (*69*)]. For colocalization analysis, the trainable weka (Waikato environment for knowledge analysis) segmentation plugin and a watershed segmentation were used in FIJI (version 2.1.0/1.53c) to improve the separation of the single proteins, which were detected. Only proteins near the plasma membrane were analyzed for colocalization. For the calculation and quantification of the colocalization of P2X4 and P2X7, a MATLAB script, based on the published study by Nauth *et al.* (*70*), was used.

Global Ca^{2+} imaging in primary T cells

Freshly isolated $CD4^+$ T cells from WT, *P2rx4*$^{-/-}$, or *P2rx7*$^{-/-}$ mice were loaded in 500 μl of RPMI (see above) with 4 μM Fura2-AM for 35 min at 37°C. After 20 min of incubation, 2 ml of medium was added. After Fura2 loading, cells were washed with Ca^{2+} buffer [140 mM NaCl, 5 mM KCl, 1 mM $MgSO_4$, 1 mM $CaCl_2$, 1 mM NaH_2PO_4, 20 mM Hepes, and 5.5 mM glucose (pH 7.4) (NaOH), sterile-filtered] (*10*). Ca^{2+} imaging was performed using a Leica IRBE microscope equipped with a 40-fold objective and an electron-multiplying charge-coupled device camera (C9100-13, Hamamatsu). As a light source, a Sutter DG-4 High Speed Wavelength Switcher with the following filter set was used: excitation, hard-coated (HC) 340/26 nm and HC 387/11 nm; beam splitter, 400DCLP; emission, 510/84 nm (*10*). Cells were imaged with an exposure time of 20 ms for 340 and 380 nm for 10 min on slides coated with 5 μl of BSA (5 mg/ml) and 5 μl of poly-L-lysine (0.1 mg/ml) and stimulated with 10 μl of soluble anti-CD3 after 2 min. Image acquisition was done in 16-bit mode with Volocity software (PerkinElmer), and postprocessing like background correction, splitting of the fluorescence channels, and selection of the regions of interest was performed with FIJI software (version 2.1.0/1.53c).

Flow cytometry

Spleen cells were isolated by pressing the organ successively through 70- and 40-μm cell strainers. Erythrocytes were depleted with lysis buffer [155 mM NH_4Cl, 10 mM $KHCO_3$, 10 μM EDTA (pH 7.2)]. Cells were incubated in 500 μl of Iscove's modified Dulbecco's medium (IMDM) supplemented with fetal calf serum, glutamine, gentamicin, and 2-mercaptoethanol. Cells were simulated for 18 hours with anti-CD3ε mAb (1 μg/ml; clone 145-2C11, BioLegend, San Diego, CA) and anti-CD28 mAb (1 μg/ml; clone 37.51, BioLegend). For extracellular antibody staining, cells were incubated in PBS with 1% rat serum and anti–Fc receptor mAb (10 μg/ml) (clone 2.4G2, BioXCell, West Lebanon, NH). Cells were incubated with a fixable dead cell stain (Alexa Flour 750 carboxylic acid, succinimidyl ester, Invitrogen, Eugene, OR), AF700-conjugated anti-CD4 mAb (clone RM4-5, BioLegend), and BV605-conjugated anti-CD69 mAb (clone H1.2F3, BioLegend) for 20 min on ice. Intracellular antibody staining was conducted with the Foxp3/Transcription Factor Staining Buffer Set (Invitrogen) according to the manufacturer's protocol. Cells were stained with phycoerythrin-conjugated anti-NUR77 mAb (clone 12.14, Invitrogen). Cells were analyzed using a FACSCelesta flow

cytometer (BD Biosciences, Franklin Lakes, NJ) and FlowJo software (Tree Star, Ashland, OR).

For the proliferation assay, spleen cells were incubated for 10 min at room temperature with carboxyfluorescein diacetate succinimidyl ester (CFSE) proliferation dye (5 μM; Invitrogen). The cells were washed twice and then incubated with anti-CD3ε mAb (1 μg/ml; clone 145-2C11, BioLegend) and anti-CD28 mAb (1 μg/ml; clone 37.51, BioLegend) in supplemented IMDM. After 3 days, cells were stained with APC-conjugated anti-CD4 mAb (clone RM4-5, eBioscience, San Diego, CA) and a fixable dead cell stain (Alexa Flour 750 carboxylic acid, succinimidyl ester, Invitrogen) and analyzed by FACS.

Statistics

All data are presented as means ± SEM of independent experiments performed as at least triplicates. Data were analyzed using MATLAB software (MathWorks) and Prism 9 (GraphPad Software). Groups were compared using Mann-Whitney *U* or Kruskal-Wallis tests or two-way analysis of variance (ANOVA) and Dunnett's multiple comparisons test. A *P* value of 0.05 was considered as significant.

SUPPLEMENTARY MATERIALS

Supplementary material for this article is available at https://science.org/doi/10.1126/sciadv.abl9770

View/request a protocol for this paper from *Bio-protocol*.

REFERENCES AND NOTES

1. R. Fliegert, J. Heeren, F. Koch-Nolte, V. O. Nikolaev, C. Lohr, C. Meier, A. H. Guse, Adenine nucleotides as paracrine mediators and intracellular second messengers in immunity and inflammation. *Biochem. Soc. Trans.* **47**, 329–337 (2019).
2. M. Trebak, J. P. Kinet, Calcium signalling in T cells. *Nat. Rev. Immunol.* **19**, 154–169 (2019).
3. S. D. Guile, L. Alcaraz, T. N. Birkinshaw, K. C. Bowers, M. R. Ebden, M. Furber, M. J. Stocks, Antagonists of the P2X(7) receptor. From lead identification to drug development. *J. Med. Chem.* **52**, 3123–3141 (2009).
4. E. C. Keystone, M. M. Wang, M. Layton, S. Hollis, I. B. McInnes, Clinical evaluation of the efficacy of the *P2X7* purinergic receptor antagonist AZD9056 on the signs and symptoms of rheumatoid arthritis in patients with active disease despite treatment with methotrexate or sulphasalazine. *Ann. Rheum. Dis.* **71**, 1630–1635 (2012).
5. M. Vaeth, J. Yang, M. Yamashita, I. Zee, M. Eckstein, C. Knosp, U. Kaufmann, P. K. Jani, R. S. Lacruz, V. Flockerzi, I. Kacskovics, M. Prakriya, S. Feske, ORAI2 modulates store-operated calcium entry and T cell-mediated immunity. *Nat. Commun.* **8**, 14714 (2017).
6. C. Cordiglieri, F. Odoardi, B. Zhang, M. Nebel, N. Kawakami, W. E. F. Klinkert, D. Lodygin, F. Lühder, E. Breunig, D. Schild, V. K. Ulaganathan, K. Dornmair, W. Dammermann, B. V. L. Potter, A. H. Guse, A. Flügel, Nicotinic acid adenine dinucleotide phosphate-mediated calcium signalling in effector T cells regulates autoimmunity of the central nervous system. *Brain* **133**, 1930–1943 (2010).
7. A. Guse, I. Ernst, R. Fliegert, NAADP signaling revisited. *Curr. Top. Med. Chem.* **13**, 2978–2990 (2013).
8. I. M. A. Wolf, B. P. Diercks, E. Gattkowski, F. Czarniak, J. Kempski, R. Werner, D. Schetelig, H. W. Mittrücker, V. Schumacher, M. Von Osten, D. Lodygin, A. Flügel, R. Fliegert, A. H. Guse, Frontrunners of T cell activation: Initial, localized Ca2+ signals mediated by NAADP and the type 1 ryanodine receptor. *Sci. Signal.* **8**, ra102 (2015).
9. B. P. Diercks, R. Werner, P. Weidemüller, F. Czarniak, L. Hernandez, C. Lehmann, A. Rosche, A. Krüger, U. Kaufmann, M. Vaeth, A. V. Failla, B. Zobiak, F. I. Kandil, D. Schetelig, A. Ruthenbeck, C. Meier, D. Lodygin, A. Flügel, D. Ren, I. M. A. Wolf, S. Feske, A. H. Guse, ORAI1, STIM1/2, and RYR1 shape subsecond Ca^{2+} microdomains upon T cell activation. *Sci. Signal.* **11**, eaat0358 (2018).
10. H. G. Roggenkamp, I. Khansahib, C. L. C. Hernandez, Y. Zhang, D. Lodygin, A. Krüger, F. Gu, F. Möckl, A. Löhndorf, V. Wolters, D. Woike, A. Rosche, A. Bauche, D. Schetelig, R. Werner, H. Schlüter, A. V. Failla, C. Meier, R. Fliegert, T. F. Walseth, A. Flügel, B. P. Diercks, A. H. Guse, HN1L/JPT2: A signaling protein that connects NAADP generation to Ca^{2+} microdomain formation. *Sci. Signal.* **14**, eabd5647 (2021).
11. G. S. Gunaratne, E. Brailoiu, S. He, E. M. Unterwald, S. Patel, J. T. Slama, T. F. Walseth, J. S. Marchant, Essential requirement for JPT2 in NAADP-evoked Ca^{2+} signaling. *Sci. Signal.* **14**, eabd5605 (2021).
12. U. Schenk, A. M. Westendorf, E. Radaelli, A. Casati, M. Ferro, M. Fumagalli, C. Verderio, J. Buer, E. Scanziani, F. Grassi, Purinergic control of T cell activation by ATP released through pannexin-1 hemichannels. *Sci. Signal.* **1**, ra6 (2008).
13. G. Burnstock, J. M. Boeynaems, Purinergic signalling and immune cells. *Purinergic Signal.* **10**, 529–564 (2014).
14. V. M. Ruiz-Rodríguez, J. D. Cortes-García, M. de Jesús Briones-Espinoza, E. Rodríguez-Varela, M. Vega-Cárdenas, A. Gómez-Otero, M. H. García-Hernández, D. P. Portales-Pérez, P2X4 receptor as a modulator in the function of P2X receptor in CD4+ T cells from peripheral blood and adipose tissue. *Mol. Immunol.* **112**, 369–377 (2019).
15. F. Grassi, The P2X7 receptor as regulator of T cell development and function. *Front. Immunol.* **11**, 1179 (2020).
16. T. Woehrle, L. Yip, A. Elkhal, Y. Sumi, Y. Chen, Y. Yao, P. A. Insel, W. G. Junger, Pannexin-1 hemichannel-mediated ATP release together with P2X1 and P2X4 receptors regulate T-cell activation at the immune synapse. *Blood* **116**, 3475–3484 (2010).
17. L. Yip, T. Woehrle, R. Corriden, M. Hirsh, Y. Chen, Y. Inoue, V. Ferrari, P. A. Insel, W. G. Junger, Autocrine regulation of T-cell activation by ATP release and P2X 7 receptors. *FASEB J.* **23**, 1685–1693 (2009).
18. C. Ledderose, Y. Bao, M. Lidicky, J. Zipperle, L. Li, K. Strasser, N. I. Shapiro, W. G. Junger, Mitochondria are gate-keepers of T cell function by producing the ATP that drives purinergic signaling. *J. Biol. Chem.* **289**, 25936–25945 (2014).
19. W. Danquah, M. S. Catherine, B. Rissiek, C. Pinto, S. P. Arnau, M. Amadi, D. Iacenda, J. H. Knop, A. Hammel, P. Bergmann, N. Schwarz, J. Assunção, W. Rotthier, F. Haag, E. Tolosa, P. Bannas, B. G. Eric, T. Magnus, T. Laeremans, C. Stortelers, F. Koch-Nolte, Nanobodies that block gating of the P2X7 ion channel ameliorate inflammation. *Sci. Transl. Med.* **8**, 366ra162 (2016).
20. C. Ledderose, K. Liu, Y. Kondo, C. J. Slubowski, T. Dertnig, S. Denicoló, M. Arbab, J. Hubner, K. Konrad, M. Fakhari, J. A. Lederer, S. C. Robson, G. A. Visner, W. G. Junger, Purinergic P2X4 receptors and mitochondrial ATP production regulate T cell migration. *J. Clin. Invest.* **128**, 3583–3594 (2018).
21. M. Er-Lukowiak, Y. Duan, F. Rassendren, L. Ulmann, A. Nicke, F. Ufer, M. A. Friese, F. Koch-Nolte, T. Magnus, B. Rissiek, A *P2rx7* passenger mutation affects the vitality and function of T cells in congenic mice. *iScience* **23**, 101870 (2020).
22. B. Balázs, T. Dankó, G. Kovács, L. Köles, M. A. Hediger, Á. Zsembery, Investigation of the inhibitory effects of the benzodiazepine derivative, 5-BDBD on P2X 4 purinergic receptors by two complementary methods. *Cell. Physiol. Biochem.* **32**, 11–24 (2013).
23. C. Coddou, R. Sandoval, M. J. Hevia, S. S. Stojilkovic, Characterization of the antagonist actions of 5-BDBD at the rat P2X4 receptor. *Neurosci. Lett.* **690**, 219–224 (2019).
24. A. Abdelrahman, V. Namasivayam, S. Hinz, A. C. Schiedel, M. Köse, M. Burton, A. El-Tayeb, M. Gillard, J. Bajorath, M. de Ryck, C. E. Müller, Characterization of P2X4 receptor agonists and antagonists by calcium influx and radioligand binding studies. *Biochem. Pharmacol.* **125**, 41–54 (2017).
25. Z. Hou, J. Cao, Comparative study of the P2X gene family in animals and plants. *Purinergic Signal.* **12**, 269–281 (2016).
26. R. Kopp, A. Krautloher, A. Ramírez-Fernández, A. Nicke, P2X7 interactions and signaling—Making head or tail of it. *Front. Mol. Neurosci.* **12**, 183 (2019).
27. M. Boumechache, M. Masin, J. M. Edwardson, D. Górecki, R. Murrell-Lagnado, Analysis of assembly and trafficking of native P2X4 and P2X7 receptor complexes in rodent immune cells. *J. Biol. Chem.* **284**, 13446–13454 (2009).
28. J. F. Ashouri, A. Weiss, Endogenous Nur77 is a specific indicator of antigen receptor signaling in human T and B cells. *J. Immunol.* **198**, 657–668 (2017).
29. F. Di Virgilio, P. Chiozzi, D. Ferrari, S. Falzoni, J. M. Sanz, A. Morelli, M. Torboli, G. Bolognesi, O. R. Baricordi, Nucleotide receptors: An emerging family of regulatory molecules in blood cells. *Blood* **97**, 587–600 (2001).
30. M. Handa, G. Guidotti, Purification and cloning of a soluble ATP-diphosphohydrolase (Apyrase) from potato tubers (Solanum tuberosum). *Biochem. Biophys. Res. Commun.* **218**, 916–923 (1996).
31. M. Tsukimoto, A. Tokunaga, H. Harada, S. Kojima, Blockade of murine T cell activation by antagonists of P2Y6 and P2X7 receptors. *Biochem. Biophys. Res. Commun.* **384**, 512–518 (2009).
32. R. Bruzzone, S. G. Hormuzdi, M. T. Barbe, A. Herb, H. Monyer, Pannexins, a family of gap junction proteins expressed in brain. *Proc. Natl. Acad. Sci. U.S.A.* **100**, 13644–13649 (2003).
33. K. F. Shoji, P. J. Sáez, P. A. Harcha, H. L. Aguila, J. C. Sáez, Pannexin1 channels act downstream of P2X7 receptors in ATP-induced murine T-cell death. *Channels* **8**, 142–156 (2014).
34. W. G. Junger, Immune cell regulation by autocrine purinergic signalling. *Nat. Rev. Immunol.* **11**, 201–212 (2011).
35. Y. H. Chiu, M. S. Schappe, B. N. Desai, D. A. Bayliss, Revisiting multimodal activation and channel properties of Pannexin 1. *J. Gen. Physiol.* **150**, 19–39 (2018).
36. P. Whyte-Fagundes, G. Zoidl, Mechanisms of pannexin1 channel gating and regulation. *Biochim. Biophys. Acta Biomembr.* **1860**, 65–71 (2018).
37. K. A. Taylor, J. R. Wright, M. P. Mahaut-Smith, Regulation of Pannexin-1 channel activity. *Biochem. Soc. Trans.* **43**, 502–507 (2015).

38. K. Kaczmarek-Hájek, É. Lörinczi, R. Hausmann, A. Nicke, Molecular and functional properties of P2X receptors-recent progress and persisting challenges. *Purinergic Signal.* **8**, 375–417 (2012).
39. Y. Gwack, S. Feske, S. Srikanth, P. G. Hogan, A. Rao, Signalling to transcription: Store-operated Ca^{2+} entry and NFAT activation in lymphocytes. *Cell Calcium* **42**, 145–156 (2007).
40. S. M. Emrich, R. E. Yoast, P. Xin, J. Sneyd, D. I. Yule, S. M. Emrich, R. E. Yoast, P. Xin, V. Arige, L. E. Wagner, N. Hempel, D. L. Gill, Article. Omnitemporal choreographies of all five STIM / Orai and IP_3Rs underlie the complexity of mammalian Il Omnitemporal choreographies of all five STIM/Orai and IP_3Rs underlie the complexity of mammalian Ca^{2+} signaling. *CellReports* **34**, 108760 (2021).
41. W. Dammermann, B. Zhang, M. Nebel, C. Cordiglieri, F. Odoardi, T. Kirchberger, N. Kawakami, J. Dowden, F. Schmid, K. Dornmair, M. Hohenegger, A. Flügel, A. H. Guse, B. V. L. Potter, NAADP-mediated Ca^{2+} signaling via type 1 ryanodine receptor in T cells revealed by a synthetic NAADP antagonist. *Proc. Natl. Acad. Sci. U.S.A.* **106**, 10678–10683 (2009).
42. E. Adinolfi, A. L. Giuliani, E. De Marchi, A. Pegoraro, E. Orioli, F. Di Virgilio, The P2X7 receptor: A main player in inflammation. *Biochem. Pharmacol.* **151**, 234–244 (2018).
43. P. Prasai, G. C. Stefos, W. Becker, Extracellular ATP activates NFAT-dependent gene expression in neuronal PC12 cells via P2X receptors. *BMC Neurosci.* **12**, 90 (2011).
44. C. Guo, M. Masin, O. S. Qureshi, R. D. Murrell-Lagnado, Evidence for functional P2X4/P2X7 heteromeric receptors. *Mol. Pharmacol.* **72**, 1447–1456 (2007).
45. A. Nicke, Homotrimeric complexes are the dominant assembly state of native P2X7 subunits. *Biochem. Biophys. Res. Commun.* **377**, 803–808 (2008).
46. C. M. Wang, C. Ploia, F. Anselmi, A. Sarukhan, A. Viola, Adenosine triphosphate acts as a paracrine signaling molecule to reduce the motility of T cells. *EMBO J.* **33**, 1354–1364 (2014).
47. L. Ulmann, H. Hirbec, F. Rassendren, P2X4 receptors mediate PGE2 release by tissue-resident macrophages and initiate inflammatory pain. *EMBO J.* **29**, 2290–2300 (2010).
48. I. P. Chessell, J. P. Hatcher, C. Bountra, A. D. Michel, J. P. Hughes, P. Green, J. Egerton, M. Murfin, J. Richardson, W. L. Peck, C. B. A. Grahames, M. Anna, Y. Yiangou, R. Birch, P. Anand, G. N. Buell, Disruption of the *P2X7* purinoceptor gene abolishes chronic inflammatory and neuropathic pain. *Pain* **114**, 386–396 (2005).
49. M. V. Zamaraeva, R. Z. Sabirov, E. Maeno, Y. Ando-Akatsuka, S. V. Bessonova, Y. Okada, Cells die with increased cytosolic ATP during apoptosis: A bioluminescence study with intracellular luciferase. *Cell Death Differ.* **12**, 1390–1397 (2005).
50. P. Pellegatti, L. Raffaghello, G. Bianchi, F. Piccardi, V. Pistoia, F. Di Virgilio, Increased level of extracellular ATP at tumor sites: In vivo imaging with plasma membrane luciferase. *PLOS ONE* **3**, e2599 (2008).
51. J. Linden, F. Koch-Nolte, G. Dahl, Purine release, metabolism, and signaling in the inflammatory response. *Annu. Rev. Immunol.* **37**, 325–347 (2019).
52. S. Trabanelli, D. Očadlíková, S. Gulinelli, A. Curti, V. Salvestrini, R. de Paula Vieira, M. Idzko, F. Di Virgilio, D. Ferrari, R. M. Lemoli, Extracellular ATP exerts opposite effects on activated and regulatory $CD4^+$ T cells via purinergic P2 receptor activation. *J. Immunol.* **189**, 1303–1310 (2012).
53. T. M. Chused, S. Apasov, M. Sitkovsky, Murine T lymphocytes modulate activity of an ATP-activated P2Z-type purinoceptor during differentiation. *J. Immunol.* **157**, 1371–1380 (1996).
54. C. Ledderose, Y. Bao, J. Zhang, W. G. Junger, Novel method for real-time monitoring of ATP release reveals multiple phases of autocrine purinergic signalling during immune cell activation. *Acta Physiol.* **213**, 334–345 (2015).
55. Z. Deng, Z. He, G. Maksaev, R. M. Bitter, M. Rau, J. A. J. Fitzpatrick, P. Yuan, Cryo-EM structures of the ATP release channel pannexin 1. *Nat. Struct. Mol. Biol.* **27**, 373–381 (2020).
56. P. S. Brookes, Y. Yoon, J. L. Robotham, M. W. Anders, S. S. Sheu, Calcium, ATP, and ROS: A mitochondrial love-hate triangle. *Am. J. Physiol. Cell Physiol.* **287**, C817–C833 (2004).
57. C. J. Fox, P. S. Hammerman, C. B. Thompson, Fuel feeds function: Energy metabolism and the T-cell response. *Nat. Rev. Immunol.* **5**, 844–852 (2005).
58. C. Ledderose, Y. Bao, S. Ledderose, T. Woehrle, M. Heinisch, L. Yip, J. Zhang, S. C. Robson, N. I. Shapiro, W. G. Junger, Mitochondrial dysfunction, depleted purinergic signaling, and defective T cell vigilance and immune defense. *J. Infect. Dis.* **213**, 456–464 (2016).
59. C. Ledderose, T. Woehrle, S. Ledderose, K. Strasser, R. Seist, Y. Bao, J. Zhang, W. G. Junger, Cutting off the power: Inhibition of leukemia cell growth by pausing basal ATP release and P2X receptor signaling? *Purinergic Signal.* **12**, 439–451 (2016).
60. D. Draganov, S. Gopalakrishna-Pillai, Y. R. Chen, N. Zuckerman, S. Moeller, C. Wang, D. Ann, P. P. Lee, Modulation of P2X4/P2X7/Pannexin-1 sensitivity to extracellular ATP via Ivermectin induces a non-apoptotic and inflammatory form of cancer cell death. *Sci. Rep.* **5**, 16222 (2015).
61. O. Kepp, L. Bezu, T. Yamazaki, F. Di Virgilio, M. J. Smyth, G. Kroemer, L. Galluzzi, ATP and cancer immunosurveillance. *EMBO J.* e108130 (2021).
62. B. Rissiek, F. Haag, O. Boyer, F. Koch-Nolte, S. Adriouch, P2X7 on mouse T cells: One channel, many functions. *Front. Immunol.* **6**, 204 (2015).
63. K. Dreisig, B. R. Kornum, A critical look at the function of the P2Y11 receptor. *Purinergic Signal.* **12**, 427–437 (2016).
64. K. Dreisig, L. Sund, M. W. Dommer, N. P. Kristensen, K. Boddum, R. Viste, S. Fredholm, N. Odum, M. Jäättelä, S. Skov, B. R. Kornum, Human $P2Y_{11}$ expression level affects human P2X7 receptor-mediated cell death. *Front. Immunol.* **9**, 1159 (2018).
65. C. Vial, A. B. Tobin, R. J. Evans, G-protein-coupled receptor regulation of P2X1 receptors does not involve direct channel phosphorylation. *Biochem. J.* **382**, 101–110 (2004).
66. B. P. Diercks, R. Werner, D. Schetelig, I. M. A. Wolf, A. H. Guse, High-resolution calcium imaging method for local calcium signaling. *Methods Mol. Biol.* **1929**, 27–39 (2019).
67. P. Pelegrin, A. Surprenant, Pannexin-1 mediates large pore formation and interleukin-1β release by the ATP-gated P2X7 receptor. *EMBO J.* **25**, 5071–5082 (2006).
68. M. Arigovindan, J. C. Fung, D. Elnatan, V. Mennella, Y. H. M. Chan, M. Pollard, E. Branlund, J. W. Sedat, D. A. Agard, High-resolution restoration of 3D structures from widefield images with extreme low signal-to-noise-ratio. *Proc. Natl. Acad. Sci. U.S.A.* **110**, 17344–17349 (2013).
69. L. M. Woelk, S. A. Kannabiran, V. J. Brock, C. E. Gee, C. Lohr, A. H. Guse, B. P. Diercks, R. Werner, Time-dependent image restoration of low-SNR live-cell Ca2+ fluorescence microscopy data. *Int. J. Mol. Sci.* **22**, 11792 (2021).
70. T. Nauth, F. Huschka, M. Schweizer, J. B. Bosse, A. Diepold, A. V. Failla, A. Steffen, T. Stradal, M. Wolters, M. Aepfelbacher, Visualization of translocons in Yersinia type III protein secretion machines during host cell infection. *PLOS Pathog.* **14**, e1007527 (2018).

Acknowledgments: We acknowledge discussions with members of The Calcium Signalling Group and members of SFB 1328. Nb13A7 can be provided by F.K.-N. pending scientific review and a completed material transfer agreement. Requests for Nb13A7 should be submitted to nolte@uke.de. **Funding:** This work was supported by Deutsche Forschungsgemeinschaft (DFG) (project number 335447717; SFB 1328, project A01 to A.H.G.; project A02 to B.-P.D. and R.W.; project A03 to H.-W.M.; project A10 and Z01 to F.K.-N.; and project A11 to C.E.M.); Joachim-Herz-Stiftung (Hamburg), Infectophysics Consortium (project 4, to A.H.G.); NCL-Stiftung Hamburg (to A.H.G.); the Hamburg Ministry of Science, Research and Equality (LFF-FV75/0070-134, to A.H.G.); and University Medical Center Hamburg-Eppendorf (M3I consortium, to A.H.G.). **Author contributions:** Conceptualization: I.M.A.W., A.H.G., and B.-P.D. Methodology: V.J.B., B.-P.D., L.-M.W., R.W., M.E.-L., B.R., T.S., F.K.-N., and C.E.M. Investigation: V.J.B., M.E.-L., N.L., and T.S. Visualization: V.J.B., I.M.A.W., N.L., A.H.G., and B.-P.D. Funding acquisition: I.M.A.W., B.-P.D., R.W., A.H.G., F.K.-N., C.E.M., and H.-W.M. Supervision: B.-P.D., I.M.A.W., R.W., A.H.G., F.K.-N., C.E.M., and H.-W.M. Writing—original draft: V.J.B. Writing—review and editing: V.J.B., B.-P.D., A.H.G., R.W., B.R., and H.-W.M. **Competing interests:** F.K.-N. is the inventor on a patent related to this work, filed by the University Medical Center Hamburg-Eppendorf and Ablynx NV (WO2013178783, filed on 31 May 2013, published on 5 December 2013). The authors declare no other competing interests. **Data and materials availability:** All data needed to evaluate the conclusions in the paper are present in the paper and/or the Supplementary Materials.

Submitted 17 August 2021
Accepted 14 December 2021
Published 4 February 2022
10.1126/sciadv.abl9770

Science Advances
AAAS

Supplementary Materials for

P2X4 and P2X7 are essential players in basal T cell activity and Ca^{2+} signaling milliseconds after T cell activation

Valerie J. Brock, Insa M. A. Wolf, Marco Er-Lukowiak, Niels Lory, Tobias Stähler, Lena-Marie Woelk, Hans-Willi Mittrücker, Christa E. Müller, Friedrich Koch-Nolte, Björn Rissiek, René Werner, Andreas H. Guse, Björn-Philipp Diercks*

*Corresponding author. Email: b.diercks@uke.de

Published 4 February 2022, *Sci. Adv.* **8**, eabl9770 (2022)
DOI: 10.1126/sciadv.abl9770

This PDF file includes:

Supplementary Material

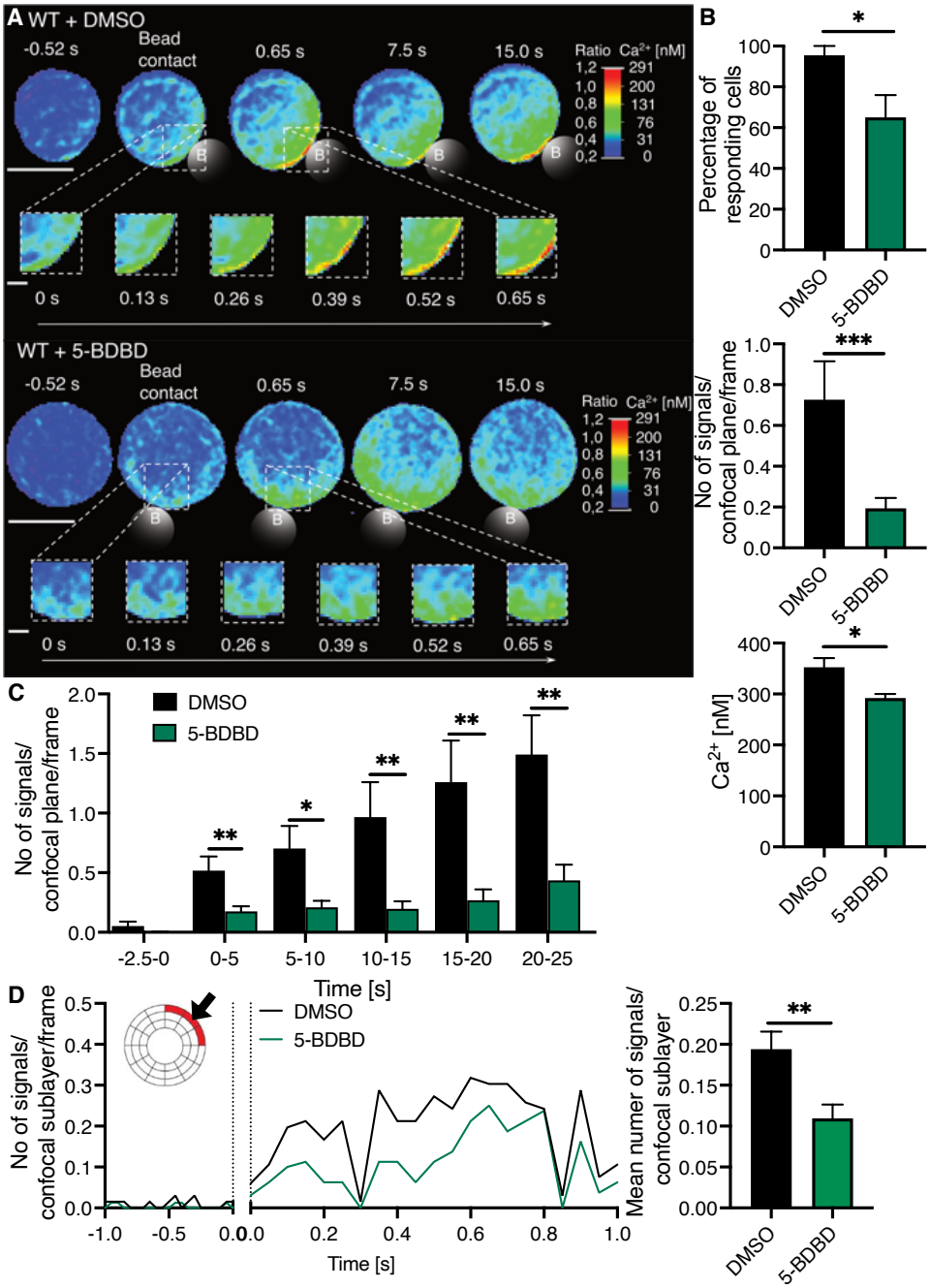

Supplementary Fig. 1: Reduced Ca^{2+} microdomains in T cells with directly inhibited P2X4 channels (5-BDBD)

$CD4^+$ T cells of WT mice were loaded with Fluo4 and FuraRed and incubated with or without 5-BDBD (10 µM) for the inhibition of P2X4. A DMSO control (0.01 %) was used. Ca^{2+} imaging was done to analyze local Ca^{2+} events as described in Materials and Methods. Six different mice were used. Data are mean ± SEM, DMSO control n = 33 cells, 5-BDBD n = 40 cells. Statistical analysis by an unpaired two-tailed Mann-Whitney test.

(A) Representative cells of WT mice with control (DMSO) or 5-BDBD treatment are shown for 0.52 s before and up to 15 s after stimulation with anti-CD3/anti-CD28 coated beads (scale bar 5 µm) as well as for 0 s up to 0.65 s in 0.13 s steps zoomed into the region of bead contact (scale bar 1 µm).

(B) Quantification of the first 15 s after bead contact for $CD4^+$ T cells of WT mice with control or 5-BDBD treatment. Percentage of responding cells, the number of Ca^{2+} microdomains per frame for whole cells (confocal plane) and the average Ca^{2+} concentration of these signals are shown.

(C) Quantification of the number of Ca^{2+} microdomains per frame for the period 2.5 to 0 s before and every 5 s after bead contact up to 25 s after bead contact.

(D) Analysis of the Ca^{2+} microdomains in the first second before and after TCR stimulation for the sublayers at the contact site (as indicated in red, left panel). Quantification of the signals in the first second after bead contact (right panel).

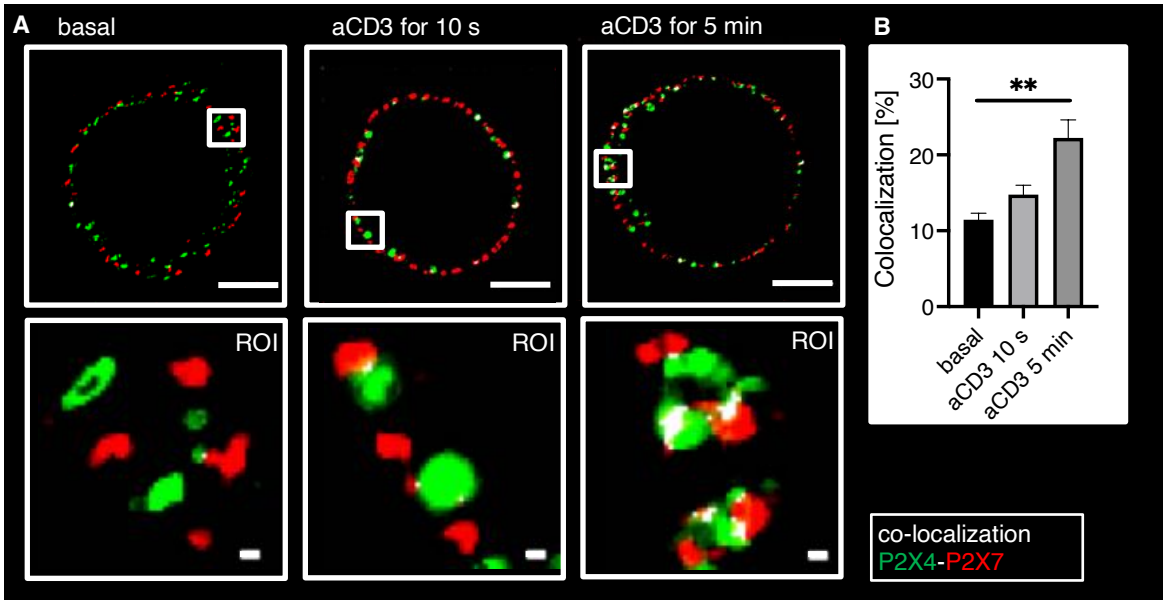

Supplementary Fig. 2: Co-localization of P2X4 and P2X7 protein in activated primary murine T cells

$CD4^+$ T cells of WT mice were stained with directly conjugated nanobodies against P2X4 (+CD568) and P2X7 (+AF647) as described in Materials and Methods and activated with 0.5 mg/ml soluble anti-CD3.

(A) Representative cell after WEKA segmentation without stimulation (basal), after 10 s of stimulation and after 5 min of stimulation with soluble anti-CD3. P2X4 proteins are indicated in green, P2X7 in red and colocalization of both proteins is indicated in white. Scale bar for whole cell image = 2 µm, for ROIs = 100 nm.

(B) Quantification of colocalization of P2X4 and P2X7 after no stimulation (basal), after short stimulation (10 s) and after longer stimulation (5 min). Data are mean ± SEM, basal n = 38 cells, 10 s of stimulation n = 56 cells and 5 min of stimulation n = 45 cells. Statistical analysis by a Kruskal-Wallis test.

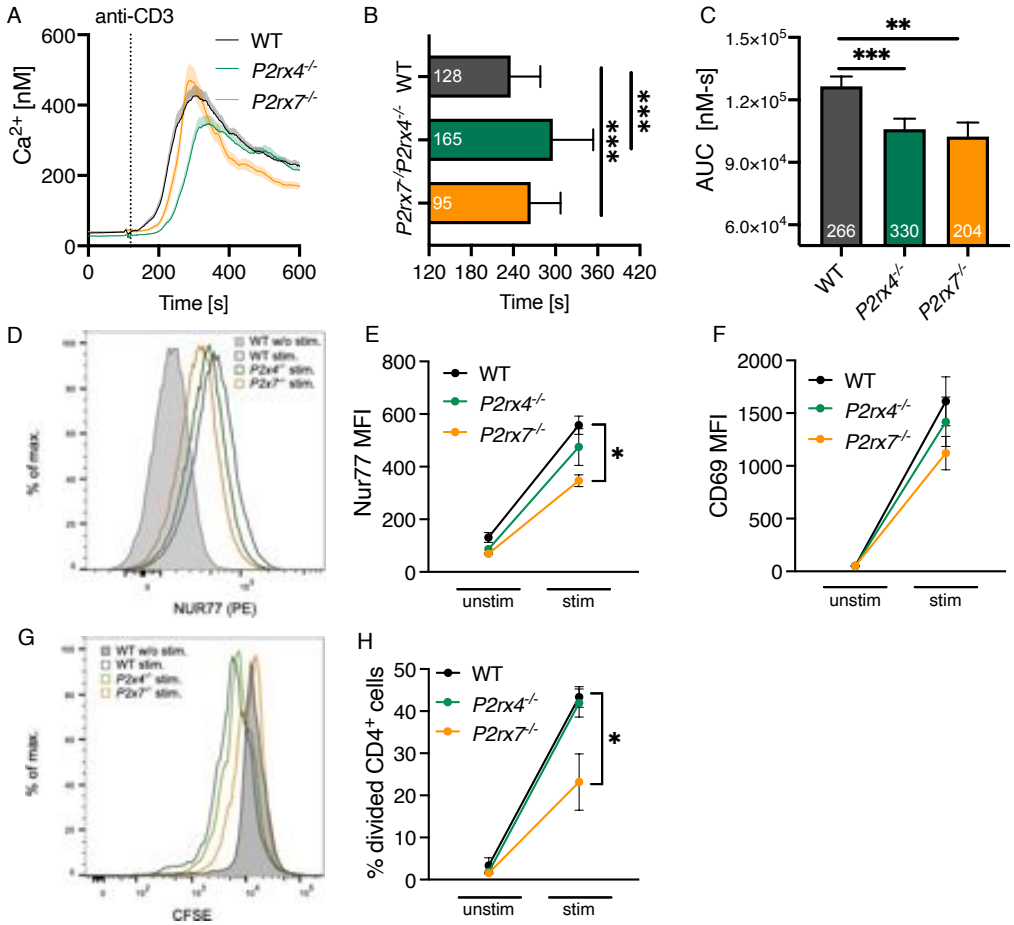

Supplementary Fig. 3: Decreased global Ca^{2+} signaling, expression of Nur77 and proliferation in *P2rx4*$^{-/-}$ or *P2rx7*$^{-/-}$ cells

$CD4^+$ T cells of WT, *P2rx4*$^{-/-}$ or *P2rx7*$^{-/-}$ mice were stimulated with 10 µg/ml soluble anti-CD3 for Fura2 Ca^{2+} imaging or stimulated with a combination of anti-CD3/anti-CD28 for flow cytometry. Three different mice for each condition were used. Data are mean ± SEM. (A) and (C) WT n = 266 cells, *P2x4*$^{-/-}$ n = 330 cells and *P2x7*$^{-/-}$ n = 204 cells. (B) WT n = 128 cells, *P2rx4*$^{-/-}$ n = 165 cells and *P2rx7*$^{-/-}$ n = 95 cells. (A) – (C) Statistical analysis by a Kruskal-Wallis test. (E, F, H) Statistical analysis by two-way ANOVA and Dunnett´s multiple comparisons test.

(A) Global Ca^{2+} response of $CD4^+$ T cells of WT or *P2rx4*$^{-/-}$ or *P2rx7*$^{-/-}$ mice stimulated with soluble anti-CD3 after 2 min of measurement as indicated.

(B) Analysis of the shift of the Ca^{2+} response indicate a faster response for WT T cells. The time difference to reach 200 nM Ca^{2+} of $CD4^+$ T cells of WT, *P2rx4*$^{-/-}$ or *P2rx7*$^{-/-}$ mice after stimulation with soluble anti-CD3 was compared.

(C) Analysis of the area under the curve (AUC) for $CD4^+$ T cells of WT, *P2rx4*$^{-/-}$ or *P2rx7*$^{-/-}$ mice stimulated with soluble anti-CD3.

(D) Nur77 expression measured by flow cytometry in WT $CD4^+$ T cells with or without stimulation and stimulated *P2rx4*$^{-/-}$ and *P2rx7*$^{-/-}$ $CD4^+$ T cells.

(E) Mean fluorescence intensity (MFI) for Nur77 expression by flow cytometry in WT, *P2rx4*$^{-/-}$ or *P2rx7*$^{-/-}$ $CD4^+$ T cells activated with anti-CD3 and anti-CD28.

(F) MFI from CD69 expression by flow cytometry in WT or *P2rx4*$^{-/-}$ or *P2rx7*$^{-/-}$ $CD4^+$ T cells activated with anti-CD3 and anti-CD28.

(G) CFSE fluorescence measured by flow cytometry in WT $CD4^+$ T cells with or without stimulation and stimulated *P2rx4*$^{-/-}$ and *P2rx7*$^{-/-}$ $CD4^+$ T cells.

(H) Percent of divided $CD4^+$ T cells of WT with or without stimulation and stimulated *P2rx4*$^{-/-}$ or *P2rx7*$^{-/-}$.

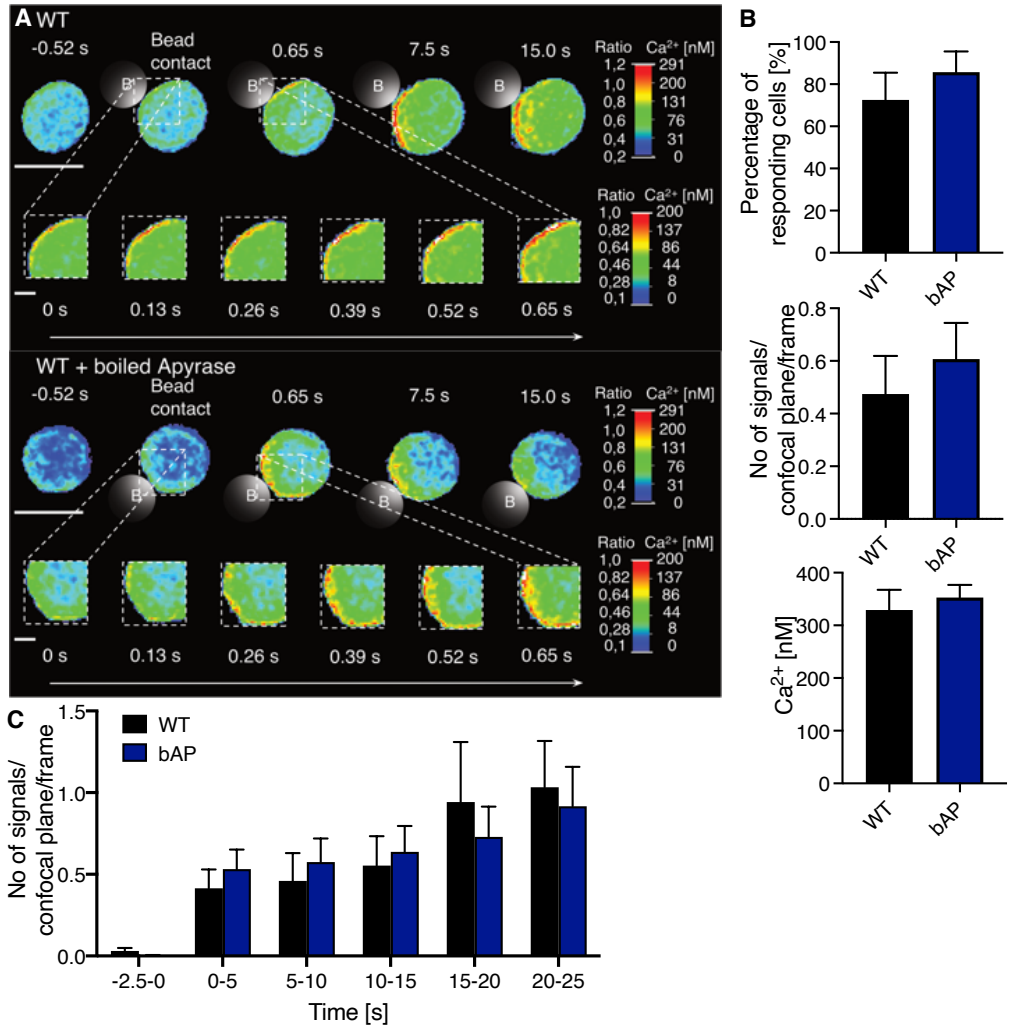

Supplementary Fig. 4: Inactivated apyrase (boiled) did not result in any alteration in Ca^{2+} microdomain formation

$CD4^+$ T cells of WT mice were loaded with Fluo4 and FuraRed and incubated with or without boiled apyrase before Ca^{2+} imaging. Local Ca^{2+} events were analyzed as described in Materials and Methods. A minimum of five different mice were used. Data are mean ± SEM, WT n = 28 cells, cells treated with boiled apyrase n = 26 cells. Statistical analysis by an unpaired two-tailed Mann-Whitney test.

(A) Representative cells of WT mice with or without treatment with boiled apyrase are shown for 0.52 s before and up to 15 s after stimulation with anti-CD3/anti-CD28 coated beads (scale bar 5 µm) as well as for 0 s up to 0.65 s in 0.13 s steps zoomed into the region of bead contact (scale bar 1 µm).

(B) Quantification of the first 15 s after bead contact for $CD4^+$ T cells of WT cells with and without treatment with inactivated apyrase. Percentage of responding cells, the number of Ca^{2+} microdomains per frame for whole cells (confocal plane) and the average Ca^{2+} concentration of these signals is shown.

(C) Quantification of the number of Ca^{2+} microdomains per frame for the period 2.5 to 0 s before and every 5 s after bead contact up to 25 s after bead contact.

3 | Methods

3.1 Mice

CD38$^{-/-}$ mice [Cockayne et al., 1998], *Trpm2*$^{-/-}$ mice (*Trpm2*^{tm1Yamo}) [Yamamoto et al., 2008], *Rag1*$^{-/-}$ mice (B6.129S7*Rag1*^{tm1Mom}/J) [Mombaerts et al., 1992], OT-1 mice (Tg(TcraTcrb)1100Mjb) [Hogquist et al., 1994], and CD90.1 congenic mice (B6.PL-*Thy1*^{a}/CyJ) were on the C57BL/6 background. P2X4 deficient (*P2x4*$^{-/-}$) (P2rx4tm1Rass) and P2X7 deficient (*P2x7*$^{-/-}$) (P2rx7tm1Gab) mice on the BALB/c background, were kindly provided by Dr. Björn RIssiek. BALB/c WT control mice were used for the respective experiments.

Animal experiments were approved by the local committee for animal experiments of the City of Hamburg (registration number N033/2018). Age- and sex-matched mice were used.

3.2 FACS staining and analysis

Antibody selection and fluorescence-activated cell sorting (FACS) staining and analysis were performed as described in Lory et al., 2022 [Lory et al., 2022]. Additional antibodies used are anti-BCL2 mAb (clone 10C4, eBioscience, Carlsbad, CA), anti-ITGA4/CD49d (clone R1-2, Thermo Fischer, Darmstadt, Germany) and the primary, polyclonal anti-ZEB (Bioss, Boston, Massachusetts) and anti-IL18rap (Bioss) which were stained with anti-rabbit IgG secondary antibody (Dianova GmbH, Hamburg, Germany).

3.3 *In vitro* stimulation

In vitro stimulation of $CD8^+$ T cells in total spleen cells was performed as described in Lory et al., 2022 [Lory et al., 2022] and Brock et al. [Brock et al., 2022]. $OVA_{257\text{-}264}$-peptides and $OVA_{257\text{-}264}$-derived peptides were used at a concentration of 10^{-6} mol/l.

3.4 Competitive T-cell transfer

Competitive T-cell transfer was performed as described in Lory et al., 2022 [Lory et al., 2022].

3.5 *Listeria monocytogenes* infection

Listeria monocytogenes infection was performed as described in Lory et al., 2022 [Lory et al., 2022].

3.6 Single cell CITE-Seq

Experimental work for the sequencing was performed by Dr. Karsten Yan. Alignment of the sequencing results to the GRCm38 mm10 *Mus musculus* reference genome was performed at the UKE Bioinformatics Core facility by Christian Casar.

A competitive T cell transfer was performed with *CD38*$^{-/-}$ T cells and wild type C57BL/6 T cells as described in Lory et al. 2022 [Lory et al., 2022]. At day 11 after infection, liver cells were isolated and sorted for CD69 positive CD8 positive T cells. Because of the increased susceptibility to cell death of *Cd38*$^{-/-}$ cells during cell isolation, mice were injected 30 μg s+16 nanobody in 100 PBS intravenously, 3 min before sacrificing the mice [Rissiek et al., 2018]. 25,000 CD69^{+} CD8^{+} cells from wild type and *CD38*$^{-/-}$ mice each were stained with Totalseq-A CITE-seq antibodies against CD90.1, CD90.2, CD8a, CD62L, CD127, CD69, CD44, CD25 and CX3CR1 (Biolegend, San Diego, California). Cells were processed for sequencing with the Totalseq-A 3'v3 Kit according to the manufacturers protocol (10X Genomics, Pleasanton, California). Sequencing was performed by BGI (Yantian District, Shenzhen, China), aiming for 50,000 reads per cell of 25,000 isolated cells per genotype.

Analysis of the sequencing results was performed using the Seurat R package for analysis and quality control of sequencing data, microarray data of sorted immune cell populations from the immunological genome project (immgen.org) as reference data and the SingleR Bioconductor package [Hao et al., 2021, Heng et al., 2008, Aran et al., 2019, Gentleman et al., 2004].

4 | Discussion

4.1 Motivation to investigate CD38 and TRPM2

The initial motivation to investigate whether a CD38 - TRPM2 signaling axis influences in $CD8^+$ T cells was based on preliminary data, which showed a disadvantage of *Cd38*$^{-/-}$ $CD8^+$ T cells in competitive T cell transfer assays. Additional preliminary experiments on *Cd38*$^{-/-}$ $CD4^+$ T cells in a T cell transfer colitis model showed a more severe disease course. TRPM2 was investigated as a putative signaling protein downstream of CD38, potentially activated by cADPR, ADPR and 2dADPR adenine nucleotide 2nd messenger molecules produced by CD38. A further reason to investigate TRPM2 in $CD8^+$ T cell function, was a study in murine T cells by Melzer et al. who showed that TRPM2 expression is up-regulated in activated $CD4^+$ T cells and that proliferation is decreased in *Trpm2*$^{-/-}$ $CD4^+$ T cells [Melzer et al., 2012].

4.2 Key findings

4.2.1 CD38 in $CD8^+$ T cells

We investigated several aspects of $CD8^+$ T cell response in the *L. monocytogenes* infection model. Experiments examining $CD8^+$ T cells in the acute phase of infection revealed no impact of CD38 on $CD8^+$ T cell function with the exception of a reduced ratio of *Cd38*$^{-/-}$ to WT $CD8^+$ OT-1 T cells we found in a competitive T cell transfer assay. We performed infection experiments with *Cd38*$^{-/-}$ mice and competitive T cell transfers and did not find an altered function or phenotype of *Cd38*$^{-/-}$ $CD8^+$ T cells at day 8 and day 5 respectively (Section 2.1).

Experiments targeting memory cell differentiation and function of $CD8^+$ memory T cells did show a more pronounced disadvantage of *Cd38*$^{-/-}$ $CD8^+$ T cells in competitive T cell transfers. Infection of *Cd38*$^{-/-}$ mice did not reveal an altered phenotype of $CD8^+$ T cells compared to wild

type CD8$^+$ T cells after 8 weeks, however, we could observe a non-significant trend of increased CX3CR1, ZEB and BCL2 but not ITGA4 and IL18R levels, which were also found in the single cell RNA CITE-seq. experiment (Section 2.2).

We analyzed *Cd38*$^{-/-}$ and WT CD8$^+$ OT-1 T cells from a T cell transfer experiment by single cell RNA CITE sequencing. The analyzed cells were isolated from the liver at day 11 post infection. *Cd38*$^{-/-}$ CD8$^+$ OT-1 T cells showed a skewed ratio of CD8$^+$ memory and effector T cell frequencies: *Cd38*$^{-/-}$ CD8$^+$ T cells showed a reduced percentage of cells with a CD8$^+$ memory T cell associated transcriptome compared to wild type CD8$^+$ T cells when compared to reference populations from immgen.org (Section 2.3) [Heng et al., 2008]. The analysis of differentially expressed genes between *Cd38*$^{-/-}$ and WT CD8$^+$ OT-1 T cells revealed, in both *Cd38*$^{-/-}$ CD8$^+$ effector and *Cd38*$^{-/-}$ CD8$^+$ memory T cells, a number of genes up-regulated which are associated with CD8$^+$ effector T cell function or expression levels.

In conclusion, our results show that absence of CD38 does not impair the acute CD8$^+$ T cell response but causes (modest) changes in CD8+ memory T cell development.

4.2.2 TRPM2 Is Not Required for T-Cell Activation and Differentiation

TRPM2 was investigated *in vitro*, in acute infection models and in assays targeting CD8$^+$ memory T cell formation. We did not observe a difference of T cell activation or proliferation of *Trpm2*$^{-/-}$ CD4$^+$ and CD8$^+$ T cells. CD4$^+$ T cell *in vitro* differentiation assays did not show an effect of TRPM2-deficiency.

CD8$^+$ T cells in an acute infection phase were investigated in *L. monocytogenes* infection and competitive T cell transfer experiments: TRPM2 did not affect the phenotype and function of CD8$^+$ T cells in both assays. To investigate CD8$^+$ memory T cells, 8 week-*L. monocytogenes* infection and competitive transfer experiments were utilized. Again, TRPM2 did not affect the function of CD8$^+$ T cells in these assays.

Trpm2$^{-/-}$ CD4$^+$ T cells were investigated in *in vitro* differentiation assays and did not differ from wild type CD4$^+$ T cells in frequencies of T_H1 cells, T_{reg} cells and T_H17 cells but showed reduced frequency of T_R1 cells when incubated with the respective differentiation cocktail, this result was however not consistent across repeated experiments. CD4$^+$ T cells were investigated in an anti-CD3ϵ mAb induced intestinal inflammation model and additionally, to exclude innate immune system affecting the T cell function, with a transfer of CD4$^+$ T cells in the model of anti-CD3ϵ mAb induced intestinal inflammation. TRPM2 deficiency did not affect the severity of the

disease or the composition of $CD4^+$ T cell subsets. [Lory et al., 2022]

In conclusion, our results show that TRPM2 is not required for a functioning $CD4^+$ and $CD8^+$ T cell response.

4.2.3 P2X4 and P2X7 are essential players in basal T cell activity and Ca^{2+} signaling milliseconds after T cell activation

Brock et al. showed that P2X4 and P2X7 deficiency in $CD4^+$ T cells and inhibition of P2X4 and P2X7 in $CD4^+$ T cells with 1 μM PSB-15417 or P2X7 inhibiting nanobody (P2X7-nb) respectively, results in a reduced frequency of Ca^{2+} microdomains which are also dependent on extracellular ATP [Brock et al., 2022]. ATP release from the cell was suppressed by the inhibition of PANX1 with 200 μM ^{10}panx1 which resulted in a decreased frequency of Ca^{2+} microdomains. Further, a basal level ofATP release from un-stimulated $CD4^+$ T cells was able to genereate Ca^{2+} microdomains without the need of TCR stimulation. Additionally, they could reproduce the findings of Woehrle et al. and show co-localization of P2X4 and P2X7 [Brock et al., 2022, Woehrle et al., 2010].

Interestingly we found that P2X7 does not only contribute to the very early events which lead to the formation of Ca^{2+} microdomains but is also important for T cell activation and proliferation.

We could show that *P2x7*$^{-/-}$ $CD4^+$ T cells but not *P2x4*$^{-/-}$ $CD4^+$ T cells exhibit reduced NUR77 levels after 16 hours of stimulation and that proliferation was decreased in *P2x7*$^{-/-}$ $CD4^+$ T cells. [Brock et al., 2022]

In conclusion, P2X7 is involved in the formation of the initial Ca^{2+} microdomains as well as signaling downstream of the TCR in $CD4^+$ T cells and is important for activation and proliferation of $CD4^+$ T cells.

4.3 Limitations of the results

It is worth mentioning that the results were obtained using the murine model system and are only to a certain degree transferable to humans. The research using animals is in its nature directed towards the human system and the understanding of disease and therefore flawed. Nevertheless, the complexity of the animal can not be replicated in *in vitro* settings thus far. Further, we primarily used the *L. monocytogenes* infection model and $CD8^+$ T cells may behave differently in other disease models.

4.4 Methodological approach

4.4.1 Infection models in *Cd38*$^{-/-}$ and *Trpm2*$^{-/-}$ mice

Both CD38 and TRPM2 have been shown to be essential for the function of innate immune cell populations, to the point where bacterial infection models in both *Cd38*$^{-/-}$ and *Trpm2*$^{-/-}$ mice show increased lethality compared to wild type mice. An impaired innate immune response not only leads to decreased survival of *Cd38*$^{-/-}$ and *Trpm2*$^{-/-}$ mice but also affects recruitment of cells to the site of infection.

In *Cd38*$^{-/-}$ and *Trpm2*$^{-/-}$ mice, not only CD8^{+} T cells but all cells including CD4^{+} T helper cells and cells of the innate immune system are transgenic. T cells rely on interactions with cells from other immune cell populations through cytokine signaling or direct cell to cell interaction as for example during antigen presentation. The frequency of dendritic cells, the main antigen presenting cell population, migrating to the site of infection was shown to be unaffected by CD38 deficiency by Lischke et al., however Partida et al. observed the opposite, showing decreased migration of dendritic cells to secondary lymph organs and additionally found a reduced efficiency of *Cd38*$^{-/-}$ dendritic cells to present antigen [Lischke et al., 2013, Partida-Sánchez et al., 2004a]. Consequently, T cells may not encounter the same environment in *Cd38*$^{-/-}$ and *Trpm2*$^{-/-}$ mice that they would in WT mice. The conditions T cells encounter in transgenic mice therefore cannot be accurately replicated in wild type mice, reducing the comparability of the wild type control group.

This circumstance creates the need of methods which exclude the influence of innate immune cell populations. In the infection *L. monocytogenes* model, we treated the mice with ampicillin to clear the infection after two days. This timing allows for an adequate priming of T cells and results in the mounting of a CD8^{+} T cell response and avoids the increased mortality of *Cd38*$^{-/-}$ and *Trpm2*$^{-/-}$ mice in bacterial infection models [Lischke et al., 2013, Mercado et al., 2000].

A second way to circumvent an influence of the innate immune system on the investigated CD8^{+} T cells was to utilize T cell transfer assays. Transfer assays are especially elegant as they exclude all cells from the donor mouse which are not the population of interest and rely on the innate immune response of the recipient mice. The transfers were performed using total spleen cells: OT-1 T cells make up 20% of the cells in the spleen of OT-1 mice. We transferred 5000 WT and 5000 *Cd38*$^{-/-}$ CD8^{+} OT-1 T cells which recognize $OVA_{257\text{-}264}$. The actual number of CD8^{+} OT-1 T cells which are transferred to the recipient mouse is lower than 5000, as not all cells survive the transfer. To set

these numbers in perspective: The number of endogenous naïve $CD8^+$ T cells of the mouse, which recognize a given antigen, varies between different antigens: Jenkins et al. found a range of 15 to 1100 specific naïve $CD8^+$ T cells per mouse [Jenkins and Moon, 2012]. The low number of specific $CD8^+$ T cells which were transferred is therefore close to the number of cells which recognize an antigen in the endogenous response to a pathogen. The number of transferred cells which are not $CD8^+$ OT-1 T cells is small and not subject to the clonal expansion which antigen specific OT-1 T cells will undergo. Additionally, all transferred $CD8^+$ OT-1 T cells encounter the same infection "environment" which makes non - $CD8^+$ OT-1 T cells which were transferred irrelevant. The second major advantage of competitive T cell transfer experiments over other infection models lies in the aforementioned encounter of the investigated cells with the exact same environment. This makes a comparison between wild type and transgenic $CD8^+$ T cells more accurate and less prone to natural variation between mice. One drawback to this model lies in the high affinity of OT-1 $CD8^+$ T cells to the secreted ovalbumin derived peptide SIINFEKL, making this approach unsuitable to investigate a more nuanced examination of $CD8^+$ T cell response. This may however be possible with *L. monocytogenes* strains which secrete OVA peptides with amino acid substitutions altering the affinity to the MHC I and could be included in an approach in the future.

4.4.2 Single cell RNA CITE sequencing of *Cd38*$^{-/-}$ $CD8^+$ T cells

While single cell RNA sequencing is a powerful tool in itself, the possibility to sequence cells from different genetic backgrounds in one run and distinguish them by cell surface protein levels made CITE sequencing an excellent choice for the analysis of $CD8^+$ T cells from competitive transfer experiments. We utilized the combination of CITE sequencing and a co-transfer assay with wild type and *Cd38*$^{-/-}$ $CD8^+$ T cells in the same infection-environment and sequencing run to achieve near identical conditions for the cells throughout the experiment. We sorted the cells for $CD69^+$ $CD8^+$ to select activated and tissue resident $CD8^+$ T cells which are involved in the response to the *L. monocytogenes* infection.

A major drawback of single cell sequencing are the costs, which restricts replication of the experiments. Therefore, results of the sequencing experiment should be considered with care and should be confirmed with other approaches such as quantitative PCR or assays based on protein expression such as FACS or Western plot. A second factor which complicates evaluation of the results is the time point at which the cells are isolated and analyzed: We chose to analyze $CD8^+$ T cells at day 11 after infection to target $CD8^+$ T cells in the process of becoming memory cells. We

wanted to analyze the transcriptional landscape that leads to the differentiation into $CD8^+$ memory T cells and how it might be affected by CD38 deficiency.

The approach we chose allowed us to analyze differential expression profiles with relatively low values of $\log_2$-fold changes for individual genes.

4.4.3 Proliferation and *in vitro* activation assays investigating *P2x4*$^{-/-}$ and *P2x7*$^{-/-}$ $CD4^+$ T cells

We investigated *P2x4*$^{-/-}$ and *P2x7*$^{-/-}$ $CD4^+$ T cells *in vitro* for activation and proliferation. $CD4^+$ T cells were stimulated with anti-CD3ϵ mAb to simulate a TCR stimulation in an interaction between an antigen presenting cell and the $CD4^+$ T cell. $CD4^+$ T cells were stimulated in presence of spleen cells which provide CD80 and CD86 as ligands for the co-factor CD28. For the proliferation assay, anti-CD3ϵ mAb were coated to the 96-well plate to further simulate clustering of TCR signals.

While *in vitro* stimulation and proliferation assays give us a good indication of the function of the investigated cells, this system excludes the complex environment cells encounter in the animal.

4.5 CD38-deficiency in $CD8^+$ T cells

Based on the single cell RNA CITE sequencing results (Section 2.3), CD38-deficiency may cause a delay of $CD8^+$ memory T cell differentiation or an increased ratio of effector to memory $CD8^+$ T cells. Additionally we observed an increased expression of several $CD8^+$ effector T cell associated genes. A more effector like state of *Cd38*$^{-/-}$ $CD8^+$ T cells could cause a decreased survival of *Cd38*$^{-/-}$ $CD8^+$ T cells. This would explain the reduced ratio of *Cd38*$^{-/-}$ to WT $CD8^+$ T cells we observed in $CD8^+$ T cell transfer experiments (Section 2.1& 2.2). Taken together this indicates a subtle influence of CD38 on the differentiation or survival of $CD8^+$ T cells.

Differentially expressed genes between *Cd38*$^{-/-}$ and WT $CD8^+$ OT-1 T cells are presented as genes up- or down-regulated in *Cd38*$^{-/-}$ $CD8^+$ T cells. We first examined the distribution of genes in the mouse genome to exclude an effect of either *Cd38*- or *Thy1*-adjacent genes being inherited non-randomly. The genes found in the differential expression analysis are dispersed within the genome. Genes which are located on the same chromosome as *Thy1* are *Cx3cr1* (76×10^6 bp distance), *S1pr5* (22×10^6 bp distance), *Ets1* (11×10^6 bp distance), *Hspa8* (3×10^6 bp distance), *Thy1*, *Nptn* (14×10^6 bp distance) and *Rora* (24×10^6 bp distance) in order of position on the chromosome 9. Genes which are located on the same chromosome as *Cd38* are *Cd38*, *Klf3* ($20 \times$

10^6 bp distance), *Fryl* (29×10^6 bp distance), *Dynll1* (71×10^6 bp distance), *Lfng* (96×10^6 bp distance) and *Hsph1* (100×10^6 bp distance) in order of position on chromosome 5. We concluded that adjacency effects did not cause artifacts in the differential expression analysis. A comparison of differentially expressed genes between *Cd38*$^{-/-}$ and WT CD8$^+$ OT-1 T cells for total CD8$^+$ T cells, the effector-like subset "T cells (T.8EFF.OT1.D10LIS)" and the memory-like subset "T cells (T.8MEM.OT1.D45.LISOVA)" is discussed in section 4.5.2. Differential expression analysis based on either subset resulted in a list of genes which is identical for the genes with the highest change of expression ($\log_2$-fold change ≥ 0.37) between *Cd38*$^{-/-}$ and WT CD8+ T cells (See section 4.5.2 and tables 4.1 and 4.2).

4.5.1 Function of differentially expressed genes in *Cd38*$^{-/-}$ CD8$^+$ T cells

We found several genes associated with CD8$^+$ effector T cells among the differentially expressed genes up-regulated in *Cd38*$^{-/-}$ OT-1 CD8$^+$. In the following, the function of proteins encoded by the genes with the highest $\log_2$-fold change ($\log_2$-fold change ≥ 0.37) in the differential expression analysis (*Cd38*$^{-/-}$ vs. WT) of total CD8$^+$ T cells, the CD8$^+$ effector subset "T cells (T.8EFF.OT1.D10LIS)" and CD8$^+$ memory T cell subset "T cells (T.8MEM.OT1.D45.LISOVA)" are discussed (See also tables 4.1 and 4.2).

The multi zinc finger transcription factor ZEB2 was found to be up-regulated in KLRG1$^+$ CD8$^+$ effector cells. Omilusik et al. describe a loss of CD8$^+$ effector cells in ZEB2 deficient mice compared to WT mice in LCMV infection. Further, they showed that ZEB2-deficiency lead to increased expression of *Cx3cr1*, *Il7r* and *Tcf7*. While we found both *Cx3cr1* expression and *Zeb2* expression increased in *Cd38*$^{-/-}$ OT-1 CD8$^+$ T cells, a link to the IL-7 receptor (IL-7R) which is important in development and survival of memory T cells and T cell factor 1 (TCF1) which regulates survival of CD8$^+$ memory T cells is very interesting. [Omilusik et al., 2015, Kim et al., 2020, Barata et al., 2019]

The chemokine receptor CX3CR1 is expressed in terminally differentiated CD8$^+$ effector T cells. CX3CR1 interacts with fractalkine (CX3CL1) which is expressed on endothelial cells. CX3CR1 is involved in adhesion and migration of T lymphocytes. [Gerlach et al., 2016]

AC149090.1 is a phosphatidylserine carboxylase. Phosphatidylserine carboxylases are enzymes in the synthesis of the phospholipid phosphatidylethanolamine which makes up a large portion of the phospholipids in the cell membrane. [Di Bartolomeo et al., 2017] As an enzyme in an anabolic synthesis pathway of an abundant membrane component, AC149090.1 could be important for anabolic

processes needed for the proliferation of effector T cells.

BCL2 is expressed in KLRG1^{low} CD127^{high} pre-memory CD8$^+$ T cells where it counteracts the apoptotic function of BIM. [Hardwick and Soane, 2013, Li et al., 2020, Kurtulus et al., 2011, Joshi et al., 2007, Kaech and Cui, 2012]. As such, BCL2 does not fit to the increase of CD8$^+$ effector over memory T cells in *Cd38*$^{-/-}$ CD8$^+$ T cells. However, its direct involvement in the survival of CD8$^+$ T cells which differentiate into CD8$^+$ memory T cells makes it an interesting finding. The differential expression of *Bcl2* could indicate a dis-regulation of the maturation towards CD8$^+$ memory T cells.

The thioredoxin-interacting protein (TXNIP) is a regulator of redox signaling in response to stress. TXNIP was found to be necessary for natural killer cell maturation and TXNIP-deficient naive mice exhibited a reduced number of CD8$^+$ T cells. This could point towards a role in survival of CD8$^+$ T cells. [Lee et al., 2005]

IL18rap interacts with the IL-18 receptor and is part of the signal transduction of the response to IL-18. IL-18 response in T cells involves the activation of JNK and NF-κB (See section 1.2). [Debets et al., 2000, Cheung et al., 2005, Born et al., 1998]

ITGA4 is an integrin which recognizes fibronectin on endothelial cells and has been found to interact with fractalkine and was hypothesized to play a role in the interaction of T cells with target cells. The expression of *Itga4* is lower in CD8$^+$ OT-1 memory T cells ($\geq$ 45 days) than in CD8$^+$ OT-1 effector T cells (Day 5 to 45), fitting to the more effector like transcriptome of *Cd38*$^{-/-}$ OT-1 CD8$^+$ T cells (immgen.org) [Fujita et al., 2012, Heng et al., 2008, UniProt, 2021].

Neuroblast differentiation-associated protein (AHNAK) was shown to be necessary for cytotoxic activity of CD8$^+$ T cells through the modulation of $Ca_V1.1$ Ca^{2+} channel activity. AHNAK1-deficient T cells show decreased global Ca^{2+} levels upon TCR stimulation, decreased killing capability, decreased granzyme B expression and decreased IFNγ production compared to WT CD8$^+$ T cells. [Alvarez et al., 2010] The up-regulation of *Ahnak* in *Cd38*$^{-/-}$ CD8$^+$ OT-1 T cells could indicate a compensatory effect on Ca^{2+} signaling potentially counteracting the loss of CD38 activity.

Because we breed mice to use CD90.1 and CD90.2, which are allelic versions of the same protein, encoded by *Thy1*, as a congenic marker, the differential expression of *Thy1* is no reliable result. Increased expression of the *Thy1* (CD90.2) gene may be caused by a difference in the promotor region of the gene, epigenetic modulation, an enhancing effect of the CD90.2 encoding sequence itself or other regions inherited in the proximity of the gene.

CACCC-box-binding protein (KLF3) or BKLF is a transcriptional repressor with a wide range

of functions. KLF3 funcion is poorly defined in T lymphocytes, however its expression is regulated by B cell receptor stimulation in B cells. KLF3 is down-regulated in activated B cells and is thought to be involved in maintaining B cell quiescence. [Pearson et al., 2011]

Atp2b1 encodes a plasma membrane Ca^{2+} ATPase 1 (PMCA1) that pumps Ca^{2+} against a concentration gradient from the cytosol out of the cell and maintains Ca^{2+} homeostasis in the cell. Korthals et al. found that PMCA1 is up-regulated after TCR stimulation and Ca^{2+} clearance from the cell is impaired in $CD4^+$ T cells with only one functioning *Atp2b1* allele. [Korthals et al., 2017]

Tsc22d3 encodes glucocorticoid-induced leucine zipper (GILZ) which was reported to be up-regulated in T cells after "IL-2 withdrawal". Activated T cells which do not sense IL-2 go into apoptosis, this is counteracted by the up-regulation of GILZ. GILZ was also reported to prohibit DNA binding of NF-κB and inhibition of the pro-apoptotic BIM through inhibition the activating transcription factor forkhead box protein O3 (FOXO3). [Asselin-Labat et al., 2004, Ayroldi et al., 2001]

Granzyme A (GZMA) induces caspase independent apoptosis in target cells of cytotoxic T lymphocytes and natural killer cells. It is expressed in $CD8^+$ effector T cells and shows low expression in $CD8^+$ memory T cells (immgen.org) [Fan et al., 2003, Van Daalen et al., 2020, Heng et al., 2008]

Protein C-ets-1 (ETS1) is a transcription factor that was shown to up-regulate proteins which are part of DNA repair, which is important for proliferating cells [Wilson et al., 2004]. However, ETS1 is expressed in $CD8^+$ T cells regardless of their differentiation status [Heng et al., 2008]. ETS1 was further shown to be important for early T cell development in the thymus [Cauchy et al., 2016]. Most relevant for $CD8^+$ T cells is a publication by Moskovitz et al., who describe that ETS1 is involved in the maintenance of a naïve like chromatin accessibility and conclude that ETS1 and SP1 are important transcription factors which maintain the naïve state of $CD8^+$ T cells. [Moskowitz et al., 2017] It is unclear whether the ETS1 has a function in $CD8^+$ effector versus memory T cell differentiation.

Arhgef18 encodes rho guanine nucleotide exchange factor 18 (AHRGI) which has been shown to interact with Mitogen-activated protein kinase kinase kinase 7 (MAP3K7), a kinase of the MAPK signaling pathway downstream of several receptors including toll-like receptors (TLRs) but also the TCR. AHRGI-deficient cells of the human monocyte cell line U937 showed decreased NF-κB activity, indicating an enhancing effect of AHRGI on MAP3K7 activity. If this translates to $CD8^+$ T cells this could mean that the increased RNA level of *Arhgef18* lead to an increased NF-κB activity in *Cd38*$^{-/-}$ $CD8^+$ T cells. [Frauenstein et al., 2021, Landström, 2010]

Phosphoinositide-3-kinase-interacting protein 1 (PIK3IP1) is a negative regulator of PI3K activity. PI3K is activated downstream of the T cell co-receptor CD28 and part of the mTOR signaling pathway. CD28 signaling further activates transcription factors such as NF-κB, NFAT and AP-1. Uche et al. showed that T cells deficient in PIK3IP1 produce more IL-2 and showed increased proliferation. Further they showed that bacterial titers in liver of *L. monocytogenes* infected mice are reduced in PIK3IP1-deficient mice compared to WT mice. [Uche et al., 2018, Acuto and Michel, 2003, Gaud et al., 2018] An increase in PIK3IP1 could therefore contribute to a decrease in cell numbers of *Cd38*$^{-/-}$ compared to WT CD8$^+$ T cells in the competitive T cell transfer experiments.

The interferon γ receptor 1 (IFNGR1) mediates IFNγ signaling and activates the JAK-STAT pathway leading to the expression of ISG which confer resistance to pathogens by directly targeting pathways used in their life cycles [Schneider et al., 2014]. Ifng which encodes IFNγ on the other hand was down-regulated in *Cd38*$^{-/-}$ T cells.

Sialophorin (SPN), also called CD43, contributes to T cell activation and is expressed to a higher level in CD8$^+$ effector T cells than in CD8$^+$ memory T cells (immgen.org) [Rosenstein et al., 1991, Heng et al., 2008].

Ras-related protein Rap-1b (RAP1b) is required for homing of lymphocytes to secondary lymph organs. If this affects *Cd38*$^{-/-}$ CD8$^+$ T cells in a way that leads to increased lymphocyte homing to secondary lymph organs they could be exposed to an increased time/frequency of antigen presentation by dendritic cells compared to WT CD8$^+$ T cells. [Su et al., 2015] Mele et al. showed increased migration of lymphocytic leukemia cells with higher levels of CD38 which they found to be caused by CD38 acting via RAP1 [Mele et al., 2018].

Finally *Ifng* was the only down-regulated gene shared between the results of differential expression analyses. IFNγ is a produced by activated CD8$^+$ T cells. IFNγ is a cytokine that is part of the effector functions of CD8$^+$ T cells and directly combats viral, selected bacterial and protozoan infections [de Araújo-Souza et al., 2015].

Taken together, the genes found up-regulated between *Cd38*$^{-/-}$ and WT CD8$^+$ OT-1 T cells regardless of the analyzed subset (See section 4.5.2) point towards a shift towards an effector like transcriptome of *Cd38*$^{-/-}$ CD8$^+$ OT-1 T cells. Although the differential expression of individual genes was not high, the sum of the discussed gene products may have a significant impact on the proliferation and/or survival of *Cd38*$^{-/-}$ CD8$^+$ OT-1 T cells in the T cell transfer experiments.

Table 4.1: **Differentially expressed genes up-regulated in *Cd38*$^{-/-}$ CD8$^+$ OT-1 T cells compared to wild type CD8$^+$ OT-1 T cells.** The table compares three differential expression analyses which were performed using three different subsets of cells: Total CD8$^+$ OT-1 T cells (Total diff. ex.) include all CD90.2$^+$ CD8$^+$ T cells measured in the single cell CITE sequencing experiment. The CD8$^+$ effector T cell subset (Effector diff. ex.) includes CD8$^+$ OT-1 T cells which were found similar to the "T cells (T.8EFF.OT1.D10LIS)" population via the SingleR R package. The CD8$^+$ OT-1 memory T cell subset (Memory diff. ex.) includes the cells which were found similar to the "T cells (T.8MEM.OT1.D45.LISOVA)" population via SingleR. The gene lists are ordered by descending $\log_2$-fold change, however Log_2-fold change is only shown for the comparison of total CD8$^+$ OT-1 T cells. A complete table can be found in tables S.4 and S.5. Columns "Total vs. effector", "Effector vs. total", "Total vs. memory" and "Memory vs. total" show genes that are not found in the list of genes to which the respective differential expression analysis result is compared to.

Total log2FC*	Total diff. ex.	Total vs. effector	Effector vs. total	Effector diff. ex.	Total vs. memory	Memory vs. total	Memory diff. ex.
0.73	Zeb2			Zeb2			Zeb2
0.66	Cx3cr1			Bcl2			Cx3cr1
0.56	AC149090.1			Cx3cr1			AC149090.1
0.51	Bcl2			AC149090.1			Txnip
0.50	Txnip			Txnip			Bcl2
0.47	Il18rap			Ahnak			Il18rap
0.43	Itga4			Il18rap			Arhgef18
0.42	Ahnak			Gzma			Pik3ip1
0.41	Thy1			Ifngr1			Itga4
0.41	Klf3			Arhgef18			Klf3
0.41	Atp2b1			Ccdc88c			Thy1
0.40	Tsc22d3			Ets1			Gzma
0.39	Gzma			Thy1			Ccnd3
0.38	Ets1			Itga4			Atp2b1
0.38	Arhgef18			Spn			Ahnak
0.38	Pik3ip1			Tsc22d3			Tsc22d3
0.37	Ifngr1			Klf3			Gm44175
0.37	Spn			Atp2b1			Ifngr1
0.36	Rap1b			Rora			Ripor2
0.35	Klrb1c	Klrb1c		Znrf2	Klrb1c		Neat1
0.35	Rora			Sppl2a			Ets1
0.34	S1pr5	S1pr5		Apbb1ip	S1pr5	Prf1	Prf1
0.33	Ccdc88c			Nptn	Ccdc88c		Rap1b
0.33	Nptn			Rap1b			Rora
0.33	Arl4c			Mirt1			Arl4c
0.33	Ccnd3			Pik3ip1			Oip5os1
0.32	Lnpep			Emp3		Kcnq1ot1	Kcnq1ot1
0.32	Gm26740		Thap3	Thap3		Picalm	Picalm

*Log_2-fold change only refers to the differential expression analysis of total CD8$^+$ cells

Continued table 4.1

Total log2FC*	Total diff. ex.	Total vs. effector	Effector vs. total	Effector diff. ex.	Total vs. memory	Memory vs. total	Memory diff. ex.
0.30	Gm44175			Arl4c			Gm26740
0.30	Zmiz1			Ccnd3			Spata13
0.30	Neat1			Gm26740			Lfng
0.30	Znrf2			Gm44175			Sept11
0.29	Emp3			Neat1	Emp3		Spn
0.29	Nkg7			Ube2g2		Ypel3	Ypel3
0.29	Nebl	Nebl	Ankrd44	Ankrd44	Nebl		Tm9sf3
0.28	Apbb1ip			Lnpep	Apbb1ip	Ctsd	Ctsd
0.28	Itgb1		Picalm	Picalm	Itgb1	Gsk3b	Gsk3b
0.28	Mirt1			Klrc1	Mirt1		Nkg7
0.28	Klf7	Klf7	Zfp36l2	Zfp36l2	Klf7	Brd9	Brd9
0.28	Oip5os1			Zmiz1		Malat1	Malat1
0.28	Sept11		Tbl1xr1	Tbl1xr1			S1pr1
0.27	Sppl2a		C85193	C85193		Atf7ip	Atf7ip
0.27	Ripor2	Ripor2	Pik3r1	Pik3r1		Cd8a	Cd8a
0.27	Fryl			Fryl	Fryl	Pds5a	Pds5a
0.27	Klrc1			Racgap1	Klrc1		Nptn
0.26	Klrg1	Klrg1	Efhd2	Efhd2	Klrg1	Kif21b	Kif21b
0.26	Lfng	Lfng	Prkacb	Prkacb		Id2	Id2
0.26	Ube2g2			Sgk1	Ube2g2	Tram1	Tram1
0.26	Sgk1			Nkg7	Sgk1	Rabgap1l	Rabgap1l
0.26	Racgap1			Ncald	Racgap1	Bcl11b	Bcl11b
0.26	S1pr1	S1pr1	Ube2q1	Ube2q1			Zmiz1
0.26	Spata13	Spata13		Zcchc7		BE692007	BE692007
0.26	Ncald			Sept11	Ncald		Sppl2a
0.25	Tm9sf3	Tm9sf3	Rasgrp2	Rasgrp2		Adgre5	Adgre5
0.25	Jak1		Atp1b3	Atp1b3	Jak1	Ppp3ca	Ppp3ca
0.25	Zcchc7		Cdk13	Cdk13	Zcchc7		Lnpep
-			Klrc2	Klrc2			Znrf2
-				Jak1		Iqgap1	Iqgap1
-			Dnajc1	Dnajc1		Itgal	Itgal
-			Nfatc3	Nfatc3		Txk	Txk
-			Gabpb2	Gabpb2			
-			Cd164	Cd164			
-				Itgb1			
-				Oip5os1			

*Log_2-fold change only refers to the differential expression analysis of total $CD8^+$ cells

Table 4.2: **Differentially expressed genes down-regulated in *Cd38*$^{-/-}$ CD8$^+$ OT-1 T cells compared to wild type CD8$^+$ OT-1 T cells.** The table compares three differential expression analyses which were performed using three different subsets of cells: Total CD8$^+$ OT-1 T cells (Total diff. ex.) include all CD90.2$^+$ CD8$^+$ T cells measured in the single cell CITE sequencing experiment. The CD8$^+$ effector T cell subset (Effector diff. ex.) includes CD8$^+$ OT-1 T cells which were found similar to the "T cells (T.8EFF.OT1.D10LIS)" population via the SingleR R package. The CD8$^+$ OT-1 memory T cell subset (Memory diff. ex.) includes the cells which were found similar to the "T cells (T.8MEM.OT1.D45.LISOVA)" population via SingleR. The gene lists are ordered by descending $\log_2$-fold change, however Log_2-fold change is only shown for the comparison of total CD8$^+$ OT-1 T cells. A complete table can be found in tables S.4 and S.5. Columns "Total vs. effector", "Effector vs. total", "Total vs. memory" and "Memory vs. total" show genes that are not found in the list of genes to which the respective differential expression analysis result is compared to.

Total log2FC*	Total	Total vs. effector	Effector vs. total	Effector	Total vs. memory	Memory vs. total	Memory
-0.38	Hsp90ab1			Hsp90ab1			Ifng
-0.38	Ifng			Hsph1			Ccl4
-0.36	Hsph1		Hist1h1c	Hist1h1c			Bst2
-0.35	Rgs1			Dnaja1			Hsph1
-0.31	Bst2	Bst2		Rgs1			Jaml
-0.31	Gapdh		Hspe1	Hspe1			Rgs1
-0.29	Isg15	Isg15		Gapdh	Isg15	Hspd1	Hspd1
-0.29	Dnaja1			Cd69	Dnaja1	Ifi203	Ifi203
-0.28	Ccl4	Ccl4		Ifng			Gapdh
-0.28	Cd69			Hspa8	Cd69		Dynll1
-0.28	Hspa8		Edf1	Edf1			Hsp90ab1
-0.28	Ly6a	Ly6a	Tnfaip3	Tnfaip3		Ifi27l2a	Ifi27l2a
-0.27	Rpl10			Rpl10		Mndal	Mndal
-0.27	Jaml	Jaml		Hsp90aa1			Ly6a
-0.27	Dynll1			Nsa2			Hspa8
-0.27	Nsa2			Dynll1			Rpl10
-0.25	Hsp90aa1		Rpl29	Rpl29		Rpl29	Rpl29

*Log_2-fold change only refers to the differential expression analysis of total CD8$^+$ cells

4.5.2 Differentially expressed genes in effector and memory subsets of *Cd38*$^{-/-}$ CD8$^+$ T cells

For the comparison of *Cd38*$^{-/-}$ with WT CD8$^+$ OT-1 T cells, the resulting list of differentially expressed genes was similar when analyzing cells of the CD8$^+$ effector subset "T cells (T.8EFF.OT1.D10LIS)" and CD8$^+$ memory T cell subset "T cells (T.8MEM.OT1.D45.LISOVA)" shown in section 5 - figure 5.

In the tables 4.1 and 4.2 the results of differential expression analysis in the different subsets are compared. Genes which are found in only one of the compared lists are shown in columns "Total vs. effector", "effector vs. total" etc.. Interestingly, the differentially expressed genes with the highest $\log_2$-fold change ($\log_2 FC \geq 0.37$) did not differ between total CD8$^+$ cell comparison and effector and memory subsets respectively. Genes with lower $\log_2$-fold change of ≤ 0.37 showed a higher variety between the lists.

This indicates that CD38-deficiency effects CD8$^+$ effector and memory T cells in a similar way, causing the up-regulation of a number of genes which we would expect up-regulated in CD8$^+$ effector T cells. If the increase of effector T cell - associated genes also influences the survival of *Cd38*$^{-/-}$ CD8$^+$ T cells, this could further explain the reduced number of *Cd38*$^{-/-}$ CD8$^+$ T cells in the competitive T cell transfer experiments.

4.6 TRPM2-deficiency in CD8$^+$ T cells

Whether TRPM2 has a function in T cells is controversial. Our data shows that TRPM2-deficiency has no effect on CD4$^+$ and CD8$^+$ T cell function. Melzer et al. however showed decreased proliferation and cytokine production of *Trpm2*$^{-/-}$ CD4$^+$ T cells *in vitro* [Melzer et al., 2012] while Wolf et al. reported that *Trpm2*$^{-/-}$ T cells show regular calcium signaling [Wolf et al., 2015]. At the moment we can not explain this discrepancy.

4.7 Outlook

4.7.1 CD38

Our results hint at a function of CD38 in the differentiation or survival of CD8$^+$ T cells. Future experiments investigating the role of CD38 for the differentiation of CD8$^+$ T cells could include

monitoring kinetics of $CD8^+$ T cell composition after infection over time. Although the flow cytometry analysis of proteins expressed by the genes identified in the single cell CITE sequencing experiment did not yield significant results, a kinetic of these targets over time could be utilized to see whether protein levels are affected at specific time points during infection and after clearance of the bacteria. Survival of *Cd38*$^{-/-}$ T cells in different conditions, including a titration of IL-7 and IL-15 concentrations could be investigated *in vitro* or in transfer experiments. *In vitro* migration experiments could reveal whether CD38 deficiency affects motility of $CD8^+$ T cells as seen in different innate immune cells [Lischke et al., 2013]. NAD metabolism in *Cd38*$^{-/-}$ $CD8^+$ T cells could be investigated with focus on poly (ADP-ribose) polymerase (PARP) family proteins which are involved in DNA repair and programmed cell death and are dependent on NAD. A member of a second NAD dependent family of proteins, SIRT 1, was shown to affect T_H17 cell activation, to positively regulate stemness of T_H17 cells, and to increase transcription of memory-associated genes through forkhead box protein O1 (FOXO1). [Kar et al., 2020, Chatterjee et al., 2018] An interesting tool to unravel the many functions of CD38 could also be to disrupt only its catalytic function by amino acid substitutions at the catalytically active site of the enzyme.

4.7.2 TRPM2

Our results demonstrated that TRPM2-deficiency does not alter $CD4^+$ and $CD8^+$ T cell function, phenotype and differentiation in the utilized models. We showed that potential compensatory effects, such as increased expression of other Ca^{2+} channels RYR1, TPC1, TPC2 and ORAI1 are not masking the effect of TRPM2-deficiency. However, a compensatory effect can never be excluded and TRPM2 could still be investigated in models utilizing combinations of transgenic mice deficient in the mentioned Ca^+ channels. Apart from activation and differentiation, TRPM2 may still have other functions in T cells, for example conferring cell death in the response to oxidative stress [Manna et al., 2015].

4.7.3 P2X4 and P2X7

We will investigate the role of P2X receptors for $CD8^+$ T cells *in vitro* following the promising results of the *in vitro* experiments investigating $CD4^+$ T cells which showed reduced activation and proliferation. We will investigate $CD8^+$ T cells in *in vitro* stimulation and proliferation assays with *P2x4*$^{-/-}$ and *P2x7*$^{-/-}$ $CD8^+$ T cells and investigate *P2x4*$^{-/-}$. Further we will investigate whether P2X4 and P2X7 is important in the T cell response to bacterial infection in the *L. monocytogenes*

infection model.

4.7.4 Other potential regulators of Ca^{2+} signaling in T cells

The role of other potential regulators of Ca^{2+} signaling in T cells should be adressed as well. Putative regulators include RYR1, TPC1 and TPC2 which also may be studied in *in vitro* stimulation assays and *in vivo* infection models utilizing *L. monocytogenes* and *Staphylococcus aureus*. RYR1 has been found to be co-localized with the NAADP-interacting protein HN1L/JPT2 and is involved in the formation of Ca^{2+} microdomains within milliseconds on TCR stimulation, making it a prime candidate to investigate regulation of Ca^{2+} signaling in $CD8^+$ T cells [Roggenkamp et al., 2021]. TPC1 was shown to interact with HN1L/JPT2 and to regulate NAADP-dependent Ca^{2+} release [Davis et al., 2012, Gunaratne et al., 2021].

Bibliography

[Aarhus et al., 1995] Aarhus, R., Graeff, R. M., Dickey, D. M., Walseth, T. F., and Hon, C. L. (1995). ADP-ribosyl Cyclase and CD38 Catalyze the Synthesis of a Calcium-mobilizing Metabolite from NADP+ (). *Journal of Biological Chemistry*, 270(51):30327–30333.

[Acuto and Michel, 2003] Acuto, O. and Michel, F. (2003). CD28-mediated co-stimulation: a quantitative support for TCR signalling. *Nature Reviews Immunology*, 3(12):939–951.

[Alvarez et al., 2010] Alvarez, J. L., Petzhold, D., Pankonien, I., Behlke, J., Kouno, M., Vassort, G., Morano, I., and Haase, H. (2010). Ahnak1 modulates L-type Ca2+ channel inactivation of rodent cardiomyocytes. *Pflügers Archiv-European Journal of Physiology*, 460(4):719–730.

[Amici et al., 2018] Amici, S. A., Young, N. A., Narvaez-Miranda, J., Jablonski, K. A., Arcos, J., Rosas, L., Papenfuss, T. L., Torrelles, J. B., Jarjour, W. N., and Guerau-de Arellano, M. (2018). CD38 is robustly induced in human macrophages and monocytes in inflammatory conditions. *Frontiers in immunology*, 9:1593.

[Aran et al., 2019] Aran, D., Looney, A. P., Liu, L., Wu, E., Fong, V., Hsu, A., Chak, S., Naikawadi, R. P., Wolters, P. J., Abate, A. R., et al. (2019). Reference-based analysis of lung single-cell sequencing reveals a transitional profibrotic macrophage. *Nature immunology*, 20(2):163–172.

[Ashburner et al., 2000] Ashburner, M., Ball, C. A., Blake, J. A., Botstein, D., Butler, H., Cherry, J. M., Davis, A. P., Dolinski, K., Dwight, S. S., Eppig, J. T., et al. (2000). Gene ontology: tool for the unification of biology. *Nature genetics*, 25(1):25–29.

[Ashouri and Weiss, 2017] Ashouri, J. F. and Weiss, A. (2017). Endogenous Nur77 is a specific indicator of antigen receptor signaling in human T and B cells. *The Journal of Immunology*, 198(2):657–668.

[Asselin-Labat et al., 2004] Asselin-Labat, M.-L., David, M., Biola-Vidamment, A., Lecoeuche, D., Zennaro, M.-C., Bertoglio, J., and Pallardy, M. (2004). GILZ, a new target for the transcription factor FoxO3, protects T lymphocytes from interleukin-2 withdrawal–induced apoptosis. *Blood*, 104(1):215–223.

[Ayroldi et al., 2001] Ayroldi, E., Migliorati, G., Bruscoli, S., Marchetti, C., Zollo, O., Cannarile, L., D'Adamio, F., and Riccardi, C. (2001). Modulation of T-cell activation by the glucocorticoid-induced leucine zipper factor via inhibition of nuclear factor κB. *Blood, The Journal of the American Society of Hematology*, 98(3):743–753.

[Bahri et al., 2012] Bahri, R., Bollinger, A., Bollinger, T., Orinska, Z., and Bulfone-Paus, S. (2012). Ectonucleotidase CD38 demarcates regulatory, memory-like CD8+ T cells with IFN-γ-mediated suppressor activities.

[Barata et al., 2019] Barata, J. T., Durum, S. K., and Seddon, B. (2019). Flip the coin: IL-7 and IL-7R in health and disease. *Nature immunology*, 20(12):1584–1593.

[Baricordi et al., 1999] Baricordi, O. R., Melchiorri, L., Adinolfi, E., Falzoni, S., Chiozzi, P., Buell, G., and Di Virgilio, F. (1999). Increased proliferation rate of lymphoid cells transfected with the P2X7 ATP receptor. *Journal of Biological Chemistry*, 274(47):33206–33208.

[Beceiro et al., 2017] Beceiro, S., Radin, J. N., Chatuvedi, R., Piazuelo, M. B., Horvarth, D., Cortado, H., Gu, Y., Dixon, B., Gu, C., Lange, I., et al. (2017). TRPM2 ion channels regulate macrophage polarization and gastric inflammation during Helicobacter pylori infection. *Mucosal immunology*, 10(2):493–507.

[Beck et al., 2006] Beck, A., Kolisek, M., Bagley, L. A., Fleig, A., Penner, R., Beck, A., Kolisek, M., Bagley, L. A., Fleig, A., and Penner, R. (2006). Nicotinic acid adenine dinucleotide phosphate and cyclic ADP-ribose regulate TRPM2 channels in T lymphocytes. *The FASEB journal*, 20(7):962–964.

[Bhan et al., 1980] Bhan, A. K., Reinherz, E. L., Poppema, S., McCluskey, R., and Schlossman, S. (1980). Location of T cell and major histocompatibility complex antigens in the human thymus. *The Journal of experimental medicine*, 152(4):771–782.

[Born et al., 1998] Born, T. L., Thomassen, E., Bird, T. A., and Sims, J. E. (1998). Cloning of a novel receptor subunit, AcPL, required for interleukin-18 signaling. *Journal of Biological Chemistry*, 273(45):29445–29450.

[Brock et al., 2022] Brock, V. J., Wolf, I. M., Er-Lukowiak, M., Lory, N., Stähler, T., Woelk, L.-M., Mittrücker, H.-W., Müller, C. E., Koch-Nolte, F., Rissiek, B., et al. (2022). P2X4 and P2X7 are essential players in basal T cell activity and Ca2+ signaling milliseconds after T cell activation. *Science Advances*, 8(5):eabl9770.

[Burnstock and Boeynaems, 2014] Burnstock, G. and Boeynaems, J.-M. (2014). Purinergic signalling and immune cells. *Purinergic signalling*, 10(4):529–564.

[Carr et al., 2010] Carr, E. L., Kelman, A., Wu, G. S., Gopaul, R., Senkevitch, E., Aghvanyan, A., Turay, A. M., and Frauwirth, K. A. (2010). Glutamine uptake and metabolism are coordinately regulated by ERK/MAPK during T lymphocyte activation. *The Journal of Immunology*, 185(2):1037–1044.

[Cauchy et al., 2016] Cauchy, P., Maqbool, M. A., Zacarias-Cabeza, J., Vanhille, L., Koch, F., Fenouil, R., Gut, M., Gut, I., Santana, M. A., Griffon, A., et al. (2016). Dynamic recruitment of Ets1 to both nucleosome-occupied and-depleted enhancer regions mediates a transcriptional program switch during early T-cell differentiation. *Nucleic acids research*, 44(8):3567–3585.

[Chakraborty and Mehrotra, 2020] Chakraborty, P. and Mehrotra, S. (2020). CD38: Modulating histone methyltransferase EZH2 activity in SLE. *Trends in Immunology*, 41(3):187–189.

[Chatterjee et al., 2018] Chatterjee, S., Daenthanasanmak, A., Chakraborty, P., Wyatt, M. W., Dhar, P., Selvam, S. P., Fu, J., Zhang, J., Nguyen, H., Kang, I., et al. (2018). CD38-NAD+ axis regulates immunotherapeutic anti-tumor T cell response. *Cell metabolism*, 27(1):85–100.

[Chatzileontiadou et al., 2021] Chatzileontiadou, D. S., Sloane, H., Nguyen, A. T., Gras, S., and Grant, E. J. (2021). The many faces of CD4+ T cells: Immunological and structural characteristics. *International Journal of Molecular Sciences*, 22(1):73.

[Chen et al., 2006] Chen, J., Chen, Y.-G., Reifsnyder, P. C., Schott, W. H., Lee, C.-H., Osborne, M., Scheuplein, F., Haag, F., Koch-Nolte, F., Serreze, D. V., et al. (2006). Targeted disruption of CD38 accelerates autoimmune diabetes in NOD/Lt mice by enhancing autoimmunity in an ADP-ribosyltransferase 2-dependent fashion. *The Journal of Immunology*, 176(8):4590–4599.

[Cheung et al., 2005] Cheung, H., Chen, N.-J., Cao, Z., Ono, N., Ohashi, P. S., and Yeh, W.-C. (2005). Accessory protein-like is essential for IL-18-mediated signaling. *The Journal of Immunology*, 174(9):5351–5357.

[Cockayne et al., 1998] Cockayne, D. A., Muchamuel, T., Grimaldi, J. C., Muller-Steffner, H., Randall, T. D., Lund, F. E., Murray, R., Schuber, F., and Howard, M. C. (1998). Mice deficient for the ecto-nicotinamide adenine dinucleotide glycohydrolase CD38 exhibit altered humoral immune responses. *Blood, The Journal of the American Society of Hematology*, 92(4):1324–1333.

[Da Silva et al., 1998] Da Silva, C. P., Schweitzer, K., Heyer, P., Malavasi, F., Mayr, G. W., and Guse, A. H. (1998). Ectocellular CD38-catalyzed synthesis and intracellular Ca2+-signalling activity of cyclic ADP-ribose in T-lymphocytes are not functionally related. *FEBS letters*, 439(3):291–296.

[Dammermann et al., 2009] Dammermann, W., Zhang, B., Nebel, M., Cordiglieri, C., Odoardi, F., Kirchberger, T., Kawakami, N., Dowden, J., Schmid, F., Dornmair, K., et al. (2009). NAADP-mediated Ca2+ signaling via type 1 ryanodine receptor in T cells revealed by a synthetic NAADP antagonist. *Proceedings of the National Academy of Sciences*, 106(26):10678–10683.

[Danquah et al., 2016] Danquah, W., Meyer-Schwesinger, C., Rissiek, B., Pinto, C., Serracant-Prat, A., Amadi, M., Iacenda, D., Knop, J.-H., Hammel, A., Bergmann, P., et al. (2016). Nanobodies that block gating of the P2X7 ion channel ameliorate inflammation. *Science translational medicine*, 8(366):366ra162–366ra162.

[Davis et al., 2012] Davis, L. C., Morgan, A. J., Chen, J.-L., Snead, C. M., Bloor-Young, D., Shenderov, E., Stanton-Humphreys, M. N., Conway, S. J., Churchill, G. C., Parrington, J., et al. (2012). NAADP activates two-pore channels on T cell cytolytic granules to stimulate exocytosis and killing. *Current Biology*, 22(24):2331–2337.

[de Araújo-Souza et al., 2015] de Araújo-Souza, P. S., Hanschke, S. C., and Viola, J. P. (2015). Epigenetic control of interferon-gamma expression in CD8 T cells. *Journal of immunology research*, 2015.

[Deaglio et al., 1998] Deaglio, S., Morra, M., Mallone, R., Ausiello, C. M., Prager, E., Garbarino, G., Dianzani, U., Stockinger, H., and Malavasi, F. (1998). Human CD38 (ADP-ribosyl cyclase) is

a counter-receptor of CD31, an Ig superfamily member. *The Journal of Immunology*, 160(1):395–402.

[Debets et al., 2000] Debets, R., Timans, J. C., Churakowa, T., Zurawski, S., de Waal Malefyt, R., Moore, K. W., Abrams, J. S., O'Garra, A., Bazan, J. F., and Kastelein, R. A. (2000). IL-18 receptors, their role in ligand binding and function: anti-IL-1RAcPL antibody, a potent antagonist of IL-18. *The Journal of Immunology*, 165(9):4950–4956.

[Di et al., 2017] Di, A., Kiya, T., Gong, H., Gao, X., and Malik, A. B. (2017). Role of the phagosomal redox-sensitive TRP channel TRPM2 in regulating bactericidal activity of macrophages. *Journal of cell science*, 130(4):735–744.

[Di Bartolomeo et al., 2017] Di Bartolomeo, F., Wagner, A., and Daum, G. (2017). Cell biology, physiology and enzymology of phosphatidylserine decarboxylase. *Biochimica et Biophysica Acta (BBA)-Molecular and Cell Biology of Lipids*, 1862(1):25–38.

[Di Virgilio et al., 2018] Di Virgilio, F., Sarti, A. C., and Grassi, F. (2018). Modulation of innate and adaptive immunity by P2X ion channels. *Current opinion in immunology*, 52:51–59.

[Diercks et al., 2018] Diercks, B.-P., Werner, R., Weidemüller, P., Czarniak, F., Hernandez, L., Lehmann, C., Rosche, A., Krüger, A., Kaufmann, U., Vaeth, M., et al. (2018). ORAI1, STIM1/2, and RYR1 shape subsecond Ca2+ microdomains upon T cell activation. *Science signaling*, 11(561).

[Doedens et al., 2013] Doedens, A. L., Phan, A. T., Stradner, M. H., Fujimoto, J. K., Nguyen, J. V., Yang, E., Johnson, R. S., and Goldrath, A. W. (2013). Hypoxia-inducible factors enhance the effector responses of CD8+ T cells to persistent antigen. *Nature immunology*, 14(11):1173–1182.

[Estrada-Figueroa et al., 2011] Estrada-Figueroa, L., Ramírez-Jiménez, Y., Osorio-Trujillo, C., Shibayama, M., NAVARRO-GARCÍA, F., GARCÍA-TOVAR, C., and TALAMÁS-ROHANA, P. (2011). Absence of CD38 delays arrival of neutrophils to the liver and innate immune response development during hepatic amoebiasis by Entamoeba histolytica. *Parasite immunology*, 33(12):661–668.

[Fan et al., 2003] Fan, Z., Beresford, P. J., Oh, D. Y., Zhang, D., and Lieberman, J. (2003). Tumor suppressor NM23-H1 is a granzyme A-activated DNase during CTL-mediated apoptosis, and the nucleosome assembly protein SET is its inhibitor. *Cell*, 112(5):659–672.

[Fedele et al., 2015] Fedele, G., Sanseverino, I., D'Agostino, K., Schiavoni, I., Locht, C., Horenstein, A. L., Malavasi, F., and Ausiello, C. M. (2015). Unconventional, adenosine-producing suppressor T cells induced by dendritic cells exposed to BPZE1 pertussis vaccine. *Journal of Leukocyte Biology*, 98(4):631–639.

[Finlay et al., 2012] Finlay, D. K., Rosenzweig, E., Sinclair, L. V., Feijoo-Carnero, C., Hukelmann, J. L., Rolf, J., Panteleyev, A. A., Okkenhaug, K., and Cantrell, D. A. (2012). PDK1 regulation of mTOR and hypoxia-inducible factor 1 integrate metabolism and migration of CD8+ T cells. *Journal of Experimental Medicine*, 209(13):2441–2453.

[Fliegert et al., 2017] Fliegert, R., Bauche, A., Pérez, A.-M. W., Watt, J. M., Rozewitz, M. D., Winzer, R., Janus, M., Gu, F., Rosche, A., Harneit, A., et al. (2017). 2-Deoxyadenosine 5-diphosphoribose is an endogenous TRPM2 superagonist. *Nature chemical biology*, 13(9):1036–1044.

[Fliegert et al., 2020] Fliegert, R., Riekehr, W. M., and Guse, A. H. (2020). Does cyclic adp-ribose (cADPR) activate the non-selective cation channel TRPM2? *Frontiers in Immunology*, page 2018.

[Frauenstein et al., 2021] Frauenstein, A., Ebner, S., Hansen, F. M., Sinha, A., Phulphagar, K., Swatek, K., Hornburg, D., Mann, M., and Meissner, F. (2021). Identification of covalent modifications regulating immune signaling complex composition and phenotype. *Molecular systems biology*, 17(7):e10125.

[Frauwirth et al., 2002] Frauwirth, K. A., Riley, J. L., Harris, M. H., Parry, R. V., Rathmell, J. C., Plas, D. R., Elstrom, R. L., June, C. H., and Thompson, C. B. (2002). The CD28 signaling pathway regulates glucose metabolism. *Immunity*, 16(6):769–777.

[Fujita et al., 2012] Fujita, M., Takada, Y. K., and Takada, Y. (2012). Integrins αvβ3 and α4β1 act as coreceptors for fractalkine, and the integrin-binding defective mutant of fractalkine is an antagonist of CX3CR1. *The Journal of Immunology*, 189(12):5809–5819.

[Gasser et al., 2006] Gasser, A., Bruhn, S., and Guse, A. H. (2006). Second messenger function of nicotinic acid adenine dinucleotide phosphate revealed by an improved enzymatic cycling assay. *Journal of Biological Chemistry*, 281(25):16906–16913.

[Gattkowski et al., 2021] Gattkowski, E., Rutherford, T. J., Möckl, F., Bauche, A., Sander, S., Fliegert, R., and Tidow, H. (2021). Analysis of ligand binding and resulting conformational changes in pyrophosphatase NUDT9. *The FEBS Journal*, 288(23):6769–6782.

[Gaud et al., 2018] Gaud, G., Lesourne, R., and Love, P. E. (2018). Regulatory mechanisms in T cell receptor signalling. *Nature Reviews Immunology*, 18(8):485–497.

[Gelderblom et al., 2014] Gelderblom, M., Melzer, N., Schattling, B., Göb, E., Hicking, G., Arunachalam, P., Bittner, S., Ufer, F., Herrmann, A. M., Bernreuther, C., et al. (2014). Transient receptor potential melastatin subfamily member 2 cation channel regulates detrimental immune cell invasion in ischemic stroke. *Stroke*, 45(11):3395–3402.

[Gentleman et al., 2004] Gentleman, R. C., Carey, V. J., Bates, D. M., Bolstad, B., Dettling, M., Dudoit, S., Ellis, B., Gautier, L., Ge, Y., Gentry, J., et al. (2004). Bioconductor: open software development for computational biology and bioinformatics. *Genome biology*, 5(10):1–16.

[Gerasimenko et al., 2003] Gerasimenko, J. V., Maruyama, Y., Yano, K., Dolman, N. J., Tepikin, A. V., Petersen, O. H., and Gerasimenko, O. V. (2003). NAADP mobilizes Ca2+ from a thapsigargin-sensitive store in the nuclear envelope by activating ryanodine receptors. *The Journal of cell biology*, 163(2):271–282.

[Gerlach et al., 2016] Gerlach, C., Moseman, E. A., Loughhead, S. M., Alvarez, D., Zwijnenburg, A. J., Waanders, L., Garg, R., Juan, C., and von Andrian, U. H. (2016). The chemokine receptor CX3CR1 defines three antigen-experienced CD8 T cell subsets with distinct roles in immune surveillance and homeostasis. *Immunity*, 45(6):1270–1284.

[Grassi, 2020] Grassi, F. (2020). The P2X7 receptor as regulator of T cell development and function. *Frontiers in Immunology*, 11:1179.

[Gu et al., 2021] Gu, F., Krüger, A., Roggenkamp, H. G., Alpers, R., Lodygin, D., Jaquet, V., Möckl, F., Hernandez C, L. C., Winterberg, K., Bauche, A., et al. (2021). Dual NADPH oxidases DUOX1 and DUOX2 synthesize NAADP and are necessary for Ca2+ signaling during T cell activation. *Science Signaling*, 14(709):eabe3800.

[Gunaratne et al., 2021] Gunaratne, G. S., Brailoiu, E., He, S., Unterwald, E. M., Patel, S., Slama, J. T., Walseth, T. F., and Marchant, J. S. (2021). Essential requirement for JPT2 in NAADP-evoked Ca2+ signaling. *Science Signaling*, 14(675).

[Guse et al., 1999] Guse, A. H., Da Silva, C. P., Berg, I., Skapenko, A. L., Weber, K., Heyer, P., Hohenegger, M., Ashamu, G. A., Schulze-Koops, H., Potter, B. V., et al. (1999). Regulation of calcium signalling in T lymphocytes by the second messenger cyclic ADP-ribose. *Nature*, 398(6722):70–73.

[Guse and Wolf, 2016] Guse, A. H. and Wolf, I. M. (2016). Ca2+ microdomains, NAADP and type 1 ryanodine receptor in cell activation. *Biochimica et Biophysica Acta (BBA)-Molecular Cell Research*, 1863(6):1379–1384.

[Hao et al., 2021] Hao, Y., Hao, S., Andersen-Nissen, E., III, W. M. M., Zheng, S., Butler, A., Lee, M. J., Wilk, A. J., Darby, C., Zagar, M., Hoffman, P., Stoeckius, M., Papalexi, E., Mimitou, E. P., Jain, J., Srivastava, A., Stuart, T., Fleming, L. B., Yeung, B., Rogers, A. J., McElrath, J. M., Blish, C. A., Gottardo, R., Smibert, P., and Satija, R. (2021). Integrated analysis of multimodal single-cell data. *Cell*.

[Hara et al., 2002] Hara, Y., Wakamori, M., Ishii, M., Maeno, E., Nishida, M., Yoshida, T., Yamada, H., Shimizu, S., Mori, E., Kudoh, J., et al. (2002). LTRPC2 Ca2+-permeable channel activated by changes in redox status confers susceptibility to cell death. *Molecular cell*, 9(1):163–173.

[Hardwick and Soane, 2013] Hardwick, J. M. and Soane, L. (2013). Multiple functions of BCL-2 family proteins. *Cold Spring Harbor perspectives in biology*, 5(2):a008722.

[Heiner et al., 2006] Heiner, I., Eisfeld, J., Warnstedt, M., and Radukina, N. (2006). Jü ngling E, Lü ckhoff A. 2006. Endogenous ADP-ribose enables calcium-regulated cation currents through TRPM2 channels in neutrophil granulocytes. *Biochemical Journal*, 398:225–232.

[Heng et al., 2008] Heng, T. S., Painter, M. W., Elpek, K., Lukacs-Kornek, V., Mauermann, N., Turley, S. J., Koller, D., Kim, F. S., Wagers, A. J., Asinovski, N., et al. (2008). The Immunological Genome Project: networks of gene expression in immune cells. *Nature immunology*, 9(10):1091–1094.

[Hofmann et al., 2003] Hofmann, T., Chubanov, V., Gudermann, T., and Montell, C. (2003). TRPM5 is a voltage-modulated and Ca2+-activated monovalent selective cation channel. *Current biology*, 13(13):1153–1158.

[Hogan, 2017] Hogan, P. G. (2017). Calcium–NFAT transcriptional signalling in T cell activation and T cell exhaustion. *Cell calcium*, 63:66–69.

[Hogquist et al., 1994] Hogquist, K. A., Jameson, S. C., Heath, W. R., Howard, J. L., Bevan, M. J., and Carbone, F. R. (1994). T cell receptor antagonist peptides induce positive selection. *Cell*, 76(1):17–27.

[Huang et al., 2020] Huang, Y., Fliegert, R., Guse, A. H., Lü, W., and Du, J. (2020). A structural overview of the ion channels of the TRPM family. *Cell Calcium*, 85:102111.

[Jenkins and Moon, 2012] Jenkins, M. K. and Moon, J. J. (2012). The role of naive T cell precursor frequency and recruitment in dictating immune response magnitude. *The Journal of Immunology*, 188(9):4135–4140.

[Joshi et al., 2007] Joshi, N. S., Cui, W., Chandele, A., Lee, H. K., Urso, D. R., Hagman, J., Gapin, L., and Kaech, S. M. (2007). Inflammation directs memory precursor and short-lived effector CD8+ T cell fates via the graded expression of T-bet transcription factor. *Immunity*, 27(2):281–295.

[Kaech and Cui, 2012] Kaech, S. M. and Cui, W. (2012). Transcriptional control of effector and memory CD8+ T cell differentiation. *Nature Reviews Immunology*, 12(11):749–761.

[Kanellopoulos et al., 2021] Kanellopoulos, J. M., Almeida-da Silva, C. L. C., Rüütel Boudinot, S., and Ojcius, D. M. (2021). Structural and functional features of the P2X4 receptor: An immunological perspective. *Frontiers in Immunology*, 12:852.

[Kar et al., 2020] Kar, A., Mehrotra, S., and Chatterjee, S. (2020). CD38: T cell immuno-metabolic modulator. *Cells*, 9(7):1716.

[Kashio et al., 2012] Kashio, M., Sokabe, T., Shintaku, K., Uematsu, T., Fukuta, N., Kobayashi, N., Mori, Y., and Tominaga, M. (2012). Redox signal-mediated sensitization of transient receptor potential melastatin 2 (TRPM2) to temperature affects macrophage functions. *Proceedings of the National Academy of Sciences*, 109(17):6745–6750.

[Katsuyama et al., 2020] Katsuyama, E., Suarez-Fueyo, A., Bradley, S. J., Mizui, M., Marin, A. V., Mulki, L., Krishfield, S., Malavasi, F., Yoon, J., Sui, S. J. H., et al. (2020). The CD38/NAD/SIRTUIN1/EZH2 axis mitigates cytotoxic CD8 T cell function and identifies patients with SLE prone to infections. *Cell reports*, 30(1):112–123.

[Kim et al., 2020] Kim, C., Jin, J., Weyand, C. M., and Goronzy, J. J. (2020). The transcription factor TCF1 in T cell differentiation and aging. *International journal of molecular sciences*, 21(18):6497.

[Klein-Hessling et al., 2017] Klein-Hessling, S., Muhammad, K., Klein, M., Pusch, T., Rudolf, R., Flöter, J., Qureischi, M., Beilhack, A., Vaeth, M., Kummerow, C., et al. (2017). NFATc1 controls the cytotoxicity of CD8+ T cells. *Nature communications*, 8(1):1–15.

[Knowles et al., 2011] Knowles, H., Heizer, J. W., Li, Y., Chapman, K., Ogden, C. A., Andreasen, K., Shapland, E., Kucera, G., Mogan, J., Humann, J., et al. (2011). Transient Receptor Potential Melastatin 2 (TRPM2) ion channel is required for innate immunity against Listeria monocytogenes. *Proceedings of the National Academy of Sciences*, 108(28):11578–11583.

[Knowles et al., 2013] Knowles, H., Li, Y., and Perraud, A.-L. (2013). The TRPM2 ion channel, an oxidative stress and metabolic sensor regulating innate immunity and inflammation. *Immunologic research*, 55(1):241–248.

[Kolisek et al., 2005] Kolisek, M., Beck, A., Fleig, A., and Penner, R. (2005). Cyclic ADP-ribose and hydrogen peroxide synergize with ADP-ribose in the activation of TRPM2 channels. *Molecular cell*, 18(1):61–69.

[Korthals et al., 2017] Korthals, M., Langnaese, K., Smalla, K.-H., Kähne, T., Herrera-Molina, R., Handschuh, J., Lehmann, A.-C., Mamula, D., Naumann, M., Seidenbecher, C., et al. (2017). A complex of neuroplastin and plasma membrane Ca2+ ATPase controls T cell activation. *Scientific reports*, 7(1):1–13.

[Krejcik et al., 2016] Krejcik, J., Casneuf, T., Nijhof, I. S., Verbist, B., Bald, J., Plesner, T., Syed, K., Liu, K., van de Donk, N. W., Weiss, B. M., et al. (2016). Daratumumab depletes CD38+ immune regulatory cells, promotes T-cell expansion, and skews T-cell repertoire in multiple myeloma. *Blood, The Journal of the American Society of Hematology*, 128(3):384–394.

[Kumar et al., 2017] Kumar, B. V., Ma, W., Miron, M., Granot, T., Guyer, R. S., Carpenter, D. J., Senda, T., Sun, X., Ho, S.-H., Lerner, H., et al. (2017). Human tissue-resident memory T cells are defined by core transcriptional and functional signatures in lymphoid and mucosal sites. *Cell reports*, 20(12):2921–2934.

[Kurtulus et al., 2011] Kurtulus, S., Tripathi, P., Moreno-Fernandez, M. E., Sholl, A., Katz, J. D., Grimes, H. L., and Hildeman, D. A. (2011). Bcl-2 allows effector and memory CD8+ T cells to tolerate higher expression of Bim. *The Journal of Immunology*, 186(10):5729–5737.

[Landström, 2010] Landström, M. (2010). The TAK1–TRAF6 signalling pathway. *The international journal of biochemistry & cell biology*, 42(5):585–589.

[Lange et al., 2008] Lange, I., Penner, R., Fleig, A., and Beck, A. (2008). Synergistic regulation of endogenous TRPM2 channels by adenine dinucleotides in primary human neutrophils. *Cell calcium*, 44(6):604–615.

[Launay et al., 2004] Launay, P., Cheng, H., Srivatsan, S., Penner, R., Fleig, A., and Kinet, J.-P. (2004). TRPM4 regulates calcium oscillations after T cell activation. *Science*, 306(5700):1374–1377.

[Launay et al., 2002] Launay, P., Fleig, A., Perraud, A.-L., Scharenberg, A. M., Penner, R., and Kinet, J.-P. (2002). TRPM4 is a Ca2+-activated nonselective cation channel mediating cell membrane depolarization. *Cell*, 109(3):397–407.

[Ledderose et al., 2014] Ledderose, C., Bao, Y., Lidicky, M., Zipperle, J., Li, L., Strasser, K., Shapiro, N. I., and Junger, W. G. (2014). Mitochondria are gate-keepers of T cell function by producing the ATP that drives purinergic signaling. *Journal of Biological Chemistry*, 289(37):25936–25945.

[Ledderose et al., 2018] Ledderose, C., Liu, K., Kondo, Y., Slubowski, C. J., Dertnig, T., Denicoló, S., Arbab, M., Hubner, J., Konrad, K., Fakhari, M., et al. (2018). Purinergic P2X4 receptors and mitochondrial ATP production regulate T cell migration. *The Journal of clinical investigation*, 128(8):3583–3594.

[Lee et al., 2018] Lee, J.-U., Kim, L.-K., and Choi, J.-M. (2018). Revisiting the concept of targeting NFAT to control T cell immunity and autoimmune diseases. *Frontiers in immunology*, 9:2747.

[Lee et al., 2005] Lee, K. N., Kang, H.-S., Jeon, J.-H., Kim, E.-M., Yoon, S.-R., Song, H., Lyu, C.-Y., Piao, Z.-H., Kim, S.-U., Han, Y.-H., et al. (2005). VDUP1 is required for the development of natural killer cells. *Immunity*, 22(2):195–208.

[Lee et al., 2008] Lee, S.-M., Gao, B., and Fang, D. (2008). FoxP3 maintains Treg unresponsiveness by selectively inhibiting the promoter DNA-binding activity of AP-1. *Blood, The Journal of the American Society of Hematology*, 111(7):3599–3606.

[Li et al., 2020] Li, K.-P., Ladle, B. H., Kurtulus, S., Sholl, A., Shanmuganad, S., and Hildeman, D. A. (2020). T-cell receptor signal strength and epigenetic control of Bim predict memory CD8+ T-cell fate. *Cell Death & Differentiation*, 27(4):1214–1224.

[Lischke et al., 2013] Lischke, T., Heesch, K., Schumacher, V., Schneider, M., Haag, F., Koch-Nolte, F., and Mittrücker, H.-W. (2013). CD38 controls the innate immune response against Listeria monocytogenes. *Infection and immunity*, 81(11):4091–4099.

[López-Cortés et al., 2021] López-Cortés, G. I., Díaz-Alvarez, L., and Ortega, E. (2021). Leukocyte Membrane Enzymes Play the Cell Adhesion Game. *Frontiers in immunology*, 12:742292–742292.

[Lory et al., 2022] Lory, N. C., Nawrocki, M., Corazza, M., Schmid, J., Schumacher, V., Bedke, T., Menzel, S., Koch-Nolte, F., Guse, A. H., Huber, S., and Mittrücker, H.-W. (2022). TRPM2 Is Not Required for T-Cell Activation and Differentiation. *Frontiers in Immunology*, 12.

[Mackay et al., 2013] Mackay, L. K., Rahimpour, A., Ma, J. Z., Collins, N., Stock, A. T., Hafon, M.-L., Vega-Ramos, J., Lauzurica, P., Mueller, S. N., Stefanovic, T., et al. (2013). The developmental pathway for CD103+ CD8+ tissue-resident memory T cells of skin. *Nature immunology*, 14(12):1294–1301.

[Malavasi et al., 2008] Malavasi, F., Deaglio, S., Funaro, A., Ferrero, E., Horenstein, A. L., Ortolan, E., Vaisitti, T., and Aydin, S. (2008). Evolution and function of the ADP ribosyl cyclase/CD38 gene family in physiology and pathology. *Physiological reviews*, 88(3):841–886.

[Malavasi et al., 1992] Malavasi, F., Funaro, A., Alessio, M., DeMonte, L. B., Ausiello, C. M., Dianzani, U., Lanza, F., Magrini, E., Momo, M., and Roggero, S. (1992). CD38: a multi-lineage cell activation molecule with a split personality. *International Journal of Clinical and Laboratory Research*, 22(1):73–80.

[Manna et al., 2015] Manna, P. T., Munsey, T. S., Abuarab, N., Li, F., Asipu, A., Howell, G., Sedo, A., Yang, W., Naylor, J., Beech, D. J., et al. (2015). TRPM2-mediated intracellular Zn2+ release triggers pancreatic beta-cell death. *Biochem J*, 466(3):537–46.

[Martins and Aguas, 1999] Martins, T. and Aguas, A. (1999). A role for CD45RBlow CD38+ T cells and costimulatory pathways of T-cell activation in protection of non-obese diabetic (NOD) mice from diabetes. *Immunology*, 96(4):600.

[McMahon and Luger, 2019] McMahon, C. M. and Luger, S. M. (2019). Relapsed T cell ALL: current approaches and new directions. *Current hematologic malignancy reports*, 14(2):83–93.

[Mele et al., 2018] Mele, S., Devereux, S., Pepper, A. G., Infante, E., and Ridley, A. J. (2018). Calcium-RasGRP2-Rap1 signaling mediates CD38-induced migration of chronic lymphocytic leukemia cells. *Blood advances*, 2(13):1551–1561.

[Melzer et al., 2012] Melzer, N., Hicking, G., Göbel, K., and Wiendl, H. (2012). TRPM2 cation channels modulate T cell effector functions and contribute to autoimmune CNS inflammation.

[Mercado et al., 2000] Mercado, R., Vijh, S., Allen, S. E., Kerksiek, K., Pilip, I. M., and Pamer, E. G. (2000). Early programming of T cell populations responding to bacterial infection. *The Journal of Immunology*, 165(12):6833–6839.

[Mi et al., 2019] Mi, H., Muruganujan, A., Ebert, D., Huang, X., and Thomas, P. D. (2019). PANTHER version 14: more genomes, a new PANTHER GO-slim and improvements in enrichment analysis tools. *Nucleic acids research*, 47(D1):D419–D426.

[Mombaerts et al., 1992] Mombaerts, P., Iacomini, J., Johnson, R. S., Herrup, K., Tonegawa, S., and Papaioannou, V. E. (1992). RAG-1-deficient mice have no mature B and T lymphocytes. *Cell*, 68(5):869–877.

[Morad et al., 2021] Morad, H., Luqman, S., Tan, C.-H., Swann, V., and McNaughton, P. A. (2021). TRPM2 ion channels steer neutrophils towards a source of hydrogen peroxide. *Scientific reports*, 11(1):1–16.

[Morandi et al., 2019] Morandi, F., Airoldi, I., Marimpietri, D., Bracci, C., Faini, A. C., and Gramignoli, R. (2019). CD38, a receptor with multifunctional activities: from modulatory functions on regulatory cell subsets and extracellular vesicles, to a target for therapeutic strategies. *Cells*, 8(12):1527.

[Moskowitz et al., 2017] Moskowitz, D. M., Zhang, D. W., Hu, B., Le Saux, S., Yanes, R. E., Ye, Z., Buenrostro, J. D., Weyand, C. M., Greenleaf, W. J., and Goronzy, J. J. (2017). Epigenomics of human CD8 T cell differentiation and aging. *Science immunology*, 2(8):eaag0192.

[Muñoz et al., 2008] Muñoz, P., Mittelbrunn, M., de la Fuente, H., Pérez-Martínez, M., García-Pérez, A., Ariza-Veguillas, A., Malavasi, F., Zubiaur, M., Sánchez-Madrid, F., and Sancho, J. (2008). Antigen-induced clustering of surface CD38 and recruitment of intracellular CD38 to the immunologic synapse. *Blood, The Journal of the American Society of Hematology*, 111(7):3653–3664.

[Murphy and Weaver, 2016] Murphy, K. and Weaver, C. (2016). *Janeway's immunobiology*. Garland science.

[Murrell-Lagnado and Frick, 2019] Murrell-Lagnado, R. D. and Frick, M. (2019). P2X4 and lysosome fusion. *Current opinion in pharmacology*, 47:126–132.

[Omilusik et al., 2015] Omilusik, K. D., Best, J. A., Yu, B., Goossens, S., Weidemann, A., Nguyen, J. V., Seuntjens, E., Stryjewska, A., Zweier, C., Roychoudhuri, R., et al. (2015). Transcriptional repressor ZEB2 promotes terminal differentiation of CD8+ effector and memory T cell populations during infection. *Journal of Experimental Medicine*, 212(12):2027–2039.

[Ontology, 2021] Ontology, G. (2021). The Gene Ontology resource: enriching a GOld mine. *Nucleic acids research*, 49(D1):D325–D334.

[Partida-Sanchez et al., 2001] Partida-Sanchez, S., Cockayne, D. A., Monard, S., Jacobson, E. L., Oppenheimer, N., Garvy, B., Kusser, K., Goodrich, S., Howard, M., Harmsen, A., et al. (2001). Cyclic ADP-ribose production by CD38 regulates intracellular calcium release, extracellular calcium influx and chemotaxis in neutrophils and is required for bacterial clearance in vivo. *Nature medicine*, 7(11):1209–1216.

[Partida-Sanchez et al., 2007] Partida-Sanchez, S., Gasser, A., Fliegert, R., Siebrands, C. C., Dammermann, W., Shi, G., Mousseau, B. J., Sumoza-Toledo, A., Bhagat, H., Walseth, T. F., et al. (2007). Chemotaxis of mouse bone marrow neutrophils and dendritic cells is controlled by adp-ribose, the major product generated by the CD38 enzyme reaction. *The Journal of Immunology*, 179(11):7827–7839.

[Partida-Sánchez et al., 2004a] Partida-Sánchez, S., Goodrich, S., Kusser, K., Oppenheimer, N., Randall, T. D., and Lund, F. E. (2004a). Regulation of dendritic cell trafficking by the ADP-ribosyl cyclase CD38: impact on the development of humoral immunity. *Immunity*, 20(3):279–291.

[Partida-Sánchez et al., 2004b] Partida-Sánchez, S., Iribarren, P., Moreno-García, M. E., Gao, J.-L., Murphy, P. M., Oppenheimer, N., Wang, J. M., and Lund, F. E. (2004b). Chemotaxis and calcium responses of phagocytes to formyl peptide receptor ligands is differentially regulated by cyclic ADP ribose. *The Journal of Immunology*, 172(3):1896–1906.

[Patton et al., 2011] Patton, D. T., Wilson, M. D., Rowan, W. C., Soond, D. R., and Okkenhaug, K. (2011). The PI3K p110δ regulates expression of CD38 on regulatory T cells. *PloS one*, 6(3):e17359.

[Paul et al., 2014] Paul, S., Traver, M. K., Kashyap, A. K., Washington, M. A., Latoche, J. R., and Schaefer, B. C. (2014). T cell receptor signals to NF-κB are transmitted by a cytosolic p62-Bcl10-Malt1-IKK signalosome. *Science signaling*, 7(325):ra45–ra45.

[Pearce et al., 2013] Pearce, E. L., Poffenberger, M. C., Chang, C.-H., and Jones, R. G. (2013). Fueling immunity: insights into metabolism and lymphocyte function. *Science*, 342(6155):1242454.

[Pearson et al., 2011] Pearson, R. C., Funnell, A. P., and Crossley, M. (2011). The mammalian zinc finger transcription factor Krüppel-like factor 3 (KLF3/BKLF). *IUBMB life*, 63(2):86–93.

[Qian et al., 2018] Qian, X., Zhao, H., Chen, X., and Li, J. (2018). Disruption of transient receptor potential melastatin 2 decreases elastase release and bacterial clearance in neutrophils. *Innate immunity*, 24(2):122–130.

[Read et al., 1998] Read, S., Mauze, S., Asseman, C., Bean, A., Coffman, R., and Powrie, F. (1998). CD38+ CD45RBlow CD4+ T cells: a population of T cells with immune regulatory activities in vitro. *European journal of immunology*, 28(11):3435–3447.

[Rissiek et al., 2018] Rissiek, B., Lukowiak, M., Raczkowski, F., Magnus, T., Mittrücker, H.-W., and Koch-Nolte, F. (2018). In vivo blockade of murine ARTC2. 2 during cell preparation preserves the vitality and function of liver tissue-resident memory T cells. *Frontiers in immunology*, 9:1580.

[Robledo-Avila et al., 2020] Robledo-Avila, F. H., Ruiz-Rosado, J. d. D., Brockman, K. L., and Partida-Sánchez, S. (2020). The TRPM2 Ion channel regulates inflammatory functions of neutrophils during listeria monocytogenes infection. *Frontiers in immunology*, 11:97.

[Roggenkamp et al., 2021] Roggenkamp, H. G., Khansahib, I., Hernandez C, L. C., Zhang, Y., Lodygin, D., Krueger, A., Gu, F., Moeckl, F., Loehndorf, A., Wolters, V., et al. (2021).

HN1L/JPT2: A signaling protein that connects NAADP generation to Ca2+ microdomain formation. *Science signaling*, 14(675):eabd5647.

[Rosenstein et al., 1991] Rosenstein, Y., Park, J. K., Hahn, W. C., Rosen, F. S., Bierer, B. E., and Burakoff, S. J. (1991). CD43, a molecule defective in Wiskott-Aldrich syndrome, binds ICAM-1. *Nature*, 354(6350):233–235.

[Ruiz-Rodríguez et al., 2019] Ruiz-Rodríguez, V. M., Cortes-García, J. D., de Jesús Briones-Espinoza, M., Rodríguez-Varela, E., Vega-Cárdenas, M., Gómez-Otero, A., García-Hernández, M. H., and Portales-Pérez, D. P. (2019). P2X4 receptor as a modulator in the function of P2X receptor in CD4+ T cells from peripheral blood and adipose tissue. *Molecular immunology*, 112:369–377.

[Schenk et al., 2011] Schenk, U., Frascoli, M., Proietti, M., Geffers, R., Traggiai, E., Buer, J., Ricordi, C., Westendorf, A. M., and Grassi, F. (2011). ATP inhibits the generation and function of regulatory T cells through the activation of purinergic P2X receptors. *Science signaling*, 4(162):ra12–ra12.

[Schenk et al., 2009] Schenk, U., Westendorf, A., Radaelli, E., Casati, A., Fumagalli, M., Verderio, C., Buer, J., Scanziani, E., and Grassi, F. (2009). Purinergic control of T cell activation by ATP released through pannexin-1 hemichannels. In *Joint annual congress of the Swiss Society for Allergology and Immunology Swiss Society for Infectious Diseases*, volume 139, pages s21–s21. EMH Swiss Medical Publishers.

[Schmid et al., 2011] Schmid, F., Bruhn, S., Weber, K., Mittrücker, H.-W., and Guse, A. H. (2011). CD38: a NAADP degrading enzyme. *FEBS letters*, 585(22):3544–3548.

[Schneider et al., 2014] Schneider, W. M., Chevillotte, M. D., and Rice, C. M. (2014). Interferon-stimulated genes: a complex web of host defenses. *Annual review of immunology*, 32:513–545.

[Sconocchia et al., 1999] Sconocchia, G., Titus, J. A., Mazzoni, A., Visintin, A., Pericle, F., Hicks, S. W., Malavasi, F., and Segal, D. M. (1999). CD38 triggers cytotoxic responses in activated human natural killer cells. *Blood, The Journal of the American Society of Hematology*, 94(11):3864–3871.

[Shi et al., 2011] Shi, L. Z., Wang, R., Huang, G., Vogel, P., Neale, G., Green, D. R., and Chi, H. (2011). HIF1α–dependent glycolytic pathway orchestrates a metabolic checkpoint for the differentiation of TH17 and Treg cells. *Journal of Experimental Medicine*, 208(7):1367–1376.

[Shimizu et al., 2015] Shimizu, S., Yonezawa, R., Negoro, T., Yamamoto, S., Numata, T., Ishii, M., Mori, Y., and Toda, T. (2015). Sensitization of H2O2-induced TRPM2 activation and subsequent interleukin-8 (CXCL8) production by intracellular Fe2+ in human monocytic U937 cells. *The international journal of biochemistry & cell biology*, 68:119–127.

[Shyer et al., 2020] Shyer, J. A., Flavell, R. A., and Bailis, W. (2020). Metabolic signaling in T cells. *Cell research*, 30(8):649–659.

[Sinclair et al., 2013] Sinclair, L. V., Rolf, J., Emslie, E., Shi, Y.-B., Taylor, P. M., and Cantrell, D. A. (2013). Control of amino-acid transport by antigen receptors coordinates the metabolic reprogramming essential for T cell differentiation. *Nature immunology*, 14(5):500–508.

[Siracusa et al., 2019] Siracusa, F., Durek, P., McGrath, M. A., Sercan-Alp, Ö., Rao, A., Du, W., Cendón, C., Chang, H.-D., Heinz, G. A., Mashreghi, M.-F., et al. (2019). CD69+ memory T lymphocytes of the bone marrow and spleen express the signature transcripts of tissue-resident memory T lymphocytes. *European journal of immunology*, 49(6):966–968.

[Su et al., 2015] Su, W., Wynne, J., Pinheiro, E. M., Strazza, M., Mor, A., Montenont, E., Berger, J., Paul, D. S., Bergmeier, W., Gertler, F. B., et al. (2015). Rap1 and its effector RIAM are required for lymphocyte trafficking. *Blood, The Journal of the American Society of Hematology*, 126(25):2695–2703.

[Sumoza-Toledo et al., 2011] Sumoza-Toledo, A., Lange, I., Cortado, H., Bhagat, H., Mori, Y., Fleig, A., Penner, R., and Partida-Sánchez, S. (2011). Dendritic cell maturation and chemotaxis is regulated by TRPM2-mediated lysosomal Ca2+ release. *The FASEB Journal*, 25(10):3529–3542.

[Sumpter et al., 2008] Sumpter, T. L., Payne, K. K., and Wilkes, D. S. (2008). Regulation of the NFAT pathway discriminates CD4+ CD25+ regulatory T cells from CD4+ CD25- helper T cells. *Journal of leukocyte biology*, 83(3):708–717.

[Syed, 2019] Syed, Y. Y. (2019). Daratumumab: a review in combination therapy for transplant-ineligible newly diagnosed multiple myeloma. *Drugs*, 79(4):447–454.

[Trebak and Kinet, 2019] Trebak, M. and Kinet, J.-P. (2019). Calcium signalling in T cells. *Nature Reviews Immunology*, 19(3):154–169.

[Tripathi et al., 2018] Tripathi, J. K., Sharma, A., Sukumaran, P., Sun, Y., Mishra, B. B., Singh, B. B., and Sharma, J. (2018). Oxidant sensor cation channel TRPM2 regulates neutrophil extracellular trap formation and protects against pneumoseptic bacterial infection. *The FASEB Journal*, 32(12):6848–6859.

[Uche et al., 2018] Uche, U. U., Piccirillo, A. R., Kataoka, S., Grebinoski, S. J., D'Cruz, L. M., and Kane, L. P. (2018). PIK3IP1/TrIP restricts activation of T cells through inhibition of PI3K/Akt. *Journal of Experimental Medicine*, 215(12):3165–3179.

[UniProt, 2021] UniProt (2021). UniProt: the universal protein knowledgebase in 2021. *Nucleic acids research*, 49(D1):D480–D489.

[Vaeth et al., 2017] Vaeth, M., Maus, M., Klein-Hessling, S., Freinkman, E., Yang, J., Eckstein, M., Cameron, S., Turvey, S. E., Serfling, E., Berberich-Siebelt, F., et al. (2017). Store-operated Ca2+ entry controls clonal expansion of T cells through metabolic reprogramming. *Immunity*, 47(4):664–679.

[Van Daalen et al., 2020] Van Daalen, K. R., Reijneveld, J. F., and Bovenschen, N. (2020). Modulation of inflammation by extracellular granzyme A. *Frontiers in Immunology*, 11:931.

[Viegas et al., 2007] Viegas, M. S., do Carmo, A., Silva, T., Seco, F., Serra, V., Lacerda, M., and Martins, T. C. (2007). CD38 plays a role in effective containment of mycobacteria within granulomata and polarization of Th1 immune responses against Mycobacterium avium. *Microbes and infection*, 9(7):847–854.

[Vig and Kinet, 2009] Vig, M. and Kinet, J.-P. (2009). Calcium signaling in immune cells. *Nature immunology*, 10(1):21–27.

[Wang et al., 2016] Wang, G., Cao, L., Liu, X., Sieracki, N. A., Di, A., Wen, X., Chen, Y., Taylor, S., Huang, X., Tiruppathi, C., et al. (2016). Oxidant sensing by TRPM2 inhibits neutrophil migration and mitigates inflammation. *Developmental cell*, 38(5):453–462.

[Wehage et al., 2002] Wehage, E., Eisfeld, J., Heiner, I., Jungling, E., Zitt, C., and Luckhoff, A. (2002). Activation of the cation channel long transient receptor potential channel 2 (LTRPC2)

by hydrogen peroxide: a splice variant reveals a mode of activation independent of ADP-ribose. *Journal of Biological Chemistry*, 277(26):23150–23156.

[Wilson et al., 2004] Wilson, L. A., Yamamoto, H., and Singh, G. (2004). Role of the transcription factor Ets-1 in cisplatin resistance. *Molecular cancer therapeutics*, 3(7):823–832.

[Woehrle et al., 2010] Woehrle, T., Yip, L., Elkhal, A., Sumi, Y., Chen, Y., Yao, Y., Insel, P. A., and Junger, W. G. (2010). Pannexin-1 hemichannel–mediated ATP release together with P2X1 and P2X4 receptors regulate T-cell activation at the immune synapse. *Blood, The Journal of the American Society of Hematology*, 116(18):3475–3484.

[Wolf et al., 2015] Wolf, I. M., Diercks, B.-P., Gattkowski, E., Czarniak, F., Kempski, J., Werner, R., Schetelig, D., Mittrücker, H.-W., Schumacher, V., von Osten, M., et al. (2015). Frontrunners of T cell activation: Initial, localized Ca2+ signals mediated by NAADP and the type 1 ryanodine receptor. *Science Signaling*, 8(398):ra102–ra102.

[Yamamoto et al., 2008] Yamamoto, S., Shimizu, S., Kiyonaka, S., Takahashi, N., Wajima, T., Hara, Y., Negoro, T., Hiroi, T., Kiuchi, Y., Okada, T., et al. (2008). TRPM2-mediated Ca 2+ influx induces chemokine production in monocytes that aggravates inflammatory neutrophil infiltration. *Nature medicine*, 14(7):738–747.

[Yamasaki et al., 2005] Yamasaki, M., Thomas, J. M., Churchill, G. C., Garnham, C., Lewis, A. M., Cancela, J.-M., Patel, S., and Galione, A. (2005). Role of NAADP and cADPR in the induction and maintenance of agonist-evoked Ca2+ spiking in mouse pancreatic acinar cells. *Current biology*, 15(9):874–878.

[Yao et al., 2016] Yao, H., Zhang, Y., Liu, L., Xu, Y., Liu, X., Lin, J., Zhou, W., Wei, P., Jin, P., and Wen, L.-P. (2016). Inhibition of lanthanide nanocrystal-induced inflammasome activation in macrophages by a surface coating peptide through abrogation of ROS production and TRPM2-mediated Ca2+ influx. *Biomaterials*, 108:143–156.

[Yip et al., 2009] Yip, L., Woehrle, T., Corriden, R., Hirsh, M., Chen, Y., Inoue, Y., Ferrari, V., Insel, P. A., and Junger, W. G. (2009). Autocrine regulation of T-cell activation by ATP release and P2X7 receptors. *The FASEB Journal*, 23(6):1685–1693.

[Zeng et al., 2016] Zeng, H., Cohen, S., Guy, C., Shrestha, S., Neale, G., Brown, S. A., Cloer, C., Kishton, R. J., Gao, X., Youngblood, B., et al. (2016). mTORC1 and mTORC2 kinase signaling and glucose metabolism drive follicular helper T cell differentiation. *Immunity*, 45(3):540–554.

[Zhao et al., 2012] Zhao, Y. J., Lam, C. M. C., and Lee, H. C. (2012). The membrane-bound enzyme CD38 exists in two opposing orientations. *Science signaling*, 5(241):ra67–ra67.

[Zou et al., 2013] Zou, J., Ainscough, J. F., Yang, W., Sedo, A., Yu, S.-P., Mei, Z.-Z., Sivaprasadarao, A., Beech, D. J., and Jiang, L.-H. (2013). A differential role of macrophage TRPM2 channels in Ca2+ signaling and cell death in early responses to H2O2. *American Journal of Physiology-Cell Physiology*, 305(1):C61–C69.

Supplementary material

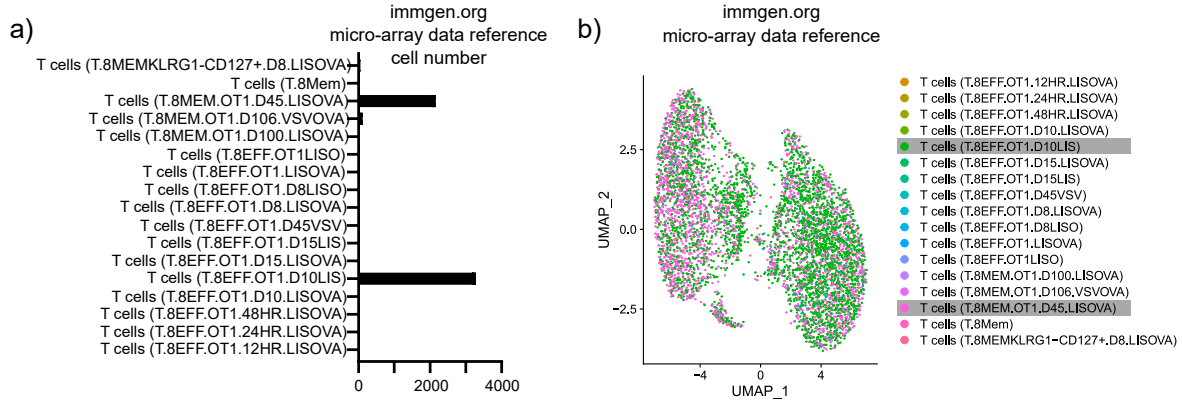

Figure S.1: **Cell numbers in immgen.org reference populations** a) Number of cells assigned to immge.org reference populations. b) Immgen.org reference populations in dimensional reduction/UMAP

Gene ontology enquiry of differentially expressed genes in *Cd38*$^{-/-}$ OT-1 vs. OT1 CD8^{+} T cells

Analysis Type: PANTHER Overrepresentation Test (Released 20220202); Annotation Version and Release Date: GO Ontology database DOI: 10.5281/zenodo.5725227 Released 2020-11-01; Analyzed List: upload_1 (Mus musculus); Reference List: Mus musculus (all genes in database); Test Type: FISHER; Correction: FDR

Table S.1: Gene ontology enquiry: *Cd38*$^{-/-}$ OT-1 vs. OT1 CD8^{+} T cells

GO_biological_process	Genes	Fold Enrich.
positive regulation of melanocyte differentiation (GO:0045636)	2	> 100
regulation of melanocyte differentiation (GO:0045634)	2	> 100
positive regulation of pigment cell differentiation (GO:0050942)	2	> 100
positive regulation of developmental pigmentation (GO:0048087)	2	> 100
regulation of pigment cell differentiation (GO:0050932)	2	99.76
leukocyte tethering or rolling (GO:0050901)	4	85.51
leukocyte adhesion to vascular endothelial cell (GO:0061756)	4	74.82
cellular extravasation (GO:0045123)	4	39.04
positive regulation of natural killer cell mediated cytotoxicity (GO:0045954)	3	38.48
positive regulation of natural killer cell mediated immunity (GO:0002717)	3	36.4
lamellipodium assembly (GO:0030032)	3	33.67
leukocyte cell-cell adhesion (GO:0007159)	4	30.44
regulation of cellular extravasation (GO:0002691)	3	29.28
regulation of T cell migration (GO:2000404)	3	28.65
lamellipodium organization (GO:0097581)	3	27.48
"CD4-positive, alpha-beta T cell activation (GO:0035710)"	3	24.94
regulation of natural killer cell mediated cytotoxicity (GO:0042269)	3	23.63
regulation of natural killer cell mediated immunity (GO:0002715)	3	22.45
alpha-beta T cell activation (GO:0046631)	4	19.95
lymphocyte activation involved in immune response (GO:0002285)	5	16.5
regulation of mononuclear cell migration (GO:0071675)	4	15.09
regulation of leukocyte mediated cytotoxicity (GO:0001910)	4	14.72
positive regulation of leukocyte migration (GO:0002687)	5	14.3
cell-matrix adhesion (GO:0007160)	4	13.92
leukocyte activation involved in immune response (GO:0002366)	6	13.33
cell activation involved in immune response (GO:0002263)	6	13.08
developmental growth involved in morphogenesis (GO:0060560)	4	12.83
regulation of cell killing (GO:0031341)	4	12.74

GO_biological_process	Genes	Fold Enrich.
negative regulation of inflammatory response (GO:0050728)	4	12.65
T cell activation (GO:0042110)	7	10.51
leukocyte migration (GO:0050900)	5	10.02
regulation of leukocyte migration (GO:0002685)	5	9.93
positive regulation of leukocyte cell-cell adhesion (GO:1903039)	5	9.01
positive regulation of cell-cell adhesion (GO:0022409)	6	9.01
leukocyte activation (GO:0045321)	11	8.46
positive regulation of response to external stimulus (GO:0032103)	8	7.95
GO_biological_process	Genes	Fold Enrich.
regulation of leukocyte cell-cell adhesion (GO:1903037)	6	7.81
lymphocyte activation (GO:0046649)	8	7.77
positive regulation of cell adhesion (GO:0045785)	8	7.42
cell activation (GO:0001775)	11	7.35
axonogenesis (GO:0007409)	6	7.34
cell-cell adhesion (GO:0098609)	7	7.13
positive regulation of cell migration (GO:0030335)	9	6.99
cell morphogenesis involved in neuron differentiation (GO:0048667)	7	6.77
axon development (GO:0061564)	6	6.7
regulation of cell-cell adhesion (GO:0022407)	7	6.69
positive regulation of cell motility (GO:2000147)	9	6.68
positive regulation of cellular component movement (GO:0051272)	9	6.5
positive regulation of locomotion (GO:0040017)	9	6.49
immune effector process (GO:0002252)	8	6.37
neuron projection morphogenesis (GO:0048812)	7	6.28
regulation of cell adhesion (GO:0030155)	11	6.28
plasma membrane bounded cell projection morphogenesis (GO:0120039)	7	6.21
cell projection morphogenesis (GO:0048858)	7	6.14
cell morphogenesis involved in differentiation (GO:0000904)	8	6.05
cell morphogenesis (GO:0000902)	10	5.87
cell part morphogenesis (GO:0032990)	7	5.83
regulation of defense response (GO:0031347)	8	5.73
cellular component morphogenesis (GO:0032989)	8	5.67
neuron projection development (GO:0031175)	9	5.53
neuron development (GO:0048666)	11	5.47
cell population proliferation (GO:0008283)	7	5.46
actin filament-based process (GO:0030029)	7	5.32
cellular metal ion homeostasis (GO:0006875)	7	5.27
head development (GO:0060322)	8	5.04
neuron differentiation (GO:0030182)	12	4.88
plasma membrane bounded cell projection organization (GO:0120036)	12	4.68
regulation of cell migration (GO:0030334)	10	4.65
regulation of response to external stimulus (GO:0032101)	10	4.64
response to cytokine (GO:0034097)	8	4.53
generation of neurons (GO:0048699)	14	4.49
cell projection organization (GO:0030030)	12	4.47
neurogenesis (GO:0022008)	15	4.4

GO_biological_process	Genes	Fold Enrich.
regulation of cell motility (GO:2000145)	10	4.39
positive regulation of cell differentiation (GO:0045597)	9	4.21
locomotion (GO:0040011)	12	4.19
regulation of locomotion (GO:0040012)	10	4.19
positive regulation of immune system process (GO:0002684)	10	4.1
regulation of anatomical structure morphogenesis (GO:0022603)	9	4.09
regulation of cellular component movement (GO:0051270)	10	4.06
positive regulation of cell population proliferation (GO:0008284)	9	4.02
regulation of multicellular organismal development (GO:2000026)	13	3.87
regulation of immune system process (GO:0002682)	14	3.84
cell development (GO:0048468)	15	3.61
movement of cell or subcellular component (GO:0006928)	12	3.57
negative regulation of cell communication (GO:0010648)	11	3.57
negative regulation of signaling (GO:0023057)	11	3.56
positive regulation of multicellular organismal process (GO:0051240)	13	3.56
cell surface receptor signaling pathway (GO:0007166)	15	3.42
nervous system development (GO:0007399)	16	3.38
positive regulation of developmental process (GO:0051094)	11	3.38
positive regulation of molecular function (GO:0044093)	11	3.35
regulation of cell differentiation (GO:0045595)	12	3.3
regulation of developmental process (GO:0050793)	19	3.28
negative regulation of response to stimulus (GO:0048585)	12	3.26
immune system process (GO:0002376)	18	3.24
positive regulation of response to stimulus (GO:0048584)	17	3.23
anatomical structure morphogenesis (GO:0009653)	16	3.13
regulation of multicellular organismal process (GO:0051239)	20	3.1
regulation of response to stimulus (GO:0048583)	27	2.99
regulation of localization (GO:0032879)	19	2.9
cell differentiation (GO:0030154)	22	2.68
cellular developmental process (GO:0048869)	22	2.65
regulation of signal transduction (GO:0009966)	17	2.65
regulation of molecular function (GO:0065009)	15	2.64
signal transduction (GO:0007165)	28	2.51
regulation of cell communication (GO:0010646)	18	2.44
signaling (GO:0023052)	29	2.44
regulation of signaling (GO:0023051)	18	2.43
cell communication (GO:0007154)	29	2.39
negative regulation of biological process (GO:0048519)	27	2.25
negative regulation of cellular process (GO:0048523)	23	2.09
positive regulation of cellular process (GO:0048522)	27	2.04
positive regulation of biological process (GO:0048518)	29	2.02
cellular response to stimulus (GO:0051716)	30	1.99
response to stimulus (GO:0050896)	35	1.81
regulation of cellular process (GO:0050794)	41	1.58
regulation of biological process (GO:0050789)	42	1.54
biological regulation (GO:0065007)	42	1.47

Gene ontology enquiry of differentially expressed genes in OT-1 vs *Cd38*$^{-/-}$ OT-1 CD8^{+} T cells

Analysis Type: PANTHER Overrepresentation Test (Released 20220202); Annotation Version and Release Date: GO Ontology database DOI: 10.5281/zenodo.5725227 Released 2020-11-01; Analyzed List: upload_1 (Mus musculus); Reference List: Mus musculus (all genes in database); Test Type: FISHER; Correction: FDR

Table S.2: Gene ontology enquiry: OT1 vs. *Cd38*$^{-/-}$ OT-1 CD8^{+} T cells

GO_biological_process	Genes	Fold Enrich.
telomerase holoenzyme complex assembly (GO:1905323)	2	> 100
negative reg. of establishm. of protein local. to mitoch. (GO:1903748)	2	> 100
regulation of tau-protein kinase activity (GO:1902947)	2	> 100
protein refolding (GO:0042026)	2	> 100
positive regulation by host of viral process (GO:0044794)	2	> 100
telomere maintenance via telomerase (GO:0007004)	2	> 100
RNA-dependent DNA biosynthetic process (GO:0006278)	2	> 100
chaperone-mediated protein complex assembly (GO:0051131)	2	> 100
telomere maintenance via telomere lengthening (GO:0010833)	2	> 100
reg. of establishm. of protein local. to mitoch. (GO:1903747)	2	> 100
positive regulation of type I interferon production (GO:0032481)	3	57.09
regulation of nitric oxide biosynthetic process (GO:0045428)	3	54.67
neutrophil chemotaxis (GO:0030593)	3	51.76
regulation of nitric oxide metabolic process (GO:0080164)	3	51.76
response to unfolded protein (GO:0006986)	4	50.74
protein localization to mitochondrion (GO:0070585)	3	48.52
granulocyte chemotaxis (GO:0071621)	3	47.34
neutrophil migration (GO:1990266)	3	44.11
response to topologically incorrect protein (GO:0035966)	4	41.74
response to interferon-gamma (GO:0034341)	4	41.08
response to heat (GO:0009408)	3	40.86
protein folding (GO:0006457)	5	40.18
regulation of muscle cell apoptotic process (GO:0010660)	3	40.02
cellular response to interferon-gamma (GO:0071346)	3	39.61
granulocyte migration (GO:0097530)	3	39.21

GO_biological_process	Genes	Fold Enrich.
regulation of type I interferon production (GO:0032479)	3	37.69
biological process involved in interaction with symbiont (GO:0051702)	3	34.35
myeloid leukocyte migration (GO:0097529)	3	30.33
positive regulation of peptidyl-serine phosphorylation (GO:0033138)	3	29.86
leukocyte chemotaxis (GO:0030595)	3	28.13
regulation of cell killing (GO:0031341)	3	27.53
biological process involved in symbiotic interaction (GO:0044403)	4	24.3
regulation of protein ubiquitination (GO:0031396)	4	23.74
reg. of protein mod. by small protein conjug. or removal (GO:1903320)	4	20.54
response to virus (GO:0009615)	4	18.03
regulation of protein stability (GO:0031647)	4	16.75
positive regulation of protein kinase activity (GO:0045860)	4	14.58
positive regulation of cytokine production (GO:0001819)	5	12.97
regulation of cytokine production (GO:0001817)	7	11.72
regulation of protein kinase activity (GO:0045859)	5	10.86
response to cytokine (GO:0034097)	6	9.8
regulation of kinase activity (GO:0043549)	5	9.22
positive regulation of catalytic activity (GO:0043085)	7	8.56
negative regulation of apoptotic process (GO:0043066)	6	8.1
biol. process involved in interspecies interact. between organisms (GO:0044419)	10	7.97
negative regulation of programmed cell death (GO:0043069)	6	7.91
negative regulation of cell death (GO:0060548)	6	6.96
response to other organism (GO:0051707)	8	6.96
response to external biotic stimulus (GO:0043207)	8	6.95
regulation of apoptotic process (GO:0042981)	8	6.77
response to biotic stimulus (GO:0009607)	8	6.77
regulation of programmed cell death (GO:0043067)	8	6.64
regulation of catalytic activity (GO:0050790)	9	6.47
positive regulation of gene expression (GO:0010628)	6	6.45
positive regulation of molecular function (GO:0044093)	7	6.14
regulation of cell death (GO:0010941)	8	5.96
response to organic substance (GO:0010033)	11	5.46
regulation of cellular protein metabolic process (GO:0032268)	9	4.89
response to external stimulus (GO:0009605)	9	4.75
cellular response to chemical stimulus (GO:0070887)	9	4.71
response to chemical (GO:0042221)	13	4.7
regulation of molecular function (GO:0065009)	9	4.57
regulation of protein metabolic process (GO:0051246)	9	4.55
negative regulation of nitrogen compound metabolic process (GO:0051172)	8	4.41
response to stress (GO:0006950)	11	4.31
regulation of signal transduction (GO:0009966)	9	4.04
negative regulation of metabolic process (GO:0009892)	9	3.92

Differentially expressed genes in *Cd38*$^{-/-}$ OT-1 CD8^{+} T cells

Table S.3: Differentially expressed genes *Cd38*$^{-/-}$ OT-1 vs. OT-1 CD8^{+} T cells

Gene	p_val	avg_log2FC	pct.1	pct.2	p_val_adj
Hsp90ab1	8.24412770502763E-78	-0.380129743335927	0.979	0.993	1.65888337680566E-73
Zeb2	6.10797180347735E-66	0.733740072407697	0.655	0.494	1.22904608629571E-61
Txnip	5.30883443449214E-65	0.501946225872765	0.894	0.867	1.06824366490851E-60
Hspa8	1.03506506300045E-56	-0.279720785097656	0.987	0.996	2.08275791976951E-52
Itga4	9.82350034975886E-55	0.42759514063572	0.926	0.917	1.97668474037848E-50
Thy1	7.76926963488145E-52	0.411569494341275	0.846	0.846	1.56333243593085E-47
Rpl10	1.69796955139315E-48	-0.272713375088656	0.953	0.974	3.4166543313133E-44
Ahnak	4.11419634877848E-46	0.422147285235976	0.88	0.872	8.27858589301205E-42
Nkg7	2.70514063032751E-45	0.285423456090466	0.991	0.99	5.44328397634503E-41
Ets1	1.48716608978707E-42	0.381753147597085	0.92	0.914	2.99247560586955E-38
Cx3cr1	1.18541015566752E-39	0.657365460191038	0.414	0.283	2.38528231523419E-35
Hsph1	1.07561662089002E-38	-0.363934227104034	0.431	0.633	2.16435576455489E-34
Dnaja1	1.35992199196047E-38	-0.288712715741425	0.856	0.926	2.73643503222286E-34
AC149090.1	1.00573893498115E-36	0.559933261221667	0.57	0.471	2.02374788496907E-32
Gapdh	7.69580700959856E-34	-0.305752639552729	0.703	0.815	1.54855028647142E-29
Ifngr1	5.82674046465873E-32	0.374187188239533	0.774	0.771	1.17245671629863E-27
Jaml	3.05545358810883E-30	-0.270776953029996	0.191	0.339	6.14818370999259E-26
Arl4c	7.67764922396844E-30	0.32948910592866	0.847	0.837	1.54489657684693E-25
Rap1b	1.78042740368618E-29	0.359881538115643	0.807	0.802	3.58257602169733E-25
Gzma	8.7573047246134E-29	0.387166659904891	0.786	0.763	1.76214485668671E-24
Atp2b1	1.69973702576176E-28	0.408485959517203	0.764	0.741	3.42021084323781E-24
Dynll1	3.37740491237673E-28	-0.271157399577657	0.617	0.774	6.79601416468445E-24
Il18rap	3.93173305895661E-28	0.473839636560427	0.582	0.522	7.9114332612325E-24
Hsp90aa1	2.39412052033258E-25	-0.254135083939648	0.825	0.909	4.81744931101321E-21
Nsa2	3.44610167888246E-25	-0.265444940857073	0.555	0.716	6.9342457982473E-21
Emp3	5.70977016501697E-25	0.287065379257443	0.868	0.858	1.14891995260471E-20
Tsc22d3	3.76140360195726E-23	0.39523626078018	0.587	0.542	7.5686963278584E-19
Klf3	4.16066089515115E-23	0.41124630976165	0.672	0.653	8.37208185322315E-19
Rgs1	4.48499760138367E-23	-0.352246571058831	0.476	0.639	9.02471217350422E-19
Cd69	9.15329335487108E-22	-0.282152728997576	0.444	0.606	1.84182568886716E-17
Bcl2	2.73209766394081E-20	0.51280942965388	0.616	0.583	5.49752691938169E-16
Ccdc88c	8.23303150524196E-19	0.334316391845951	0.651	0.623	1.65665059948479E-14
Ifng	2.48168921909614E-18	-0.377997724429074	0.416	0.563	4.99365504666525E-14
Itgb1	4.27162846090201E-18	0.279921253190198	0.899	0.907	8.59537078902702E-14
Ccnd3	9.36581173669353E-18	0.327147592765596	0.635	0.631	1.88458863765747E-13
Bst2	9.86122384797741E-18	-0.308882744402029	0.263	0.385	1.98427546269001E-13
Gm26740	1.71749168231473E-17	0.322393807243419	0.659	0.646	3.45593676315369E-13
Arhgef18	6.62200891851058E-17	0.380703192299729	0.501	0.461	1.3324806345827E-12
Pik3ip1	1.23431091278461E-16	0.375084493630466	0.325	0.252	2.48368041870518E-12
Spn	1.5284114663765E-16	0.369457155815516	0.633	0.629	3.07546955264279E-12

Gene	p_val	avg_log2FC	pct.1	pct.2	p_val_adj
Ly6a	2.83232681626391E-16	-0.27643325624167	0.525	0.661	5.69920801968624E-12
S1pr5	2.65382641161968E-15	0.335041282095671	0.238	0.165	5.34002950546112E-11
Jak1	4.53299040549707E-15	0.250476296331298	0.841	0.872	9.1212832939412E-11
Ripor2	7.0749270792655E-15	0.270389527855437	0.674	0.661	1.4236168268898E-10
Apbb1ip	1.1351277855849E-13	0.281004778253903	0.672	0.679	2.28410413015393E-09
Klrc1	1.47867652245467E-12	0.265295378454538	0.711	0.737	2.97539289848329E-08
Isg15	4.7120483152304E-12	-0.293379942508198	0.095	0.156	9.48158361990661E-08
Lnpep	4.75460505426828E-12	0.324623467486522	0.566	0.565	9.56721629019863E-08
Znrf2	1.05301221334698E-11	0.300495540530973	0.59	0.594	2.1188711756968E-07
Klrb1c	7.98701512255409E-11	0.350648049071616	0.221	0.167	1.60714718296033E-06
Rora	2.40439295880585E-10	0.346572911083304	0.566	0.562	4.83811951170912E-06
Klrg1	1.88797209268679E-09	0.26434570484235	0.196	0.145	3.79897744490437E-05
Nptn	9.00888448713492E-09	0.332887549805964	0.437	0.417	0.00018127677365
Neat1	9.9244888943305E-09	0.300559172078108	0.538	0.531	0.000199700565532
S1pr1	1.2410946861658E-08	0.260237138725472	0.586	0.597	0.00024973307275
Zcchc7	1.38680139235974E-08	0.25046359957901	0.588	0.602	0.000279052176171
Zmiz1	2.81813396354149E-08	0.301939290576284	0.365	0.328	0.000567064916144
Lfng	2.69272294101921E-07	0.263234404942452	0.507	0.511	0.005418297101919
Gm44175	3.61847596744225E-07	0.302687141247878	0.328	0.294	0.007281097341687
Fryl	3.35812261854468E-06	0.269926625370428	0.451	0.445	0.067572143330356
Oip5os1	3.86294433451027E-06	0.27658649472063	0.455	0.454	0.077730165899016
Sept11	6.52616447600317E-06	0.27596143379008	0.413	0.402	0.131319481586136
Mirt1	2.1672104860005E-05	0.278578878466986	0.366	0.349	0.436086093993021
Klf7	2.19689090081399E-05	0.277972539813751	0.222	0.192	0.442058387061792
Nebl	3.20726715617633E-05	0.285336555027148	0.19	0.16	0.645366297165802
Ncald	3.62223997174946E-05	0.256741925941047	0.298	0.274	0.728867127115426
Racgap1	7.15613812226449E-05	0.260913901224869	0.262	0.237	1
Ube2g2	0.000110078150623	0.261963539986559	0.313	0.297	1
Sppl2a	0.00014198953191	0.272957177670736	0.317	0.307	1
Tm9sf3	0.000178926325344	0.251383860412635	0.498	0.527	1
Spata13	0.000273484612121	0.259008792969894	0.367	0.367	1
Sgk1	0.001081339743815	0.261447561203342	0.3	0.287	1
Ccl4	0.088331203781024	-0.283232031065493	0.638	0.692	1

Table S.4: Differentially expressed genes in "T cells (T.8EFF.OT1.D10LIS)": *Cd38*$^{-/-}$ OT-1 vs. OT-1 CD8^{+} T cells

Gene	p_val	avg_log2FC	pct.1	pct.2	p_val_adj
Zeb2	3.83675561114612E-27	0.675365828499133	0.68	0.529	7.72031964074822E-23
Bcl2	4.32211197043874E-13	0.583075429095148	0.602	0.529	8.69695370691682E-09
Cx3cr1	6.51211294422603E-14	0.582929473152927	0.435	0.324	1.31036736663716E-09
AC149090.1	6.35441908934515E-16	0.536823067950821	0.57	0.459	1.27863620915803E-11
Txnip	1.66116302247073E-28	0.468678366729447	0.902	0.868	3.3425922338156E-24
Ahnak	1.82911899728764E-22	0.448494810221737	0.874	0.868	3.68055324634218E-18
Il18rap	2.75569170071584E-12	0.419245198389576	0.582	0.501	5.54500284018042E-08
Gzma	1.07392447518542E-11	0.407220768951847	0.802	0.785	2.1609508289681E-07
Ifngr1	1.24908862285668E-14	0.401343475210616	0.762	0.758	2.51341612691221E-10
Arhgef18	1.15475130696724E-10	0.399434544573057	0.514	0.448	2.32359057987947E-06
Ccdc88c	1.22254252068146E-11	0.394783867599833	0.666	0.616	2.46000006011524E-07
Ets1	6.04654223037548E-22	0.388393876955814	0.92	0.905	1.21668522759615E-17
Thy1	3.27100682824431E-19	0.387759443748443	0.829	0.83	6.5819199397932E-15
Itga4	6.77854334681334E-23	0.386551674293548	0.929	0.913	1.36397849224578E-18
Spn	6.01412047969541E-09	0.382282624360132	0.649	0.634	0.000121016132292
Tsc22d3	9.13644207056158E-09	0.379550382752181	0.564	0.52	0.000183843487344
Klf3	2.3378658871493E-07	0.368113472337227	0.653	0.657	0.004704253738122
Atp2b1	1.7762053578412E-10	0.363163156958928	0.76	0.741	3.57408042104807E-06
Rora	2.58844754932995E-06	0.348988851840152	0.549	0.529	0.052084741587617
Znrf2	1.23146954480123E-09	0.344703026807256	0.619	0.571	2.47796301804904E-05
Sppl2a	0.000156865711679	0.334896113892701	0.312	0.273	1
Apbb1ip	4.28471372024636E-08	0.33357972338415	0.657	0.654	0.000862170094788
Nptn	3.90839102863106E-05	0.33320221191718	0.442	0.413	0.786446442781143
Rap1b	2.89160360382883E-11	0.328350402518371	0.803	0.791	5.81848477162438E-07
Mirt1	0.000413993720167	0.325074756692156	0.398	0.37	1
Pik3ip1	1.1528750251987E-05	0.312553341661285	0.323	0.268	0.231981512570483
Emp3	1.85289090861795E-14	0.309099815638088	0.885	0.864	3.72838708632104E-10
Thap3	0.00106657683676	0.306139708106038	0.402	0.391	1
Arl4c	2.13195453523787E-14	0.302096243200993	0.85	0.817	4.28991891580563E-10
Ccnd3	1.0397856427849E-07	0.297468639547441	0.634	0.614	0.002092256670412
Gm26740	1.20963155975467E-06	0.293710865211556	0.65	0.644	0.024340206245384
Gm44175	0.005098641015815	0.292795997216549	0.334	0.31	1
Neat1	4.95708199138448E-05	0.289421990864013	0.543	0.522	0.997464038306386
Ube2g2	0.002677942655965	0.289022824397494	0.327	0.305	1
Ankrd44	2.11738789526042E-06	0.283393605629971	0.7	0.71	0.04260607922843
Lnpep	0.000204493651512	0.283216448390769	0.555	0.562	1
Picalm	0.000131140502189	0.283036865377048	0.457	0.43	1
Klrc1	2.45100538896384E-06	0.281231334897365	0.662	0.665	0.04931913043673
Zfp36l2	4.02745745248533E-10	0.281207611963397	0.869	0.854	8.10404988589099E-06
Zmiz1	0.00116955648238	0.277660149336979	0.367	0.335	1
Tbl1xr1	0.01599237250243	0.277126774061147	0.287	0.273	1
4833420G17Rik	0.003165476968235	0.2768435657956	0.329	0.305	1
Pik3r1	0.001490656515239	0.275815476144459	0.454	0.439	1
Fryl	0.000623463581599	0.27487580709942	0.456	0.436	1
Racgap1	0.001899090506886	0.274722394717349	0.266	0.23	1

Gene	p_val	avg_log2FC	pct.1	pct.2	p_val_adj
Efhd2	0.001672761921997	0.271863598935961	0.41	0.389	1
Prkacb	0.010081875726474	0.271742389319197	0.365	0.357	1
Sgk1	0.016354319773145	0.27076788771777	0.305	0.284	1
Nkg7	3.62251028050059E-18	0.270354107675895	0.989	0.987	7.28921518642329E-14
Ncald	0.004788480680848	0.270033749209782	0.29	0.263	1
Ube2q1	0.001240490696369	0.269726652136056	0.313	0.282	1
Zcchc7	1.55014534916555E-06	0.268122476135312	0.597	0.58	0.031192024715909
Sept11	0.00164183641143	0.267630362515798	0.406	0.378	1
Rasgrp2	0.004101725197559	0.267067904448273	0.52	0.533	1
Atp1b3	8.53183728970587E-08	0.26551829916559	0.775	0.779	0.001716776299435
Cdk13	0.09592426466352	0.260257882888204	0.302	0.304	1
Klrc2	9.38077236718663E-05	0.258093025245908	0.594	0.583	1
Jak1	1.97444373283267E-06	0.257302470468747	0.83	0.853	0.039729756792059
Dnajc1	0.003008303191966	0.256894923160319	0.48	0.485	1
Nfatc3	0.014066656678994	0.25363842050719	0.514	0.537	1
Gabpb2	0.007930677026885	0.253290227174758	0.376	0.365	1
Cd164	0.003441750176494	0.252816284146395	0.457	0.457	1
Itgb1	9.59635436171918E-07	0.251985868695453	0.911	0.911	0.019309784246651
Oip5os1	0.013685551900744	0.250408172514373	0.459	0.461	1
Rpl29	6.34381389699149E-20	-0.252484308712173	0.977	0.986	1.27650223235263E-15
Dynll1	7.3927212566084E-13	-0.256381571536214	0.582	0.753	1.48756337125474E-08
Hsp90aa1	7.75017338928289E-12	-0.256451525328489	0.806	0.895	1.5594898893915E-07
Nsa2	3.11544092475706E-10	-0.261705028401349	0.529	0.68	6.26889022879616E-06
Rpl10	2.38326968643244E-18	-0.261931342866015	0.946	0.969	4.79561526303937E-14
Tnfaip3	1.03081206889732E-10	-0.265523476045971	0.347	0.506	2.07420004503519E-06
Edf1	1.08906613563374E-12	-0.265972368703613	0.405	0.592	2.19141887812222E-08
Hspa8	1.30577403007096E-23	-0.273755912267315	0.986	0.997	2.62747850330879E-19
Ifng	2.5438446894172E-05	-0.274164218936747	0.386	0.497	0.511872428404529
Cd69	4.16191584391616E-09	-0.274561567448615	0.351	0.494	8.37460706112809E-05
Gapdh	2.50841816477937E-13	-0.277658647712495	0.676	0.789	5.04743903116905E-09
Hspe1	5.10349020036301E-14	-0.280122671978461	0.762	0.878	1.02692429811705E-09
Rgs1	7.73903257314877E-07	-0.287932593235918	0.424	0.559	0.01557248134369
Dnaja1	1.68248529168138E-19	-0.314964754536783	0.853	0.92	3.38549690392127E-15
Hist1h1c	1.30546086595501E-12	-0.324642673540095	0.203	0.341	2.62684835447468E-08
Hsph1	9.47418333722408E-17	-0.394651112166088	0.418	0.614	1.90639517111623E-12
Hsp90ab1	1.93344714352482E-38	-0.410622606360498	0.978	0.993	3.89048234220065E-34

Table S.5: Differentially expressed genes in "T cells (T.8MEM.OT1.D45.LISOVA)" *Cd38*$^{-/-}$ OT-1 vs. OT-1 CD8^{+} T cells

Gene	p_val	avg_log2FC	pct.1	pct.2	p_val_adj
Zeb2	1.07533129865292E-17	0.765242188401777	0.592	0.424	2.1637816391494E-13
Cx3cr1	3.68231383754827E-13	0.705550175621223	0.364	0.224	7.40955190391463E-09
AC149090.1	4.44512813323099E-13	0.590112390961395	0.575	0.469	8.94448682968739E-09
Txnip	8.23886093006311E-17	0.511031625065421	0.889	0.873	1.6578235963473E-12
Bcl2	2.99352176175022E-07	0.492594507818305	0.673	0.642	0.006023564488994
Il18rap	2.4633000825714E-05	0.456875094844497	0.525	0.514	0.495665242615016
Arhgef18	3.29085852777469E-07	0.452759766074686	0.522	0.471	0.006621865529588
Pik3ip1	1.37558447637723E-08	0.446931070749512	0.358	0.258	0.000276795108337
Itga4	3.09580309375702E-16	0.439467983575696	0.932	0.915	6.22937498525787E-12
Klf3	2.20337233269786E-09	0.425388253162386	0.704	0.66	4.43362580785463E-05
Thy1	3.32607943415245E-18	0.423015465445747	0.867	0.873	6.69273703740156E-14
Gzma	9.65760402720862E-10	0.413062454573128	0.786	0.77	1.94330308235492E-05
Ccnd3	5.04311380957289E-08	0.409869739061538	0.658	0.648	0.001014775360762
Atp2b1	9.52579036859662E-09	0.408703668437695	0.758	0.76	0.000191677953797
Ahnak	1.10098765313782E-11	0.40767987042346	0.887	0.872	2.21540735564391E-07
Tsc22d3	3.58974868505318E-09	0.396533740458136	0.642	0.586	7.22329230406402E-05
Gm44175	2.01284327739401E-05	0.384721844594247	0.341	0.27	0.405024324277223
Ifngr1	3.67455518981382E-12	0.37385390369861	0.796	0.795	7.39393995294337E-08
Ripor2	6.80219078227849E-08	0.369254063973486	0.692	0.659	0.00136873682921
Neat1	0.007812040027785	0.364609823392936	0.522	0.535	1
Ets1	1.64910339340895E-09	0.358721034823712	0.917	0.929	3.31832584821748E-05
Prf1	0.00046194186832	0.344426377195667	0.569	0.583	1
Rap1b	1.71698198237829E-08	0.340500102600941	0.807	0.811	0.000345491114494
Rora	0.03047677646517	0.337773521973533	0.551	0.576	1
Arl4c	8.88490200832198E-08	0.323080942154626	0.855	0.865	0.001787819982115
Oip5os1	0.008831220313609	0.322484586304993	0.444	0.45	1
Kcnq1ot1	0.348691419789883	0.318690034112775	0.322	0.333	1
Picalm	0.001424614694186	0.316934688065437	0.486	0.472	1
Gm26740	4.27102973928221E-06	0.313997351549233	0.68	0.684	0.085941660413837
Spata13	0.008891509494967	0.309074012534559	0.381	0.368	1
Lfng	0.001583587082756	0.306427639096822	0.52	0.53	1
Sept11	0.008085618450238	0.302659845810241	0.437	0.431	1
Spn	0.001133438966573	0.302617639508155	0.615	0.624	1
Ypel3	0.001567801390381	0.29819769376398	0.502	0.494	1
Tm9sf3	0.017680957596768	0.296397978682744	0.51	0.533	1
Ctsd	5.2517802522957E-05	0.293479293446443	0.787	0.797	1
Gsk3b	0.021234187378514	0.291065520978856	0.516	0.522	1
Nkg7	6.02731955821299E-13	0.289275987947075	0.997	0.993	1.21281724150362E-08
Brd9	0.006633619536488	0.285976599401664	0.403	0.388	1
Malat1	1.96847811215219E-23	0.285965234896588	1	1	3.96097165727263E-19
S1pr1	0.00105141080108	0.285388721954224	0.616	0.657	1
Atf7ip	0.095671146716311	0.281787720315389	0.52	0.565	1
Cd8a	1.66288062999624E-11	0.281757894255442	1	1	3.34604840367843E-07
Pds5a	0.086997990071382	0.281097305235163	0.339	0.342	1
Nptn	0.034141862810824	0.277493648593795	0.437	0.438	1

Gene	p_val	avg_log2FC	pct.1	pct.2	p_val_adj
Kif21b	0.048814173595684	0.275454579486196	0.464	0.486	1
Id2	2.83653697018067E-07	0.274495270712336	0.919	0.926	0.005707679691398
Tram1	0.123612523962938	0.268692225008068	0.444	0.46	1
Rabgap1l	0.023502471887531	0.268616308993845	0.411	0.407	1
Bcl11b	0.000145280110106	0.266533558612038	0.824	0.844	1
Zmiz1	0.045238610706793	0.264280032090074	0.347	0.333	1
BE692007	0.086384181923081	0.26084270403536	0.562	0.616	1
Sppl2a	0.147892972539843	0.260723855424566	0.339	0.347	1
Adgre5	0.000337815577535	0.260519506633492	0.621	0.618	1
Ppp3ca	0.0822677697353	0.259669249684752	0.37	0.382	1
Lnpep	0.002872511585683	0.257589249157059	0.559	0.562	1
Znrf2	0.029099406884709	0.252308341674034	0.566	0.605	1
Iqgap1	0.001108917823051	0.252303828899541	0.718	0.759	1
Itgal	0.001489585477237	0.251989688716323	0.706	0.732	1
Txk	0.023967946429981	0.251631382257409	0.655	0.698	1
Rpl29	9.70324787303207E-16	-0.253213556543791	0.982	0.998	1.95248753701151E-11
Rpl10	9.59979548784856E-15	-0.254567409871833	0.962	0.976	1.93167084806489E-10
Ly6a	2.80413803360744E-05	-0.262848667918345	0.578	0.716	0.564248655122489
Hspa8	2.20498795592396E-16	-0.268397394130818	0.989	0.998	4.43687676491019E-12
Mndal	1.06112356810675E-05	-0.269772191669972	0.623	0.772	0.21351928437444
Ifi27l2a	0.003556091143234	-0.280106201467224	0.311	0.394	1
Hsp90ab1	1.37021275898388E-15	-0.291571369241874	0.978	0.994	2.75714211362735E-11
Dynll1	1.34206275005351E-10	-0.300304024960704	0.674	0.823	2.70049866565767E-06
Gapdh	1.3246252394964E-11	-0.30346388597417	0.737	0.854	2.66541090691465E-07
Ifi203	4.01089486853239E-09	-0.3037442597201	0.655	0.827	8.07072265446088E-05
Hspd1	4.9130045770457E-09	-0.304118373791153	0.507	0.676	9.88594780993135E-05
Rgs1	1.15181894314024E-07	-0.311799616655766	0.469	0.634	0.002317690077387
Jaml	5.52248529911714E-14	-0.321504055317239	0.194	0.379	1.11123449188835E-09
Hsph1	1.0926418567231E-11	-0.322861131385586	0.459	0.655	2.19861394409822E-07
Bst2	9.72027337850322E-09	-0.402514733893725	0.286	0.438	0.000195591340922
Ccl4	0.190314509790339	-0.443703299626647	0.64	0.692	1
Ifng	2.20935538504275E-09	-0.471801529537733	0.412	0.586	4.44566490578303E-05

Declaration

Hiermit bestätige ich an Eides statt, dass die vorliegende Arbeit von mir selbständig verfasst wurde und ich keine anderen als die angegebenen Hilfsmittel – insbesondere keine im Quellenverzeichnis nicht benannten Internet–Quellen – benutzt habe und die Arbeit von mir vorher nicht einem anderen Prüfungsverfahren eingereicht wurde. Die eingereichte schriftliche Fassung entspricht der auf dem elektronischen Speichermedium. Ich bin damit einverstanden, dass die Dissertation veröffentlicht wird.

_____

Datum, Unterschrift